Assessing Fuels in European Temperate Forests and Heathlands Using Remote Sensing

Zur Erlangung des akademischen Grades einer
DOKTORIN DER NATURWISSENSCHAFTEN
(Dr. rer. nat.)

bei der KIT-Fakultät für
Bauingenieur-, Geo- und Umweltwissenschaften
des Karlsruher Instituts für Technologie (KIT)
eingereichte

DISSERTATION

von

Pia Labenski
aus Heilbronn

Tag der mündlichen Prüfung: 03.06.2024

Hauptreferent: Prof. Dr. Sebastian Schmidtlein
Korreferent: Prof. Dr. Fabian Fassnacht
Korreferentin: PD Dr. Sina Keller

Karlsruhe, 2024

Danksagung

Zunächst möchte ich mich bei Prof. Dr. Sebastian Schmidtlein für die Möglichkeit bedanken, meine Doktorarbeit am Institut für Geographie und Geoökologie in einer angenehmen Arbeitsatmosphäre anfertigen zu können. Für die Begutachtung der vorliegenden Arbeit danke ich ihm sowie Prof. Dr. Fabian Fassnacht und PD Dr. Sina Keller.
Meinem Betreuer Fabian Fassnacht bin ich außerdem zutiefst dankbar für die stetige Unterstützung während der letzten Jahre, die wertvollen Diskussionen, aufbauenden Worte und seine nicht nachlassende Begeisterung für neue Ideen. Ihm sowie allen Koautorinnen und Koautoren danke ich für die konstruktiven Rückmeldungen und Beiträge zu meinen Publikationen.
Ganz herzlich möchte ich mich bei Michael Ewald für die angenehme, engagierte Zusammenarbeit und für seine Gelassenheit bedanken, insbesondere bei den umfangreichen Feldarbeiten, sowie für die geduldige Lektüre und das wertvolle Feedback zu meinen Texten.
Johannes Senn und Martina Ettlin bin ich sehr dankbar für ihren tatkräftigen Einsatz bei den Feldarbeiten im Peak District bei bestem englischen Wetter und für alle Unterstützung darüber hinaus.
Mein besonderer Dank gilt Jannika Schäfer, Felix Schiefer, Elham Shafeian, Anne Lewerentz, Johannes Senn und Michael Ewald für die tägliche Begleitung auf dem Weg zur Promotion, die vielen hilfreichen Gespräche im Büro, die gemeinsamen Unternehmungen und die gegenseitige Unterstützung in jeder Phase. Ohne euch wäre die Zeit nur halb so schön gewesen.
Allen Kolleginnen und Kollegen aus der Vegetations-Arbeitsgruppe und dem IfGG danke ich für die gemeinsam verbrachten Mittagessen, Kaffeepausen und Feierabende und die dabei ausgetauschten Geschichten und Ratschläge.
Gareth Clay danke ich für die Betreuung während meines Forschungsaufenthaltes an der Universität Manchester, sowie Ana María Pacheco-Pascagaza und Gail Millin-Chalabi für die produktive Zusammenarbeit. Mein Dank gilt allen Mitgliedern der EPRG-Gruppe und des Geography-Departments für die freundliche Aufnahme und die schönen Erlebnisse während dieser Zeit.
Ohne die Förderung durch das Karlsruhe House of Young Scientists wäre dieser Forschungsaufenthalt nicht möglich gewesen. Die Teilnahme an mehreren Konferenzen und Summer Schools wurde mir dank der finanziellen Unterstützung durch die Graduiertenschule GRACE ermöglicht.
Schließlich möchte ich mich bei allen bedanken, die mich in dieser Zeit und darüber hinaus mit ihrer Freundschaft begleitet haben, die mir emotionalen Rückhalt und genügend Ablenkung beim Radfahren, Klettern, Segeln, Kochen, Spazierengehen oder Tischtennisspielen und bei ausgiebigen Gesprächen gegeben haben.
Von ganzem Herzen danke ich meinen Eltern und meinen Schwestern für ihre Unterstützung und ihr Vertrauen in mich und dafür, dass ich meine Qualitäten als Tante unter Beweis stellen darf.
Schließlich danke ich Carl für seinen Zuspruch und für die wunderbare Reise, die wir miteinander begonnen haben.

Summary

Wildfires are occurring with increasing frequency and intensity in European temperate ecosystems. Severe fires can affect the health and safety of the population, emit large amounts of smoke and carbon dioxide, cause economic damage, and have negative impacts on biodiversity and carbon storage. Mitigating the adverse impacts of wildfires through preventive management and effective suppression strategies requires a thorough understanding of how ignitions and fire behaviour are related to the characteristics of the local vegetation that provides the fuel. The ignition and spread of a surface fire is influenced in particular by the availability, condition, and small-scale heterogeneity of live and dead fuels close to the ground, i.e. the surface fuels. Accurate and spatially explicit characterisation of surface fuels is therefore essential to determine flammability, calculate potential fire behaviour and estimate fire effects across the landscape. Because fuel inventories in the field are laborious and time-consuming, remote sensing has been proposed as a means to collect fuel information over large areas in a cost- and time-effective manner. However, the large spatial and temporal variability of fuels complicates the accurate mapping of fuels, especially in the case of surface fuels, which are often weakly perceptible from a remote sensing perspective. Therefore, fuel mapping efforts have mainly focused on broad fuel categories, such as fuel types, which have been defined to simplify the high complexity of fuels but inevitably result in a loss of information. Hence, there is a need to develop new and improve existing surface fuel characterisation techniques capable of capturing fuel variability at fine scales, particularly for the application in previously less fire-prone and therefore in this regard understudied ecosystems such as temperate forests and dwarf shrub heaths.

This thesis aims to investigate the potential of different methods based on proximal and remote sensing datasets to characterise surface fuels in European temperate forests and Atlantic dwarf shrub heaths, resolving both spatial and temporal fuel variation. It includes three separate studies.

In the first study, a fine-grained classification of surface fuel types in central European forests is presented, and a deep learning model is developed to identify these fuel types from forest photographs and multispectral satellite time series. By incorporating below-canopy observations from handheld camera devices, the approach aims to improve the discrimination of different understory and litter fuel types using simple geo-referenced RGB images. Different input data combinations and model output aggregation techniques are tested to further increase classification accuracies. The results show that both understory types and litter types can be reasonably well distinguished based on forest photographs, while including multispectral satellite time series only improves litter classification. Further improvements can be achieved by making predictions on multiple photographs of the same stand and filtering outputs based on the class prediction probability. The algorithm thus effectively provides fuel information based on photographs, without the need for human visual interpretation and expert knowledge.

The second study focuses on mapping fine-scale variability of surface fuel loads in central European forests using detailed airborne laserscanning and multispectral satellite data in a machine learning approach. A large set of structural and spectral predictors across different forest strata is used to develop random forest regression models for different surface fuel components. Surface fuel maps calculated from these models are used to predict potential fire behaviour in two forest stands under typical summer weather conditions. Additionally, a sensitivity analysis of the fire behaviour predictions to variations in the load of different

surface fuel components is carried out. The findings confirm that accurately quantifying surface fuels from remote sensing is difficult, even when detailed remote sensing data are available. Nevertheless, the analyses identify the predictors that are most suitable for predicting the different surface fuel components, thereby informing future mapping efforts. The inevitable uncertainties in fuel load estimates are likely to continue to have a major impact on fire behaviour predictions.
In the third study, temporal dynamics of surface fuels in Atlantic dwarf shrub heaths are analysed based on multispectral satellite time series. By fitting harmonic models to the annual cycle of various optical vegetation indices, seasonal changes in fuel state and hence flammability due to phenology are effectively captured. Changes in fuels due to wildfire disturbance and subsequent vegetation regeneration are assessed by analysing the recovery trajectories of the spectral indices, unveiling significant differences between indices and between life forms. A driver analysis of the calculated recovery times based on multiple linear regression shows that burn severity, land cover class, season, and winter snow cover are important variables influencing the estimated recovery rate. While spectral recovery times underestimate true vegetation recovery for slow growing life forms due to the lack of structural information, they still provide insight into post-disturbance fuel development in these open landscapes. In this way, they help to inform models that describe fuel dynamics and can be used to update fuel maps.

The analyses in this thesis are an important step towards a more efficient and more precise description of surface fuels that is also more closely linked to ecological processes. They further advance the knowledge of fuels in European temperate ecosystems, a long-neglected research topic. Future fuel characterisation and mapping efforts will benefit from the insights into the potential and limitations of the proximal and remote sensing datasets that have been thoroughly investigated for this purpose. Future studies should further explore synergies with other remote sensing products at different scales, leveraging the capabilities offered by artificial intelligence methods for processing and fusing different types of data, and they should also strongly focus on the integration of temporal fuel dynamics by using process-based vegetation models to better describe fuels. In addition, there is a need to harmonise and extend fuel reference datasets, conduct field and laboratory experiments on fire behaviour, and collect observational data from real wildfires to address the upcoming challenge of wildfire management in Europe's temperate ecosystems.

Kurzfassung

Feuer treten in den temperierten Ökosystemen Europas zunehmend häufiger und mit größerer Intensität auf. Schwere Brände können die Gesundheit und Sicherheit der Bevölkerung gefährden, große Mengen Rauch und Kohlendioxid freisetzen, wirtschaftliche Schäden verursachen und negative Folgen für Biodiversität und Kohlenstoffspeicherung haben. Um negative Auswirkungen von Bränden durch vorbeugendes Management und wirksame Bekämpfungsstrategien zu reduzieren, ist es wichtig, die Zusammenhänge zwischen dem Brandverhalten und den Eigenschaften der Vegetation, die das Brennmaterial liefert, zu verstehen. Die Entzündung und Ausbreitung von Oberflächenfeuern wird durch Verfügbarkeit, Zustand und kleinräumige Heterogenität von Brennmaterialien in Bodennähe beeinflusst. Eine genaue, räumlich eindeutige Charakterisierung dieser Brennmaterialien ist daher für die Bestimmung der Entflammbarkeit, die Berechnung des Feuerverhaltens und die Abschätzung der Auswirkungen von Bränden unerlässlich. Da die Inventarisierung von Brennmaterialien im Feld sehr zeitaufwändig ist, werden Fernerkundungsmethoden eingesetzt, um Informationen über Brennmaterialien in größeren Gebieten kostengünstig und zeitsparend zu sammeln. Die große räumliche und zeitliche Variabilität der Brennmaterialien erschwert jedoch eine genaue Kartierung, besonders bei oberflächennahen Brennmaterialien, die aus Fernerkundungsperspektive oft nur schwach erkennbar sind. Daher konzentrieren sich bisherige Kartierungsbemühungen meist auf weit gefasste Brennmaterialkategorien, die definiert wurden, um die Komplexität von Brennmaterialien zu vereinfachen, was jedoch unweigerlich zu Informationsverlust führt. Daher ist es nötig, neue Methoden zur Charakterisierung von oberflächennahen Brennmaterialien zu entwickeln und bestehende Techniken zu verbessern, die in der Lage sind, feinskalige Brennmaterialvariabilität zu erfassen, insbesondere für die Anwendung in bisher weniger feuergefährdeten und daher wenig untersuchten Ökosystemen wie temperierten Wäldern und Zwergstrauchheiden.

Ziel dieser Arbeit ist es, im Rahmen von drei Studien das Potenzial verschiedener Methoden auf der Grundlage von Nah- und Fernerkundungsdatensätzen zur Charakterisierung von oberflächennahen Brennmaterialien in mitteleuropäischen Wäldern und atlantischen Zwergstrauchheiden zu untersuchen, wobei sowohl räumliche als auch zeitliche Brennstoffvariationen aufgelöst werden sollen. In der ersten Studie wird eine feinkörnige Klassifikation von oberflächennahen Brennmaterialien in mitteleuropäischen Wäldern vorgestellt, und ein Deep Learning-Modell entwickelt, um diese Brennmaterialtypen anhand von Waldfotos und multispektralen Satellitenzeitreihen zu identifizieren. Das Einbeziehen von Kameraaufnahmen unterhalb der Baumkrone soll die Unterscheidung zwischen verschiedenen Unterwuchs- und Streu-Brennmaterialtypen mittels einfacher georeferenzierter RGB-Bilder erleichtern. Um die Klassifikationsgenauigkeit zu verbessern, werden verschiedene Kombinationen von Eingangsdaten und Techniken zur Aggregation der Modellausgaben getestet. Die Ergebnisse zeigen, dass sowohl Unterwuchs- als auch Streutypen auf der Grundlage von Waldfotos recht gut unterschieden werden können, während die Einbeziehung multispektraler Satellitenzeitreihen nur die Streuklassifizierung verbessert. Weitere Verbesserungen können erzielt werden, indem Vorhersagen für mehrere Fotos desselben Bestandes getroffen und basierend auf der Wahrscheinlichkeit der Klassenvorhersage gefiltert werden. Der Algorithmus liefert somit effektiv Brennmaterialinformationen basierend auf Fotos, ohne dass eine menschliche visuelle Interpretation oder Expertenwissen erforderlich ist.
Die zweite Studie befasst sich mit der Kartierung der feinskaligen Variabilität der oberflächennahen Brennmaterialmengen in mitteleuropäischen Wäldern unter Verwendung detail-

lierter luftgestützter Laserscans und multispektraler Satellitendaten in einem maschinellen Lernverfahren. Basierend auf einem umfangreichen Satz struktureller und spektraler Prädiktoren zur Beschreibung verschiedener Waldstrata werden Regressionsmodelle für verschiedene oberflächennahe Brennmaterialkomponenten entwickelt. Die mithilfe dieser Modelle berechneten Brennmaterialkarten werden zur Vorhersage des potenziellen Brandverhaltens in zwei Waldbeständen unter typischen sommerlichen Wetterbedingungen verwendet. Zusätzlich wird die Sensitivität der Vorhersagen des Brandverhaltens in Bezug auf Variationen in der Menge der verschiedenen Brennmaterialkomponenten analysiert. Die Ergebnisse bestätigen, dass eine genaue Quantifizierung des oberflächennahen Brennmaterials mittels Fernerkundung schwierig ist, selbst wenn detaillierte Fernerkundungsdaten verfügbar sind. Dennoch zeigen die Analysen, welche Prädiktoren sich am besten für die Vorhersage der verschiedenen Brennmaterialkomponenten eignen, und liefern damit wichtige Informationen für zukünftige Kartierungsbemühungen. Die unvermeidlichen Unsicherheiten bei der Schätzung der Brennmaterialmengen haben jedoch einen erheblichen Einfluss auf die Vorhersage des Brandverhaltens.
In der dritten Studie werden zeitliche Dynamiken des oberflächennahen Brennmaterials in atlantischen Zwergstrauchheiden anhand von multispektralen Satellitenzeitreihen analysiert. Durch die Anpassung harmonischer Modelle an den Jahresgang verschiedener optischer Vegetationsindizes werden saisonale Schwankungen des Brennmaterialzustandes und damit der Entflammbarkeit aufgrund phänologischer Veränderungen effektiv erfasst. Veränderungen des Brennmaterials durch Störungen wie Brände und die anschließende Regeneration der Vegetation werden durch eine Analyse der Erholungsverläufe der spektralen Indizes bewertet, wobei signifikante Unterschiede zwischen den verwendeten Indizes und zwischen den untersuchten Lebensformen aufgedeckt werden. Eine Auswertung der potentiellen Einflussfaktoren auf die berechneten Erholungszeiten mittels multipler linearer Regression zeigt, dass Brandschwere, Landbedeckungsklasse, Jahreszeit und winterliche Schneebedeckung wichtige Variablen sind, die die geschätzte Erholungsrate beeinflussen. Obwohl die spektralen Erholungszeiten die tatsächliche Erholung der Vegetation für langsam wachsende Lebensformen aufgrund fehlender struktureller Informationen unterschätzen, geben sie dennoch Aufschluss über die Entwicklung des Brennmaterials nach einer Störung. Auf diese Weise helfen sie bei der Erstellung von Modellen zur Beschreibung der Brennmaterialdynamik, welche zur Aktualisierung von Brennmaterialkarten verwendet werden können.

Die in dieser Arbeit vorgestellten Analysen sind ein wichtiger Schritt hin zu einer effizienteren, genaueren und stärker an ökologischen Prozessen orientierten Beschreibung oberflächennaher Brennmaterialien. Sie erweitern das Wissen über Brennmaterialien in temperierten europäischen Ökosystemen, welche in dieser Hinsicht bisher wenig erforscht wurden. Zukünftige Arbeiten zur Charakterisierung und Kartierung von Brennmaterialien werden von den Erkenntnissen über das Potenzial und die Grenzen der zu diesem Zweck eingehend untersuchten Nah- und Fernerkundungsdatensätze profitieren. Künftige Studien sollten Synergien mit anderen Fernerkundungsprodukten auf verschiedenen räumlichen Skalen weiter untersuchen und dabei die Möglichkeiten von Methoden der künstlichen Intelligenz zur Verarbeitung und Zusammenführung verschiedener Datentypen nutzen, sich aber auch auf die Integration der zeitlichen Dynamik von Brennmaterialien konzentrieren, indem sie prozessbasierte Vegetationsmodelle verwenden. Zudem sollten Referenzdatensätze für Brennmaterialien erweitert, Feld- und Laborexperimente zum Brandverhalten durchgeführt und Beobachtungsdaten von realen Bränden gesammelt werden, um die künftige Herausforderung des Feuermanagements in temperierten Ökosystemen Europas zu bewältigen.

Contents

Part I

Introduction

Motivation

Wildfires have long been a rare phenomenon in the temperate ecosystems of Europe, where wildfire activity has been largely confined to the Mediterranean region. The emergence of severe fires in temperate regions of Europe in recent years yet provides clear evidence that these areas, traditionally not considered fire-prone, are now increasingly at risk (San-Miguel-Ayanz et al., 2022). The simultaneous occurrence of large wildfires across European ecosystems in exceptional drought years, such as 2018 and 2022, points to an emerging change in fire dynamics and increased fire impacts in Europe driven by global warming and land use change (Carnicer et al., 2022). In 2022, the European Forest Fire Information System (EFFIS) recorded the highest frequency and second largest extent of wildfires in central-western European countries since 2006 (EFFIS, 2023). Increased wildfire activity in temperate regions has the potential to seriously affect biodiversity and carbon storage in forests and peatlands (Kirkland et al., 2023), as well as posing threats to the health and safety of the population. These developments emphasise the urgent need to better understand fire behaviour, its drivers, and its impacts in previously less affected ecosystems, in order to make informed decisions about how to create fire-resistant and resilient landscapes.

Despite the current trend towards increased fire risk in the temperate ecosystems of Europe, research on wildfires in these areas lags behind the research carried out in the traditionally more fire-prone Mediterranean or North American ecosystems by several decades. While the scarcity of observational data from wildfires or experimental burns in temperate regions of Europe makes it difficult to gain insight into ignition conditions and fire dynamics based on real fires, modelling approaches can help shed light on potential fire behaviour and effects. These models rely on information about the quantity and properties of the combustible material present in the area, known as fuel. Therefore, a detailed characterisation of the local vegetation regarding its availability to act as fuel is required, but such information is largely lacking in temperate European ecosystems. Hence, the objective of this thesis is to expand the knowledge on vegetation fuels in these regions whilst developing new and improving existing methods to collect this information in an effective way using proximal and remote sensing.

1 European temperate forests and heathlands

This work focuses on the temperate broadleaved and mixed forests of central Europe and the open landscapes of the Atlantic dwarf shrub heaths in western Europe. They are presently located in the zone of temperate oceanic climate and partly in the humid continental zone (Köppen climate classification Cfb and Dfb), with moderately warm to warm summers and mild to cold winters, depending on the continentality of the location. Precipitation amount does not differ significantly between the seasons, except in years with extended summer droughts, which are occurring with increasing frequency (Hänsel et al., 2022). The seasonality in temperature and day length means that plants experience a period favourable for growth over spring, summer and parts of autumn, and a period of dormancy over the winter.
The forests and heathlands of central-western Europe differ in several ways from the ecosystems analysed in previous fuel and wildfire studies, e.g. from southern Europe or North America. Important aspects are differences in the local species composition, which are linked to physiological and morphological traits that result in different combustion behaviour, and differences in vegetation structure, which determines the distribution and continuity of fuel and therefore the spread of fire across the landscape. In addition, species may possess or lack protective or survival strategies to cope with the occurrence of fire. In the following, the specific characteristics of forests and heathlands in central-western Europe (comprising Austria, Belgium, France, Germany, Ireland, Liechtenstein, Luxembourg, Netherlands, Switzerland, and United Kingdom according to Forest Europe, 2020) are outlined.

1.1 Temperate broadleaved and mixed forests

1.1.1 Vegetation development and composition

The temperate and relatively humid climatic conditions of central-western Europe are suitable for the growth of deciduous broadleaved tree species, such as European beech (*Fagus sylvatica* L.) or pedunculate oak (*Quercus robur* L.), which are equipped with corresponding traits like mesomorphic leaves (Leuschner & Ellenberg, 2017a). Consequently, large parts of central-western Europe are dominated by broadleaved forest. Coniferous forests, including forests dominated by silver fir (*Abies alba* Mill.), occur naturally only at higher elevations or where specific edaphic and environmental conditions allow them to outcompete broadleaved species (Leuschner & Ellenberg, 2017a). However, today's forest landscape in central and western Europe has been created by humans over thousands of years through the use of forests for livestock feeding and grazing, through clearing activities to obtain land for agriculture and wood as fuel and building material, and through systematic forestry with a primarily economically oriented species selection (Puhe & Ulrich, 2001). The latter has led to plantings of fast-growing monocultures of Norway spruce (*Picea abies* (L.) H. Karst.) and Scots pine (*Pinus sylvestris* L.) in broadleaved forest habitats, such as in the North German Plain or in the Harz. Species that are not native to Europe have also been introduced for timber production and now occupy a significant proportion of the forest area in the temperate regions of Europe, e.g. Douglas fir (*Pseudotsuga menziesii* (Mirb.) Franco) (Forest Europe, 2020). Despite the species-poor and often even-aged overstory in managed forests,

understory composition can be very variable, consisting of regeneration of conifer seedlings, broadleaved trees and shrubs, dwarf shrubs, herbs, and mosses (Leuschner & Ellenberg, 2017a). More recently, the formation of semi-natural mixed broadleaved forests has been promoted more intensively, which has led to a greater diversity of tree species and also to higher quantities of deadwood in European forests in the past years (Forest Europe, 2020). In addition, these forests feature vegetation layers with trees in different stages of development, providing small-scale habitat heterogeneity for the forest floor vegetation and a wide range of forest species (Muys et al., 2022). According to Forest Europe (2020), mixed forests currently account for 24.1 % of the forest area in central-western Europe, while predominantly broadleaved forests occupy 45.9 %, and predominantly coniferous forests represent 30.0 %. Hence, the forest ecosystems in central-western Europe show a wide range of structural and compositional diversity depending on the degree of human intervention and forest management objectives, likely resulting in differences in potential fire behaviour.

1.1.2 Fire-adaptive traits of the vegetation

Although there is clear evidence of prehistoric and historic fire use in central-western Europe (Tinner et al., 2005), e.g. slash-and-burn agriculture in southwestern Germany during the Neolithic (Clark et al., 1989) and the persistence of similar practices in many European regions until the Second World War (Conedera et al., 2007), there is hardly any fire use in central-western European forests today. Wildfires in central-western European forest ecosystems neither play a major role in the natural disturbance regime, contrary to Mediterranean ecosystems or Northern European boreal forests. However, there are regions where periodic fires appear to be important in maintaining forests dominated by Scots pine (Adámek et al., 2015). Scots pine is considered the most fire-prone but at the same time most fire-resistant tree species in the European temperate zone (Adámek et al., 2016; Päätalo, 1998). The litter of Scots pine is highly flammable due to its high terpene content and leaf morphology (Ewald et al., 2023), and the comparably low canopy density allows the growth of a dense understory that can dry to low moisture levels (Hille et al., 2005; Tanskanen et al., 2006). Scots pine further exhibits several fire-adaptation traits, such as a thick and heat-insulating bark, a deep root system that is less susceptible to damage, a cambium that can recover from fire damage, and the ability to regenerate successfully after low-frequency fires (Fernandes et al., 2008; Zackrisson, 1977).
Most other tree species of central-western European forests are not well adapted to fire. Norway spruce, for example, has a thin bark and a shallow root system, making it more vulnerable to fire damage and increasing the likelihood of post-fire mortality (Ryan & Reinhardt, 1988). In addition, due to its low hanging branches, fires are more easily transferred from the surface to the tree crown, bearing the potential for severe crown fires (Blauw et al., 2017; Päätalo, 1998). Norway spruce in particular is suffering from widespread bark beetle outbreaks in European temperate forests in response to warming trends, increasing the amount of dead fuel and thus potentially intensifying wildfires in these forests (Romeiro et al., 2022). Norway spruce is commonly classified as fire-intolerant or fire avoider species, as is silver fir (Tinner et al., 2013). In contrast, North American Douglas fir exhibits high fire resistance owing to its thick bark and deep roots (Moris et al., 2022; Spalt & Reifsnyder, 1962). Deciduous species that dominate European temperate forests are considered to be less fire-prone than coniferous species, and are also fire-sensitive (Bobek et al., 2019; Tinner et al., 2000). European beech lacks fire adaptive traits such as a thick

bark or resprouting capacity and can suffer from severe damage and stand-replacing effects even after low-intensity fires (Conedera et al., 2010). The presence of beech forests has been associated with little fire activity historically (Bobek et al., 2019), but more recently, large wildfires associated with summer heat waves have affected beech forests in the Southwestern Alps (Müller et al., 2020). However, studies by Ascoli et al. (2013) and Maringer et al. (2016) indicate that there is some resilience of beech in response to single fire events: mast seeding of surviving mature trees, triggered by warm summers, coinciding with suitable seedbed conditions created by the fire has been observed as a successful post-fire recovery strategy in beech forests. Deciduous oak species such as pendunculate oak and sessile oak have shown varying fire resistance depending on the level of fire severity (Conedera et al., 2010; Tinner et al., 2000). Their thicker bark protects them from low-intensity fires, but not from moderate or high-intensity fires, and their resprouting capability has been shown to be rather weak (Conedera et al., 2010).

1.1.3 Vulnerability to wildfires

Due to the mostly poorly fire-adapted tree species in central-western Europe and their increasing vulnerability to multiple climate-mediated stressors, these forests may experience strong impacts by wildfires of increasing frequency and severity (Tinner et al., 2005), which can also lead to alterations in species composition and key forest services. The weakened health of temperate forests has been shown in recent decades by increased defoliation, canopy dieback, and mortality (Millar & Stephenson, 2015). However, temperate forests are fundamental for carbon sequestration and provide a habitat for endangered species when managed appropriately. Large areas of central-western European forests (46.5 %) are protected for landscape and biodiversity conservation (Forest Europe, 2020). Carbon stocks in forest biomass are currently highest in central-western Europe (93.0 t/ha) compared to other European regions (Forest Europe, 2020), but this could change under increased wildfire activity (Millar & Stephenson, 2015). Forests provide numerous other ecosystem services that benefit society and people. In central-western Europe, forested areas and human settlements are particularly closely interwoven, as demonstrated by the highest rural population density (37.8 people per km) in Europe and the high distribution of Wildland-Urban Interface (WUI) areas (Forest Europe, 2020; Modugno et al., 2016). This means that many people directly profit from recreational opportunities and health effects of forests, but also that a considerable proportion of the population is exposed to smoke and air pollution and their safety is threatened in the case of wildfire (Costa et al., 2020). At the same time, human activities at the interface between populated or agricultural areas and the forest or within the forest are the most common source of ignitions (Adámek et al., 2018). These circumstances emphasise the sensitivity to and the distinctive nature of wildfires in the forests of central-western Europe.

1.2 Atlantic dwarf shrub heaths

1.2.1 Vegetation development and composition

In oceanic north-west Europe, the creation of open wood-pastures in forested areas in the late Neolithic led to the expansion of dwarf shrub heaths and grassland during the Bronze Age (Puhe & Ulrich, 2001). This development was particularly rapid on poor soils, where practices such as sod cutting for crop fertilisation had led to considerable nutrient depletion (Leuschner & Ellenberg, 2017a). Dwarf shrub heaths can be found both on freely draining, sandy soils (dry heaths) and on peat soils (wet heaths). The establishment of heathland vegetation promotes the podsolisation of the already base-poor soils through its acidic litter and leads to the formation of raw humus. In areas with high rainfall and/or impeded drainage, such as the uplands of the north and west of the United Kingdom (UK), soils can remain waterlogged for longer periods, inhibiting decomposition and encouraging further accumulation of raw humus, which eventually turns into peat (W. G. Smith, 1902). The development of today's heathlands back into woodland has been prevented over centuries by constant disturbance from grazing, periodic burning or other use, maintaining an open landscape composed of low shrubs, grasses, herbs, and bryophytes. Atlantic heathlands of north-western Europe can be found in parts of Belgium, Sweden, Denmark, the Netherlands, Norway, the UK, and Germany (Weir & Scasta, 2022). The typical heathland vegetation is dominated by members of the Ericaceae family, such as common heather (*Calluna vulgaris* (L.) Hull) and bilberry (*Vaccinium myrtillus* L.), but grassland species such as wavy hair-grass (*Deschampsia flexuosa* (L.) Trin.) and, in wet habitats, purple moor-grass (*Molinia caerulea* (L.) Moench), hare's tail cottongrass (*Eriophorum vaginatum* L.) and bog mosses (*Sphagnum spp.*) also occur (Leuschner & Ellenberg, 2017b). Heathland habitats are closely associated with acid grasslands and blanket bogs in upland areas, and so they often co-exist in dynamic vegetation mosaics (Ausden, 2007).

1.2.2 Fire-adaptive traits of the vegetation

Due to the high conservation value of open heathland habitats, there is a wealth of literature on heathland ecology and the heather plant itself, including the relation to fire (Diemont et al., 2013; Gimingham, 1972; G. R. Miller & Miles, 1970; Schellenberg & Bergmeier, 2022). Common heather is a fire-adapted species, with the capacity to resprout rapidly after fires and increased seed germination in response to fires (Måren et al., 2010). Periodic fires therefore help to rejuvenate heathlands by enhancing new plant growth from seed or triggering a secondary life cycle through vegetative regeneration (Schellenberg & Bergmeier, 2022). Common heather is a highly flammable species due to its low moisture content (Davies, 2005) and emits considerable amounts of biogenic volatile organic compounds (VOC), mainly consisting of monoterpenes (Isidorov et al., 2022), which have been shown to strongly influence combustion dynamics (Ormeño et al., 2009). Furthermore, common heather forms rather dense and continuous fuel beds with high fuel loads, which can support intense fires (Plucinski et al., 2009; Weir & Scasta, 2022). Grasses and mosses associated with heathland habitats also provide easily combustible fuels depending on their moisture status and can either thrive or decline in response to fire. Wavy hair-grass, for example, suffers from more deeply burning fires due to its shallow roots (Päätalo, 1998), while purple moor-grass has shown high growth rates and the ability to expand even after intense

fires (Brys et al., 2005). Similarly, invasive bracken (*Pteridium aquilinum* (L.) Kuhn) is able to survive and spread after fire due to the large number of underground buds on its rhizome (Marrs et al., 2000). It has also been observed that the abundance of acrocarpous mosses increases, while pleurocarpous mosses decrease following high-intensity fires (Grau-Andrés et al., 2019; Sedláková & Chytrỳ, 1999). Severe wildfires therefore have the potential to induce changes in the community composition and structure of heathlands.

1.2.3 Fire use and vulnerability to wildfires

In contrast to temperate forest ecosystems, fire management still plays an important role today in the heathlands of north-west Europe, particularly in the UK, where heather-dominated landscapes in upland areas are often referred to as moorlands (Weir & Scasta, 2022). Traditional heathland land use in north-west Europe mainly involved burning to promote the regrowth of young heather shoots for livestock grazing with a fire rotation of 15-25 years, and burns were usually carried out in winter to avoid damage to soils and the seed bank (Weir & Scasta, 2022). Current heathland management practices involving fire in the UK are strongly associated with enhancing the population of red grouse, which is used for game shooting on privately owned shooting estates (Davies et al., 2016). Burning also still serves to improve the grazing conditions for sheep and deer, and helps to retain habitat functions and biodiversity (Davies et al., 2008). However, prescribed burning and its impacts are still a controversial subject in the UK, particularly when it comes to burning on deep peat and associated effects on carbon dynamics (see Heinemeyer & Ashby, 2023). Owing to the increasing risk of wildfires across coastal heathlands, prescribed burning is also used to manage fuel loads to reduce the risk of severe wildfires (Weir & Scasta, 2022). Management fires are usually low-severity fires that consume surface vegetation and litter, but leave the soil organic layer intact (Davies, Smith, et al., 2010). Their use is usually regulated in some form by good-practice burning codes, for example by restricting the size of burn areas and the legal burn period, which in upland areas of England lasts from 1 October to 15 April (Defra, 2007). In contrast to prescribed burns, wildfires in heathlands tend to occur when vegetation is dry and therefore highly flammable, which can result in the complete consumption of above-ground vegetation and substantial amounts of organic soil or peat (e.g. Maltby et al., 1990). High-intensity fires may lead to the mortality of dwarf shrubs by burning their rootstock and can also produce lethal temperatures for the seeds buried in the soil, thereby hindering successful regeneration of dwarf shrubs and facilitating colonisation by grasses (Ausden, 2007). This may ultimately lead to the decline of these valuable ecosystems, which are already subject to severe pressure from historical drainage, climate warming, and pollution (Weir & Scasta, 2022). Measures to restore areas severely damaged by wildfires require considerable investment and may not guarantee complete restoration (McMorrow, 2011). Given that UK moorlands are a globally significant carbon sink (Billett et al., 2010), large wildfires contribute to further climate feedbacks. As in temperate forests, wildfires in moorlands can threaten live and livelihoods of the rural population, and the amount of smoke released from burning peat may affect human health more seriously than is the case with forest fires.

1.3 Wildfire regime

1.3.1 Meteorological drivers

The temperate regions of Europe have long experienced limited exposure to wildfires. They are commonly classified as moisture-limited systems, where fuel moisture driven by weather conditions is the main factor limiting fire activity, as opposed to fuel-limited systems such as some shrublands, where the amount and connectivity of combustible biomass are the limiting factor for fire (Kelley et al., 2019; Krawchuk & Moritz, 2011). Therefore, changes in weather conditions that promote greater fuel dryness in temperate ecosystems make these highly productive systems more flammable (Duane et al., 2021; Krawchuk et al., 2009) and add to the lengthening of fire seasons (Jolly et al., 2015). An increased frequency and severity of fire weather has been observed for various regions of the world in recent decades (Abatzoglou et al., 2019), and models also suggest a strong increase in fire weather across central-western Europe by the end of the 21st century under a high emissions scenario (**Figure 1.1**) (Costa et al., 2020; de Rigo et al., 2017). More persistent, extreme summer weather events in north-west Europe, such as heatwaves and droughts, have been linked to a slower and wavier flow of the North Atlantic polar jet stream, most likely resulting from a reduction in the temperature gradient between the Equator and the North Pole caused by global warming (Trouet et al., 2018). Associated with increasing fire weather, fire probability is predicted to rise substantially in temperate biomes towards the end of the century (Moritz et al., 2012). For the period from 2000 to 2014, an increase in the burned area in temperate forests of 2.4 % per year has already been estimated as a result of changing controls on fire regimes (Duane et al., 2021), suggesting that global warming may cause further shifts in the fire regime of temperate ecosystems.

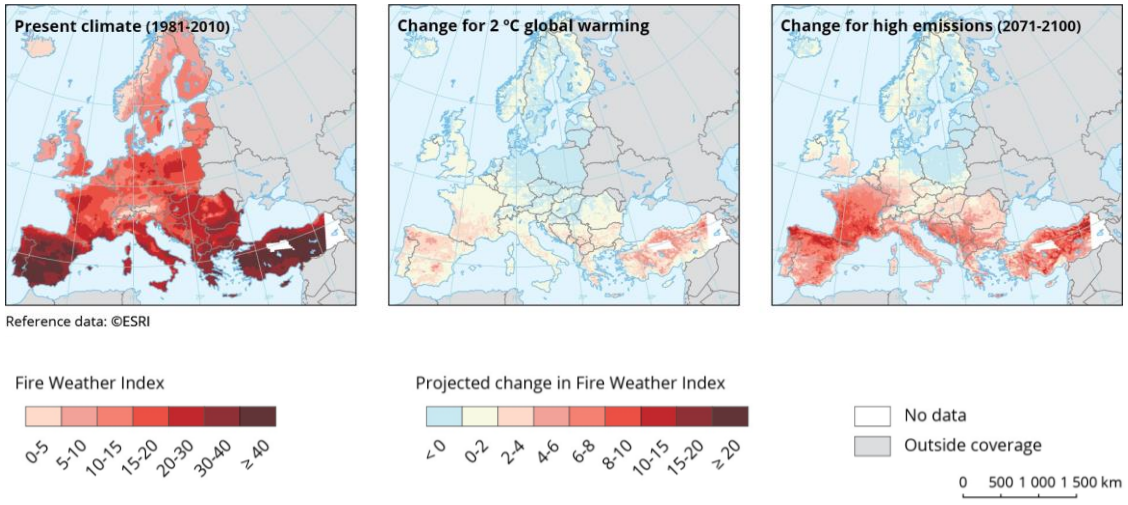

Figure 1.1: Fire Weather Index (FWI) for Europe in the present and FWI change under two climate change scenarios (2 °C global warming and RCP8.5). Adapted from Figure 8 of de Rigo et al. (2017).

1.3.2 Current figures

Understanding of current and potential future fire regimes in central-western Europe requires knowledge of the long-term patterns of fire frequency, intensity, and seasonality, as

well as fuel consumption, burned area size, and distribution (Keeley et al., 2011). However, statistics on the occurrence of wildfires in central-western European countries only cover a few decades, and the different national documentation systems vary in the fire attributes collected, the most common being fire cause and area burned (Müller et al., 2020; San-Miguel-Ayanz et al., 2022). These records show that most wildfires are less than 1 ha in size, but also that there is a large inter-annual variability in the area burned (San-Miguel-Ayanz et al., 2022). Small fires are difficult to detect with coarse-resolution satellite sensors such as MODIS or VIIRS, which are currently employed by the European Forest Fire Information System (EFFIS) to monitor wildfires in Europe, as they can only resolve fires >30 ha (EFFIS, 2023). Still, EFFIS statistics provide insight into the occurrence of larger wildfires, indicating that frequency and extent of these fires in central and western European countries have increased since monitoring began in 2006 (**Figure 1.2**). Still, consistent and detailed fire records across countries are lacking, and particularly data on fire behaviour are scarce (Fernandez-Anez et al., 2021).

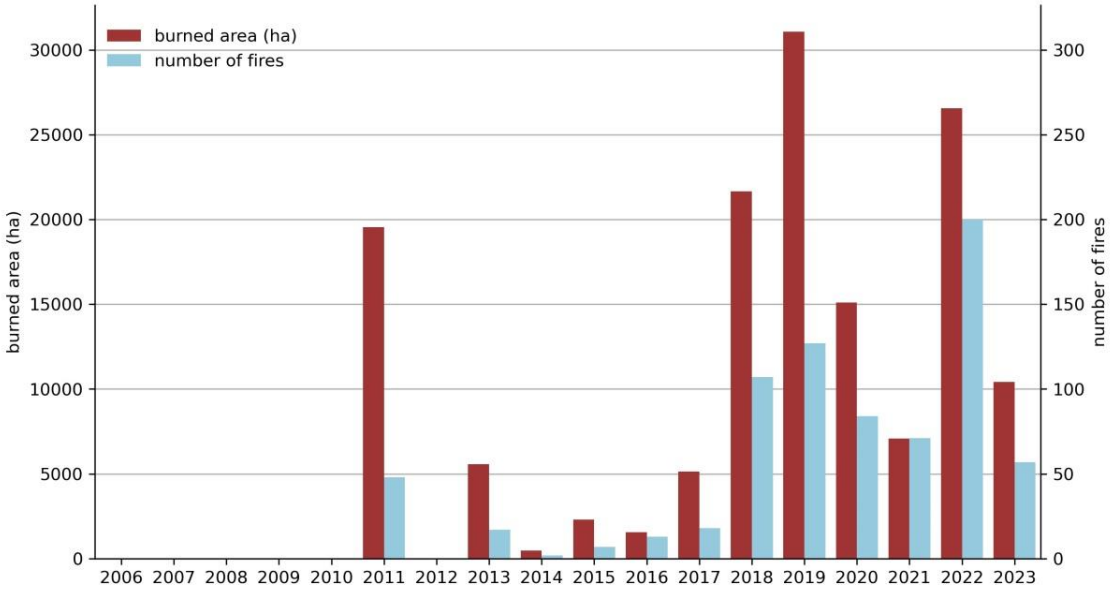

Figure 1.2: Country statistics available in EFFIS (2023) for central-western European countries (Austria, Belgium, Germany, Netherlands, Switzerland, United Kingdom). France is excluded, as the Mediterranean part of the country differs greatly in terms of vegetation composition and wildfire occurrence.

Nevertheless, some of the few available observations on the wildfire regime in central-western Europe are summarised in the following. The fire season can be largely restricted to the period from March to September (Venäläinen et al., 2014), and usually exhibits two peaks, specifically in early spring and late summer (Cardíl et al., 2023; Müller et al., 2020). Ignition sources are almost exclusively anthropogenic, with fires being started either through negligence or deliberately, and only 0.5 % of fires in central Europe in the period from 2006 to 2010 were of natural origin, i.e., ignited by lightning strikes (Ganteaume et al., 2013). As forest areas are often highly fragmented and easily accessible (Forest Europe, 2020), wildfires are detected and extinguished relatively rapidly, contributing to smaller fire sizes. However, research suggests that current fire suppression capabilities may not be sufficient under changing fire-weather conditions (Carnicer et al., 2022). Generally, most wildfires under central-western European conditions burn as low-intensity surface fires, but

single fires burning at high intensities have also been observed (San-Miguel-Ayanz et al., 2019, 2022), suggesting that there is a wide range in the potential fire behaviour.
In areas of temperate forest, national statistics show that coniferous forests are generally affected by larger burned areas compared to deciduous forests (e.g. BLE, 2023). In boreal Scots pine forests with bilberry understory, experimental burns in wind speeds up to 14 km/h typically had spread rates of less than 5 m/min, but in wind speeds of 29 km/h, fires propagated about 15 m/min (Schimmel & Granström, 1997). Fire spread was found to be slower in younger stands, where only a thin and compact layer of fine fuels had accumulated on the forest floor. Experimental fires in Scots pine forests with grass-dominated understory of north-eastern Germany showed fire spread rates of 4 to 10 m/min in wind speeds ranging from 4 to 10.5 km/h. Little is known about fire behaviour in other forest types, particularly deciduous forests. Satellite-based analyses of average fire spread rates in different land cover types across Atlantic north-west Europe revealed that wildfires spread fastest in coniferous forests (3.2 m/min) (Cardíl et al., 2023). Generally, reported spread rates were low to moderate, ranging between 1.3 and 2.3 m/min in grassland, bog, moor, and heathland, but these average values are likely to underestimate actual fire spread. Measured spread rates of experimental fires in Scottish heathland ranged from 0.5 to 12.6 m/min at wind speeds between 7 and 32 km/h, and fire behaviour was also strongly dependent on stand age (Davies et al., 2009). Experimental burns in heathland of north-eastern Germany showed spread rates of about 4 to 6 m/min at wind speeds of 6 to 13 km/h (Hille, 2006).

However, it is difficult to draw conclusions from such data because each fire has its own set of conditions that need to be known precisely, and in particular experimental burns and wildfires cannot be easily compared. This emphasises the need to better understand flammability and fire behaviour in different vegetation types and structures in order to define preventive measures. As the current fire regime in central-western Europe is strongly influenced by anthropogenic factors, it is additionally challenging to decipher the effect of natural drivers on fire behaviour and impacts.

2 Fire-relevant vegetation fuel characteristics

2.1 Fundamentals of fuels and fire behaviour

Fires require heat, fuel, and oxygen to ignite and burn. Plant biomass, which consists mainly of cellulose, hemicellulose and lignin in varying proportions, acts as fuel in wildfires (Resco De Dios, 2020). Before combustion starts, the fuel is heated by an ignition source, causing cell water to evaporate and organic compounds to volatilise. Ignition typically occurs when the temperature of the volatiles reaches 450-500 °C, and the oxidation of these volatiles generates heat and light, i.e., flames (Keane, 2015). Fire spread across an area is determined by fuel properties, weather, and topography, which are therefore the drivers of fire behaviour at coarser scales (Moritz et al., 2005). While weather and topography are beyond human control, fuels can be modified. Therefore, knowledge on the relationship between fuels and fire behaviour is essential for managing fire risk.

As fires act at different scales, the fuel characteristics governing fire behaviour can be assessed at various scales, ranging from individual particles (leaf, grass blade), fuel components (herbaceous fuels, woody fuels), fuel layers (ground, surface, canopy) to the entire fuelbed (assemblage of fuel components) (Keane, 2015). In this work, I additionally use the term 'fuel type' to refer to the dominant fuel in a given area. Fuels are highly variable in space due to the complex interaction of environmental factors influencing the amount and arrangement of the vegetation. They are also highly variable in time as vegetation is formed by dynamic ecological processes such as plant development, mortality, and succession, and fuels are further altered through biophysical processes such as deposition and decomposition (Prichard et al., 2023). The spatial and temporal heterogeneity of fuels is difficult to integrate with the estimation of fire behaviour over large areas needed for fuel management decisions (Keane et al., 2012). Therefore, the fuel properties selected to predict fire behaviour using operational fire behaviour models have been identified through empirical relationships and are often simplified, e.g. by representing an average across the particles of one fuel component in a given area (Keane, 2015). The fuel properties considered most important for fire behaviour estimation are presented in the following. The focus is placed on surface fuels, i.e. all fuels within 2 m above the ground surface, as these determine fire spread in most wildfires. In particular, low-intensity surface fires, which are common under central-western European conditions, are strongly influenced by fine-scale surface fuel heterogeneity (Prichard et al., 2022). Surface fuels comprise litter, lichens, mosses, herbaceous vegetation, shrubs, and dead woody material (Sandberg et al., 2001). In this work, all living woody species in the surface fuel layer are considered as shrub fuels, including tree regeneration, as seedlings and saplings are more abundant than true shrubs in the understory of central-western European forests.

2.2 Fuel traits

Combustion properties of the vegetation depend on the physical, chemical, morphological, and ecophysiological characteristics (traits) of the individual species (Popović et al., 2021). Most of these fuel traits influence fire behaviour at the fuel particle scale by affecting ignition, heat yield and heat transfer.

2.2.1 Fuel chemical composition

The chemical composition of a fuel determines its heat content, i.e. the heat yield per unit mass (kJ/kg) (Keane, 2015). Fuels with high mineral (inorganic) content, such as litter and duff, have a lower heat content than, for example, woody fuels (Keane et al., 2012; Philpot, 1970), which is one reason why the former often burn at lower intensities and have a higher proportion of smouldering combustion (Keane, 2015; Varner et al., 2015). In contrast, secondary plant metabolites such as resins, oils, waxes, and VOC can increase the heat content of a fuel (Resco De Dios, 2020). Higher concentrations of such compounds are a typical feature of many coniferous species and have been associated with increased flammability compared to deciduous species (Terrier et al., 2013). Pinus species in particular store a variety of VOCs, known as terpenes, in their leaves, which increase ignitability and heat release of fresh leaves and litter (Dewhirst et al., 2020; Ewald et al., 2023). The chemical composition of a fuel can also change over time. For example, Weikert et al. (1989) observed that the mineral content of Norway spruce needles increases with age, while various species show reductions in leaf mineral content before leaf senescence an litter fall (Maillard et al., 2015; Mak, 1982). It has also been observed that the emission of VOC varies over the growing season and additionally has a diurnal cycle in heather and other VOC-emitting plant species, showing a positive correlation with temperature and often peaking in the summer months (Kesselmeier et al., 2002; Tiiva et al., 2017). The accumulation of emitted VOC near the ground surface, particularly in response to the heating effect of an already burning fire, may enhance flammability and intensify fires (Chetehouna et al., 2013). Generally, there is comparatively little variation in the heat content of different forest understory plants in central-western European forests, but highest heat contents have been measured for heather and juniper with 21-22 kJ/kg (Mißbach, 1982). Varying proportions of lignin, cellulose, and hemi-cellulose in different plant parts also affect combustion properties, as lignin is more stable thermally and therefore takes longer to combust than cellulose and hemi-cellulose (Liodakis et al., 2002). Lignin content is higher in wood than in foliage (Resco De Dios, 2020), and differs between deciduous and coniferous foliage (N. A. Scott & Binkley, 1997), but the effects on flammability are currently not included in operational fire behaviour models.

2.2.2 Fuel morphology

Morphological characteristics of different fuel particles, such as size and shape, also play an important role in flammability (Engber & Varner, 2012; R. H. White & Zipperer, 2010). Dead woody fuel particles are often stratified by diameter, as this property strongly influences their rate of drying, and thus amongst others affects the time to ignition (Pyne, 1984). Particle geometry is also commonly expressed as surface-area-to-volume ratio (SAV in 1/m) and is included as such in fire spread equations (Rothermel, 1972). SAV determines

the rate of response of a fuel particle to temperature and moisture variations (Brown, 1970) and also affects the packing ratio (m^3/m^3, i.e. dimensionless) of the fuelbed and hence the degree of aeration, thereby influencing various fire behaviour characteristics (Resco De Dios, 2020). SAV is high in graminoids, mosses, and other herbaceous species, and higher in leaf litter compared to needle litter (Schimmel & Granström, 1997), resulting in faster spread rates and shorter burning times (Grootemaat et al., 2017). However, the latter study suggests that leaf mass per area (LMA) (kg/m^2) is more closely related to flammability than SAV, as it includes particle (tissue) density and influences the bulk density of the fuelbed (kg/m^3), which also determines heat production and transfer. In close relation to these morphological metrics, leaf length has been shown to influence the flammability of litterbeds by controlling density and ventilation of the litter layer, with longer leaves resulting in loosely packed and better aerated litterbeds (Schwilk & Caprio, 2011). Similarly, leaf curl influences the structure of the litterbed (Burton et al., 2021).
Changes in fuel particle density, size, and shape, as well as in the chemical composition of litter and dead woody fuels, are driven by decomposition processes, i.e. leaching of solubles, fragmentation, and microbial respiration (Resco De Dios, 2020). Live plant parts experience alterations in size and shape through processes such as growth, e.g. increases in leaf length at the beginning of the growing season or the thickening of conifer needles with age (Keane, 2015).
Despite the importance of fuel particle morphology and chemical composition in the combustion process, it has been argued that other factors, such as the morphology of whole plants and plant arrangement, are more relevant to the overall landscape flammability (Doran et al., 2004). This refers for example to branching patterns of plants, with shade-tolerant species usually having their leaves more homogeneously distributed vertically than shade-intolerant species, thereby enabling fire spread from lower parts of their canopy to higher parts, as for example in some coniferous species (Brown, 1978; Päätalo, 1998). In addition to the multi-layered canopy of some conifers, they also tend to have more and thinner branches to sustain their leaves than deciduous species, and are therefore easier to burn (Johnson, 1996).

2.3 Fuel load

Fuel load, i.e. the amount of combustible biomass (dry weight) per area (kg/m^2), is the most important fuel property used in fire management applications, including the calculation of fire intensity and emissions (Restaino, 2019). Fuel loads are usually quantified separately for different fuel components such as litter, woody fuels, herbaceous fuels and shrub fuels, when used as input to operational fire behaviour models (Heinsch, 2019). Fuel load influences fire behaviour more at fuelbed scale, especially in connection with the horizontal and vertical distribution of the fuel, and also determines total heat release.

2.3.1 Surface fuel load variability

Spatial variation in fuel loads is determined by site conditions such as the availability of nutrients, water, and light, as well as by the local species composition. For example, understory cover and species richness in temperate forests vary across a stand depending on canopy closure, being higher in light conditions such as canopy gaps or at forest edges (Dormann et al., 2020), thereby affecting the loads of herbaceous and shrub vegetation.

However, research from North American ecosystems suggests that surface fuel loads in forested areas often poorly correlate with canopy properties, stand attributes, or other surface fuel components, and exhibit significantly higher variability than canopy fuels (Brown, 1986; Keane et al., 2012). The latter study also showed that finer surface fuel components, such as small twigs, vary on scales of meters to tens of meters, while larger fuel components, such as logs, vary on scales of tens to hundreds of meters.
In addition to the biophysical environment, variability in live surface fuels is driven on annual to decadal time scales by the life cycle of plants through establishment, growth, phenology, mortality, as well as recovery and successional patterns following disturbance (Prichard et al., 2023). For example, herbaceous vegetation may reach high loads in an early stage of development after disturbance and decrease afterwards (Brown, 1981). Hence, the effectiveness of individual regeneration strategies of the affected species plays an important role, as does the degree to which other environmental factors, e.g. soil conditions, are altered by the disturbance (Pérez-Cabello et al., 2021). Additionally, plant anatomical characteristics such as size, morphology and density as well as individual growth rates influence live fuel loads (Resco De Dios, 2020). For example, dwarf shrubs such as heather have denser foliage but slower growth rates than for example grasses (Sedláková & Chytrỳ, 1999).
Fuel loads may also change over the course of a season, as for example some annual plant species only appear at a specific time of the year (Leuschner & Ellenberg, 2017a). Dead fuels accumulate as a result of the deposition of plant material from living plants, with a seasonal peak in deciduous species, and in response to disturbances such as windthrow or insect outbreaks in forests. Loads are reduced by decomposition, with slower decay rates for large fuel particles, or through consumption, particularly of fine fuel particles, in the event of fire. As a result, surface fuelbeds are constantly changing (Restaino, 2019). However, studies mostly report average surface fuel loads at one point in time across a specific area.

2.3.2 Characteristic surface fuel loads

Fuel loads as high as 3.4 kg/m^2 have been reported for heather-dominated fuelbeds in the UK (Weir & Scasta, 2022), while fuel loads of heathland in north-eastern Germany ranged from 0.9 to 1.5 kg/m^2 (Hille, 2006). Both fuel loads and canopy heterogeneity have been shown to increase with the development stage of heather, leading to deeper air penetration into the canopy and more extreme fire behaviour in older stands (Davies et al., 2009). Total surface fuel loads sampled in a forest of north-western Germany were similar among stands dominated by either European beech, red oak or Scots pine (2.55 to 2.91 kg/m^2), but the stands differed in the loads of individual fuel components, particularly in fine woody fuels and live fuels. Comparatively lower surface fuel loads were reported from pine-forests in north-eastern Germany with 0.5 to 1.5 kg/m^2 (Hille, 2006). Surface fuel loads in mixed forests of silver fir, Norway spruce and European beech with sparse understory in the western Alps totalled 1.2 kg/m^2 (Fréjaville et al., 2016). Still, there are no studies that provide continuous, spatially explicit information on surface fuels in central-western European ecosystems at scales below the stand-level. Spatial arrangement and continuity of fuels yet play an important role for fire behaviour (Drury, 2019; Prichard et al., 2023). Limited horizontal continuity of fuels or insufficient fuel loads may cause fire spread to cease under moderate weather conditions, while high quantity and connectivity of fuels

both horizontally and vertically can lead to the most intense fires, including crown fires (Agee & Skinner, 2005; Knapp & Keeley, 2006; C. Miller & Urban, 2000).

2.4 Fuel condition

The most dynamic property of fuels affecting fire behaviour is their moisture status. It is therefore also sometimes referred to as fuel state or fuel condition (DeBano et al., 1998). Fuel moisture content, i.e. the mass of water relative to the mass of dry material (%), determines the amount of energy needed to initiate and sustain combustion (Kane & Prat-Guitart, 2018). Before the fuel is heated to ignition temperature, a sufficient amount of water needs to be removed by volatilisation, otherwise the fuel will not ignite (Resco De Dios, 2020). High fuel moisture therefore retards combustion and also reduces the heat produced by the fire. It leads to a higher proportion of smouldering combustion and decreases the rate of fuel consumption (Keane, 2015).

2.4.1 Drivers of fuel moisture dynamics

Fuel moisture is closely related to the live/dead status of the fuel. While dead fuel moisture is strongly driven by atmospheric conditions and resulting water adsorption and desorption (evaporation) processes, live fuel moisture is mediated by ecophysiological processes (transpiration) and soil water dynamics (Keane, 2015; Schunk et al., 2013). As most plants have the ability to control water loss by closing their stomata, the moisture content of live fuels is more stable and generally higher than that of dead fuels. Live fuel moisture content differs between coniferous and broadleaved species, with deciduous leaves having a moisture content of around 150-200 %, whereas conifer needles usually contain <100-150 % moisture (Johnson, 1996; Keyes, 2006). This is another reason why the flammability of deciduous forests is lower than that of coniferous forests (Girardin et al., 2013). In addition, broadleaved trees tend to form forests with more closed canopies, which have a sparser understory and a sheltering effect on local microclimate, resulting in slower drying of below-canopy fuels after rain (Fréjaville et al., 2016). Fuel moisture also depends on the chemical composition of the fuel. Fuel particles with higher cellulose and hemi-cellulose content, such as leaves, can hold significantly more water than woody fuel particles, which have less cellulose but more lignin, due to the different molecular structure of these compounds (Resco De Dios, 2020; Talhelm & Smith, 2018). Physical properties of fuel particles such as density and size further influence moisture dynamics, particularly of dead fuels. As described in Chapter 2.2.2, dead fuels are often stratified into different diameter classes. These are 1 hr (<0.6 cm), 10 hr (0.6-2.5 cm), 100 hr (2.5-7.5 cm) and 1000 hr (>7.5 cm), and refer to the time needed for a fuel particle to reduce the difference between its original and equilibrium moisture content by two thirds (by adsorption or desorption) under constant temperature and humidity conditions (Fosberg, 1971). This equilibrium moisture content has been shown to be higher in leaf litter than in needle litter because of their different physical and chemical properties (Schunk et al., 2013).

Fuel moisture not only changes in response to weather but is also strongly influenced by ecological processes. Plant phenology shifts fuels between live and dead components throughout the year, e.g. grasses cure at the end of the growing season, which has a substantial impact on flammability (Duff et al., 2019). Fuel moisture in living plants is highest

during the active growing phase, when new foliage and thin branches can reach moisture contents of up to 300 % (Pyne, 1984). Ageing of foliage in coniferous species is often associated with lower fuel moisture contents (Keyes, 2006), and therefore moisture also varies between lower and upper parts, as well as inner and out parts of a conifer crown (Agee et al., 2002; Brown, 1978). Live fuel moisture in new conifer foliage has been shown to be more variable over the course of a season than in old foliage, with the lowest values usually reached in late summer, but several studies show that changes in dry matter content are a more important driver of these changes than water content (Jolly et al., 2014; Qi et al., 2014). Decomposition processes in litter beds initially increase pore spaces, resulting in faster wetting and drying, but subsequently lead to higher compactness resulting in higher moisture retention (Plamondon et al., 1972 after Keane, 2015).

2.4.2 Critical moisture thresholds

It has been found that fire spread is usually not sustained when dead fuel moisture exceeds 30 % (Burgan & Rothermel, 1984), but at moisture contents below 14 %, ignition probability rises rapidly and extreme fire behaviour has been observed (Boer et al., 2017). In contrast, critical flammability thresholds in live fuels are around 70-100 % (Resco De Dios, 2020). The role of live fuel moisture content in fire ignition and spread dynamics is not yet fully understood, but studies suggest that leaf chemistry and volatile emissions from live fuels partly explain why combustion is possible at higher moisture contents than in dead fuels (Darwish Ahmad et al., 2021; McAllister et al., 2012). In heathland and moorland areas, critical moisture thresholds of 35-59 % were observed, at which peat and litter began to ignite, while sustained ignition (i.e. fire spread) occurred at fuel moisture levels between 19 and 55 % (Santana & Marrs, 2014). This contrasts with experiments by Rein et al. (2008), who reported that Scottish peat samples ignited already at moisture contents below 125 % when a more intense ignition source was used, suggesting that peat ignition strongly depends on the energy produced by the fire. Santana & Marrs (2014) confirmed previous observations by Davies & Legg (2011) that heather flammability depends on the proportion of dead fuel and its fuel moisture content in the canopy, with the probability of successful ignition rising with the amount of dead fuel, and the critical fuel moisture increasing from 19 to 35 % as the proportion of dead fuel increases.

3 Methods for characterising and mapping fuels

Knowledge of vegetation fuel characteristics and their spatio-temporal dynamics in a given area is obtained by fuel sampling. This chapter presents both field-based fuel sampling methods and fuel mapping efforts using remote sensing data. The latter are needed to obtain fuel information over large areas and for the operationalisation of knowledge about fuels, especially for fire management applications that can support decision-making. The methods described in the following are used for measuring and mapping surface fuels.

3.1 Field-based methods

Field-based methods for characterising fuels involve different direct and indirect methods. Direct methods involve the measurement of fuel properties in situ or in the laboratory, while indirect methods quantify fuel characteristics based on other available data (Prichard et al., 2022). Because field campaigns are costly and time-consuming, they are usually constrained to limited spatial and temporal extents. Still, they are required as a fundamental source of data for creating and validating fuel maps.

3.1.1 Measuring fuel traits

Fuel properties such as SAV can be estimated from measurements of perimeter, cross-sectional area, and length of the fuel particles (Brown, 1970). Another technique estimates SAV by immersion of fuel particles in water and requires knowledge of fuel particle density and measurements of fuel particle weight before and after immersion (Fernandes & Rego, 1998). Particle density is determined by measuring oven-dry weight and particle volume by immersing the particle in liquid and measuring the volume or mass displacement of the liquid (Keane, 2015). Heat content is usually measured using oxygen bomb calorimetry (Rivera et al., 2012), but other techniques such as thermal analysis, ignition tests, and oxygen consumption calorimetry are also commonly applied to assess flammability properties of fuels such as ignition time, total heat release, mass loss rate, and smoke development (R. H. White & Zipperer, 2010). Fuel moisture content is determined from weighting fuels before and after drying in an oven and dividing mass of lost water by dry fuel mass (Matthews, 2013). Fuel moisture content is more difficult to measure in the field, and a few species-specific and more or less sophisticated methods have been developed. For example, fuel moisture sensors measure electrical signals that are related to moisture content, such as resistance or capacitance, when pulsing an electric charge through a fuel particle (e.g. Chatto & Tolhurst, 1997), but the sensors also require accurate calibration of physico-chemical fuel properties (Kane & Prat-Guitart, 2018). Since gravimetric measurements are more reliable, dead fuel moisture is sometimes measured indirectly using wooden sticks of standardised size and weight that are repeatedly weighed to approximate 10 hr fuel moisture content, and these estimates are also used to derive the moisture of other fuel components using empirical relationships (J. D. Cohen, 1985). Other methods for estimating fuel moisture include process-based models based on energy and water balance equations, which rely on weather inputs and fuel information to simulate fuel moisture, and some of these models are used operationally as part of fire danger rating systems (e.g. Nelson, 2000; Wotton et

al., 2009). Generally, for most applications, relatively rough assumptions are made about the various fuel traits, often representing an average over a fuel component.

3.1.2 Measuring fuel loads

Fuel loads are measured in the field, often using fixed-area plots, where fuel material is destructively sampled, then dried and weighed in the laboratory (Brown et al., 1982). Alternatively, the mass of fuel particles such as dead woody material is determined from measurements of diameter and length, assuming a certain geometric shape and particle density (Woodall & Monleon, 2008). A common sampling strategy for woody fuels is the planar intersect technique, where fuel particles are counted by diameter class as they intersect a vertical sampling plane, and the counts are then converted to loads (Brown et al., 1982). Litter fuel load is sometimes estimated from depth measurements after litter bulk density has been determined from a subset of samples in the laboratory (Keane et al., 2012). As an alternative to destructive sampling, herb and shrub fuel loads are determined from field measurements of cover and height combined with species information (Lutes et al., 2006).
As fuel inventories involving direct measurements are very time-consuming, several indirect methods to estimate fuel loads have been developed. These include visual techniques such as the photoload method (Keane & Dickinson, 2007), where a series of downward-looking photographs of synthetic fuelbeds with gradually increasing fuel loads are compared with field conditions to estimate loads of fine woody debris, herbs, shrubs, and logs. Another comparative visual method is the photo series, where photographs of representative stands in a geographical region where fuel loads have been measured are compared with the observed conditions in the field, and the fuel loads of the best matching photograph are assigned to the stand (Restaino, 2019). This is a popular and rapid technique applied in different geographical areas (Maxwell, 1980; Morfin-Rios et al., 2008; Ottmar et al., 2004; Vihnanek et al., 2009), but inaccuracies in fuel load estimates and difficulties in repeating assignments between different observers have been reported (Sikkink & Keane, 2008). However, load estimates using photo series are mostly sufficient for management decisions (Keane, 2015).

3.1.3 Mapping fuel classes

Irrespective of the individual advantages and disadvantages of the aforementioned methods for characterising fuels, it is difficult to capture the complex and highly variable nature of different surface fuel components. Therefore, fire management uses fuel description systems which simplify the quantification of fuel characteristics for different applications by classifying fuels into groups (Keane, 2013; Weise & Wright, 2014). These fuel classifications summarise fuel component properties and loads for different categories of vegetation based on fuel data collected in the field or based on different observed or expected fire behaviour (e.g. Albini, 1976; Lutes et al., 2009; J. H. Scott & Burgan, 2005). Fuel maps can then be created by recording fuel classes in the field or by linking the fuel classes to existing map categories, such as vegetation types (e.g. Reeves et al., 2006; Reinhardt, 1997). However, there is often poor agreement between fuel information classified by vegetation categories and field-measured fuels characteristics due to their different scales of variation (Keane et al., 2012). Furthermore, when fuel classes are determined based on fire behaviour variables, fuel information is often adjusted to achieve observed fire behaviour with semi-

empirical fire behaviour models and does not precisely describe the actual fuel situation (Finney, 2019). Therefore, this fuel information cannot be used in other applications, such as fire effects models (Weise & Wright, 2014). Another drawback is that the identification and mapping of such fuel classes strongly relies on expert knowledge to evaluate potential fire behaviour and therefore requires well-trained personnel (Keane, 2013). Still, mapping fuel classes through association to vegetation categories is the most common technique to create fuel maps because it is quick and inexpensive, and vegetation classification maps are usually readily available.

3.1.4 Measuring vegetation recovery

Temporal changes in vegetation fuels after disturbance can be assessed in permanent field plots, where measurements are conducted repeatedly for several years post-disturbance. Field methods for evaluating vegetation recovery involve measuring different structural and/or floristic characteristics in fixed-area plots or along transects (Szpakowski & Jensen, 2019). The variables assessed include for example seedling germination, survival and growth, resprouting vigour, or more generally species composition, cover, condition, and other vegetation attributes (Gitas et al., 2012). Comparing these measurements with pre-disturbance characteristics helps to quantify the immediate impact of the disturbance on the landscape, and their long-term monitoring allows assessing the ecosystem-specific recovery rates. These cannot be easily generalised, as the vegetation response to disturbance is influenced by a large number of factors, such as topographic parameters, soil characteristics, climatic effects, and more (Gitas et al., 2012). Closely monitoring the recovery process is important for analysing ecosystem resilience and landscape dynamics (Pérez-Cabello et al., 2021), while it also helps to understand the temporal changes in fuels. Additionally, the information is useful to select and prioritise restoration activities and treatment sites, and provides the basis for future monitoring (Gitas et al., 2012). However, as such field campaigns are labour-intensive and need to cover large time spans, they are not always feasible.

3.2 Remote sensing methods

Remote sensing data are useful for vegetation fuel characterisation across large areas and particularly in remote regions. They expand field sampling methods by providing a spatially explicit representation of the landscape, and observations can be obtained repeatedly and non-destructively. Remote sensing techniques allow to analyse the fuel situation time- and cost-effectively, and with some sensors in near real-time. Therefore, remote sensing data from both spaceborne and airborne passive and active sensors with different resolutions have been used to map fuel properties or fuel classification categories in various ecosystems.

3.2.1 Passive sensors

Passive sensors measure the electromagnetic energy reflected from the Earth's surface, which originates from radiation emitted by the Sun, and radiation naturally emitted by the Earth itself. Different surface materials have unique patterns of reflectance and absorption over various wavelength domains of the electromagnetic spectrum (**Figure 3.1**). The spectral signature of plants mainly depends on leaf pigments (visible region, 400-700 nm), cell

structure (near-infrared, NIR, 700-1300 nm), and water content (shortwave infrared, SWIR, 1300-2500 nm) (Huete, 2004). Additionally, the reflectance of vegetation canopies depends on vegetation cover, canopy architecture, and morphological characteristics of leaves and varies with phenological state. This allows different vegetation types and conditions to be distinguished, e.g., broadleaf and coniferous vegetation, grasses and trees, photosynthetically active (green tissues) and non-photosynthetically active vegetation (senescent foliage, litter, woody stems, dormant grass), or healthy and drought-stressed vegetation (Caturegli et al., 2020; Jia et al., 2006; Silván-Cárdenas et al., 2015; Verrelst et al., 2023). Reflectance values in different wavelength domains are often combined in mathematical formulations known as vegetation indices, which maximise the sensitivity to specific vegetation attributes while minimising the influence of confounding factors such as atmospheric and soil background effects.

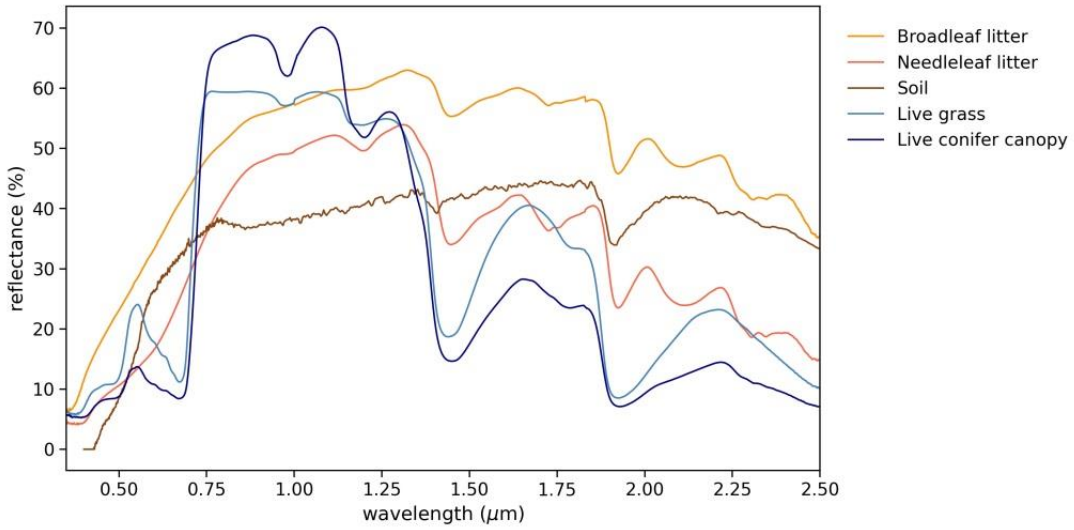

Figure 3.1: Reflectance spectra of different photosynthetic and non-photosynthetic vegetation types and soil from the ECOSTRESS spectral library (Baldridge et al., 2009; Meerdink et al., 2019).

Multispectral data

Spectral reflectance data have been frequently used to characterise and map vegetation fuels. Most often, mapping efforts focus on overstory fuels and categorical representations of fuel characteristics (Gale et al., 2021). For example, medium to coarse-resolution multispectral data from spaceborne sensors such as those onboard the Landsat satellite fleet (30 m spatial resolution), the Moderate Resolution Imaging Spectroradiometer (MODIS) onboard the Terra and Aqua satellites (1 km), the Advanced Spaceborne Thermal Emission and Reflection Radiometer (ASTER) onboard Terra (15-90 m), and more recently the finer-resolution sensors onboard the Sentinel-2 satellites (10-20 m) have been used in classification approaches to map fuel types and fire behaviour fuel models based on spectral bands and vegetation indices (DeCastro et al., 2022; Falkowski et al., 2005; Lanorte & Lasaponara, 2008; Lasaponara & Lanorte, 2007b; Riaño et al., 2002; Van Wagtendonk & Root, 2003; B. A. Wilson et al., 1994). The researchers employed different pixel-based classification algorithms such as maximum likelihood (ML), support vector machine (SVM), neural network (NN), random forest (RF), as well as spectral mixture analysis (SMA), which uses spectral unmixing to derive the contribution of different ground cover

(endmembers) to the spectral signature of a pixel. However, such pixel-based approaches do not take into account spatial interactions with neighbouring pixels, which can lead to a salt-and-pepper appearance of the classification (Tompoulidou et al., 2016). Therefore, object-based image analysis (OBIA) that integrates contextual information by employing multi-scale image segmentation has been implemented to map fuel types and achieved enhanced classification accuracies (Alonso-Benito et al., 2012; Stefanidou et al., 2018, 2022; Tompoulidou et al., 2016). However, applying OBIA is challenging because of the need to identify the appropriate scale for image segmentation and to select suitable features for classification (Mallinis et al., 2008).
Most recently, motivated by promising results in other classification tasks and vegetation mapping (Kattenborn et al., 2021), deep learning techniques such as convolutional neural network (CNN) have also been applied to map fuel types. CNN-based classification approaches can overcome the limitations of conventional machine learning techniques by automatically extracting and identifying relevant image features at different scales, allowing them to extract complex (spectral and spatial) patterns from raw images (X. X. Zhu et al., 2017). Carbone et al. (2023) successfully used a 1D-CNN to discriminate between seven fuel types (broadleaf, conifer, shrub, grass, grass-shrub, timber-shrub, and timber-shrub-grass) in a Sentinel-2 scene from Sardinia and refined them to the Scott & Burgan (2005) fuel models using ancillary above-ground biomass and climate maps. Pickell et al. (2021) used a shallow neural network with two hidden layers to classify fuel types of the Canadian Fire Behavior Prediction System from MODIS and Landsat imagery in British Columbia, and obtained moderate accuracies. Alipour et al. (2023) used a multi-layer neural network to classify Scott & Burgan (2005) fuel models from Landsat scenes for the state of California, combining the spectral information with biophysical data and high-resolution imagery. Overall accuracy ranged from 55 to 75 % and depended on the level of granularity of the fuel types included. Deep learning techniques have thus already shown potential to perform well on fuel classification tasks based on multispectral data. However, the potential of 2D-CNNs that include spatial context has not been fully explored for fuel type classification. Such networks could also be useful in validating remotely sensed fuel type maps, which often require a laborious procedure involving expert knowledge and visual interpretation of photographs of the mapped forest stands (see Chapter 3.2.3). The ability of CNNs to extract vegetation attributes and identify plant species from simple RGB images has already been demonstrated (Goëau et al., 2013; Kattenborn et al., 2019), so it is likely that they also have potential for identifying fuel types from forest photographs.

Compared to the large number of fuel studies that have focused on fuel classification from multispectral remote sensing data, fuel properties are rarely assessed as continuous variables that reflect their true heterogeneity. In particular, surface fuels in forested ecosystems have not been studied frequently because the view from remote sensing platforms is obstructed by the canopy. Fuel loads of dead woody fuel categories discretised into three ordinal classes have for example been mapped by Peterson et al. (2013) in Yosemite National Park using Landsat data and additional environmental data layers, however, with limited accuracies. Fuel conditions in the more open landscapes of the Brazilian Cerrado were derived from Landsat 8 and Sentinel-2 data through partial unmixing and were then used to predict total fine surface fuel loads with good accuracy (Franke et al., 2018). However, estimates of total surface fuel load in pine stands in northwest Spain based on spectral bands and vegetation indices derived from Sentinel-2 were poor owing to the limited penetration of the forest canopy by the optical sensor (Arellano-Pérez et al., 2018). Still, results by He

et al. (2019) showed that the fractional cover of woody, herbaceous, and nonvascular components in Alaskan tundra could be mapped with good accuracy at subpixel resolution using multi-step RF based on Landsat observations. D'Este et al. (2021) used Sentinel-2 data along with other remote sensing datasets to estimate fine dead fuel loads across different land cover classes in southern Italy, showing that while RF achieved better predictive performance than SVM and multiple linear regression models, overall accuracies were limited. Also Ensley-Field et al. (2023) reported high uncertainty in the prediction of fine fuel loads based on herbaceous productivity derived from Landsat and MODIS data in the grasslands and shrublands of the Great Basin in the north-western United States.
The highly diverse results of these previous studies suggest that the ability of multispectral remote sensing data to estimate surface fuel load and conditions depends much on the ecosystem and the specific fuel component under assessment, with overall higher potential in open landscapes compared to forested ecosystems due to the canopy obstruction problem. For surface fuel characterisation in the latter, Gale et al. (2021) note in their review that the usefulness of remote sensing data in general has yet to be adequately proven or disproven.

Due to their repeated acquisition, multispectral satellite data have also been used to detect disturbance and monitor post-fire vegetation recovery across different ecosystems. Such satellite-based monitoring approaches can be useful to assess the temporal dynamics of vegetation in a cost- and time-effective way. While some studies use classification and/or SMA to discriminate different post-fire vegetation classes and fractional vegetation cover (Polychronaki et al., 2013; Solans Vila & Barbosa, 2010; Veraverbeke et al., 2012), most studies rely on time series of vegetation indices for the identification of disturbance events and monitoring vegetation growth by analysing spectral trajectories (Pérez-Cabello et al., 2021). For example, forest disturbances in northern temperate forest of the United States have been detected by using multitemporal normalised difference moisture index (NDMI) and tasselled cap wetness derived from Landsat data (Jin & Sader, 2005). Results by Schroeder et al. (2011) confirm the utility of SWIR-based indices in mapping boreal forest disturbances at different timesteps after disturbance, and highlight the unreliability of NIR-based indices such as normalised difference vegetation index (NDVI) that are primarily associated with green leaf area. Consequently, more recent studies on post-wildfire vegetation recovery in forest ecosystems also rely on SWIR-based indices such as normalised burn ratio (NBR) to track longer recovery timeframes (Hislop et al., 2018; J. White et al., 2017).
Contrastingly, in open landscapes, the use of NDVI to assess post-disturbance vegetation dynamics is very common due to the strong NIR reflectance of healthy vegetation (Lees et al., 2021; Potter, 2018; Sankey et al., 2013). A review by Szpakowski & Jensen (2019) reported that NDVI was the most frequently used vegetation index in studies of post-fire vegetation recovery, despite its known limitations related among others to saturation issues. Also, monitoring of fuel seasonality is often based on phenological metrics extracted from NDVI time series, such as in the studies by De Angelis et al. (2012) and Bajocco et al. (2015), who used MODIS NDVI profiles to identify phenological clusters as proxies for potential fuel load and flammability in Sardinia (Bajocco et al., 2015; De Angelis et al., 2012). However, a study by Villarreal et al. (2016) showed that NDVI was not ideal to monitor post-fire vegetation dynamics in semidesert grassland due to the presence of woody species with small leaf area that absorb less radiation in the red wavelengths compared to grasses. Furthermore, vegetation dynamics during senescence periods were not adequately captured by NDVI. Studies in other dryland ecosystems suggested that combin-

ing indices based on red-edge, mid-, and shortwave infrared bands is more effective in monitoring vegetation state and condition, especially when different life forms are present (Hill, 2013; Sesnie et al., 2018). Models predicting annual fine-fuel recovery after prescribed fire in semi-arid grasslands based on various spectral bands of Sentinel-2 imagery from the growing and dormant season performed reasonably well (Wells et al., 2021), suggesting that the data are generally suitable for monitoring fuel load changes. Also live fuel moisture content has been estimated in various ecosystems based on NIR and SWIR reflectance derived from multispectral sensors, using either empirical relationships or radiative transfer models (Argañaraz et al., 2016; García et al., 2020; Yebra et al., 2018; L. Zhu et al., 2021). However, these approaches mostly relied on rather coarse spatial and high temporal resolution data and showed difficulties in relating the moisture signal to different fuel components or layers (Yebra et al., 2018).
Despite the demonstrated potential of multispectral satellite data for vegetation monitoring, different methods might be appropriate depending on the ecosystem under examination, as the seasonal dynamics and vegetation response after disturbance are unique (Szpakowski & Jensen, 2019). Changes in fire risk due to phenological change and vegetation recovery after wildfires in temperate heathland ecosystems have not yet been thoroughly assessed from a multispectral satellite perspective, so the suitability of different spectral indices to monitor fuel changes in these mosaicked landscapes is unknown to date.

Overall, multispectral satellite imagery has the advantage of global coverage and availability, is easily accessible at low or no cost, and provides multi-temporal spectral information. However, the spatial resolution is limited and the spectral signal often contains both the signature of canopy and surface materials. This makes it difficult to determine surface fuel characteristics in forested areas (Abdollahi & Yebra, 2023). Spectral data also have little ability to discriminate the vertical structure of fuels. Cloud cover can further limit the use of the data, posing challenges in the monitoring of fuel status and vegetation recovery based on time series.

Hyperspectral data

Hyperspectral data provide spectral information in a large number of narrow wavelength domains and thus allow a very detailed characterisation of surface materials. This includes the specific composition of different fuel types and the fuel status (Abdollahi & Yebra, 2023). Studies using hyperspectral data from sensors mounted on satellites (e.g., Hyperion, PRISMA) and aircrafts (e.g., AVIRIS) have shown good results in discriminating a larger numbers of classes of different fuel types, primarily using SMA and classification techniques (Jia et al., 2006; Keramitsoglou et al., 2008; Mallinis et al., 2014; Shaik et al., 2022; C. W. Smith et al., 2021). Hyperion imagery has also been used in mapping post-fire vegetation recovery of different forest species employing object-based classification (Mitri & Gitas, 2010), while airborne hyperspectral imagery with high spatial resolution was useful for monitoring peatland restoration in the UK by estimating the coverage of different plant functional types using a regression approach (Cole et al., 2014a). However, the area coverage of hyperspectral sensors is smaller and the data cost is higher than with multispectral data. The high volume of data requires greater storage and computing capacities and a more complex pre-processing. Additionally, the high dimensionality of hyperspectral images can be challenging to handle in classification approaches (Abdollahi & Yebra, 2023). As with multispectral data, cloud cover can be a restriction, but substitute images are more difficult to obtain as the revisit time of the satellite platforms is longer.

Very high-resolution data

Very high-resolution (VHR) imagery from satellites such as WorldView and QuickBird provides spectral information in fewer bands, but at high spatial resolution (<1-3 m). This allows to characterise small-scale variations in surface properties, which has been beneficial for fuel type mapping in Mediterranean landscapes (Alonso-Benito et al., 2016; Gitas et al., 2006; Lasaponara & Lanorte, 2007a; Mallinis et al., 2008). Fuel mapping efforts based on VHR imagery achieved higher accuracies compared to approaches based on Landsat data, indicating that spatial resolution may be more important than spectral resolution (Mallinis et al., 2014; Sesnie et al., 2018). Fernández-Guisuraga et al. (2019) achieved good accuracies in assessing post-fire structure of pine seedlings and understory community using generalised linear models based on spectral indices and textural data derived from WorldView-2 imagery and suggested this would not be possible using coarser resolution data. Vegetation indices derived from WorldView-3 data at annual intervals also helped assess post-fire recovery trajectories in semi-arid grasslands and open woodlands (McKenna et al., 2018). However, the spatial extent of VHR images is limited and their utility is impacted by image acquisition parameters as well as scene configuration (Mallinis et al., 2014). Monitoring changes in fuel status over time and across large areas can therefore be more difficult based on these data, and cloud cover can lead to substantial data gaps (McKenna et al., 2018). Similar to multi- and hyperspectral sensors, VHR sensors have limited ability to penetrate vegetation canopies to derive information on vertical fuel layers in forested ecosystems. Ultimately, image costs of commercially owned VHR satellites limit their use in the development of new methods by research institutions.

3.2.2 Active sensors

Unlike passive remote sensing systems, active sensors have their own radiation source to emit pulses of electromagnetic energy that are reflected or backscattered by the illuminated target, so that the radiation returning to the sensor can be measured. By recording the time delay between transmission and reception and/or the strength of the returned signal, information about the distance to the target (and hence elevation of the target) as well as target properties (e.g., surface roughness) can be retrieved (Lillesand et al., 2008). As active sensors do not rely on the energy emitted by Sun and Earth, which mainly covers the electromagnetic spectrum between ultraviolet and thermal infrared, they can operate regardless of the time of day, and, depending on the wavelength used, they can also be weather independent. While light detection and ranging (lidar) systems use laser light with wavelengths most commonly located in the near-infrared spectrum, radio detection and ranging (radar) uses microwave radiation with wavelengths typically between 3 and 30 cm (Agrawal & Khairnar, 2019).

Lidar data

Because lidar has the ability to penetrate vegetation in canopy gaps and thus allows to obtain information on both the horizontal and vertical structure of the vegetation, airborne lidar (ALS) has been widely used in fuel mapping efforts. Discrete lidar systems provide 3D point clouds based on the distribution of signal returns, which have primarily been used to estimate canopy fuel attributes such as canopy cover, bulk density, canopy height, canopy base height, and canopy fuel load (Andersen et al., 2005; Botequim et al., 2019; Engelstad et al., 2019; González-Ferreiro et al., 2014). Unsurprisingly, lidar metrics outperformed

spectral imagery in estimating these canopy properties (Erdody & Moskal, 2010). Jakubowksi et al. (2013) used lidar point densities in different height bins to map surface fuel types and fuel models in Sierra Nevada mixed conifer forests, but found that it was difficult to obtain accurate predictions based on the rather low-density lidar dataset (9 pulses/m² on average). Still, in a study by Mutlu et al. (2008), combining ALS data with even lower density (2.6 points/m²) and QuickBird imagery improved fuel model classification accuracy by 13 percentage points compared to using QuickBird imagery alone, indicating that complementing spectral information with structural metrics is beneficial for surface fuel characterisation. Also mapping of Prometheus fuel types in Mediterranean ecosystems was improved by fusing low-density ALS data (<6 points/m²) with aerial imagery in Spain (García et al., 2011), and with WorldView-2 imagery in the Canary Islands (Alonso-Benito et al., 2016), confirming the synergetic effect of lidar and optical data for fuel type mapping.

However, continuous estimates of surface fuel characteristics using ALS data are also rare. One reason for this is that the density of lidar returns decreases because the lidar pulse weakens as it penetrates down through the canopy, leading to increasingly weaker results for fuels located nearer to the ground level (Jakubowksi et al., 2013). In their review, Szpakowski & Jensen (2019) go so far as to state that lidar alone cannot measure surface fuels. Studies estimating understory metrics showed varying results: while understory density estimated from ALS density metrics reached only limited accuracy even at higher point densities (16.4 points/m²) (Campbell et al., 2018), understory cover was estimated from low-density lidar (6.9 points/m²) with reasonable accuracy when filtering understory points by return intensity (Wing et al., 2012). Even better results were achieved when understory height, cover, and volume were estimated using additional energy-related metrics derived from full-waveform lidar (14 pulses/m²) (Crespo-Peremarch et al., 2018), suggesting that the full potential of ALS data had not been harnessed yet. In a study by Bright et al. (2017) ground-based fuels such as litter and dead wood, as well as total surface fuel loads, were predicted with low accuracies although the authors combined low-density lidar (2 pulses/m²) with Landsat time series. Contrastingly, surface fuel load estimates in dense coniferous forests in Greece based on height and intensity metrics derived from multispectral lidar with high point density (83 points/m²) achieved good accuracies (Stefanidou et al., 2020). The role of different lidar-derived metrics and lidar point density in estimating different surface fuel components is therefore not yet fully understood. Particularly in the heterogeneous mixed temperate forests of central Europe, the potential of spectral and structural remote sensing data to estimate surface fuel loads has not been explored.

One limitation of airborne lidar data is that the area coverage is restricted and acquisition costs are still high, which makes repeated surveys to monitor fuel changes rather difficult. However, lidar systems mounted on uncrewed aerial vehicles (UAVs) or the generation of photogrammetric point clouds using Structure-from-Motion (SfM) from UAV images may provide a solution to obtain local-scale 3D models at smaller temporal intervals (Szpakowski & Jensen, 2019). This may be particularly useful in the monitoring of vegetation recovery. However, while photogrammetric systems offer interesting true-colour and multispectral options, image-based point-clouds only capture the outer canopy envelope and do not penetrate to deeper layers (D. L. Peterson et al., 2022; J. C. White et al., 2013). Given that it is still an open question what resolution is required to obtain accurate surface fuel estimates with airborne lidar systems, and whether this is possible at all, airborne photogrammetric systems may not be too promising for surface fuel estimation in forest ecosystems either. Lidar systems mounted on satellite platforms such as GEDI (Global Ecosystem Dynamics

Investigation) provide information on vegetation structure at footprint level nearly globally, but do not offer continuous coverage and footprint size is larger than with airborne lidar (Dubayah et al., 2020). Nevertheless, a study in the Brazilian Cerrado suggests that there is some potential to estimate surface fuel loads from GEDI waveform metrics (Leite et al., 2022). Terrestrial lidar overcomes the canopy obstruction problem and offers high resolution to characterise below-canopy fuels (e.g., Chen et al., 2017; Wallace et al., 2017), but costs are also high and area coverage is even more limited. Stereophotogrammetric approaches from smartphone systems may present an interesting low-cost alternative (e.g., Spits et al., 2017). Therefore, airborne lidar is still the most viable option to obtain spatially continuous information on the vertical structure of fuels at landscape-scale.

Radar data

Airborne and spaceborne imaging radar systems have the advantage of being weather independent due to the long-wave radiation they use, which allows them to penetrate clouds and thus provide measurements at high temporal frequency. Radar antennas transmit microwave energy and measure the intensity of the radiation that is backscattered by a surface. The backscatter signal from vegetation is sensitive to plant components that resonate with the radar wavelength due to their size, and to their moisture content, among other factors (Lillesand et al., 2008). Consequently, differences in the radar signal in response to differences in forest structural parameters, such as density, tree size, and hence the amount of biomass components, can also be related to canopy fuel characteristics (Saatchi et al., 2007). In the latter study, canopy fuel load and foliage moisture content were retrieved from airborne polarimetric Synthetic Aperture Radar (SAR) measurements over Yellowstone National Park based on semi-empirical models with good accuracy. Wang et al. (2019) used spaceborne SAR data from the Sentinel-1A satellite to estimate forest fuel moisture content in Texas and achieved more accurate results compared to estimations based on optical Landsat 8 data. Combining Sentinel-1 microwave backscatter and optical reflectance data led to improved predictions for live fuel moisture content over the western United States compared to predictions on optical data alone (Rao et al., 2020), confirming the usefulness of the strong relationship between the microwave signal and vegetation water content. The first global live fuel moisture content product is therefore also based on passive microwave data (Forkel et al., 2023). Still, coarse-scale estimates of live fuel moisture content only provide an average moisture value of the canopy, neglecting the distinction between live and dead material (Resco De Dios, 2020).

While canopy biomass components such as branch and foliage fuel loads have been successfully estimated from polarimetric SAR backscatter data (e.g., Li et al., 2021; Zeng et al., 2022), radar signals have been less frequently employed to characterise surface fuels. Huang et al. (2009) used airborne SAR backscatter values to estimate the quantity of standing and downed coarse woody debris in Yellowstone National Park, achieving only limited accuracy due to many confounding factors. D'Este et al. (2021) reported that airborne lidar variables were more important than Sentinel-2 and Sentinel-1 variables in estimating fine dead fuel loads in southern Italy, but suggested that radar sensors operating at longer wavelength bands might also be more useful. In-situ ground-penetrating radar allowed to successfully retrieve litter thicknesses of beech forest litter (Andre et al., 2015), indicating potential of future SAR missions operating at longer wavelengths such as the ESA Biomass mission. Chrysafis et al. (2023) used both Sentinel-2 and Sentinel-1 data together with topographic information for fuel type mapping in Greece, and found that the inclusion of SAR data

slightly increased classification accuracy. Millin-Chalabi (2016) found that burn scars and burn scar persistence in peat moorlands could be detected from SAR backscatter intensity and coherence data obtained with interferometric SAR techniques, especially under wet post-fire conditions. Drought conditions that lead to increased wildfire vulnerability in boreal peatlands could also be identified from seasonally decomposed Sentinel-1 backscatter (Millard et al., 2022). These previous studies show that radar backscatter is well suited to monitor the moisture state of vegetation, while the potential for surface fuel characterisation has not been fully explored. This may be due to the complexity of drivers and scattering mechanisms contributing to the radar signal, the limited understanding of the influence of different forest structural properties (Joshi et al., 2017), and the need to carefully select appropriate wavelengths and polarisations (Chrysafis et al., 2023; Huang et al., 2009).

3.2.3 European fuel maps

Two fuel maps for the whole of Europe have been published to date. The fuel map created by the European Forest Fire Information System (EFFIS, 2017) is based on the fire behaviour fuel models developed by Anderson (1982) for the United States. They assigned 10 of these 13 fuel models to vegetation complexes across Europe using land cover and vegetation maps (**Figure 3.2 a**). However, there has been no comprehensive evaluation of whether these fuel models represent actual fire behaviour in central-western European conditions. Moreover, the map distinguishes between a very limited number of different fuel models in central-western Europe, despite the large heterogeneity of the vegetation.
A first fuel typology adapted to European environments has been developed in the FUELMAP project led by the Joint Research Centre (JRC, 2011). The 42 FUELMAP classes comprise forest, shrubland, grassland, and other surface fuel classes in different ecoregions. They have been mapped in the ArcFUEL project using existing European spatial datasets (land cover, forest type, ecoregion, tree cover, terrain) and multi-temporal remote sensing imagery; however, the methodology has only been tested and validated in Mediterranean countries (Bonazountas et al., 2014; Toukiloglou et al., 2013).
The first pan-European fuel map at 1 km spatial resolution has been produced by Aragoneses et al. (2023), who developed a classification system that includes six main fuel types (forest, shrubland, grassland, cropland, wet and peat/semi-peat land, urban) and further distinguishes forest fuel types based on overstory and understory characteristics (overstory leaf type and cover, understory type and depth). These classes were mapped based on several satellite-based land cover maps and bioclimatic modelling to calculate shrubland and grassland productivity, and fuelbed depth (**Figure 3.2 b**). The resulting map product was validated using LUCAS (Land Use and Coverage Area frame Survey) data, which provide information on land use and land cover together with landscape photographs at specific points across the EU (Eurostat, 2022), as well as Google Earth and Google Street View images. The validation was performed on 5,016 validation points and a 20 % subset was used for visual interpretation of the fuel types in the photographs, resulting in an overall accuracy of the map product of 80.9 %, while the accuracy of individual fuel types ranged from 20-100 %. In addition, based on expert knowledge, they assigned to each fuel type one of the Scott & Burgan (2005) fire behaviour fuel models to serve fire modelling purposes. These maps are a first step towards characterising fuels across Europe, albeit with a fairly coarse resolution and limited granularity of fuel types.

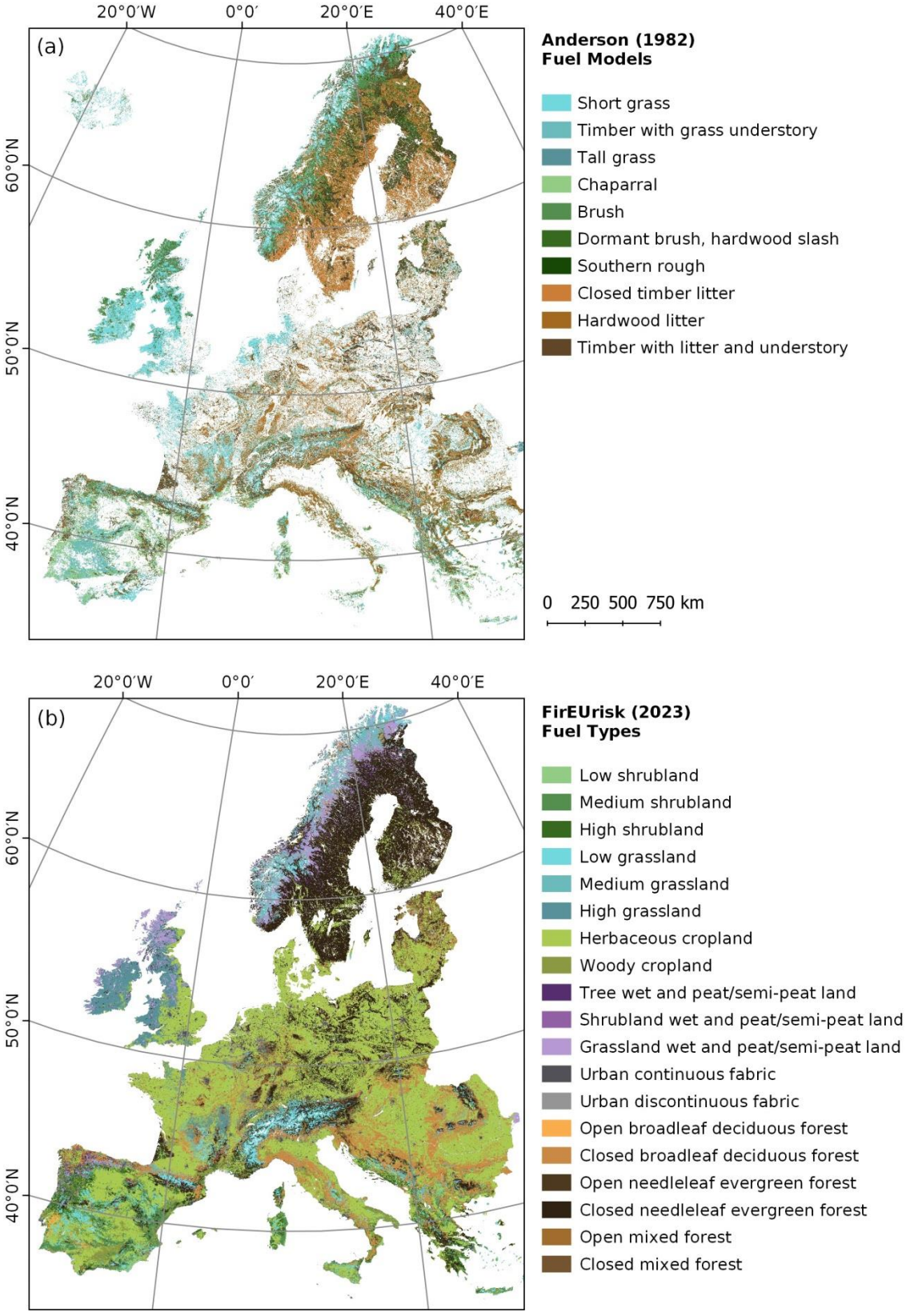

Figure 3.2: European maps of (a) the fire behaviour fuel models by Anderson (1982) and (b) the FireEUrisk fuel types (Aragoneses, 2023).

4 Research gap and thesis outline

In view of the increasing fire risk in the temperate ecosystems of Europe, detailed knowledge of vegetation fuels and fire behaviour is necessary in order to take precautionary measures and management decisions. Fuels as part of dynamic ecosystems are highly complex in space and time, which makes their characterisation a challenging task (Skowronski & Gallagher, 2018). Particularly, current methods fo characterising surface fuels need improvement to enable a more efficient, accurate, and universal way of describing and mapping fuels (Fares et al., 2017).

Geo-referenced fuel data are a key requirement for producing accurate fuel maps from other remotely sensed datasets. However, field inventories are laborious and costly, and some fuel inventory techniques have remained nearly unchanged for the past decades, despite their low repeatability and high uncertainty (D. L. Peterson et al., 2022). Alternatives to small-scale plot-based destructive sampling for the estimation of fuel bed composition are needed (Skowronski & Gallagher, 2018), which facilitate easy replication and updating. For practical purposes, classification into fuel categories has proved useful, which therefore represent the most commonly mapped entities for fire management applications. Field reference data for such maps are often generated from photo series, which rely on visual interpretation by trained observers (see Chapters 3.1.2 and 3.2.3). Deep learning algorithms such as CNNs offer a more efficient and objective method to analyse and interpret visual data, which has already been demonstrated in other applications (Chapter 3.2.1). Therefore, in the first study of this thesis (Chapter 5), a new method for classifying surface fuel types from forest stand photographs using CNNs is proposed. This technique would allow a rapid and observer-independent identification of the dominant below-canopy fuel that influences surface fire behaviour due to its specific compositional and morphological characteristics. Furthermore, the usefulness of integrating widely available multispectral remote sensing time series with the proximal image data in a deep learning framework is tested. Since existing fuel type classifications for Europe (see Chapter 3.2.3) are highly simplified and neglect the possible diverse composition of the surface fuel layer, a more fine-grained fuel type classification for surface fuels in central-western European forest types based on field surveys and expert knowledge is proposed along with the new methodology.

Despite their usefulness for operational purposes, the simplistic representation of fuels in fuel classifications limits the transferability of fuel information to different applications (D. L. Peterson et al., 2022). Therefore, there is a consensus in the fire research community that fuel properties should rather be mapped as continuous variables (Fares et al., 2017; Keane, 2015; Prichard et al., 2023), particularly key properties such as fuel load. Spatially explicit fuel properties can be obtained from remote sensing data, but this has primarily been demonstrated for canopy fuel attributes (Gale et al., 2021). Wall-to-wall estimates of surface fuel loads at the landscape scale are not widely available and previous studies often reported limited accuracies, particularly in comparison to overstory fuels. Although the combination of passive and active remote sensing datasets has been shown to improve fuel type classification (Chapter 3.2.2; Skowronski & Gallagher, 2018), the role of remotely sensed spectral and structural information for surface fuel load mapping in forested areas is not clear. Additionally, previous research has focused on fuel mapping in Mediterranean and North American ecosystems (Abdollahi & Yebra, 2023), while studies in European

temperate forests are not available, and particularly all of the individual surface fuel components have rarely been mapped. Therefore, in the second study of this thesis (Chapter 6), a multi-source remote sensing approach combining the currently best available multispectral and airborne lidar datasets is used to assess their potential for surface fuel load mapping in European temperate forests. The work focuses on all surface fuel components needed for fire behaviour modelling with current operational fire spread models and analyses the sensitivity of modelled fire behaviour to the remote sensing-based predictions of surface fuels.

The largest knowledge gap in wildland fuel science relates to understanding fuel dynamics and incorporating fuel ecology into the creation of up-to-date fuel maps (Duff et al., 2017; Keane, 2015; Prichard et al., 2022). Therefore, understanding the life cycle of fuels and how it influences their availability to burn is essential (Prichard et al., 2022). For example, methods to reliably extract phenological metrics from remotely sensed time series are needed to explore the relationships between fuel state and fire occurrence, as this is also highly relevant when considering climate change scenarios (Fares et al., 2017). Furthermore, monitoring the vegetation recovery of burned areas is important to plan restoration activities, particularly in landscapes of special conservation value, and to understand the longer-term effect of the disturbance on fuels. Knowledge of fuel dynamics is especially important in ecosystems that are disturbed frequently by wildfire or active management (Prichard et al., 2022), as for example the Atlantic dwarf shrub heaths. The usefulness of multispectral satellite data for monitoring vegetation changes is well known, but has rarely been applied in the context of fuel dynamics, especially in heavily cloud-affected areas in temperate ecosystems. Therefore, the modelling of time series of vegetation indices derived from multispectral satellite data is explored as a means to monitor both phenological and post-disturbance changes in fuels in Atlantic dwarf shrub heaths of the UK. The third study of this thesis (Chapter 7) presents this analysis and provides an estimate of the specific recovery rates of the life forms present, which can be used to update fuel maps.

The three studies outlined above have been published as research articles in peer-reviewed scientific journals (Chapters 5 and 6) or have been submitted for publication (Chapter 7). To summarise, they seek to answer the following research questions:

i. Are deep learning algorithms capable of classifying surface fuel types in central European forests from forest stand photographs and multispectral satellite time series? (Chapter 5)

ii. Do detailed multispectral satellite data and airborne laserscanning data allow to reliably quantify surface fuel components for fire behaviour modelling in central European forests? (Chapter 6)

iii. Can time series of multispectral satellite data capture fuel dynamics driven by phenology and post-wildfire recovery in western European dwarf shrub heaths? (Chapter 7)

Part II

Research Papers

5 Classifying surface fuel types

This chapter has been published as:
Labenski, P., Ewald, M., Schmidtlein, S., & Fassnacht, F. E. (2022). Classifying surface fuel types based on forest stand photographs and satellite time series using deep learning. *International Journal of Applied Earth Observation and Geoinformation*, 109, 102799.
https://doi.org/10.1016/j.jag.2022.102799

Abstract

With the increasing threat of wildfires globally, improving the availability of accurate, spatially explicit fuel type information is critical for fire behaviour predictions that can support fuel management decisions to mitigate fire hazards. For a later training of wall-to-wall fuel and finally fire risk maps using remote sensing, we propose a novel proximate sensing-based approach for classifying surface fuel types from in-forest RGB photographs using convolutional neural networks (CNNs). We test different configurations of deep learning models that integrate photographs of the forest stand and the forest floor as well as time series of multispectral satellite data from Sentinel-2 using long short-term memory (LSTM), and compare their performance in classifying understory and litter fuel types of Central European forests. We also investigate how ensemble approaches based on majority voting can help to improve classification results. We found that understory fuel types were classified with highest accuracy after cross-validation (0.78) using a combination of horizontal stand photos and forest floor photos. This accuracy could be further improved by post-classification decision fusion of model predictions on multiple photographs of a forest stand while additionally considering the model's confidence in its predictions (0.85). Litter fuel types were classified with lower overall accuracy based on forest photographs (0.60), but using model ensemble predictions on both photographs and Sentinel-2 time series significantly improved the results (0.72). We found that the accuracy of our models was mostly limited by naturally smooth transitions between the defined fuel type classes and the co-occurrence of multiple fuel types in a photograph. This study shows that deep learning methods can provide an efficient means to assess fuel types from GNSS-located photos of forest stands as a basis for a later training and validation of wall-to-wall fuel and finally fire risk maps. The necessary data can be readily collected by forest managers or in citizen science initiatives.

5.1 Introduction

Forests of Central Europe are becoming increasingly vulnerable to wildland fires as a consequence of global warming (de Rigo et al., 2017; Forzieri et al., 2021). Higher temperatures, more frequent and intense droughts in combination with other abiotic and biotic stressors affect the health of temperate forests and increase vegetation flammability (IPCC, 2019; Millar & Stephenson, 2015; Spinoni et al., 2018). In the drought years 2018 and 2019, several Central European countries reported a higher number of fires and a few exceptionally large burnt areas compared to the 10-year average from 2008 to 2017 (EFFIS, 2021), indicating a link between extreme droughts and enhanced wildfire activity. This is in accordance with future projections of climate-driven wildfire activity that predict higher fire probabilities in highly productive, previously flammability-limited regions due to longer fire weather seasons (Abatzoglou et al., 2019; Jolly et al., 2015). Model simulations suggest a lengthening of mid-latitude and boreal fire season by up to three months by the end of the 21st century (Veira et al., 2016), leading to an expansion of fire-prone regions in Europe. Wildfires can pose a serious threat to environment and society, in addition to causing major damage to timber volume and loss of carbon stocks, if adaptation measures are not taken (Khabarov et al., 2016; Seidl et al., 2014). As fire behaviour is strongly determined by fuel characteristics, suitable management practices to reduce forest fire hazard require spatially explicit information about forest fuel availability, composition, and structure (Keane, 2013).

The complex arrangement of fuels in a forest is often vertically stratified into canopy, surface, and ground fuels. Surface fuels by definition comprise all biomass within two meters above the ground surface: senesced leaves, needles and other nonwoody discarded plant material (litter), fine and coarse woody debris from trees and shrubs (twigs, branches and logs), vascular plant biomass (grasses, herbs, forbs, shrubs and young trees) as well as lichens and mosses. These fuel components are each characterised by a specific particle size and shape, mineral and heat content, and are arranged with a certain compactness and continuity, thus showing distinct combustion properties (Countryman, 1964; Chuvieco et al., 2003). Fuel composition and structure strongly vary across spatio-temporal scales due to different environmental conditions and management practices. For simplification, it is common among practitioners to summarise the fuel properties relevant for fire hazard estimation of a forest stand as "fuel types", which are usually determined by the dominant fuel component in an area (Keane, 2015). A fuel type is assumed to "exhibit characteristic fire behaviour under defined burning conditions" (Merrill & Alexander, 1987), as manifested by ease of ignition, rate of spread, fireline intensity, and fuel consumption (Varner et al., 2015). Commonly distinguished are i) herbaceous fuel types that form loosely packed fuelbeds that are easy to ignite and foster rapid fire spread, ii) shrub fuel types with diverse size and distribution of fuel particles which can burn at high intensities depending on species composition and compactness, iii) litter fuel types that dry quickly and ignite easily, but burn at low intensities, and iv) woody fuel types dominated by dead woody fuel particles with different rates of drying depending on particle size, that can foster intense surface fires (Keane, 2015; Sandberg et al., 2001). The detailed numerical description of the physical properties of a fuel type is referred to as "fuel model" (Andrews & Queen, 2001) and is often used as a set of inputs to fire behaviour models (Andrews, 2014; Finney, 2006) to help forest managers predict potential fire behaviour and decide for effective fuel management options.

Accurate spatial information on surface fuels is fundamental for appropriate forest and fire management strategies, but mapping surface fuel types remains a difficult task. Traditional mapping methods based on recordings of fuel situations in the field are very time consuming and costly; nevertheless, such field surveys are still required as primary source of data and as ground reference for fuel type maps produced using other datasets, including those collected by remote sensing (Arroyo et al., 2008). Recording fuel types can be aided by the use of photographs of representative fuel types that can be matched by the observer in the field to the forest stand situation encountered to facilitate classification (Keane, 2015). Extensive photo series have been developed for fuelbeds across the USA (Vihnanek et al., 2009; Wright et al., 2010), and also in other countries (Morfin-Rios et al., 2008; Ottmar et al., 2004). These even allow to estimate fuel component loadings, but the technique is prone to assignment errors and limited repeatability across observers has been reported (Keane, 2015; Sikkink & Keane, 2008). Fuel type maps are often generated using other land classifications such as vegetation maps by assigning fuel types to existing map categories (McKenzie et al., 2007); however, fuels are not always related to vegetation categories and map resolutions can be much coarser than the scale of fuel variation (Keane, 2015). Remote sensing methods offer another means to create fuel type maps across large areas: multispectral and hyperspectral data from passive sensors like Landsat TM, ASTER, AVIRIS and Hyperion have been extensively used in classification approaches (Jia et al., 2006; Keramitsoglou et al., 2008; Lasaponara & Lanorte, 2007b; Riaño et al., 2002), many of them again relying on associations with vegetation categories. In terms of mapping surface fuel types, the main drawback of passive optical sensors is their incapability to penetrate the forest canopy. Active sensors like lidar systems partly overcome the problem and have been successfully used to extract information about vertical fuel structure (Botequim et al., 2019; Erdody & Moskal, 2010; Riaño, 2003), often in combined approaches with multispectral data (Chirici et al., 2013; Domingo et al., 2020; García et al., 2011; Mutlu et al., 2008). However, acquisition costs still limit the availability of lidar data across large areas. Moreover, lidar data hardly provide information about the type of fuel encountered beneath the tree crown, which is yet essential to fire behaviour predictions.

Field photographs obtained within forest stands capture the relevant information about surface fuel types and are often used by fuel researchers as ancillary information to determine ground truth and validate fuel type maps (Alonso-Benito et al., 2016; Botequim et al., 2019; García et al., 2011; Mutlu et al., 2008). However, visual interpretation of photos carried out by humans is time-consuming and subjective, whereas automated interpretation of images by deep neural networks can significantly reduce the time required for this task and also increase the repeatability of the interpretation. Such deep learning-based models allow to operationalise expert knowledge and make this knowledge available to interested parties as for example demonstrated in several projects providing deep learning models in applications to automatically identify plants and animals, e.g., Pl@ntNet or BirdNET (Goëau et al., 2013; Kahl et al., 2021).

In this study, we apply convolutional neural networks (CNNs), a class of deep learning models that are particularly suited for analysing image data. CNNs process images through multiple layers of convolutional filters, thereby extracting contextual 2D spatial features of varying levels of abstraction, allowing the models to effectively learn features relevant to a specific task in an end-to-end training directly from the data. They have been applied with great success in computer vision tasks such as image classification (Krizhevsky et al., 2017; Sladojevic et al., 2016), object detection (X. Chen et al., 2014; Tompson et al., 2015), and

semantic segmentation (L.-C. Chen et al., 2018; Long et al., 2015), but have only recently been explored in ecology and vegetation science (see reviews by Christin et al., 2019 and Kattenborn et al., 2021). Vegetation properties such as species information and plant traits have been successfully extracted from plant photographs (Schiller et al., 2021; Wäldchen & Mäder, 2018), while highly accurate vegetation mapping has been achieved on different types of remote sensing data (Guirado et al., 2020; Langford et al., 2019; Schiefer et al., 2020). Most studies applying CNNs to field photographs are found in agriculture, e.g., for identification of crop types (Ringland et al., 2019; S. Wang et al., 2020) or the detection of weed infestations (J. Gao et al., 2020), as well as in land use or land cover classifications (Cao et al., 2018; G. Xu et al., 2017), while rather few studies from the field of forest ecology exist: these have attempted, for example, to detect the regrowth of woody vegetation (Bayr & Puschmann, 2019), classify tree species and estimate stock volume by segmentation (J. Liu et al., 2019), monitor plant phenology stages (Correia et al., 2020) or estimate defoliation of forest trees from ground-level images (Kälin et al., 2019). Despite the increasing use of deep learning models in ecological research, few studies currently aim to understand the behaviour of a network and, thus, increase the interpretability and trustworthiness of the predictions; although this would also help to better evaluate the potential and limitations of deep learning models for these applications. Moreover, it has rarely been assessed how ground-based imagery can be coupled with remote sensing data to harness multiple data sources to make more reliable predictions for a task. In the context of fuel research in forest ecosystems, the ubiquitous availability of multispectral satellite data with high spatiotemporal resolution provided by the Sentinel-2 satellites provides an excellent opportunity to test whether time series of Sentinel-2 data can complement field-level information derived from forest photographs to predict surface fuel types in Central European forests. Since multi-temporal satellite data have proven useful to classify tree species and crops based on their different phenological cycles using varieties of recurrent neural networks (RNN) such as Long Short-Term Memory (LSTM) (Campos-Taberner et al., 2020; Xi et al., 2021; Zhong et al., 2019), they also hold the potential to differentiate between fuel types, which are influenced by dominating tree species and stand density. In this work, we present a new approach for classifying surface fuel types using RGB imagery from within a forest stand in combination with Sentinel-2 time series in a deep learning framework. We specifically address the following research questions:

i) How accurately can we classify surface fuel types from different types of within stand forest photographs using CNNs?

ii) Does the integration of Sentinel-2 satellite time series with LSTM improve classification results and does it have the potential to be used as a stand-alone methodology?

iii) Do ensemble approaches help to improve the results?

iv) Which image regions of forest photographs and which spectral and temporal features from Sentinel-2 time series are important for classifying surface fuel types?

5.2 Methods

5.2.1 Study area

We collected surface fuel data from 278 plots in temperate forests in Germany from May to October in 2020 and 2021, focusing on two main study areas. One is located in south-western Germany, encompassing lowland pine-dominated (*Pinus sylvestris* L.) mixed forests on sandy soils of the upper Rhine plain (**Figure 5.1-1**), submontane mixed forests with beech (*Fagus sylvatica* L.), oak (*Quercus petraea* Liebl.), and Douglas fir (*Pseudotsuga menziesii* (Mirb.) Franco) in the hilly landscape of the Kraichgau (**Figure 5.1-2**), submontane beech, spruce (*Picea abies* (L.) H. Karst.), and silver fir (*Abies alba* Mill.) forests in the northern Black Forest (**Figure 5.1-3**), and dry submontane pine forests on sandstones of the Palatine Forest (**Figure 5.1-4**). The other study area is located in the state of Brandenburg in north-eastern Germany and consists of lowland pine forests on very dry sandy soils (**Figure 5.1-5**), which are the most fire-affected forest sites in Germany. We thus covered the six main overstory tree species in Central Europe, but also included less frequently occurring *Larix decidua* Mill., *Quercus rubra* L., *Carpinus betulus* L., and *Robinia pseudoacacia* L. stands. We attempted to cover different age classes and stand structures, ranging from very young stands consisting only of regenerated trees with heights of less than 5 m, to stands with larger trees and closed canopies, to old stands with low tree density and more open canopies.

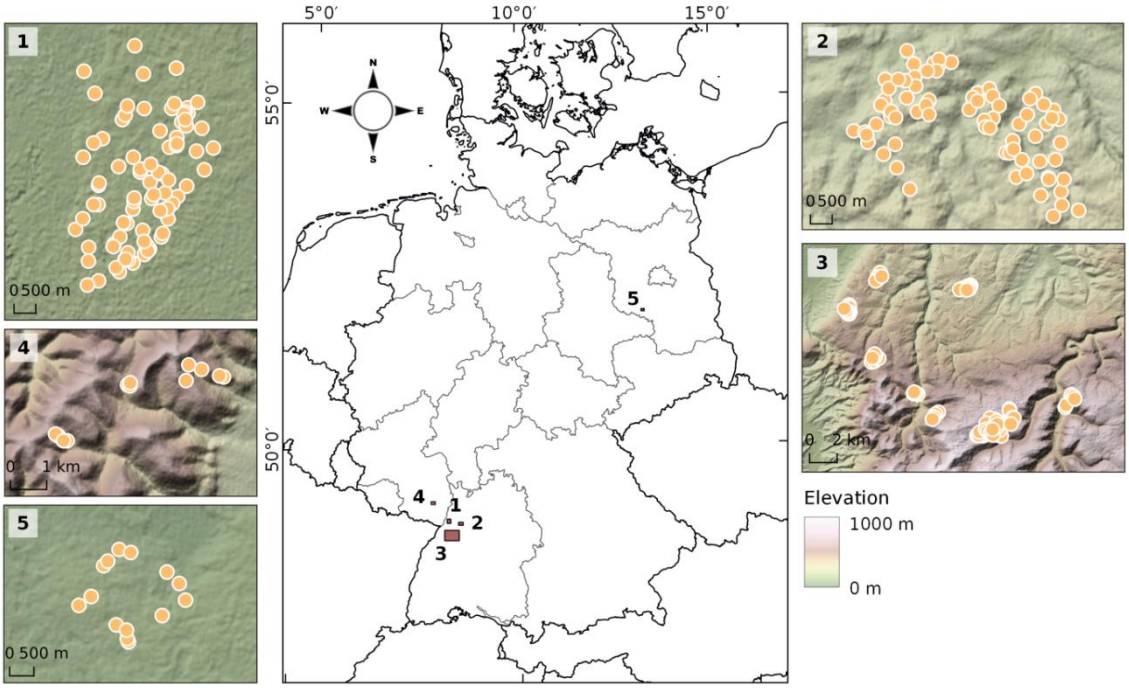

Figure 5.1: Study areas for fuel type sampling in south-western and north-eastern German: 1) upper Rhine valley 2) Kraichgau 3) northern Black Forest 4) Palatine Forest 5) Brandenburg.

5.2.2 Field measurements

We recorded overstory tree species and cover, understory tree/shrub cover and average height, herb cover and height, moss and litter cover on 278 circular plots with a radius of 7.5 m (176.6 m²). We also recorded the litter type and the presence of fine woody fuels. In 179 of the plots, we sampled all surface fuel components (seedlings, shrubs, herbaceous species, dead woody fuels, litter) following an established protocol of the USDA Forest Service (Woodall & Monleon, 2008), to later calculate fuel loadings for each component. Details of the sampling procedure and data preparation can be found in Appendix A. Before sampling, we systematically photographed all plots. Twelve horizontal photos were taken from a circle with 10 m radius, facing the center of the plot, with a spacing of 30° between the photos. We also photographed the transects along which dead woody fuels were measured (see Appendix A), from four directions at 90° to each other, obtaining 12 forest floor photos per plot.

5.2.3 Fuel type classification

Unsupervised k-means clustering was performed on the fuel loading data to identify the most important clusters in the data. The data were then presented along with the photographs to two fuel experts, who related fuel and species information to effects on fire behaviour. The final fuel type classification and respective thresholds to separate between classes were based on field data and expert opinion. Understory and litter type were considered most decisive to fire behaviour and were thus used as sub-classification systems to constitute a fuel type.

Seven understory fuel types with expected different effects on fire behaviour were identified (**Figure 5.2**): 1) Broadleaved tree or shrub understory (hereafter referred to as *shrub-broadleaf*) mainly encountered as regeneration of *Fagus sylvatica, Carpinus betulus,* and *Prunus serotina,* with large leaves that have high surface area-to-volume (SAV) ratio and water content, and the largest share of biomass allocated in stem and coarse branch wood. 2) Needle-leaved trees in the understory (*shrub-needle*) from regeneration of *Abies alba*, *Picea abies*, *Pseudotsuga menziesii* or *Pinus sylvestris,* that have leaves with smaller SAV ratio, higher lignin and terpenoid content (Bohlmann & Keeling, 2008; D. A. Perry et al., 1987; N. A. Scott & Binkley, 1997), and generally more biomass allocated in fine plant parts. 3) Herbaceous non-grassy species (*forb*) with high water content (we also included low-growing *Rubus fruticosus* agg. in this group due to its high moisture), which have a lower fire hazard than 4) grass species (*grass*) such as *Brachypodium sylvaticum* (Huds.) Beauv. or *Deschampsia flexuosa* (L.) Trin., especially after curing of the latter at the end of the season, 5) dwarf shrubs (*dwarf shrub*), in particular *Calluna vulgaris* (L.) Hull and *Vaccinium myrtillus* L., which can burn well even when green, and 6) thick, continuous moss layers (*moss*) of species such as *Polytrichum formosum* Hedw. or *Pleurozium schreberi* (Brid.) Mitt. that can dry to very low moisture contents and provide significant fuel loadings. Cover of at least 50 % (within 2 m above the ground) of the respective understory type was considered necessary to achieve significant loading and continuity that would impact fire spread and was therefore chosen as threshold for the class assignment. If none of the aforementioned understory types was present with sufficient cover, the plots were assigned to the 7) litter (*litter*) fuel complex.

Figure 5.2: Different understory fuel types. From top left to bottom right: Two examples of shrub-broadleaf (a-b), two examples of shrub-needle (c-d), then one example each of forb (e), grass (f), dwarf-shrub (g), moss (h), and litter (i).

The litter fuel types relevant to fire behaviour were distinguished based on leaf morphology of the litter, assuming that its relation with the compactness of the litter layer strongly influences the availability of oxygen in the combustion process. We therefore distinguished between broadleaf (*bl*), short-needle (*sn*), and long-needle (*ln*) litter (**Figure 5.3**). We also assumed that the different chemical composition, especially of broadleaf and coniferous litter (Philpot, 1970; N. A. Scott & Binkley, 1997), affects the combustion properties. As mixtures between these litter types are very common in Central European forests, we also included the mixed classes broadleaf-short-needle (*bl-sn)* and broadleaf-long-needle (*bl-ln*), assuming altered combustion properties compared to stands with pure litter types. In our study areas, we rarely encountered a mix of long-needle and short-needle litter and therefore assigned these plots to the dominating litter type. We found very high loads of fine woody debris in some short-needle stands, which could strongly alter the intensity of a fire, and therefore defined a separate litter type (*sn-fwd*). A simplified litter classification with only four different litter types, achieved by combining the classes *bl-ln* with *bl-sn* and *sn* with *sn-fwd*, was also tested. **Table 5.1** provides an overview of the fuel type classifications and the number of plots surveyed for each class.

Table 5.1: Overview of the number (N) of recorded plots in each fuel type classification.

understory fuel type	N plots	litter fuel type	N plots	simplified litter fuel type	N plots
shrub-broadleaf	39	bl	73	bl	73
shrub-needle	33	bl-ln	45	ln	44
forb	34	bl-sn	37	sn	79
grass	32	ln	44	mixed	82
moss	28	sn	61		
dwarf-shrub	19	sn-fwd	18		
litter	93				

5.2.4 Image data preprocessing

Our dataset consisted of 3336 horizontal forest stand photos (12 per plot) and the same amount of forest floor photos, each 4000 × 3000 pixels in size. Single missing or damaged photos were replaced by duplicating a randomly selected photo from the same plot to ensure equal sample size for each plot. Horizontal photos were resized to 512 × 512 pixels before feeding them into the model and pixel values were normalised to the interval (0, 1) to allow faster convergence of the model. During model training, on-the-fly data augmentation was performed, i.e. slight transformations were applied to the photos to increase the variation in the dataset during each epoch of training. These transformations included small image rotations, horizontal and vertical shifts, random horizontal flips, and brightness changes within a range of values that was previously identified to produce realistic results. Forest floor photos were processed differently to avoid a loss of details when resizing the images to smaller sizes processible by the model: We randomly cropped nine small image patches (224 × 224 pixels) from the forest floor photos and reassembled them to a 3 × 3 mosaic with a size of 672 × 672 pixels (**Figure 5.3**). Strong illumination variations within an image due to shadow effects were reduced by applying contrast limited adaptive histogram equalization (CLAHE) (Pizer et al., 1987) to each image before cropping. Similar to the horizontal photos, pixel values of the mosaics were normalised to the interval (0, 1). During training, forest floor mosaics were randomly rotated by 90° degrees, but received no further transformations.

Figure 5.3: Examples of forest floor mosaics for a) broadleaf (bl), b) short-needle (sn), c) long-needle (ln), and d) short-needle fine woody debris (sn-fwd) litter.

5.2.5 Satellite data preprocessing

We constructed time series of multispectral Sentinel-2 satellite data from the Level-2A surface reflectance product using Google Colab as Python interface to Google Earth Engine (GEE). Therefore, we selected all available scenes with less than 70 % cloud cover above our study areas in the 3-year period from July 2018 to June 2021. We used the Sentinel-2 cloud probability product and near-infrared reflectance to mask out cloud and cloud shadow pixels in the individual scenes. We then extracted pixel reflectance from 10 spectral bands with 10 to 20 m spatial resolution (visible, red-edge, near-infrared, shortwave-infrared bands) at our field plot locations. In addition to the spectral bands, we calculated the normalised difference vegetation index (NDVI) as an indicator of photosynthetic activity / vegetation greenness for each observation. To obtain a time series dataset equal in size to our photo dataset (3336 samples, 12 per plot) and increase the variability among time series of one plot, we binned the Sentinel-2 observations into 14-day intervals and randomly selected one observation from each 14-day interval to construct 12 slightly different time series for each of the 11 features per plot, with 72 time steps in each feature. Due to the cloud masking procedure, we obtained varying amounts of valid data points in the time series depending on the plot location. We linearly interpolated missing observations and smoothed the time series using a Savitzky-Golay filter (Savitzky & Golay, 1964). The final input to the LSTM model was a 72 × 11 matrix (time steps × features) for each sample.

5.2.6 CNN architecture

We tested different CNN architectures typically used for image classification tasks, including *VGG*, *Inception*, and *EfficientNet*. We achieved the best results using *VGG-16* (Simonyan & Zisserman, 2015) with weights pre-trained on the ImageNet dataset as backbone. *VGG-16* uses 5 blocks of consecutive 2D convolutions with a filter size of 3 × 3 and Rectified Linear Unit (ReLU) activation. Each block is followed by a max-pooling layer with stride 2 that reduces the resolution of the layers, allowing the transition from lower-level to higher-level image feature extraction. To reduce the number of trainable parameters in the model, we froze the layers in the first two convolutional blocks, i.e. their weights were not updated during training, so that low-level image features such as edge detectors were directly adopted from the pre-trained model. The convolutional layers deeper in the model were re-trained on our dataset to allow the model to learn the higher-level concepts specific to our problem. The outputs from the *VGG-16* backbone were then summarised in a global average-pooling layer and processed through a classifier model consisting of two fully connected layers and a final classifier with softmax activation, computing the class probabilities for the litter and understory fuel types, respectively. To limit overfitting and improve the model's ability to generalise, a 50 % dropout layer and L2 weight regularization with the regularization rate set to 0.01 were used. A multi-input model was constructed using two *VGG-16* branches, which were concatenated before the final classifier model, to process horizontal and forest floor photos in parallel. A summary of the architecture of the CNN model is provided in **Figure 5.4**.

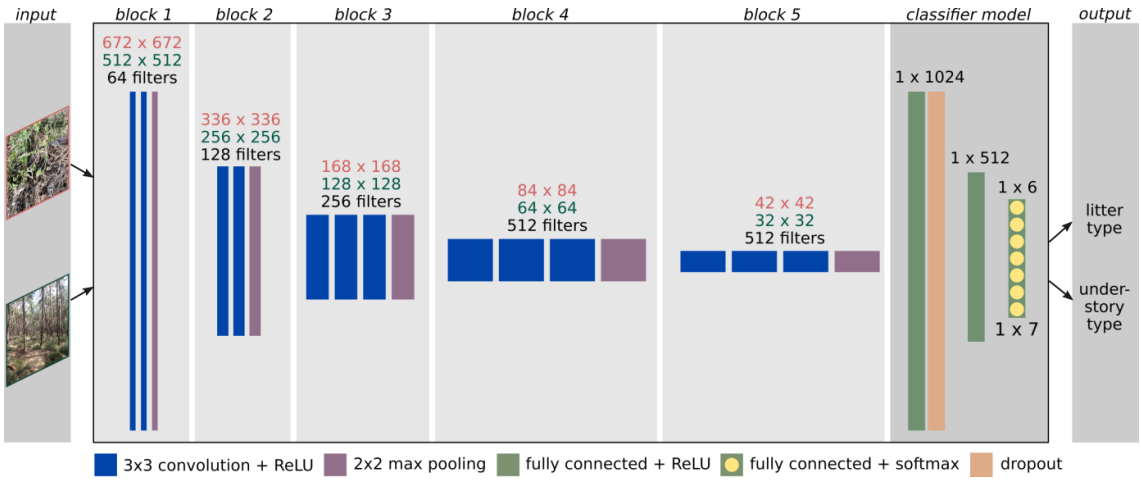

Figure 5.4: Architecture of the CNN model based on VGG-16 for the classification into litter and understory fuel types. The model accepts either horizontal or forest floor photos as inputs. These are processed through five blocks of convolutional layers with increasing number of filters, while their resolution is decreased through pooling operations. The last fully-connected layer in the classifier model consists of six neurons in litter classification and seven neurons in understory classification which give the probability values for a photo belonging to the respective classes.

5.2.7 LSTM architecture

We used a long short-term memory network (LSTM) to classify litter and understory fuel types based on the time series extracted from Sentinel-2 acquisitions. LSTM can learn long-term dependencies in sequences of data without suffering from the vanishing gradient problem that can occur when training normal recurrent neural networks (RNN) (Hochreiter & Schmidhuber, 1997). This is achieved by enforcing a constant error flow through the network by regulating the information flow through LSTM units called cells. The memory content of a cell (cell state c) is controlled and protected by three sigmoid gate units (σ): the forget, input, and output gates. The forget gate takes the output of the previous cell (h_{t-1}) and the current input (x_t) and decides which part of the memory content of the cell (c_{t-1}) will be thrown away. The input gate similarly uses the inflowing information to decide which parts of the memory will be updated, and a tanh layer gives weights to the respective values to be added to the current state. The new cell state (c_t) is then passed through another tanh layer (to scale the values between -1 and 1) and finally through the output gate, which decides what part of the cell state will be passed on to other cells (output values h_t). In this way the cells effectively discriminate between currently useful and irrelevant memory contents while ensuring constant error backpropagation to bridge even extended time intervals. As an extension of normal LSTMs, bidirectional LSTMs look at a time series from both forward and backward directions, allowing them to learn temporal dependencies using information from past *and* future time steps (Schuster & Paliwal, 1997). We used three bidirectional LSTM layers with 100 hidden units and 20 % dropout each to process the time series of the 10 spectral bands and NDVI from Sentinel-2, followed by a fully-connected layer and a final softmax layer to compute the class probabilities for the desired outputs. A summary of the architecture of the LSTM model is provided in **Figure 5.5**.

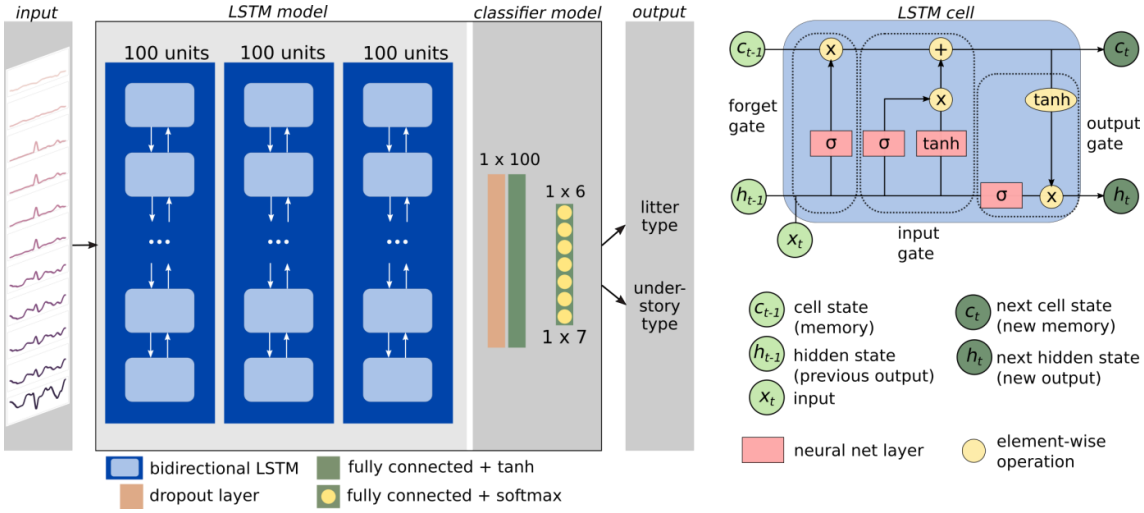

Figure 5.5: Architecture of the LSTM model (left) and structure of a LSTM cell (right). The LSTM model accepts the 11 time series (features) derived from Sentinel-2 images, with 72 time steps in each series. The time series data is processed through three bidirectional LSTM layers, each of which contains a LSTM cell as repeating module that passes the (filtered) information from each time step in forward and backward direction and outputs a vector of length 100 (hidden state vector). Based on this output, the time series are assigned to different understory and litter fuel types.

5.2.8 Model training

The dataset was split into a training/validation set and an independent test set using stratified 10-fold cross validation. The test set thus contained 336 samples (photos / time series) from plots that the model had never seen during training, and it had the same distribution of classes as the full dataset. The training/validation set was split in a ratio of 80/20, resulting in 2400 samples for training and 600 for validation. Litter and understory fuel types were converted to one-hot encoded target variables before being fed into the network. The network was trained for a maximum of 50 epochs with a batch size of 32, i.e. 32 samples of the training dataset were shown to the network before the parameters were updated, while the entire training dataset was shown to the network a maximum of 50 times. To account for the imbalanced distribution of classes in our dataset, class weights were calculated by inversely relating occurrences per class to the total number of samples and used in training to weight up underrepresented classes. We tested five different combinations of input data with our models (**Table 5.2**): Two CNNs were trained with only horizontal forest photos or only forest floor photos, respectively. Another CNN was trained with both horizontal and forest floor photos in two parallel VGG-16 branches. The LSTM model was trained with the Sentinel-2 time series, and a combined CNN-LSTM model was trained with all three data sources simultaneously in three parallel branches. The individual branches of the multi-input models were concatenated before the final classifier to arrive at a single joint prediction. For the CNN models and the multi-input models, we used the robust Adam optimizer with a learning rate of 0.0001 as optimization algorithm. The LSTM was optimised using RMSprop with a learning rate of 0.0001 and momentum set to 0.8., as determined by a hyperparameter grid search. The loss function to be minimised was categorical cross-entropy for all outputs. The learning rate was reduced during training when validation loss stopped improving for two epochs and training was stopped early if the loss did not improve for four epochs.

Table 5.2: Overview of the 5 model configurations tested.

input	forest floor photos	horizontal forest photos	Sentinel-2 time series	forest floor photos, horizontal photos	forest floor photos, horizontal photos, and Sentinel-2 time series
model architecture	single-input CNN	single-input CNN	LSTM	multi-input CNN with two VGG-16 branches	multi-input CNN-LSTM model with two VGG-16 branches and one LSTM branch
output	litter fuel type:	*bl, bl-ln, bl-sn, ln, sn, sn-fwd*			
	simplified litter fuel type:	*bl, ln, mixed, sn*			
	understory fuel type:	*dwarf-shrub, grass, forb, litter, shrub-broadleaf, shrub-needle*			

Model development and training were implemented in Python version 3.8 (van Rossum & Drake, 2009) using the Keras library (Chollet, 2015) as interface to the TensorFlow backend. For model training, we used 4 NVIDIA Tesla V100 GPUs provided by the bwUniCluster 2.0 within the Baden-Württemberg High Performance Computing (bwHPC) framework.

5.2.9 Model evaluation

Model performance was evaluated by calculating overall accuracy (1), class-wise precision (2), recall (3), f1-score (4) (harmonic mean of precision and recall), as well as Cohen's kappa (5) for predictions on the independent test sets that were generated using stratified 10-fold cross validation. All photos in the test set were considered as independent samples in these calculations. Confusion matrices were computed to gain further insights into which classes are difficult to separate using the models. Class prediction probabilities output by the final softmax layer of the best-performing model were examined for their informative value about the confidence of the model predictions. Python libraries Pandas (McKinney, 2010) and Scikit-learn (Pedregosa et al., 2011) were used for all computations.

$$\text{accuracy} = \frac{\text{true positives} + \text{true negatives}}{\text{true positives} + \text{true negatives} + \text{false positives} + \text{false negatives}} \quad (1)$$

$$\text{precision} = \frac{\text{true positives}}{\text{true positives} + \text{false positives}} \quad (2)$$

$$\text{recall} = \frac{\text{true positives}}{\text{true positives} + \text{false negatives}} \quad (3)$$

$$\text{f1-score} = 2 \times \frac{\text{precision} \times \text{recall}}{\text{precision} + \text{recall}} \quad (4)$$

$$\text{Cohen's kappa} = \frac{\text{observed agreement - expected agreement}}{\text{1 - expected agreement}} \quad (5)$$

5.2.10 Ensemble approaches

Due to our data structure with 12 different photos acquired from one plot (forest stand), we had the opportunity to test the effect of decision fusion methods to improve final classification results. Two different approaches based on majority voting were tested: First, we aggregated the predictions from the same model on multiple photographs of the same forest stand and determined the final class label based on the most frequently predicted class. When two classes appeared to have the same number of votes, the final class was randomly chosen from the two. We additionally tested the effect of considering only the most certain model predictions by setting a threshold for the minimum required probability of the predicted class (tested values were 80 % and 90 %). Second, we aggregated the predictions from the single-input models that used the three different available data sources forest floor photos, horizontal photos, and Sentinel-2 time series individually. Final class assignment was similarly based on majority voting from the ensemble of model predictions, and prediction probabilities were taken into account as described above.

5.2.11 Assessment of model explainability

Feature importance via random permutation in LSTM model

We assessed the relative importance of different spectral bands and different acquisition times to the classification of understory and litter fuel types by using feature permutations: We randomly permuted the reflectance values of one band across all samples in the test set, applied the trained LSTM model to the modified data and recorded the change in accuracy compared to the baseline performance of the model on the unperturbed test set. Likewise, we permuted the reflectance values of all bands from each acquisition month across all samples in the test set and recorded the change in classification accuracy. Hence, the importance of each feature (band or month) was calculated as the decrease in classification accuracy of model predictions when the feature was permuted, normalised with respect to the most important feature.

Importance of image regions via Grad-CAM in CNN model

We used Gradient-weighted Class Activation Mapping (Grad-CAM) (Selvaraju et al., 2017) to visualise the image regions that were important for the classification decision of the CNN model. Grad-CAM computes the gradient of the score (raw output before the softmax) for any class with respect to the activations of the feature maps produced by a convolutional layer to derive the weight for each feature map. A weighted combination of feature maps is computed and followed by a ReLU operation to emphasise only pixels that have a positive influence on the class of interest. The output is a coarse localization map, which is upsampled to the resolution of the input image to highlight the pixels that were important for the class decision. We computed Grad-CAM heatmaps for randomly selected, correctly predicted images of each class based on the activations of the last two convolutional layers of our model.

5.3 Results

5.3.1 Model training

All models converged within 50 epochs of training or earlier for both outputs (**Figure 5.6** and **Figure 5.7**). Multi-input models and the LSTM model generally showed slower convergence compared to the single-input CNN models. Except for the LSTM model, slight overfitting to the training data was observed for all models especially in litter classification and when using forest floor photos, despite the regularization techniques applied. When classifying understory, a single CNN-model trained on horizontal photos got stuck in a local minimum at an early epoch and remained at near-zero accuracy throughout training. Training and validation loss stabilised for all models after about 20 epochs.

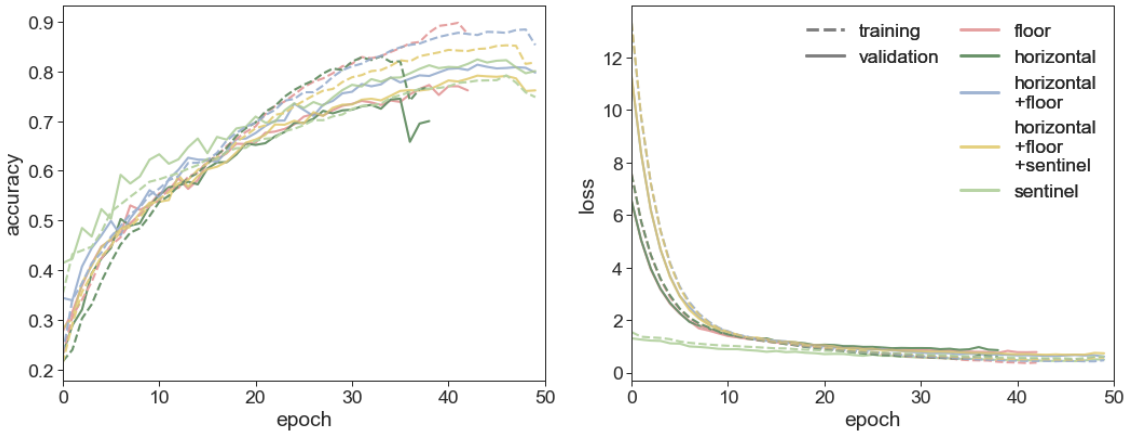

Figure 5.6: Averaged evolvement of training and validation accuracy and loss across 10 cross-validation runs for litter classification models.

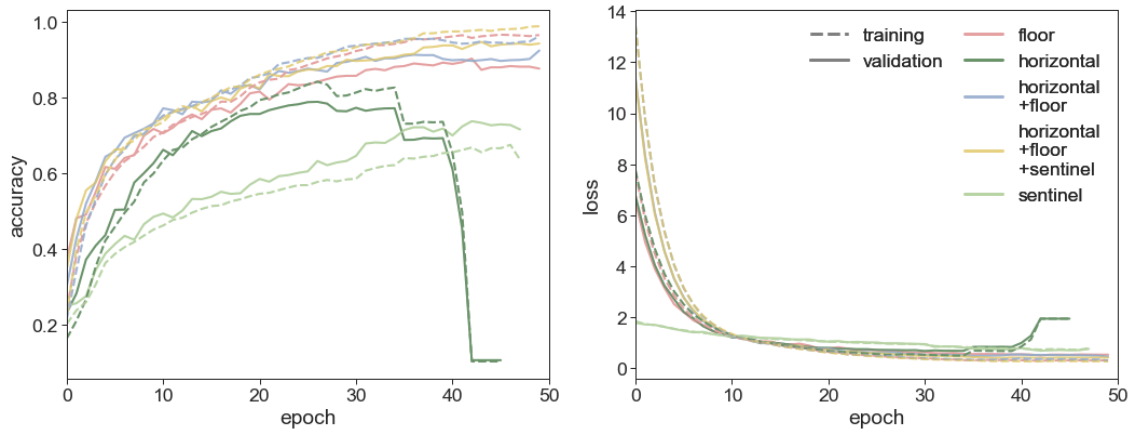

Figure 5.7: Averaged evolvement of training and validation accuracy and loss across 10 cross-validation runs for understory classification models. The curves for the CNN trained on horizontal photos are strongly distorted by a model stuck in a local minimum during training.

5.3.2 Accuracy assessment

Average classification accuracy differed only marginally among the models using different input data, except for a lower understory classification accuracy (0.41) of the LSTM model using Sentinel-2 data only (**Figure 5.8**). Highest accuracy for understory classification was achieved using the combined CNN model with horizontal and forest floor photos as input (OA=0.78, f1-score=0.76).

For the full litter classification with six litter types, different input data yielded very similar results, but the models using multiple data sources had lower variance compared to the single-input models (**Figure 5.8**). Highest accuracy was obtained using forest floor photos (OA=0.60, f1-score=0.55). Simplifying the litter classification to only four different classes resulted in increased overall accuracy. Highest accuracy was achieved using the combination of horizontal and forest floor photos (OA=0.70, f1-score=0.70). In contrast to the understory classification, the LSTM based on Sentinel-2 data performed only slightly worse than the CNN models in litter classification, yet with high variability especially for the simplified litter fuel types (**Figure 5.8**). Integrating Sentinel-2 data with the forest photos into a multi-input model improved overall classification accuracy only marginally for both understory and litter fuel types.

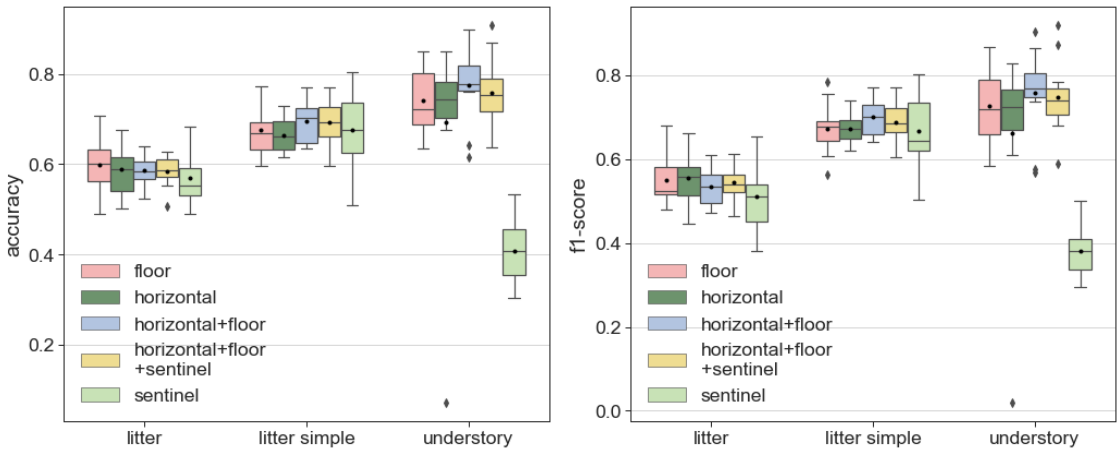

Figure 5.8: Test accuracy (left) and f1-score (right) after cross-validation for different input data for original (six classes) and simplified litter fuel types (four classes), and understory fuel types (seven classes).

Confusion matrices (**Figure 5.9**) show that pure litter types *bl*, *ln*, and *sn* were highly distinguishable based on either forest photos or Sentinel-2 time series, whereas mixed litter classes were difficult to separate from each other and the pure litter types included in the mixtures. Class-wise precision, recall and f1-scores can be found in **T**able **A1** in Appendix A. In understory classification, *dwarf-shrub* was classified correctly in almost all predictions based on forest photos. The other understory types were also identified well based on forest photos and in combination with Sentinel-2 time series, with a few confusions between *grass* and *forb*, and between the classes *shrub-needle*, *moss*, and *litter*.

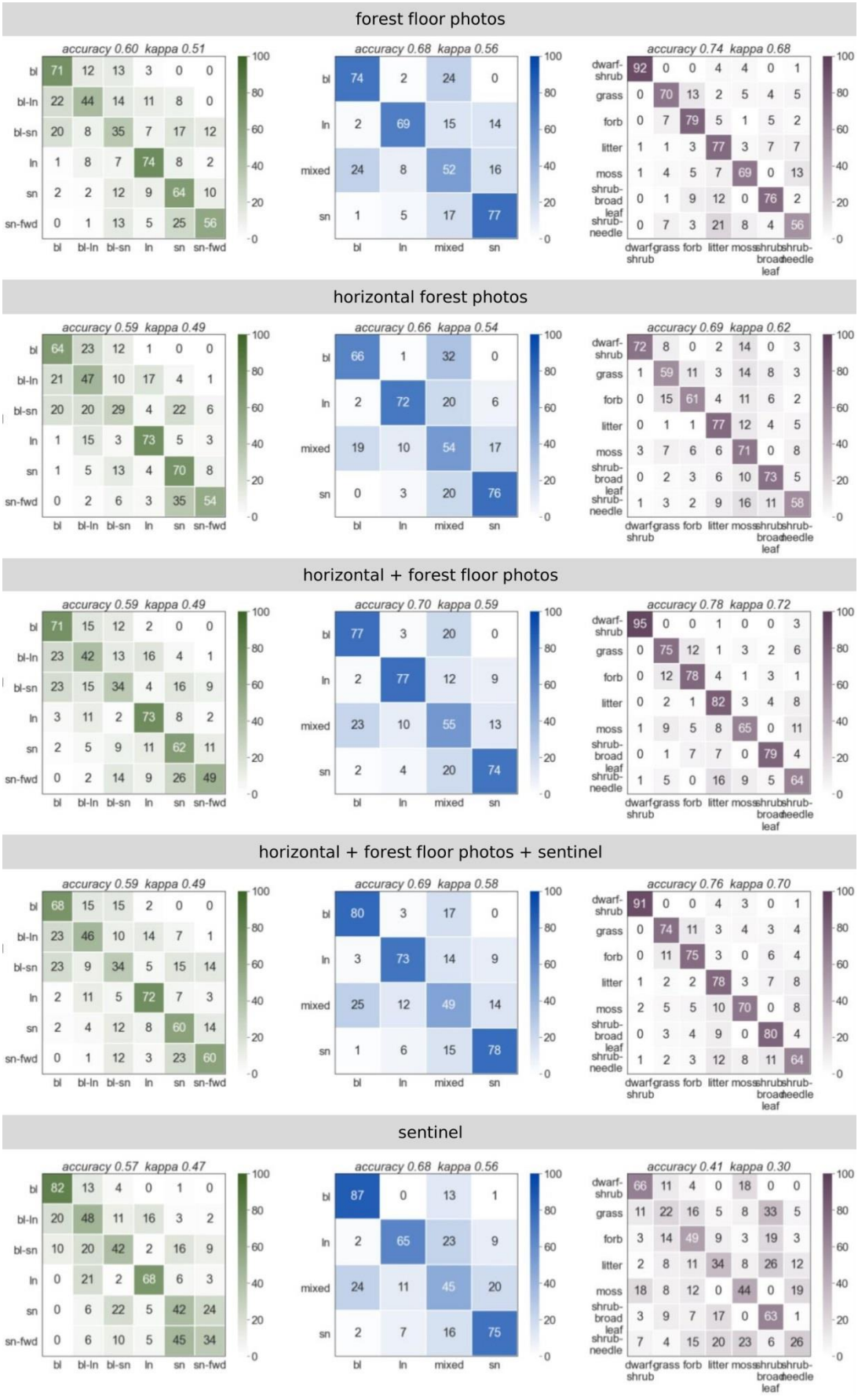

Figure 5.9: Confusion matrices for litter classification (left column: six classes, middle column: four classes) and understory classification (right column). The matrices were averaged across all 10

cross-validation folds and normalised so that each row (predicted classes) sums to 100 for easier comparison across the imbalanced dataset. Note that training of a CNN on horizontal photos in one fold did not succeed and the model predicted all instances into the moss class.

5.3.3 Assessment of prediction probabilities

Correctly classified photos generally received a higher class assignment probability score than misclassified photos, indicating the model's confidence for a correct class prediction (**Figure 5.10**). Mean prediction probability was 95 % for correct understory predictions, whereas incorrect predictions had a mean probability of 80 %. Class-wise prediction probabilities were partly in line with the results from accuracy assessment, showing that classes with high f1-scores such as *dwarf-shrub* were more confidently predicted (99 % for true labels) than classes that were confused more frequently such as *forb* (93 % for true labels). For the classification of litter fuel types, prediction probabilities were generally lower, with an average of 88 % for correct and 79 % for incorrect predictions. Probability distributions in litter classification highlight the model's uncertainty with respect to mixed litter types and *sn-fwd*, suggesting difficulties in finding appropriate decision boundaries for the class assignment.

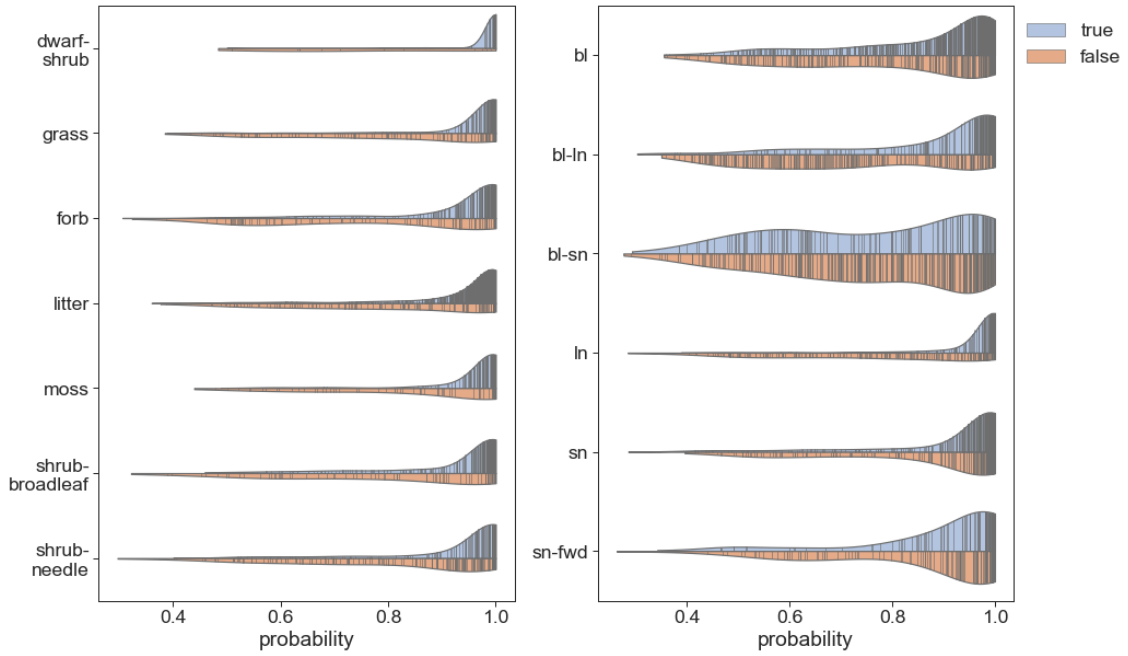

Figure 5.10: Violin plots showing the distribution of prediction probabilities for understory fuel types (left) and litter fuel types (right) from the multi-input CNN trained on horizontal and forest floor photos. Blue: true predictions, orange: false predictions.

5.3.4 Effect of ensemble approaches on classification results

Post-classification aggregation procedures provided a means to improve final classification results. While understory classification improved up to an accuracy of 0.85 (baseline 0.78), litter classification improved up to an accuracy of 0.72 (baseline 0.60). Our analysis showed that understory fuel type classification was best improved using majority voting from multiple photographs of the same stand and additionally using only the most certain predictions (**Figure 5.11**). Ensemble predictions based on the predictions from three single-input

models (two CNNs and LSTM) failed to improve classification results in case of understory (**Table 5.3**) when uncertain predictions were not omitted, due to the low accuracy of the Sentinel-2 predictions. In contrast, the ensemble prediction of litter types (**Table 5.3**) clearly outperformed the prediction resulting from majority voting based on multiple photographs (**Figure 5.11**).

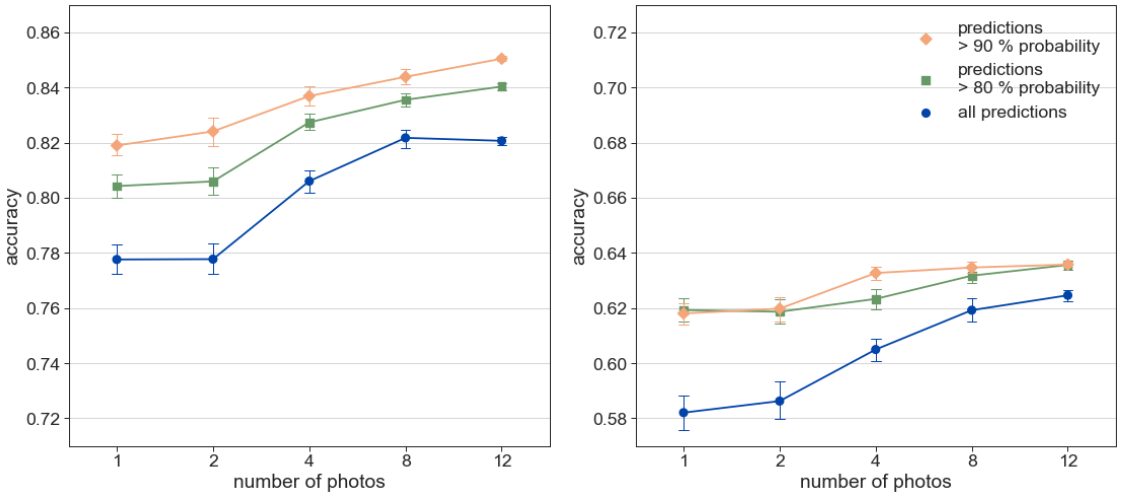

Figure 5.11: Average classification accuracy depending on different numbers of photos used to determine class assignment for a forest stand by majority voting for understory fuel types (left) and litter fuel types (right, original classification with six litter types).

Table 5.3: Average classification accuracy for model ensemble predictions with and without filtering based on prediction probability.

	understory		**litter**	
	overall accuracy	no. of predicted instances	overall accuracy	no. of predicted instances
all predictions	0.72	3336	0.65	3336
predictions >80 % probability	0.78	3175	0.70	2897
predictions >90 % probability	0.81	2982	0.72	2530

5.3.5 Feature importance in LSTM model

Time series of Sentinel-2's shortwave infrared band (SWIR, B11) were most important in litter classification, followed by a narrow near infrared band (narrow NIR, B8A) and the second SWIR band (B12) (**Figure 5.12**). Patterns changed for the simplified litter classes, where the blue band (B2), NDVI, and SWIR (B11) were most important. Little importance in litter classification was given to the red band (B4), vegetation red-edge bands (B5-7), and NIR band (B8). Understory classification relied on vegetation red-edge (B8A), SWIR bands, and NDVI. Summer acquisitions were more important in all classification tasks than winter acquisitions. Litter classification strongly relied on the months July and August, while the most important dates for understory classification were slightly earlier in the year, in May and June.

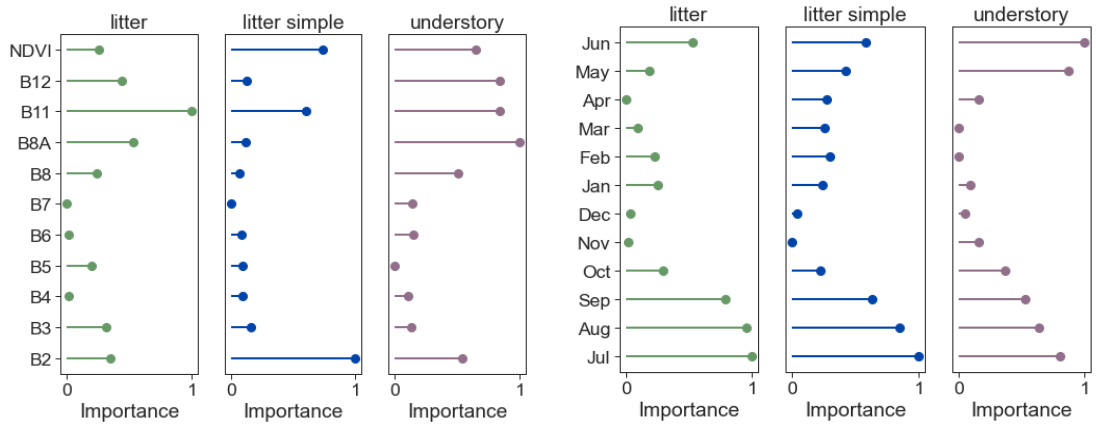

Figure 5.12: Normalised relative feature importance calculated from decreases in overall classification accuracy when reflectance values of a Sentinel-2 band (left) or acquisition month (right) were randomly permuted.

5.3.6 Importance of image regions in CNN model

In many cases, the most salient image regions in understory classification coincide with the occurrence of (or parts of) the particular understory fuel type in the image, especially in forest floor photos (**Figure 5.13 a**). Colour and texture appear to be important for the distinction of relevant from irrelevant image content (see for example *dwarf shrub, forb*, *litter*). However, sometimes only small regions are highlighted even though the fuel type covers large parts of the image (**Figure 5.13 b**), for example *grass, forb, shrub-broadleaf*), or even the fuel type is not highlighted at all, but another image feature is (e.g., grass blade instead of *moss*). In most horizontal photos of *dwarf-shrub*, *grass*, and *litter* fuel types (**Figure 5.13 c**), the bottom parts of the image are correctly identified as the relevant regions the model has to look for. The salient image regions in photos of *forb* fuel types seem to follow no clear patterns, while for *moss* either forest floor regions or stems are highlighted. In case of *shrub-broadleaf* and *shrub-needle*, mostly foreground image features such as branches and leaves seem to be relevant. For *litter* and *shrub-needle,* however, also stems in the image background can be a decisive feature (note the clear demarcation from the forest floor or foreground vegetation).

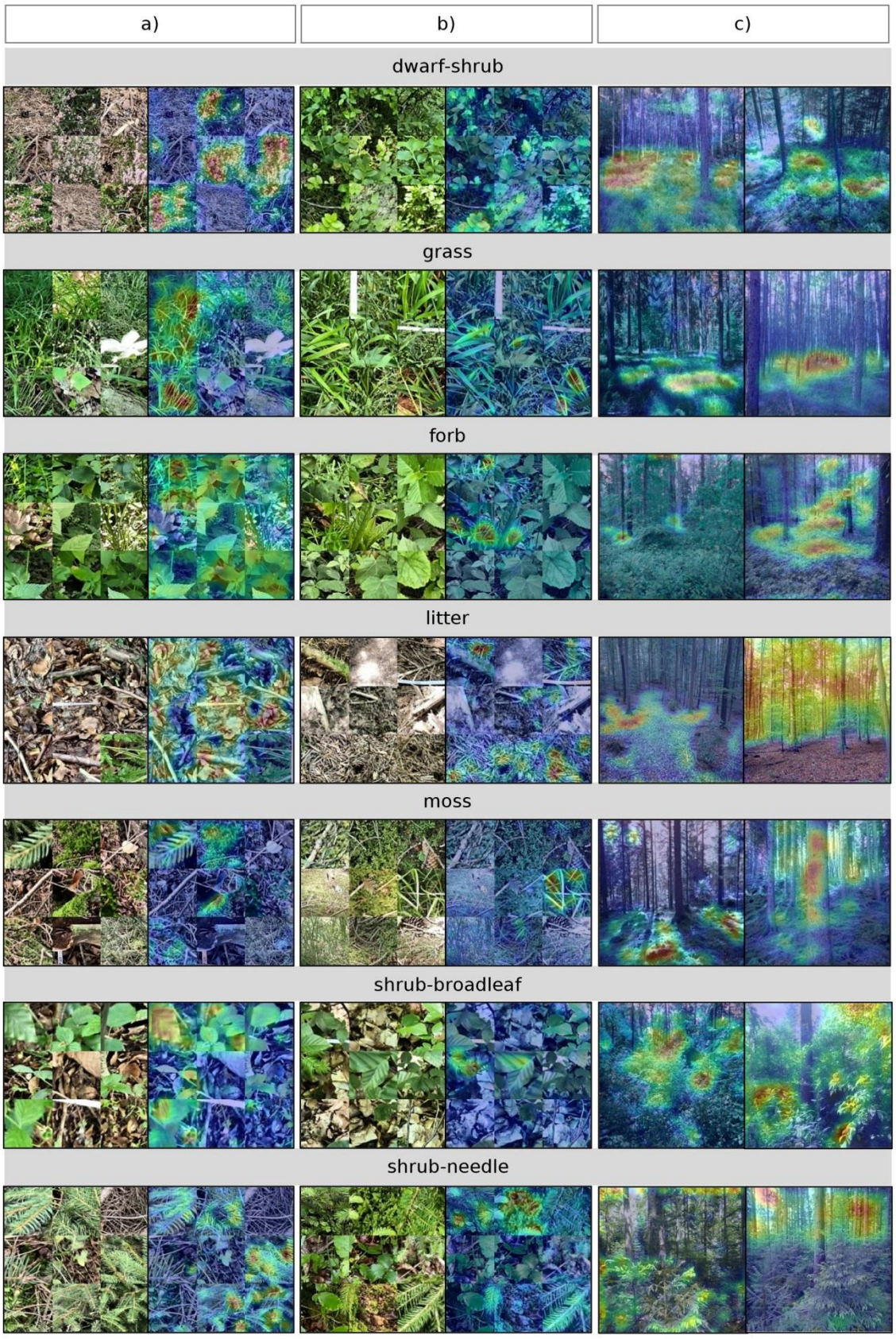

Figure 5.13: Most salient image regions (coloured in red) in the last convolutional layers of the CNN models for understory fuel type classification. Columns a) and b) show forest floor photos in the original (left) and overlaid with Grad-CAM heatmap (right); column c) shows horizontal photos overlaid with a Grad-CAM heatmap.

5.4 Discussion

5.4.1 Potential of forest photographs to classify surface fuel types

Our results showed that forest photographs are suitable to classify litter fuel types with moderate overall accuracy (60 %) and understory fuel types with fairly high accuracy (78 %) using CNNs. The small differences in performance using horizontal stand photos compared to forest floor photos indicate that both can be used for surface fuel type classification, depending on which of the two is available, and combining both can stabilise results and improve accuracy in case of understory fuel type classifications.

Litter fuel types

The good discrimination between the three basic types of short-needle, long-needle, and broadleaf litter by our models show that CNNs are able to extract the necessary information that is relevant to estimate surface fire spread for the included forest types based on photographs. However, our results revealed that it is difficult to correctly identify mixtures of different litter types: The challenge lies in the almost continuous transition from litter accumulations consisting of only one type of litter to few mixed-in leaves of, e.g., broadleaf litter, to more balanced mixtures between different litter types, where all components are assumed to have an effect on fire behaviour. Leaves of broadleaf litter in particular have a disproportionate influence on the appearance of a photograph compared to their actual abundance, leading to misclassifications also by human observers. This explains the frequent confusions of mixed types *bl-ln* and *bl-sn* with *bl*. However, the influence of mixtures of different litter types on the combustion process, and thus the level of detail required for litter characterization, remains to be investigated.
Learning critical features for litter discrimination, particularly from forest floor photos, is difficult also when the litter layer itself is not visible due to continuous understory vegetation. Although there are some relationships of litter types with understory vegetation, e.g., a continuous moss or herbaceous layer is rarely encountered underneath broadleaved trees in our target region Central Europe, we cannot be sure whether a model learns these patterns. It can be argued that in such cases litter is also less relevant for fire behaviour than the understory fuel type; however, there are situations where both are important, for example a pine forest with grass understory will burn more intense than an oak forest with grass understory due to the greater heat release from long-needle pine litter (Hough, 1969). Nevertheless, litter classification based on forest floor photos is expected to improve when excluding photos where the litter layer itself is not visible, whereas correct classifications based on horizontal photos may be still possible based on indirect relationships, e.g., to stems and crown morphologies of different tree species.

Understory fuel types

Understory fuel types were easier to distinguish based on forest photographs than litter fuel types. One reason for this might be that understory can be readily identified in an image and can have a unique appearance, such as in the case of *dwarf-shrub*. Since *dwarf-shrub* is the potentially most fire-prone understory fuel type included in this study (severe fires can occur in *Calluna vulgaris* habitats, e.g., Davies, Smith, et al., 2010), its reliable detection by the CNN allows for the successful identification of high-risk forest areas. Fires can also spread rapidly through cured *grass* fuel types; here a better discrimination from the moister *forb* fuel

types would be required, which is likely to be feasible with more training data. In other cases correct class attribution was more difficult because different understory fuel types appeared within the same photograph, e.g., *moss* and *shrub-needle*. This type of misclassification also occurred in the study by Xu et al. (2017), where a single land cover label was used for each photo. In the context of our study, the "confusion" of classes by the model merely reflects real-world conditions, if both fuel types contribute significantly to the fuel complex, and raises the question of whether a separation is actually meaningful in this case; or whether classification by presence/absence for different fuel types is more appropriate. However, a meaningful threshold for the minimum abundance of a fuel type to be effective in the context of fire behaviour needs to be defined. Area-based thresholds like a minimum cover as in our study are commonly used in fuel type classifications (e.g., Arroyo et al., 2008), but these may be easier to detect from an aerial than a horizontal perspective. This is where photo interpretation (CNN-based or by humans) reaches its limits: multiple branches in the foreground of an image or a photograph taken from a path where there is sufficient light for understory vegetation to grow, will result in the visual impression of high understory cover, but this is not necessarily representative of the forest stand behind. Therefore, standardised requirements for photo acquisitions are needed to ensure representativeness. Avoiding acquisitions close to occluding objects, however, can also result in subjective and potentially biased sampling. Until other well-established means are available to assess in-forest understory vegetation from a more nadir perspective, variation in the "footprint" of a photograph with understory density and height needs to be taken into account. One way to overcome this problem in the future may be under-canopy drone acquisitions, which have recently been introduced (Krisanski et al., 2020; Kuželka & Surový, 2018).

Comparison with other studies

We found no studies that have used forest photographs in a similar task before. Several studies have used CNNs to classify road view images in an agricultural context. For example, Ringland et al. (2019) characterised food production along roads in Thailand by using Google Street View (GSV) panoramas and achieved an overall accuracy of 83.3 % for seven different plant species. Yan & Ryu (2021) similarly employed GSV imagery to generate ground truth data for crop type mapping in the Central Valley in California, with an accuracy of 92 % for seven different crop types. Both studies used a considerably larger dataset than ours, with more than 2,000 images per class in the first study, and 500 to 1,000 images per class in the second study. Xu et al. (2017) used CNN-based feature extraction from 30,000 geo-tagged field photos in a multinomial logistic regression model to classify 19 land cover types, and achieved an accuracy of 48.4 % for top-1 prediction and 76.3 % for top-3 prediction (true class matches one of the three most probable predicted classes). Few studies focused on categorization problems using ground-taken imagery in a more ecological context. Habitat classification is one of such tasks and has been addressed by extracting visual features and contextual information from ground photographs, feeding them into a random forest classifier and adding information about geographical closeness of the georeferenced images (Torres & Qiu, 2016). Reported accuracy metrics range from f1-scores of about 0.2 for heathland to 0.7 for woodland and scrub habitats. Understory density has been estimated from understory images by distinguishing between vegetation-covered and background pixels using logistic regression on spectral variables (Campbell et al., 2018) or CNN-based segmentation (Abrams et al., 2019). However, these studies require that an

artificial background is used during data collection to separate understory from background areas in the photographs.

Although the aforementioned studies differ substantially from our work in terms of research context, specific aims and employed learning algorithms, we assume that model results strongly rely on the dataset size available for the task, on data cleaning procedures and on the human effort involved in the correct annotation of the training data. The highly complex and heterogeneous data from natural environments further complicate the correct interpretation of images, even for human surveyors. Reducing this complexity by categorising data allows more effective characterization and comparison, but class boundaries need to be set artificially and yet often remain fuzzy, making it difficult to clearly identify and separate classes. We consider this the most important limitation of our approach and it has remained largely unexplored how CNNs deal with such complexity outside of simple object recognition. We will discuss this further in Chapter 5.4.4.

5.4.2 Effect of integrating Sentinel-2 time series and utility as stand-alone methodology

Our results indicate that Sentinel-2 time series alone are of limited use for surface fuel type classifications: While they were similarly useful as forest photographs for classifying litter fuel types, they were of little value for distinguishing understory fuel types. Integrating them with the forest photographs in a multi-input model did not notably improve classification results for both litter and understory.

Litter fuel types

Sentinel-2 predictions of litter fuel types rely on the spectral reflectance of the pixel(s) covering the field plots, which is dominated by overstory tree species (see also Chapter 5.4.4). While tree species classification has been performed with good accuracies on multi-temporal Sentinel-2 data (Grabska et al., 2019; Persson et al., 2018), our study showed that predicting litter fuel types based on tree species information alone is difficult: small understory trees and shrubs can contribute significantly to the litter layer, and especially broadleaf litter from neighbouring stands can be blown into a stand. Data that was recorded during field work showed that litter fuel types cannot be perfectly predicted based on the basal areas of the tree species present using a random forest classifier (OA=0.68). This may explain why the litter fuel type classifications from Sentinel-2 time series achieved only moderate accuracy (OA=0.59).

Understory fuel types

Understory characterization, especially species classification, based on remote sensing data is a challenging task, as shown by the few attempts that have been made so far (Hall et al., 2000; Korpela et al., 2008; Landry et al., 2020). The fact that Sentinel-2 time series are insufficient to distinguish understory fuel types is due to multiple reasons: first, the same fuel type may occur in the understory (e.g., *litter* or *grass*) under completely different tree species in the overstory; and even in case of open stands, the spectral signal from the understory is superimposed by overstory reflectance, resulting in a complex mixture of reflectance values contributing to the final pixel reflectance (Kobayashi et al., 2018; Singh & Gray, 2020). Second, it is not clear whether the spectral signal from small understory trees, e.g., regeneration of beech, differs significantly from a closed-canopy of mature beech trees, which

could explain confusions between *shrub-broadleaf* and *litter* understory fuel types. In such cases, integrating information on vertical forest structure derived from active remote sensing systems such as lidar would help to distinguish between overstory and understory vegetation. Including Sentinel-2 data can lead to small improvements in case of understory fuel types such as *moss* that are related with a certain type of overstory (mostly coniferous); yet effects are too small to justify the additional effort.

5.4.3 Improving classification results by ensemble approaches

Ensemble approaches helped notably to improve base model predictions. Our results showed that a forest stand can be characterised more reliably using multiple photographs from different perspectives and additionally using only the most certain predictions.

Our findings also showed that aggregating the predictions of several single-input models is more useful than using a multi-input model from the start, if all inputs have similar predictive power, such as in the case of litter classification. This could also be due to the greater difficulty in finding optimal hyperparameters for a complex model with multiple inputs, e.g., with respect to the best optimization algorithm, which may be different for the CNN and the LSTM branch of a model. In this sense it is recommended to optimise the smaller and less computationally demanding single-input models and then aggregate their predictions. However, there is still room for experimentation with different fusion schemes, as the increasing availability of multiple, heterogeneous datasets with different scales and dimensions for a given task has recently driven advances in deep multimodal learning (see review by Bayoudh et al., 2021).
Using prediction probabilities as additional filter criterion further improves the results from decision fusion approaches, but always needs to be weighed against the associated discarding of data. At the same time, it can be worth to have a closer look at the more 'unsure' predictions: often the prediction probabilities contain much additional information, such as when a forest stand is actually better represented by a mixture of different fuel types than by a single one (**Figure 5.14**). In any case, providing the prediction probabilities along with the predictions helps in assessing the reliability of the prediction.

Figure 5.14: Predicted probabilities in understory fuel type classification based on horizontal photos. a) *grass* 0.59, *shrub-broadleaf* 0.23, and *forb* 0.18. b) *litter* 0.63 and *shrub-needle* 0.34. c) *litter* 0.44, *moss* 0.56.

5.4.4 Assessment of model explainability

Feature importance in LSTM model

Our results on variable importance of Sentinel-2 bands for classifying litter fuel types in the LSTM model (SWIR, blue band, see **Figure A1** in Appendix A, and NDVI) are consistent with previous studies that have classified tree species using multi-temporal Sentinel-2 data: Immitzer et al. (2016) similarly identified the SWIR band (related to leaf water content) and the blue band (absorbed by chlorophyll) as the two most important bands for tree species mapping in Germany, while the study of Persson et al. (2018) also ranked the red-edge bands very high for tree species classification in Sweden. The latter were found to be insignificant in our study, which could be related to the high correlation between these bands. Grabska et al. (2019) confirmed the importance of SWIR bands, red-edge bands, blue and red bands for the discrimination of tree species in the Polish Carpathians, while Ottosen et al. (2020) found that similar features (blue, green, red-edge, SWIR bands) were also most suited to map tree cover in Europe based on Sentinel-2 images, indicating that these bands are generally useful for mapping and differentiating canopy characteristics. Understory discrimination in our study relied somewhat more on NIR and SWIR bands, but a detailed discussion is omitted due to the rather low accuracy of the classification. The aforementioned studies mostly agreed that late spring and early summer acquisitions were most helpful for tree species discrimination, while our study revealed that midsummer acquisitions were more suitable for litter fuel type classifications; potentially due to fully developed tree canopies at this time of the year. Understory, however, is better identified earlier in the year, when phenological variations of the undergrowth may be more pronounced and better sensed through a less dense canopy. The choice of spectral variables in this study was guided by the aforementioned studies that attempted to map tree species and tree cover. However, other spectral indices have been found to be more sensitive to vegetation structure, such as the tasseled cap indices (especially the wetness feature) or the Normalised Difference Moisture Index (NDMI) (W. B. Cohen & Spies, 1992; Jin & Sader, 2005). Therefore, we trained another LSTM model on Sentinel-2 time series, adding tasselled cap wetness, tasselled cap greenness, and NDMI, but did not observe any improvement in classification results (see **Figure A2** in Appendix A).

Importance of image regions in CNN model

Due to the great heterogeneity of the input data in this study, it is challenging to assess what information from an image the CNN uses for its classification decision. Although it seems that the model generally responds to the parts of a photograph that also appear relevant to a human observer, there are still many cases where an (for the human observer) irrelevant image region drives the model towards the correct class decision. The concepts the model learns may be entirely different from what we expect in the first place; for example, we cannot be sure whether the decision for a moss or litter fuel type in a horizontal photo is actually driven by the texture and colour of these two types, or whether the model is responding to coarse deadwood on the forest floor that is barely visible in photos of other understory fuel types. Since Grad-CAM heatmaps as well as other feature attribution algorithms are specific to the input image, displayed material will always reflect only a (potentially human-biased) minimal portion of the data, making it difficult to find generalizable rules. Visualising the features the model responds to by generating synthetic images that maximise the activations of a particular convolutional filter reveals that the model mainly

learns small-scale geometric features, even in late convolutional layers (**Figure A3** in Appendix A). Although one might suspect that some of them resemble the shapes of leaves, small twigs or the texture of moss; such interpretations should be taken with caution (Kattenborn et al., 2021). Filter activations showed that maximally activated filters are very similar for photos of different fuel types, since all contain plant parts, but in slightly different compositions.

5.4.5 Outlook

We have taken a first step towards the application of deep learning methods to classify surface fuel types for fire behaviour and fire risk assessment from forest photographs and satellite time series. As with all deep learning problems, the availability of labelled training data is a bottleneck. To improve the capabilities of the model and to apply it to a larger geographical area, the dataset should be further expanded using (crowd-sourced) photos annotated by trained individuals. In our study, we identified the most common surface fuel types in temperate forests of Central Europe; however, the targeted fuel type classification scheme could be arbitrarily detailed, provided a large enough data set. For the validation of fuel type maps across larger areas, the challenge will be to obtain sufficient imagery also from remote locations and ensure quality in terms of geolocation accuracy. Incorporating point cloud data from ALS, TLS or drones, if available, could further improve or even refine fuel type classification, and also forest inventory data or biophysical factors could be included. The model itself could be improved by leveraging a more efficient architecture that requires less parameters, which would speed up training and inference times. Testing alternative approaches such as segmentation of, for example, understory vegetation on forest photographs is laborious, but could help the model to learn the relevant features and not be distracted by artefacts. Another exciting area of research would be to explore whether it is also possible to move away from classifications and retrieve quantitative information such as estimates of fuel loadings from a photograph. In addition, many other interesting use cases for forest photos are conceivable, just to mention forest health and biodiversity assessments, which have been already examined from photographs using other methodical approaches (e.g., Gyllin & Grahn, 2015; Murray et al., 2018).

In terms of practical applications, GNSS-located photos of forest stands obtained by local forest managers or through citizen science can be used not only to validate and improve fuel type maps, but also to provide forest practitioners and firefighters with immediate information about potential fire behaviour at their location, for example via a cloud-based smartphone application: The extracted fuel type information could be used to approximate the available burnable biomass and to derive relevant physical properties that determine the combustion process in order to calculate fire behaviour in a forest stand, e.g., under different moisture scenarios. Knowledge from fire experts could also be incorporated to help practitioners decide, for example, whether understory vegetation needs to be removed to reduce fire hazard in critical areas, or to understand the extent to which moist green vegetation can even serve as fire barrier. This would greatly advance knowledge exchange on fuel-related forest fire risk, particularly in temperate forests of Central Europe, which have been poorly studied in this regard to date.

5.5 Conclusion

In this work, we investigated the usefulness of deep neural networks (CNNs and LSTM) to classify surface fuel types of Central European forests based on within-stand photographs and Sentinel-2 time series. Our results demonstrated that understory fuel types can be classified with good accuracy from a combination of horizontal stand photos and forest floor photos using CNNs. Litter fuel types were classified with moderate accuracy from both types of photographs. The main limitation of the approach was the occurrence of multiple fuel types within the same photograph, leading to confusions especially in litter classification. Our study further showed that Sentinel-2 time series alone are insufficient for understory classification, but that they have potential for litter fuel type classifications both as additional predictor in ensemble approaches and as stand-alone methodology when photographs of a forest stand are not available. The decisive spectral features were reflectance differences associated with canopy characteristics, manifested primarily in NDVI, SWIR, and blue bands during summer. From a practical perspective, our research showed that a forest stand can be better characterised the more photos are available, especially concerning understory fuel types. For litter fuel types, it has proven useful to make predictions on multiple types of data separately, i.e., photographs and satellite time series, and combine the predictions of all models by majority voting. Class prediction probabilities were found to be a useful filter criterion for the most reliable predictions and provided insights into the complexity of fuel type composition in a forest stand. While our study has demonstrated that artificial intelligence can help with classification problems in complex natural environments, it has also shown that the model's capabilities are limited by fuzzy class boundaries, as humans are; and although influential image regions in CNNs often contain features that appear relevant to the observer (i.e., the respective fuel), we are unable to fully comprehend the model's decisions. Translating the task into a regression problem to quantify individual fuel components could help deal with natural gradients, but would also require extensive collection of reference data. Nonetheless, results from this study indicate that automatic processing of within-stand photographs by CNNs has the potential to facilitate validation of fuel type maps and provide forest practitioners with the information needed to mitigate fire hazard. We hope that our work can contribute to opening a new field of research for deep learning-based applications to characterise forest fuels for fire behaviour and risk assessment in light of the increasing threat of wildfires, even in temperate forests, under a changing climate.

Acknowledgements

This work was funded by the German Federal Ministry of Food and Agriculture and Federal Ministry for the Environment, Nature Conservation and Nuclear Safety as part of the project "ErWiN" (code 2219WK54A4). The authors acknowledge support by the state of Baden-Württemberg through bwHPC. We would like to thank Paulo Fernandes and Davide Ascoli for their valuable support in developing the fuel type classification. We also want to thank Gabriel Cabezas for his help with the fieldwork and Felix Schiefer for fruitful discussions on deep learning issues. Furthermore, we are grateful to the anonymous reviewers, who gave valuable comments to improve our manuscript.

6 Quantifying surface fuel loads

This chapter has been published as:
Labenski, P., Ewald, M., Schmidtlein, S., Heinsch, F. A., & Fassnacht, F. E. (2023). Quantifying surface fuels for fire modelling in temperate forests using airborne lidar and Sentinel-2: potential and limitations. *Remote Sensing of Environment*, 295, 113711.
https://doi.org/10.1016/j.rse.2023.113711

Abstract

Surface fuel information is an essential input for models of fire behaviour and fire effects. However, spatially explicit, continuous information on surface fuel loads and fuelbed depth is scarce because the collection of field data is laborious, while suitable methods for deriving estimates from remote sensing data are still at an early stage of development. Fine-scale surface fuel mapping using both passive and active remote sensing has not yet been carried out in Central European forest types, and it remains unexplored how prediction uncertainties of different fuel components affect modelled fire behaviour. This study combines very detailed airborne lidar and multispectral satellite data to extract metrics describing forest structure and composition in two forested areas in south-western Germany. These metrics were used to predict field-sampled surface fuel components using random forest regression. Accuracies of continuous fuel load predictions were compared to accuracies that could be achieved if only forest type-specific average fuels were assigned. Results revealed that models based on remotely sensed metrics explain part of the variance in litter and fine dead woody fuels (R^2=0.27-0.41), but not in coarser dead woody fuels. Estimates for herb and shrub fuels were fairly accurate (R^2=0.55-0.64) but limited for the more fire-relevant fine fraction of shrub fuels (R^2=0.39). Fuelbed depth was moderately well predicted based on remote sensing data (R^2=0.44). Lidar-derived metrics were particularly useful for predicting understory fuels and fuelbed depth. Litter and fine woody fuel predictions were linked to canopy characteristics captured with both lidar and multispectral data and similarly accurate estimates could be obtained using average values based on forest type. We used the fine-scale surface fuel maps derived from remote sensing to predict potential surface fire behaviour in the study area and analysed the sensitivity of modelled fire behaviour to errors in the predicted loads of different surface fuel components: fire behaviour was most sensitive to errors in litter and especially shrub fuel loads, hence estimates of these components need to be improved. Overall, this study showed that statistical relationships between remotely sensed metrics describing forest composition and structure and surface fuels have some potential for estimating fuel loads in Central European forest types and should be further developed to provide starting points for realistic fire behaviour models.

6.1 Introduction

Fire risk in temperate forests of Central Europe has long been of minor concern to many countries. However, recently the danger of catastrophic fire events in these formerly low-risk areas has risen as result of climate change (de Rigo et al., 2017). The year 2022 has shown that the trend of increased wildfire activity associated with prolonged droughts in Central Europe continues, with the number of fires and areas burned exceeding long-term averages (EFFIS, 2023). Weather conditions favouring wildfire ignition and spread are projected to become more frequent (IPCC, 2021), making the occurrence of catastrophic fires worldwide 1.31 to 1.57 times more likely by the end of the century (UNEP, 2022). While fires are an integral part of the natural disturbance regime in some ecosystems (Battisti et al., 2016), uncontrolled wildfires can have serious social, economic, and environmental impacts, such as loss of wildlife habitats, disease from toxic smoke, destruction of infrastructure and property, and feedbacks to climate change through greenhouse gas emissions (UNEP, 2022). To mitigate adverse effects of wildfires under global warming, it is important to better understand fire behaviour especially in ecosystems where this has not been studied extensively. The latter include temperate forests of Central Europe. One important aspect to investigate is how fire behaviour and fire effects are related to forest stand properties such as the amount and distribution of combustible organic material, i.e. fuel.

Spatially explicit fuel information is used for simulations of fire spread, intensity and severity (Finney, 2006; Tymstra et al., 2010), planning of management activities such as fuel reduction treatments (Furlaud et al., 2018; Moghaddas et al., 2010), and strategic planning of fire suppression efforts (Page et al., 2013; Plucinski, 2019). It is also needed to estimate emissions of greenhouse gases and particulate matter from burned areas (Ottmar, 2014; Weise & Wright, 2014). Several concepts have been developed to describe fuels and their characteristics, often with focus on specific applications like fire behaviour prediction (Burgan & Rothermel, 1984; Cruz & Fernandes, 2008) or fire effects and emission modelling (Prichard et al., 2007; Reinhardt, 1997). However, one fuel variable that is used in almost all fire management applications is fuel load, i.e. biomass per unit area (Keane, 2015). Fuel load is commonly specified for each fuel component of a fuelbed: surface fuelbeds (<2 m) are composed of litter, shrubs, and herbs as well as down woody material stratified into different particle diameter classes based on their rate of drying (Fosberg et al., 1970). Surface fuel loads vary at very fine spatial scales (metres to submetres) (Keane, 2015) and drive local fire behaviour: The heterogeneous distribution of dense woody fuels has for example been linked to variations in fire intensity (Loudermilk et al., 2012), which has implications for tree mortality, post-fire plant diversity, and other long-term ecosystem effects (Dell et al., 2017; Mitchell et al., 2009). Understory vegetation such as grasses, forbs, and shrubs form loosely packed fuelbeds and thus have a strong influence on fire dynamics (Keane, 2015), which can be important to consider when developing effective firefighting tactics. An important variable in this context is fuelbed depth (average height of the surface fuels), which together with fuel load determines the bulk density of the fuelbed. In forest stands without understory and without coarse deadwood, the fuelbed depth is equal to the litter depth. Litter provides a continuous, easily ignitable fuel source in almost all forest stands, capable of supporting the contagious spread of surface fires. As most fires burn through surface fuels (Albini, 1984), fine-scale maps of surface fuel loads and fuelbed depth are useful for assessing spatial patterns in fire behaviour characteristics and fire effects. High-

resolution surface fuel maps are particularly important when fires are generally small in size and crown fires do not play a major role, as is the case for most forest fires in Central Europe (San-Miguel-Ayanz et al., 2021).

Remote sensing approaches offer the potential to efficiently create and update continuous fuel maps across large areas. However, as pointed out by Gale et al. (2021), the focus in current fuel remote sensing literature is on estimating overstory fuel variables (Andersen et al., 2005; Botequim et al., 2019; García et al., 2012; González-Ferreiro et al., 2014; Riaño, 2003), while studies on surface fuel variables are underrepresented. This may be due to the difficulty of estimating fuel properties beneath canopies using airborne or spaceborne sensors. Gale et al. (2021) also noticed a tendency towards discrete mapping of surface fuels as fuel types or fuel models instead of mapping continuous fuel variables (Chirici et al., 2013; Domingo et al., 2020; García et al., 2011; Marino et al., 2016; Mutlu et al., 2008; Seielstad & Queen, 2003). Such classifications into fuel types or fuel models summarise the fuel information needed for specific modelling purposes in broad categories (Lutes et al., 2009), which are usually assigned to an entire stand, disregarding the more complex and fine-scale distribution of fuels in the forest (Loudermilk et al., 2022). Categorising fuel information, e.g. by averaging field-measured loads and associating them with a forest type, may be useful for rapid fuel assessments, but fuel loads and fuelbed depth are inherently continuous variables (Keane, 2015). Accurate quantification of continuous variables is challenging due to the high spatial and temporal variability of surface fuels, which can also differ for the individual fuel components (Keane, 2015). Studies predicting different components of surface fuels using passive and active remote sensing technologies report strongly varying model performances depending on study area, sensor used and scale of the investigation as well as the inclusion of auxiliary variables (**Table 6.1**). Hence, the utility of remote sensing for fine-scale mapping of surface fuel loads in previously unexplored ecosystems remains an open question. A comparison between the accuracy of continuous fuel estimates and average values associated with forest types may be helpful in future decisions on how to efficiently map fuel components in these forest types. In addition, there are no studies that have investigated the extent to which errors in remotely sensed surface fuel estimates affect fire models based on them.

Table 6.1: Overview of studies estimating surface fuel loads with remote sensing data.

	sensor (spatial resolution)	**fuel component**	**study area**	**explained variance**	**method**	**independent variables**
Brandis and Jacobson (2003)	Landsat TM (30 m)	litter and fine fuel load	eucalypt forest, woodland, shrubland, Australia	-	classification techniques	vegetation type, vegetation indices, fire history data, biomass turnover rates
Jin and Chen (2012)	Landsat (30 m), QuickBird (2m)	litter, 1 hr, 10 hr, 100 hr, 1000 hr loads	larch-dominated boreal forest, China	5-57 %	linear regression	spectral bands, stand-characteristics
Reich et al. (2004)	Landsat TM (30 m)	litter, duff, 1 hr, 10 hr, 100 hr, 1000 hr	Black Hills National Forest, South Dakota	34-45 % 55-72 %	multiple regression analysis, binary regression trees	spectral bands, topography, forest class
Duff et al. (2013)	Landsat 5, remotely sensed bio-	litter, elevated fuels (shrubs,	eucalyptus woodland, Australia	30-51 %	generalised additive models	NDVI, topography, climate, soil properties, fire

	physical data (50 m)	herbs), bark fuel				history
Peterson et al. (2013)	Landsat TM	1 hr live fuels, 1 hr, 10 hr, 100 hr fuels; discretised into three classes	chaparral shrublands to subalpine forests, Yosemite National Park, California	-	random forest	spectral bands, vegetation indices, topography, climate, soil properties, fire history
Arellano-Pérez et al. (2018)	Sentinel-2 (10-20 m)	total surface fuel load	even-aged pine stands, North western Spain	12 %	random forest, multivariate adaptive regression splines	spectral bands and vegetation indices
Franke et al. (2018)	Landsat 8, Sentinel-2	total surface fine fuel load	Cerrado, Brazil	86 %	mixture tuned matched filtering	Non-photosynthetic dry vegetation and soil fractions per pixel
Skowronski et al. (2007)	ALS (pulse spacing 0.125 m)	presence of ladder fuels	Pinelands, New Jersey	-	-	vertical height bins of lidar returns
Jakubowksi et al. (2013)	ALS (9 pts/m²), multispectral imagery (1 m)	total surface fuel load, 1000 hr load, understory shrub cover and height	mixed-conifer forest, Nevada	32-48 % 59-62 %	support vector machines, linear and additive regression	spectral values, topography, lidar metrics
Hudak et al. (2016)	ALS (6.9 pts/m²)	total surface fuel load	longleaf pine forest, Florida	32-44 %	multiple linear regression	lidar metrics
Wallace et al. (2017)	TLS (0.018 ° between points), image derived point-clouds	surface vegetation biomass up to 25 cm	eucalypt forest, Australia	74 %	linear regression	TLS derived and point-cloud derived vegetation volume
Li et al. (2021)	TLS (>1 pt/cm³)	herb and shrub layer biomass	temperate forests, north-eastern China	69-72 %	linear and nonlinear regression	TLS-derived understory height, cover and vegetation volume
Chen et al. (2017)	TLS, ALS (footprint: 0.26 m)	total surface fuel load	eucalypt forest, Australia	89 %	multiple regression analysis	terrain features, forest structural characteristics, fire disturbance, fuel and burn types
Alonso-Rego et al. (2021)	ALS (0.5 pts/m²), TLS (130 pts/m²)	litter and duff, understory load, down woody debris load	even-aged pine stands, NW Spain	35-49 %	multivariate adaptive regression splines	TLS and ALS metrics
Bright et al. (2017)	ALS (2 pts/m²), Landsat time series (30 m)	litter, duff, 1 hr, 10 hr, 100 hr, 1000 hr loads	coniferous montane forest, Colorado	24-32 %	random forest	lidar height and density metrics, LandTrendr variables, topography
Stefanidou et al. (2020)	multispectral ALS, (83 pts/m²)	litter, grass and forbs, 1 hr, 10 hr, total surface fuel load	*Abies borisii*, hybrid fir, dense coniferous forest, Greece	59-71 %	multiple linear regression analysis	lidar height and intensity metrics

Multispectral remote sensing data have been used to classify vegetation types and extract stand characteristics, which are then used to estimate surface fuel loads with empirically derived relationships (Brandis & Jacobson, 2003; Jin & Chen, 2012). However, surface fuel loads are not always correlated with forest stand attributes (Keane et al., 2012) and can vary

considerably within a vegetation type (Keane, 2015). Other studies have integrated multispectral information with other remotely sensed biophysical variables and fire history data to explain surface fuel load variation (Duff et al., 2013; S. H. Peterson et al., 2013; Reich et al., 2004). Topography, climate variables and time since last fire were found to be important predictors of fuel load variation in these study areas encompassing rather complex terrain with multiple vegetation types and/or frequent fire disturbance. Comparatively little variation in surface fuel load could be explained by spectral information and vegetation indices alone at more homogeneous sites (Arellano-Pérez et al., 2018), while satellite-derived fractions of vegetation cover were useful to explain surface fuel load variation across diverse Cerrado vegetation types (Franke et al., 2018). These results indicate that multispectral remote sensing data from passive sensors such as Landsat and Sentinel-2 can explain a certain fraction of surface fuel load variability, as they carry information related to vegetation density and species composition, which are likely to drive understory presence and the type and amount of litter.

However, fine-scale variation of surface fuel components is not adequately captured with these data; hence active remote sensing systems like airborne lidar (ALS), which are able to partly penetrate canopies and collect information about vertical forest structure and the forest floor, may be useful in the direct mapping of laying trunks, shrubs or even the presence of herbs and grasses. Accordingly, ALS has been used in several studies to estimate components of surface fuels based on statistical relationships with height, density, and intensity metrics of the reflected laser pulses (Hudak et al., 2016; Jakubowksi et al., 2013; Skowronski et al., 2007); however, so far with only moderate reliability for predictions of ground-based fuels. One reason for this might have been limited point densities which lead to comparably sparse information on understory vegetation and forest floor roughness, particularly if rather dense overstory vegetation is present, which is the case in most Central European forests. As an alternative, terrestrial laser scanning (TLS) and photogrammetric approaches allow to collect dense point clouds for more accurate surface fuel estimations (Y. Chen et al., 2017; S. Li et al., 2021; Wallace et al., 2017). However, these techniques are less suitable for mapping fuels across large areas, although they provide detailed information about below-canopy structure that can support models based on ALS data (Alonso-Rego et al., 2021).

Fusion of ALS with multispectral data can provide both direct and indirect measurements of surface fuels and may thus lead to more accurate mapping both within and across different forest types. Studies combining ALS with multispectral information have found moderate improvements in predicting surface fuel load variation in coniferous forests (Bright et al., 2017; Stefanidou et al., 2020). However, it remains unclear whether a combination of multispectral satellite and airborne lidar data is suitable to map surface fuel load and fuelbed depth variation in temperate mixed broadleaf and conifer forests characterised by high structural heterogeneity at fine spatial scales. The focus of this study is on mixed stands of deciduous beech and oak as well as pine and Douglas fir in lowland to colline regions. The relationship between overstory composition and surface fuel loads needs to be better understood for these forests in order to assess whether simplistic associations of surface fuel loads with broader vegetation categories such as forest types are justified to predict variability in potential fire behaviour and can be used as an alternative to fine-scaled remote sensing maps. At last, given the frequently reported inaccuracies in surface fuel estimation, it is critical to understand the sensitivity of current fire behaviour models to such inaccuracies.

Therefore, the aim of this work is to

i) explore the ability to predict surface fuel loads and fuelbed depth in heterogeneous mixed forests of Central Europe using freely available high-resolution Sentinel-2 data (10-20 m) combined with high-density ALS data (>72 points/m²)

ii) improve our understanding of remote sensing-based predictions of surface fuels by analysing a large set of features as proxies for vegetation structure and composition across vertical forest strata and investigate whether average fuel loads based on forest types can be used in practice

iii) assess the influence of errors in surface fuel load estimates on modelled fire behaviour by performing a sensitivity analysis.

6.2 Methods

6.2.1 Overview

The main steps of the analysis are summarised in **Figure 6.1**. First, we preprocessed the field measurements of surface fuel loads as well as litter and fuelbed depth in our study area (Chapter 6.2.2 and 6.2.3). We obtained average surface fuel loads for the main four forest types of our study area. We then processed the high density lidar and multispectral datasets by using a combination of different techniques and obtained a large number of potential predictors of surface fuels (Chapter 6.2.4 and 6.2.5). After feature selection (Chapter 6.2.6), we trained random forest models to predict surface fuel loads based on the selected remotely sensed predictors (Chapter 6.2.7) and compared the errors of the method with the errors of using average surface fuel loads per forest type (Chapter 6.2.8). Furthermore, we investigated the importance of different predictors to better understand the relationship between surface fuels and forest composition and structure (Chapter 6.2.9). Then, we predicted surface fuel maps for our study area (Chapter 6.2.10) and modelled the potential fire behaviour (Chapter 6.2.11). Finally, we performed a sensitivity analysis to assess the influence of the predicted fuel components on modelled fire behaviour (Chapter 6.2.12).

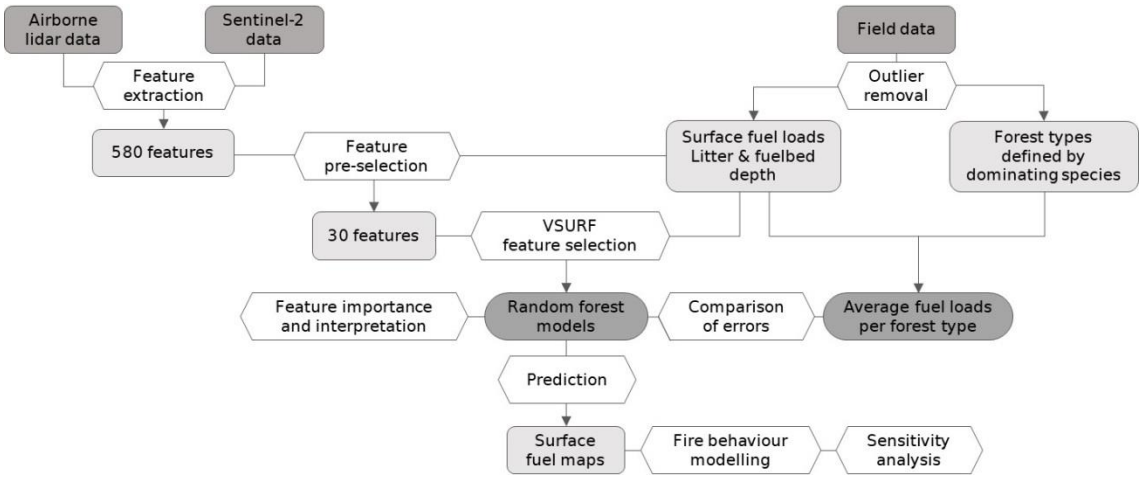

Figure 6.1: Overview of the data used and analyses carried out in this study.

6.2.2 Study area

Field data were collected in two study areas of temperate mixed forest in south-western Germany. The *Hardtwald* forest (19.6 km²) is located in the flat upper Rhine valley (49.037 N, 8.416 E) at 120 m a.s.l., and the *Bretten* municipal forest (10.5 km²) in the Kraichgau hills (49.006 N, 8.699 E) at 180 to 300 m a.s.l. (**Figure 6.2**). The two study areas are characterised by temperate climate with mean annual temperatures of 11.4 °C (*Hardtwald*) and 10.2 °C (*Bretten*) in the reference period from 1991–2020 (DWD Climate Data Center, 2023), with monthly mean temperatures varying between 1.1 and 21.5 °C at the *Hardtwald* site, and between 0.2 and 19.8 °C in *Bretten*. Mean annual precipitation amounts to 746 mm in *Hardtwald* and 792 mm in *Bretten*.

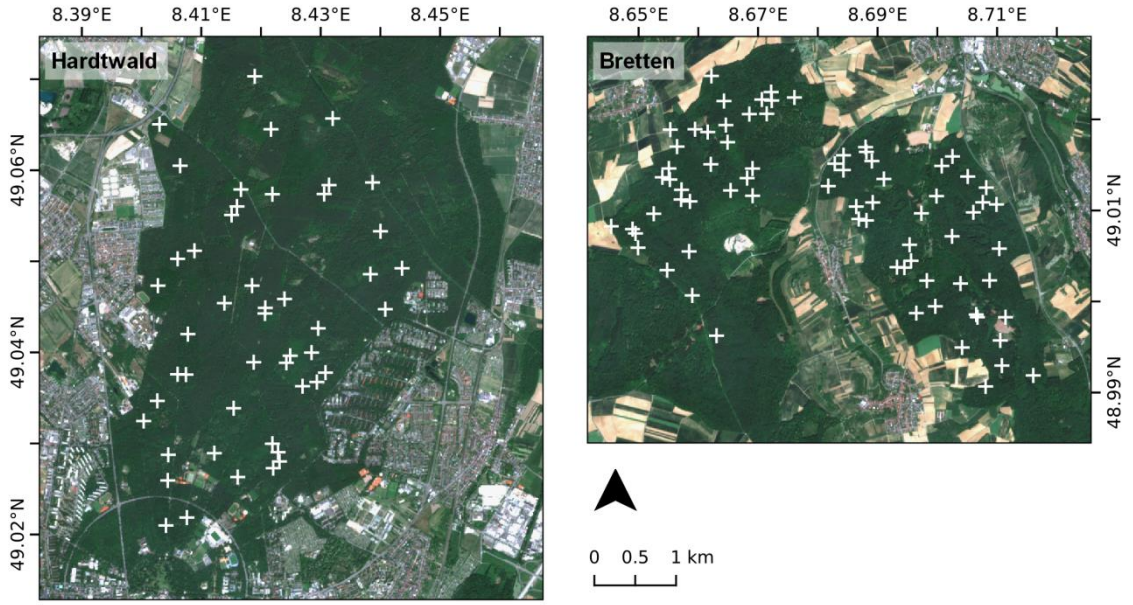

Figure 6.2: Overview of the two study areas 'Hardtwald' (left) and 'Bretten' (right). White crosses indicate the center locations of the field plots. Background image is a Sentinel-2 scene from May 2020 obtained from USGS Earth Explorer (U.S. Geological Survey, 2023).

The examined forest stands are diverse in age and structure (**Table 6.2**), encompassing dense, young planted stands of Scots pine (*Pinus sylvestris* L.) as well as older, pine-dominated stands with an understory of black cherry (*Prunus serotina* Ehrh.) or European beech (*Fagus sylvatica* L.). They further include mature beech stands with closed canopies and areas dominated by natural regeneration of beech. There are old, open stands of sessile oak (*Quercus petraea* Liebl.), as well as row-wise plantations of sessile oak and red oak (*Quercus rubra* L.), and finally young and mature stands of Douglas fir (*Pseudotsuga menziesii* (Mirb.) Franco), the latter either pure or mixed with beech. Other, less frequently occurring species include hornbeam (*Carpinus betulus L.*), European larch (*Larix decidua* Mill.), Norway spruce (*Picea abies* (L.) H. Karst), pendunculate oak (*Quercus robur* L.), silver fir (*Abies Alba* Mill.), and poplar (*Populus* spp.). The area share of the main forest types is 69 % pine, 12 % oak, 7 % beech, 3 % Douglas fir, and 9 % other in the *Hardtwald* (ForstBW, 2023), and 44 % beech, 27 % Douglas fir, 13 % pine, 9 % oak, and 7 % other in the *Bretten* forest (ForstBW, 2019).

Table 6.2: Area share of the four main forest types in each study area, as well as the area share of different age classes within each forest type. Data extracted from ForstBW (2019) and ForstBW (2023).

forest type	study area	% study area occupied	% forest type area occupied			
			age <40	age 40-80	age 80-120	age >120
pine	Hardtwald	69	7	32	26	35
	Bretten	13	0	34	66	0
beech	Hardtwald	9	6	56	35	3
	Bretten	44	7	23	39	31
oak	Hardtwald	12	5	95	0	0
	Bretten	9	18	28	46	8
Douglas fir	Hardtwald	3	3	86	10	0
	Bretten	27	12	48	40	0

Although precipitation in the region is generally evenly distributed throughout the year, an increase in heat days and prolonged droughts during the summer months has been observed in recent years (DWD Climate Data Center, 2023), leading to increased drought stress and damage to various tree species, especially on the sandy soils of the Rhine valley. So far, there have been no major forest fires in the study area (and no recordings by EFFIS (2023) between 2018 and 2023), but in the hot and dry August of 2022 there were several smaller fires (0.1 to 5 ha) in the *Hardtwald*, presumably caused by arson (ka-news, 2022). Given the expected increase in fire risk in the future, an understanding of the fuel situation in these forests and its relationship to fire behaviour is needed to better prepare for managing such fires.

6.2.3 Field data

Surface fuels were inventoried from May to September 2020 and 2021 in 119 circular field plots (radius=7.5 m, area=176.6 m²) distributed in a stratified random sampling across the study areas. Information on dominating canopy tree species, as available from stand maps based on forest inventories that are part of the German Forsteinrichtung (ForstBW, 2019, 2023), was used for stratification. The measured surface fuel components in each field plot include all dead and live fuels within 2 m above the ground: litter, dead woody fuels separated into 1 hr, 10 hr, 100 hr, and 1000 hr fuels, live herbaceous fuels (hereafter referred to as herb fuels), mosses, and live woody fuels (young trees and shrubs, hereafter referred to as shrub fuels). Fuel loads were obtained for all surface fuel components following the protocol by Woodall and Monleon (2008) As most operational fire behaviour models are based on the Rothermel equation (Rothermel, 1972), which assumes that only the fine biomass of the shrubs (plant parts <6 mm in diameter, i.e. foliage and fine twigs) within 2 m above the forest floor contributes to surface fire spread, we calculated both total shrub woody biomass and shrub fine biomass within this 2 m height-layer to describe the shrub fuels. Details of the field measurements and data preparation are given in Appendix B. In addition to the fuel loads, we measured litter depth and the height of herbaceous and shrub layers and calculated the depth of the fuelbed by weighting the different fuel heights based on their contribution to total surface fuel load (Burgan & Rothermel, 1984). Species and diameter at breast height (DBH) of all trees in the plots were recorded, and the dominant overstory tree species in each plot was determined from the basal areas of the occurring tree species. This information was used to define the forest type (**Table 6.3**).

Table 6.3: Overview of the number of field plots in different forest types and per class of mean DBH and tree count.

	all	**mean DBH <=20 cm** (tree count >15)	**20 cm< mean DBH <=40 cm** (5< tree count <=15)	**mean DBH >40 cm** (tree count <=5)
beech	25	5 (11)	14 (11)	6 (3)
oak	25	10 (7)	11 (14)	4 (4)
pine	29	6 (7)	19 (13)	4 (9)
Douglas	29	3 (15)	8 (10)	18 (4)
other	11	0 (5)	7 (6)	4 (0)

The field dataset was checked for outliers in the individual fuel components. In four fuel components, we removed 1-2 plots with loads far above the remaining data (>5 times the standard deviation away from the mean of the data), which were not representative for the study area.

6.2.4 Lidar data

Lidar data of the study area were acquired in July 2019 using a Riegl LMS-VQ780i scanner on board a Cessna C207 aircraft. The flight was operated at an altitude of 650 m with a flight line overlap of 76 %. The lidar system acquired data at a pulse repetition rate of 1000 kHz with a scanning angle of ±30° from nadir. The signal was recorded as full waveforms with a footprint diameter of 0.16 m and then transformed into discrete points with an average spacing of 0.28 m, resulting in a point density of >16 points/m² in a single flight line and a point density of >72 points/m² with overlap in the final dataset. There was a time lag between the lidar acquisition (2019) and the field measurements (2020 and 2021), but no major disturbances (fire, windthrow or disease) occurred in the study area in the meantime.

A digital terrain model (DTM) at 0.5 m spatial resolution was calculated from the lidar point cloud using a surface estimation method based on active contours that matches an elastic surface to the assumed terrain points (lowest point in each cell of a raster area) by minimising an energy function (Elmqvist et al., 2001). The DTM was then subtracted from the raw point cloud to obtain a normalised point cloud. DTM calculation and subtraction were performed in TreesVis (Weinacker et al., 2004). From the normalised point cloud, all points falling into a field plot were extracted using FUSION (McGaughey, 2022). For each plot, a large number of metrics were calculated to comprehensively describe the arrangement of reflected pulses across vertical forest stand layers (herb layer from 0 to 0.5 m, shrub layer from 0.5 to 5 m and canopy from 5 m to top) and thus characterise vegetation structure at the plot-level (**Table 6.4**). In each stand layer, metrics computation was carried ut separately for several vertical strata. Sometimes the upper and lower heights of the vertical stratum deviate from the definition of the stand layer, e.g. in case of the herb layer. For this layer we found that the height of grasses and forbs often exceeded 0.5 m. Thus, we attributed features up to 1 m to the herb group. Also, some features require a neighbourhood of points outside the stratum for their calculation, in which case the lower height does not start at 0 m.

The lidar metrics were grouped into five predictor groups: 1) geometric features as proposed by Weinmann et al. (2015) were used to describe the local 3D shape of the point cloud within a neighbourhood radius of 0.5 and 1 m. We assumed that these features might help to distinguish for example vertically oriented objects like stems from more volumi-

nous objects like shrubs. Nine geometric features based on the eigenvalues and eigenvectors of the 3D structure tensor were calculated. 2) density features such as the number of points in a vertical stratum, either normalised by the total number of points in the vertical column or the number of points within and below the stratum. Such features been used extensively to describe vegetation cover and density in a given layer (Campbell et al., 2018; Ewald et al., 2014) and have been shown to correlate with fuel load (Bright et al., 2017; Skowronski et al., 2007). 3) intensity information of the lidar returns has been used successfully to filter live (higher intensity returns) and dead tree biomass (lower intensity returns) (Kim et al., 2009) or distinguish live understory components from coarse woody debris (Wing et al., 2012) and could therefore yield information about the presence of different surface fuel components. We did not apply intensity normalisation to our data because elevation differences in our study area were small and only minor improvements were expected according to previous studies (Korpela et al., 2010; You et al., 2017). 4) height metrics were computed to characterise the distribution of returns along the vertical profile of the forest, which has proven useful in previous fuel studies (Bright et al., 2017; Jakubowksi et al., 2013; Stefanidou et al., 2020) and 5) voxel metrics derived from voxelisation of the point cloud into 0.5 m cubic voxels were used to capture horizontal variation of point densities within a vertical stratum (e.g. leaf area density as described in (Carrasco et al., 2019) to account for potential effects of fuel continuity on fuel loads. Density, intensity, height and voxel metrics were computed in Python 3.8 (van Rossum & Drake, 2009), geometric features were calculated with the Python package 'jakteristics' (Caron & Messal, 2020).

6.2.5 Multispectral satellite data

We obtained five cloud-free (<10 % cloud cover) Sentinel-2 scenes as surface reflectance products from five acquisition dates in 2020 (2020-04-04, 2020-05-19, 2020-07-23, 2020-09-21, 2020-11-30). We extracted area-weighted means of the reflectance in the 10 and 20 m bands (bands 2, 3, 4, 5, 6, 7, 8, 8A, 11, 12) from the pixels covering our field plots and additionally calculated a set of spectral indices and biophysical canopy traits using ESA's Sentinel-2 processing toolbox SNAP and Python 3.8 to enhance specific vegetation characteristics. These included leaf area index (LAI), fractional vegetation cover (FCOVER), fraction of absorbed photosynthetically active radiation (FAPAR) (Weiss & Baret, 2016), normalised difference vegetation index (NDVI) (Tucker, 1979), enhanced vegetation index (EVI) (H. Q. Liu & Huete, 1995), normalised difference moisture index using both SWIR bands 11 and 12 (NDMI, NDMI_2) (Hardisky et al., 1983), soil adjusted vegetation index (SAVI) (Huete, 1988), as well as tasseled cap wetness and greenness (TCW, TCG) (Kauth & Thomas, 1976). A total of 480 lidar metrics and 100 features derived from Sentinel-2 data were calculated, resulting in 580 potential predictors of surface fuel loads, litter, and fuelbed depth (**Table 6.4**)

Table 6.4: Overview of the predictors calculated from airborne lidar and Sentinel-2 data.

source	predictor type	features	aggregation on plot-level	stand layer	vertical strata (lower height - upper height in m)	no. of features
Lidar	geometry	anisotropy, eigenentropy, omnivariance, sum of eigenvalues, linearity, planarity, sphericity, verticality, surface variation for neighborhood radii 0.5 and 1 m *(equations in **Table B1** in Appendix B)*	mean	herb	0.1-0.5, 0.25-0.5, 0.5-1	54
				shrub	1-2, 2-3, 3-4, 4-5, 0.5-2, 0.5-5	108
				canopy	5-10, 10-15, 15-20, 20-25, 25-30, 30-max, (max-1)-max, (max-2)-max, (max-5)-max	162
	density	no. points in each stratum relative to no. points within and below the stratum, no. points in each stratum relative to no. points in vertical column	-	herb	0.1-0.5, 0.25-0.5, 0.5-1	6
				shrub	1-2, 2-3, 3-4, 4-5, 0.5-2, 0.5-5	12
				canopy	5-10, 10-15, 15-20, 20-25, 25-30, 30-max, (max-1)-max, (max-2)-max, (max-5)-max, 5-max, mean-max	16
	intensity	return intensity	mean, variation, standard deviation, coefficient of variation, skewness	herb	0-0.5	5
				shrub	0.5-2, 0.5-5	10
				canopy	(max-1)-max, (max-2)-max, (max-5)-max	15
	voxel	no. non-empty voxels per stratum, mean no. points per voxel per stratum, standard deviation of no. points per voxel per stratum, coefficient of variation of no. points per voxel per stratum, coefficient of variation of leaf area density per voxel per stratum, standard deviation of leaf area density per voxel per stratum	mean	herb	0-0.5, 0.5-1	12
				shrub	1-2, 2-3, 3-4, 4-5	24
				canopy	5-10, 10-15, 15-20, 20-25, 25-30, 30-max	36
	height	return height	maximum, quantiles (q99, q95, q90, q75, q50, q25, q10), mean, variance, standard deviation, coefficient of variation, skewness, kurtosis	all layers	-	15
			variance	herb	0.1-0.5, 0.25-0.5	2
				canopy	(max-1)-max, (max-2)-max, (max-5)-max	3
Sentinel-2 5 scenes	bands	B2, B3, B4, B5, B6, B7, B8, B8A, B11, B12 reflectances	area-weighted mean of plot-overlapping pixels	all/canopy	-	50
	indices	LAI, FCOVER, FAPAR, NDVI, EVI, NDMI, NDMI_2, SAVI, TCW, TCG	area-weighted mean of plot-overlapping pixels	all/canopy	-	50
total						580

6.2.6 Feature selection

From the 580 calculated features, a pre-selection was made for modelling each surface fuel component. For this purpose, lidar and multispectral predictors were grouped according to their type (geometry, density, intensity, height, voxel, spectral bands, indices) and the forest stand layer for which they were calculated (herb, shrub, canopy; or all stand layers together in the case of height metrics, spectral bands and indices). This resulted in 15 different groups of predictors (see columns in **Figure 6.3** in Results section), e.g. one group would contain only geometric predictors within the herb layer. A pre-selection of two features from each group was conducted to remove redundancy and multicollinearity among predictors by choosing the ones with the highest Spearman correlation with the modelled target and a correlation coefficient <0.7 between the two features. The set of 30 pre-selected features was further reduced by using the automated "Variable Selection Using Random Forests" (VSURF) algorithm (Genuer et al., 2015) in R (v4.2.2, R Core Team, 2022) to obtain a subset optimised for predicting the respective fuel component.

6.2.7 Random forest modelling

Random forest (RF) regression was chosen to explain the variability in loads of different surface fuel components across the study area, as the method generally reaches good performance on datasets with a large number of predictors that may have non-linear relationships with the response variable (Breiman, 2001; Strobl et al., 2009). Furthermore, it does not make any formal distributional assumptions about the response variables, which is useful in case of the right-skewed fuel load data, and allows to estimate the importance of different predictor variables. For each fuel component, we trained an RF model on the predictor subset obtained from VSURF using all available samples, and performed a grid search on hyperparameters to optimise the out-of-bag (oob) score of the model and thus reduce overfitting. A new model was trained with the best-scoring hyperparameters and validated using leave-one-out cross-validation (LOOCV). Model performance was evaluated using the coefficient of determination (R^2), root mean squared error (RMSE), relative RMSE (rRMSE) and RMSE normalised with the data range (nRMSE) between random forest predictions and observed fuel load values of the validation data. Our limited sample size of n=117-118 (depending on the fuel component and outliers removed) did not allow an additional hold-out test set; however, RF oob score and cross-validation results showed high agreement and were thus considered reliable estimates of model performance. In addition to the RF model trained on the predictor subset obtained from all predictor types after applying VSURF, we modelled surface fuel loads based on individual predictor types to assess their respective predictive power. For this, we used the pre-selected features from each vertical forest stratum that belonged to the same predictor type, and repeated the VSURF and model training procedure on the new variable subset.

6.2.8 Comparison of remote sensing-based estimates and average fuel loads

We compared the errors of remote sensing-based continuous fuel load estimates with errors of average fuel loads for different forest types (defined by the dominant overstory tree species). In this approach, the fuel loads in a field plot were estimated based on the fuel loads in all other plots of the same forest type. The average of the other plots' fuel loads

was taken (separately for each fuel component) and assigned to the plot under consideration, similar to a leave-one-out procedure. RMSE between the forest type-based average values and the observed fuel loads was compared to the RMSE of the RF model based on remote sensing data. Furthermore, we tested for differences in surface fuel loads between forest types defined by dominant tree species using a non-parametric Kruskal-Wallis test (Kruskal & Wallis, 1952) followed by Dunn's test (Dunn, 1964) as post hoc non-parametric test.

6.2.9 Predictor importance and interpretation

To assess the relevance of the selected variables for predicting the different fuel components, we calculated the permutation feature importance for each feature (Breiman, 2001). This importance metric reveals how much the model relies on a feature by breaking the relationship between feature and target through random permutation of the feature (Molnar, 2022). Additionally, to better understand the relationships between features and modelled target, we computed the accumulated local effect (ALE) of each feature (Apley & Zhu, 2020). ALE gives the relative effect of changing the feature on the prediction within a small interval of the feature. ALE plots are better suited than partial dependence plots to assess the influence of a feature on the prediction when features are correlated (Molnar, 2022). The latter applied to some extent to our dataset even after removing highly correlated features. ALE plots were produced using the python package 'ALEpython' (Jumelle et al., 2020), which allows to create many Monte Carlo replicas by randomly drawing samples from the data and computing ALE on them, thus reflecting its potential variability.

6.2.10 Surface fuel maps

To obtain fuel load maps at a spatial resolution reflecting the size of our field plots, we resampled the Sentinel-2 data to a pixel size of 14 m using bilinear interpolation, binned the lidar point cloud into 14 m grid cells, and calculated all features relevant for the predictions for each grid cell. We predicted fuel load maps for the entire study area using the RF models trained on all samples. Fuelbed depth was predicted using separate RF models to ensure meaningful values that matched the spatial patterns of predicted surface fuels. These models were trained based on field-measured loads of the different fuel components. Maps of fuelbed depth were then predicted with these models using the fuel loads from the prediction maps for the individual fuel components created in the preceding step.

6.2.11 Modelling potential surface fire behaviour

We used spatial predictions of surface fuel loads and fuelbed depth to estimate potential surface fire behaviour in the forest stands of our study area based on the quasi-empirical Rothermel model (Rothermel, 1972). In the underlying basic model, the rate of spread (R in m min^{-1}) of a surface fire through a fuelbed (up to 2 m above the forest floor) is the ratio between the heat flux received (heat source) and the energy required to preheat and ignite the unburned fuel (heat sink) ahead of the fire (Andrews, 2018):

$$R = \frac{\text{heat source}}{\text{heat sink}} = \frac{I_R \ \xi(1+\phi_w+\phi_s)}{\varrho_b \ \varepsilon \ Q_{ig}} \quad (1)$$

Equation (1) accounts for the effects of wind and slope (ϕ_w, ϕ_s) on the proportion of heat transferred to the fuel (propagating flux ratio ξ) from the energy release at the fire front (reaction intensity I_R in kJ/(m^2 s)). The heat required to ignite the fuel depends on the bulk density of the fuel (ϱ_b in kg/m^3, calculated from load and depth), the proportion of fuel heated to ignition temperature before combustion starts (effective heating number ε), and the heat of preignition (Q_{ig} in kJ/kg), which is a function of fuel moisture, specific heat of the fuel, and assumed ignition temperature (Andrews, 2018; Sandberg et al., 2007). The basic model includes only a single size class of dead fuel, but since surface fuelbeds are a mixture of live and dead fuels of various size classes, the final model includes weighting factors based on the surface area of the fuel in each size class (giving more weight to the finer fuels). Other fire behaviour characteristics commonly modelled are fireline intensity (I_B in kJ/(m s)) as product of reaction intensity (I_R), reaction time (t_r in min), and rate of spread (R), and flame length (F_B in m) as a function of reaction intensity, both proposed by Byram (1959):

$$I_B = I_R \ t_r \ R/60 \quad (2)$$

$$F_B = 0.45 \ I_B^{0.46} \quad (3)$$

We used an implementation of the Rothermel equation and related models in R (package 'firebehavioR', Ziegler et al., 2019). All required parameters except fuel loads and fuelbed depth were held constant across the study area and set to the values shown in **Table B2** (Appendix B). Due to the low performance of our models for the prediction of coarser dead fuels, 10 hr and 100 hr loads were set to the median of all measured values (1.65 and 2.39 t/ha, respectively). Open wind speed was set to 15 km/h and fuel moisture values were based on Scott & Burgan's (2005) very low fuel moisture scenario D1L1 to reflect severe drought conditions. Fire behaviour characteristics modelled were rate of spread, fireline intensity and flame length.

6.2.12 Sensitivity analysis

We analysed the sensitivity of the Rothermel model to variations in the different surface fuel components to assess the impact that inaccuracies in fuel load estimation can have on predicted fire behaviour. To this end, we trained a random forest model using the remotely sensed loads of the fine surface fuel components (litter, dead 1 hr, live herbaceous, and live fine shrub fuels) across the study area as predictors of the fire behaviour characteristics calculated with the Rothermel model, thus ensuring realistic combinations of the different fuel components for each instance. We treated each pixel in the study area as an individual sample, since potential fire behaviour is modelled independently of the neighbouring cells. In this way, the random forest model learns the internal relationships and the weighting of the individual fuel components in the Rothermel model and can provide information on which fuel component most strongly influences the predictions. The effect of fuel load variations on predicted fire behaviour characteristics as learned by the random forest model was assessed and visualised using ALE (see Chapter 6.2.9).

6.3 Results

6.3.1 Feature selection

Spearman correlations between field-measured surface fuel components and remotely sensed predictors (**Figure 6.3**) revealed strongest correlations of lidar-derived metrics with understory fuels such as shrubs and herbs, and also fuelbed depth. The most useful lidar metrics for predicting shrub loads were found among geometric, density, and voxel features in the corresponding forest stratum. Herb load correlated most strongly with geometric, density, and intensity features within the herb layer, but multispectral satellite data also provided information on loads of herbaceous vegetation and mosses. Among the dead woody fuels, only the smallest particle size class (1 hr fuels) showed a notable correlation with multispectral predictors. All coarser dead fuels were not significantly correlated with the predictors, making them difficult to predict using a regression approach. Correlations of litter load and litter depth with the predictors were similarly weak as for dead 1 hr fuels, but were more pronounced for multispectral predictors. After running VSURF on the correlation-based pre-selected feature set (**Table B.3** in Appendix B), subsets with three to eight variables were obtained for predicting the surface fuel components. The VSURF-selected features for each surface fuel component are listed in order of their permutation feature importance in **Table 6.5**.

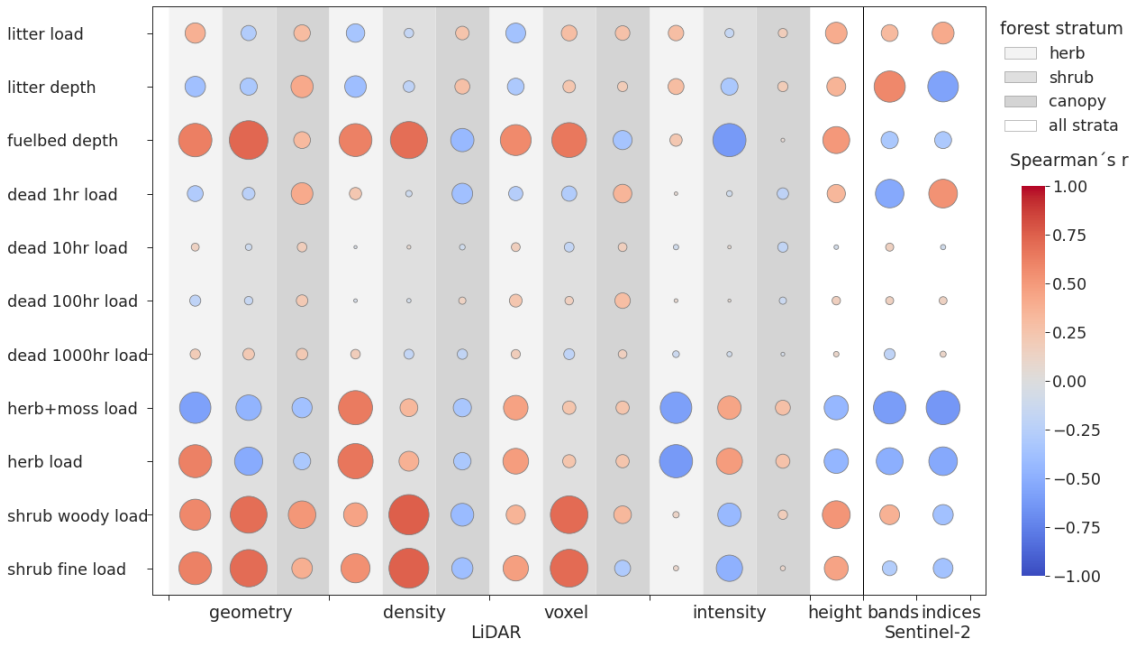

Figure 6.3: Highest Spearman correlations of the predictors in each group (defined by forest stratum and predictor type) with the fuel components. Circles are scaled such that the diameters reflect the correlation coefficient, while the column width corresponds to a correlation coefficient of 1.

Table 6.5: VSURF-selected predictors for the different surface fuel components (omitting 10-1000 hr fuels due to the poor model performance), sorted by their permutation feature importance (first feature has highest importance).

fuel component	predictors
litter load	10th percentile of lidar heights
	blue reflectance in summer
	NDVI in summer
litter depth	NDVI in early spring
	10th percentile of lidar heights
	FAPAR in autumn
	standard deviation of leaf area density between 1 and 2 m
fuelbed depth	mean omnivariance between 0.5 and 5 m (neighbourhood radius = 1 m)
	relative point density between 0.5 and 2 m
	mean return intensity in the herb layer
	relative point density between 0.5 and 1 m
dead 1 hr load	green reflectance in early spring
	NDWI in early spring
	SWIR reflectance (2190 nm) in autumn
	mean planarity between 10 and 15 m (neighbourhood radius = 0.5 m)
	number of returns in the uppermost meter of the canopy relative to vertical column
	number of returns in the 5 uppermost meter of the canopy relative to vertical column
herb+moss load	NIR reflectance (842 nm) in autumn
	EVI in autumn
	number of returns between 0.1 and 0.5 m relative to vertical column
	coefficient of variation of return intensity in the uppermost meter of the canopy
	mean linearity between 0.25 and 0.5 m (neighbourhood radius = 0.5 m)
	skewness of return intensity in the herb layer
herb load	coefficient of variation of return intensity in the uppermost meter of the canopy
	skewness of return intensity in the herb layer
	number of returns between 0.25 and 0.5 m relative to vertical column
	EVI in autumn
	NIR reflectance (842 nm) in autumn
	10th percentile of lidar heights
shrub woody load	relative point density between 0.5 and 5 m
	number of non-empty voxels between 2 and 3 m
	mean linearity between 4 and 5 m (neighbourhood radius = 1 m)
	mean anisotropy between 0.5 and 5 m (neighbourhood radius = 1 m)
	mean linearity between 10 and 15 m(neighbourhood radius = 0.5 m)
	skewness of return intensity between 0.5 and 5 m
shrub fine load	mean eigenentropy between 1 and 2 m (neighbourhood radius = 1 m)
	relative point density between 1 and 2 m
	mean linearity between 3 and 4 m (neighbourhood radius = 1 m)
	visible and NIR reflectance (783 nm) in winter
	mean omnivariance between 0.5 and 1 m (neighbourhood radius = 1 m)
	coefficient of variation of return intensity between 0.5 and 5 m
	mean return intensity in the herb layer
	skewness of lidar heights

6.3.2 Random forest modelling

Random forest models best explained variation in shrub woody load (R^2=0.64, **Figure 6.4 e**), while explained variation in shrub fine load was notably lower (R^2=0.39, **Figure 6.4 f**). Herb load variation was moderately well explained (R^2=0.55-0.56, **Figure 6.4 c-d**), while model performance for litter and dead 1 hr loads was rather low (R^2=0.27 and R^2=0.41, **Figure 6.4 a-b**). RMSE was highest for litter loads (2.57 t/ha), followed by shrub woody loads (2.08 t/ha), while the other fuel components had errors between 0.30 and

0.49 t/ha. The nRMSE was around 15 % for all fuel components, but rRMSE was highest for shrub and herb loads (84.2 % to 126.7 %) due to the many plots with very small fuel loads in these components (**Figure 6.4 c-f**). As expected from the weak correlations between the remotely sensed predictors and the coarser dead fuel loads (10, 100, and 1000 hr fuels, **Figure 6.3**), the RF models explained very little variation (R^2=0.02-0.12) and are not shown here. These fuel components are not included in the further analysis (the 1000 hr fuels are also not considered in Rothermel's fire spread model). Litter and fuelbed depth were modelled with rather low accuracies based on remotely sensed predictors (R^2=0.40-0.44, **Figure 6.4 g-h**), but fuelbed depth was reasonably well modelled using loads of the different fuel components (R^2=0.72, **Figure 6.4 i**).

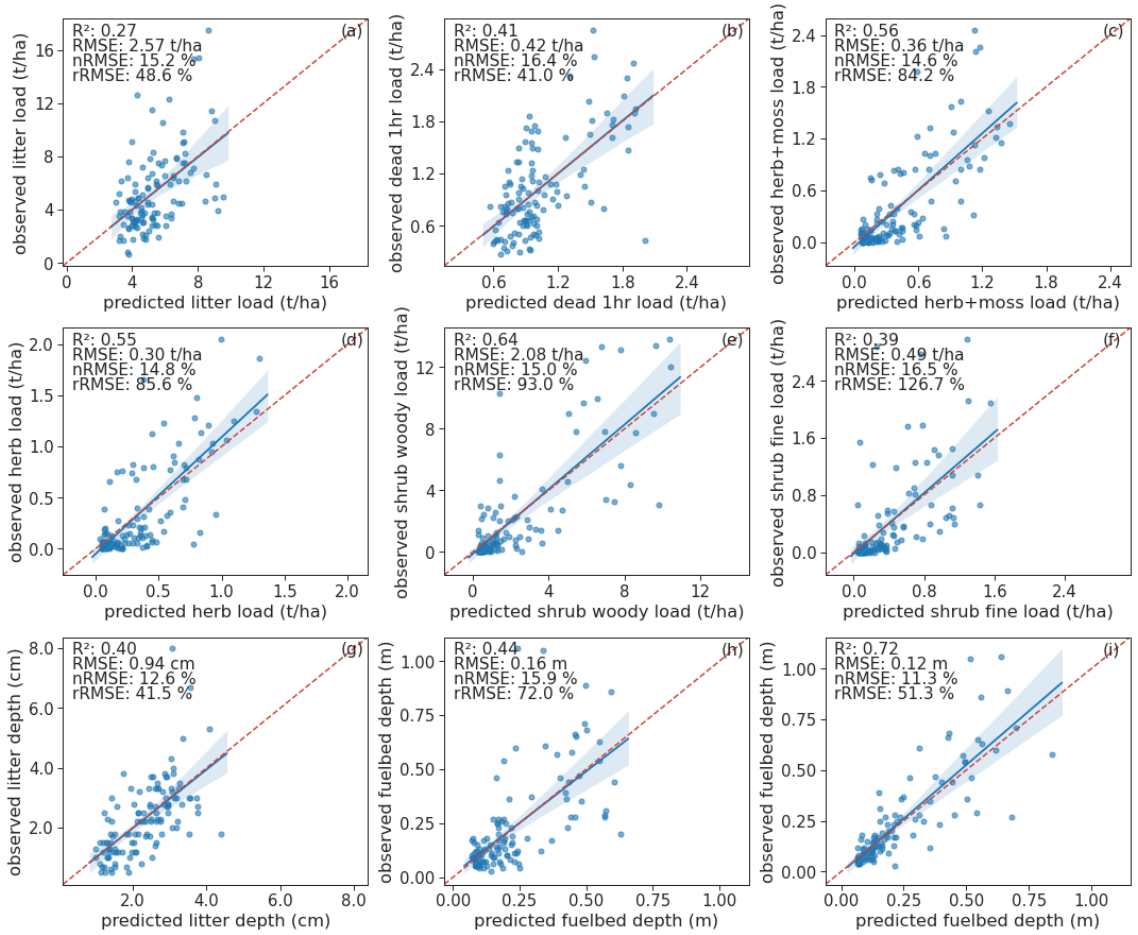

Figure 6.4: Scatterplots showing observed (y) and predicted (x) surface fuel loads, litter and fuelbed depth from random forest regression and the model evaluation scores. Blue solid lines show the estimated regression line between predicted and observed values together with the 95 % confidence band, the red dashed line is the 1:1 line. Plots h) and i) both show results for fuelbed depth, h) shows the predictions based on remote sensing metrics and i) the predictions based on fuel loads.

We tested mixed effect random forests and included forest type as a random effect in the model; however, this did not improve the overall results. We also tested a multi-output regression with random forest to predict all surface fuels using a single model, as dependencies between the fuel components are present, albeit weak, but this approach did not improve the results either.

6.3.3 Results for individual predictor types

Model performance based on individual predictor types (**Table 6.6**) reflected the observed patterns of correlation strength (**Figure 6.3**). Results show that modelling surface fuel components benefits from the synergetic use of different predictor types, as models based on variables from all predictor types (described in **Table 6.4**) consistently performed best. esults also reveal that stand attributes such as height are insufficient for modelling surface fuel loads and that all other lidar-derived features are mostly relevant for predicting understory fuels rather than litter fuels. Litter loads are generally the most difficult to model, while models for litter depth are slightly better. Both litter and dead 1 hr fuels benefit from combining lidar and spectral predictors, whereas shrub loads and fuelbed depth are not well predicted from spectral features and rely more on lidar features alone. Herb biomass is slightly better predicted from all lidar features than from spectral predictors, but estimates are improved by combining both. Interestingly, previously unexplored variables such as geometric features have the potential to adequately describe point clouds for fuel mapping, as models based on them sometimes even outperform models based on density features.

Table 6.6: R^2 and RMSE of models based on predictors of different types. Modelling was omitted if the number of VSURF selected predictors was <2. The best metrics per fuel component are shown in bold.

		geo-metry	den-sity	voxel	inten-sity	height	all lidar	spec-tral	all predic-tor types
litter load	R^2	0.12	0.12	0.03	0.03	-	0.13	0.15	**0.27**
	RMSE (t/ha)	2.84	2.82	3.06	3.03	-	2.87	2.80	**2.57**
dead 1 hr	R^2	0.23	0.25	0.12	0.09	0.09	0.35	0.36	**0.41**
load	RMSE (t/ha)	0.49	0.48	0.52	0.53	0.54	0.44	0.44	**0.42**
herb+moss	R^2	0.47	0.38	0.30	0.27	0.14	0.53	0.41	**0.56**
load	RMSE (t/ha)	0.39	0.43	0.45	0.47	0.50	0.38	0.42	**0.36**
herb load	R^2	0.34	0.33	0.33	0.30	0.14	0.48	0.31	**0.55**
	RMSE (t/ha)	0.37	0.37	0.37	0.38	0.43	0.33	0.38	**0.30**
shrub fine	R^2	0.32	0.25	0.25	0.18	-	0.33	0.13	**0.39**
load	RMSE (t/ha)	0.53	0.55	0.55	0.57	-	0.51	0.59	**0.49**
shrub woody	R^2	0.53	0.54	0.36	0.33	0.01	**0.64**	0.13	**0.64**
load	RMSE (t/ha)	2.38	2.33	2.79	2.83	3.43	**2.08**	3.24	**2.08**
litter depth	R^2	0.22	0.16	0.05	0.08	-	0.30	0.25	**0.40**
	RMSE (cm)	1.09	1.14	1.20	1.18	-	1.02	1.07	**0.94**
fuelbed	R^2	0.42	0.34	0.31	0.26	0.20	**0.45**	0.07	0.44
depth	RMSE (m)	0.17	0.18	0.18	0.19	0.20	**0.16**	0.22	**0.16**

6.3.4 Predictor importance and interpretation

ALE plots are presented and explained for the feature with highest permutation importance (**Table 6.5**). Litter loads are predicted using spectral features and the 10^{th} percentile of lidar heights (**Figure 6.5 a**), which describes the height below which 10 % of returns fall: the higher it is, the more returns are found in elevated stand layers, i.e. the canopy, and the lower this value is, the more returns are found near the ground. In the latter case, returns are most likely produced by understory, the presence of which indicates more light penetration and thus a less dense canopy that produces less litter. Litter depth is predicted using similar features and decreases most with higher NDVI in early spring (**Figure 6.5 b**): NDVI at this time of the year is higher in the younger pine and in the Douglas fir stands of

our study area, where understory herbs are developing, and lower in the deciduous beech stands, where highest litter layers accumulate. Fuelbed depth is predicted using lidar features only and increases most with the mean local omnivariance in the shrub layer (0.5 to 5 m) (**Figure 6.5 c**): higher omnivariance corresponds to a more inhomogeneous spread of points over a 3D volume (Waldhauser et al., 2014), indicating the presence of objects with high roughness, such as shrubs or small trees with voluminous structure. Dead 1 hr loads are predicted by spectral rather than lidar features: Reflectance in the green band in early spring is negatively related to predicted loads of dead 1 hr fuels (**Figure 6.5 d**) and lowest reflectance is found in Douglas fir stands, which, due to their crown structure with a high proportion of fine twigs, produce the largest amount of fine dead fuel. The most important features for predicting herb load including mosses are also spectral ones: Predicted loads are higher when reflectance in the NIR band (842 nm) in autumn is lower (**Figure 6.5 e**), which is the case for the coniferous species in the study area. When mosses are excluded from herb biomass, lidar features become more important, but the model still relies on a canopy trait as most important predictor: as the coefficient of variation of lidar return intensity in the uppermost canopy layer increases, modelled herb loads increase (**Figure 6.5 f**). Higher variation in intensity values could be related to the more discontinuous canopy of coniferous trees and less dense canopies in general (e.g. oaks compared to beech), favouring the interaction of the laser beam with different types of surfaces (leaves, exposed branches) of different reflectivity (Fassnacht et al., 2016; Kim et al., 2009). Shrub loads are modelled using lidar features only: While shrub woody loads increase with mean point density in the layer between 0.5 and 5 m (**Figure 6.5 g**), the model for fire-relevant shrub fine load is more sensitive to returns between 1 and 2 m (**Figure 6.5 h**), which corresponds to the requirement to stay within 2 m above the forest floor. The higher the eigenentropy of the point cloud in this layer, i.e. the higher the disorder of points, the more fine shrub material is predicted.

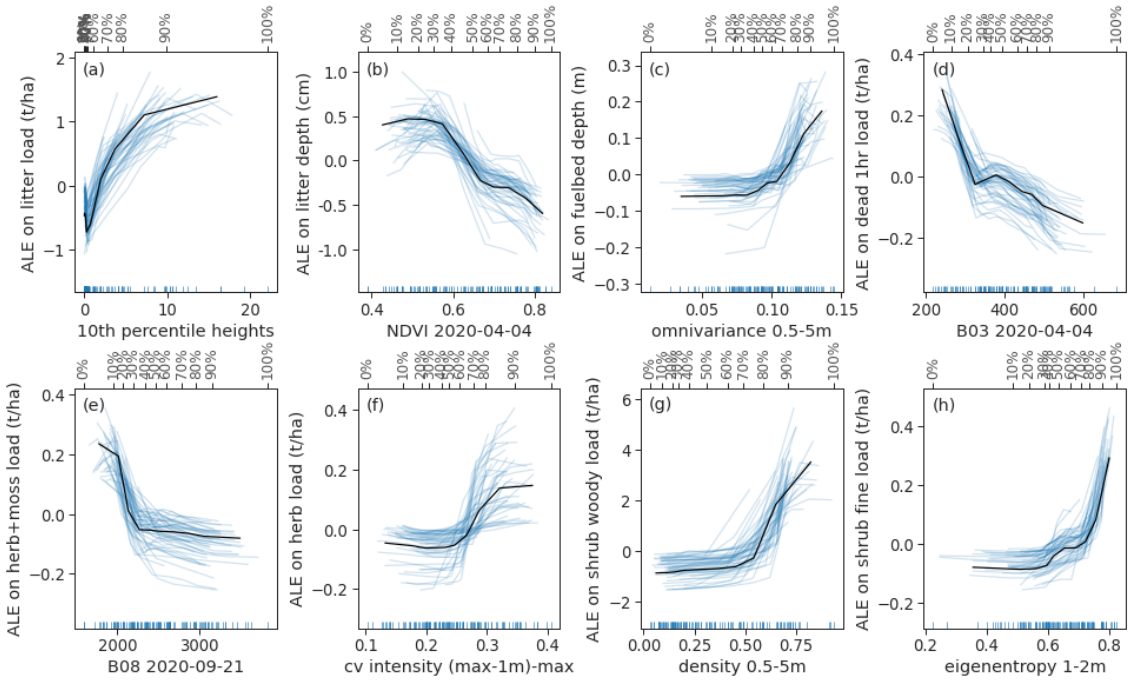

Figure 6.5: ALE plots for the most important predictor of each surface fuel component. Effects are centered at zero, which means that an ALE of zero is simply the average prediction and deviations from zero indicate that the prediction is lower/higher than the average prediction by that

value. Blue thin lines show the Monte Carlo replicas. Quantiles of the predictor are plotted on the upper axis (percentage values).

6.3.5 Comparison of remote sensing-based estimates and average fuel loads

Comparison between errors of the remote sensing-based fuel load estimates and errors of the average fuel load estimates based on the four main forest types (**Table 6.7**) shows that canopy-related fuels such as litter and dead 1 hr fuels can be predicted with comparable accuracy by forest type alone. In our study area, litter loads were significantly higher in beech stands than oak, Douglas fir and pine stands, while dead 1 hr loads were significantly higher in Douglas fir stands compared to pine, beech and oak stands (**Figure 6.6**). Understory vegetation was predicted with lower RMSE using the remote sensing-based models compared to forest type-based predictions. Maximum error reduction (40 %) using the RF model based on remote sensing data was achieved for shrub woody load (**Table 6.7**). In our study area, differences in herb load (both with and without moss) and shrub load between forest types were small. Significant differences were only found in herb load between Douglas fir and beech stands and in shrub woody load between Douglas fir and beech or pine stands. Shrub fine biomass was significantly higher only in pine stands compared to Douglas fir stands (**Figure 6.6**).

Table 6.7: Comparison of RMSE of fuel loads between random forest models based on remotely sensed metrics and predictions based on average values per forest type.

	RMSE of RF model (t/ha)	RMSE of average fuel loads (t/ha)	error reduction when using RF models (%)
litter	2.57	2.83	9
dead 1 hr	0.42	0.45	7
herb+moss	0.36	0.50	28
herb	0.30	0.44	32
shrub fine	0.49	0.65	25
shrub woody	2.08	3.49	40

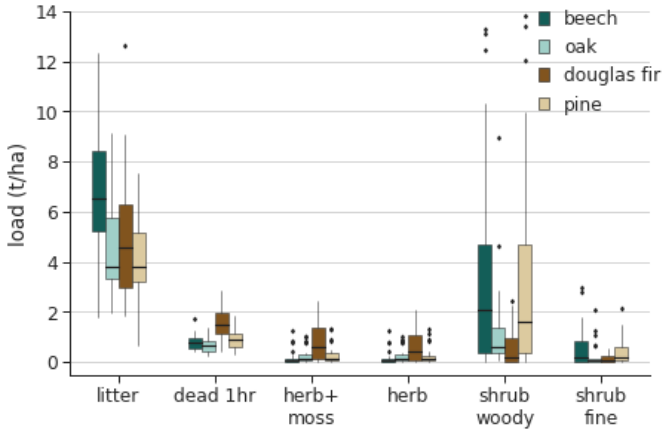

Figure 6.6: Loads of surface fuels for the four main forest types. Three outlier points of litter loads are beyond the y-axis range shown.

6.3.6 Surface fuel maps

Maps are shown for fuel components that have the greatest influence on surface fire behaviour, i.e., the fine dead and live fuels (**Figure 6.7**). Litter load ranges from 2.8 to 9.9 t/ha in the study areas, with higher mean and variance (6.4 ± 1.3 t/ha) in *Bretten* compared to *Hardtwald* (5.2 ± 0.9 t/ha). Dead 1 hr load varies between 0.5 and 2.0 t/ha and is again slightly higher and more variable in *Bretten* (1.0 ± 0.3 t/ha) than in *Hardtwald* (0.9 ± 0.2 t/ha). Herb load ranges from 0 to 1.8 t/ha with similar mean and variance (0.4 ± 0.3 t/ha) in both study areas. Fine shrub load ranges between 0 and 2.0 t/ha and is lower on average in *Bretten* (0.4 t/ha) than in *Hardtwald* (0.5 t/ha), but equally variable (± 0.3 t/ha).

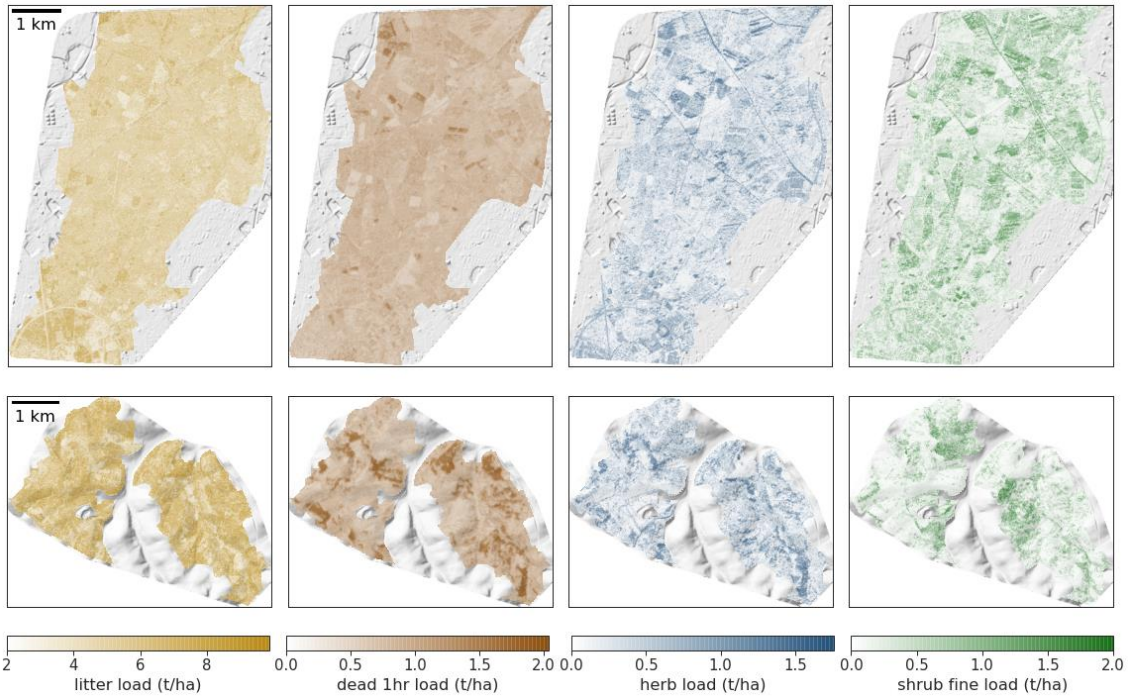

Figure 6.7: Predicted fuel load maps on hillshades of the study areas *Hardtwald* (upper panels) and *Bretten* (lower panels).

6.3.7 Potential surface fire behaviour

Surface fires are predicted to have low intensity in large parts of the study area (mean fireline intensity = 228 kW/m) under the given parametrisation of physical fuel properties, moisture and wind speed (**Figure 6.8**). The highest fireline intensity (1269 kW/m) can be found in a part of the eastern *Bretten* forest, where predicted flame length and spread rate also show maximum values (2.1 m and 5.4 m/min, respectively). Mean potential flame length for the study areas is 0.9 m, and mean rate of spread is 1.6 m/min. All three fire behaviour characteristics show similar patterns across the study areas and suggest a high correlation with the underlying fuel load patterns.

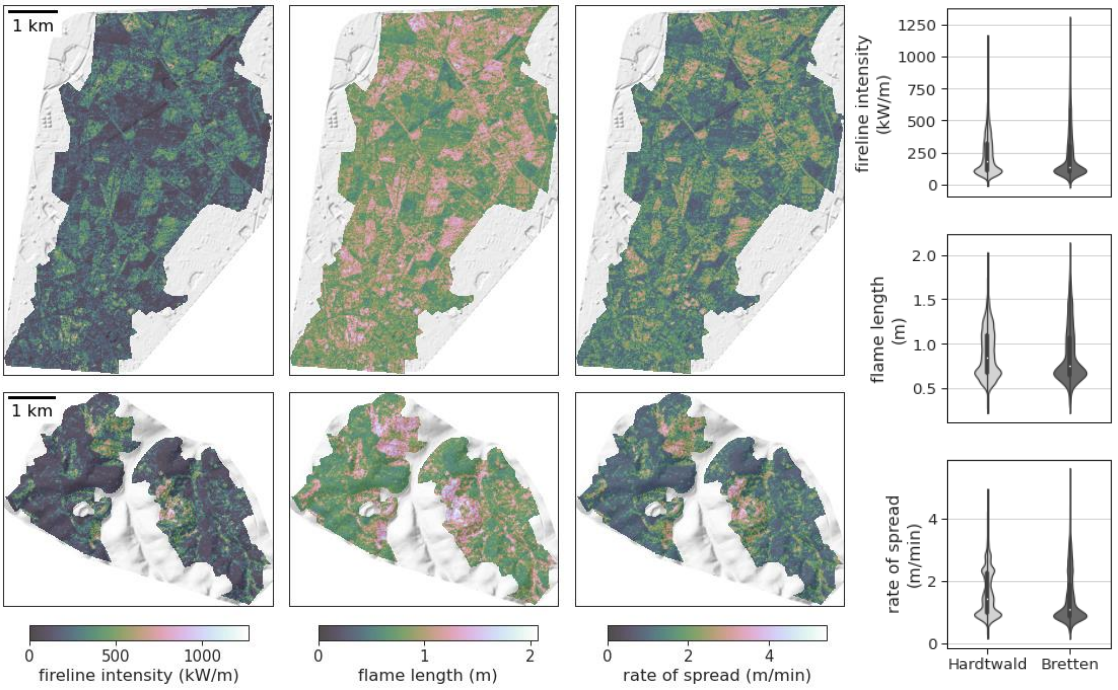

Figure 6.8: Potential surface fire behaviour in the study areas as characterised by fireline intensity (left), flame length (middle) and rate of spread (right), and violinplots for the three characteristics per study area. Fire behaviour was calculated assuming 15 km/h open wind speed and extremely low fuel moisture (scenario D1L1, see Scott and Burgan, 2005).

6.3.8 Sensitivity analysis

Examining the effects of individual fuel components on modelled fire behaviour characteristics using a random forest model (R^2=0.92-0.96 on independent test set, **Figure B1** in Appendix B) reveals that shrub load has by far the highest influence on the modelled output, despite the small range of values in the study area, as indicated by the steepness of the ALE curve (**Figure 6.9**). All fire behaviour characteristics become more severe with increasing shrub load, while dead 1 hr fuels and herb fuels seem to have a negligible effect. Increasing litter load also leads to higher modelled intensities and flame lengths, while the effect on spread rate is minor. Errors in shrub and litter load predictions thus have the greatest impact on modelled potential fire behaviour and underestimated loads in particular can lead to severly underestimated fire behaviour. **Figure B2** (Appendix B) shows how modelled fire behaviour in the study areas changes when loads of fine shrub and litter fuels are both increased by their model RMSE (0.49 t/ha and 2.57 t/ha, respectively, and fuelbed depth adjusted accordingly).

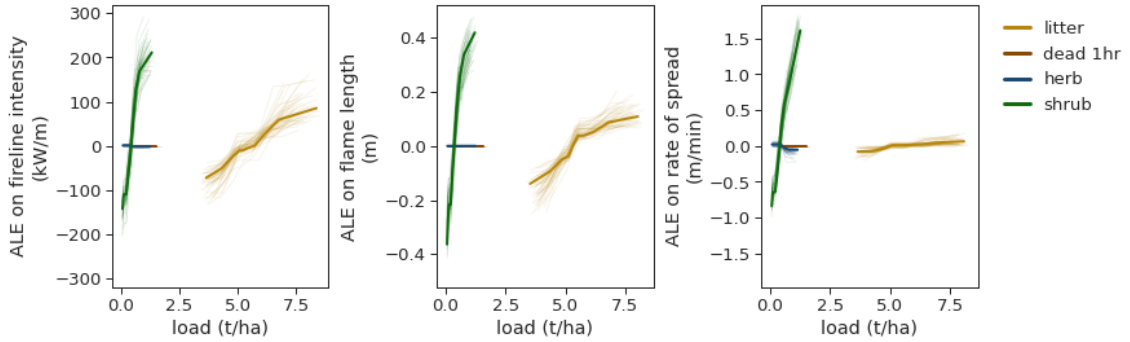

Figure 6.9: ALE of surface fuel loads on the fire behaviour characteristics in the study area.

6.4 Discussion

6.4.1 Potential and limitation of surface fuel load predictions using remote sensing

Our results show that random forest regression models based on lidar and multispectral variables describing forest composition and structure are able to predict loads of surface fuel components in heterogenous mixed forests of Central Europe with moderate to low accuracy.

Litter and fine woody fuels

Consistent with previous studies from different ecosystems (e.g. Alonso-Rego et al., 2021; Bright et al., 2017; Jakubowksi et al., 2013), ground-based fuels such as litter and deadwood were the most difficult to estimate accurately from remote sensing data. We found that the variability in litter and dead 1 hr loads was mostly explained by remotely sensed predictors capturing canopy properties, rather than by lidar reflections near the ground itself, and that the accuracy of the predictions was generally low. A possible reason for this is that litter and fine woody fuels (dead 1 hr) can vary at centimeter scales depending on the microtopography of the forest floor, the presence of herbaceous plants and mosses, or fallen branches under which especially dead needles and fine twigs accumulate. This heterogeneity may not be adequately represented in the field data, and additionally airborne lidar data were probably not fully capable of capturing this variation, both of which add uncertainty. Previous studies have shown that even with terrestrial laser scanning it is not possible to obtain information on litter or 1 hr fuel loads with sufficient accuracy (Arkin et al., 2023). Our results indicate that the captured variability in litter and fine woody fuels is mostly explained by differences in litter and fine fuel production between different tree species and canopy densities, which are reflected in the multispectral data. However, the low observed accuracies suggest that litter and 1 hr fuel loads are determined by additional factors that cannot be captured with the remote sensing data used. For example, litter loads are closely linked to decomposition rates, which depend not only on litter chemistry but also on temperature and humidity, soil conditions and microbial activity (Krishna & Mohan, 2017) and are therefore related to the general site conditions. As fuel sampling was performed from May to October in two consecutive years, different stages of litter decomposition may have added further variability to the data. We also sometimes found leaf litter from neighbouring trees blown into our field plots. The comparable error when using aver-

age fuel loads based on forest types suggests that detailed remote sensing data provide only little added value in predicting litter and 1 hr fuel loads. This is in line with the finding of Alonso-Rego et al. (2021), who report as little as 10 % variance explained in litter and duff loads of pure even-aged pine stands based on ALS metrics, and those of Bright et al. (2017), who explain 16 % (24 %) of variation in litter and duff loads using ALS only (in combination with disturbance-related metrics derived from Landsat time series), and 21 % (28 %) in 1–100 hr fuels in a study area with multiple coniferous species. However, it is contrasting the findings of Stefanidou et al. (2020), who explain 69 % of variation in litter loads and 59 % in dead 1 hr loads using multispectral lidar in a study area with pure fir overstory and suggest that lidar is interacting with the litter fuels in a direct manner. One reason for the rather low accuracies in our study may be the structurally and compositionally complex forest stands, making it difficult to disentangle the different drivers (e.g. tree species, age, and stand or canopy density) of measured fine fuel loads at the forest floor, unless these relationships are studied based on a substantially larger dataset. Our study suggests that in such cases, multispectral remote sensing data that allow reliable classification of forest types can be considered the most efficient option for predicting litter and fine woody fuel components through association with average loads that need to be determined for a forest type and site, even though this method has limited accuracy. The forest type-specific fuel loads could be refined by either coupling them with a biophysical model predicting rates of fine fuel accumulation and decomposition throughout the year (e.g., Hanan et al., 2022), or an empirically derived model that links seasonal variations in fine fuel loads to remotely sensed phenological variations in trees (e.g., Zeilhofer et al., 2012).

Coarse woody fuels

For the coarser dead fuels, we could not develop a model that was able to explain the variation in loads. While Jakubowksi et al. (2013) similarly reported little correlation between ALS metrics and 1000 hr fuels, Bright et al. (2017) explained 30 % variance in 1000 hr loads based on ALS metrics only and 32 % in combination with Landsat-derived disturbance metrics, and Alonso-Rego et al. (2021) reported 41 % variance explained in combined woody debris load using ALS. Combined estimates were not made in our study, and the weak results for the individual woody fuel components can be explained by the variability and many zeros in the observed loads in our study area, especially for the coarsest particle size class of the 1000 hr fuels, for which the calculated loads depend strongly on the geometry of the lying stems (diameter and length). Furthermore, the occurrence of these fuel particles is highly heterogeneous both within a field plot and in the entire forest stand. The field plot size thus influences the fuel variability captured, and additionally determines the sensitivity to registration errors between field plots and lidar or satellite data (especially when only few pixels overlap with the field plots, as in our case). Due to the heterogeneous distribution of downed wood, detecting logs in high-resolution optical imagery (preferably acquired from below canopies) or lidar point clouds and then determining the volume of the individual logs, as has been done successfully by e.g. Lopes Queiroz et al. (2020) and Jarron et al. (2021), would be better suited to approximate loads. Accurate localisations of lying logs may actually be more useful for fine-scale fire behaviour analyses and for assessing the accessibility of forest areas for firefighting, but fuel models for spatial fire applications still include area-based loads for coarse fuels. However, a manual examination of our lidar point cloud suggested that in heterogeneous stands with understory presence, even large logs are difficult to resolve and lidar penetration to the ground is sometimes significantly reduced depending on canopy density. Also 10 hr (0.63-2.54 cm diameter) and

100 hr (2.55-7.62 cm diameter) fuel loads are difficult to map, which is not surprising given the relatively large footprint of several centimetres in airborne lidar acquisitions. But even with terrestrial lidar, it is difficult to quantify loads of 10 hr and 100 hr fuels (Arkin et al., 2023). Lastly, the amount of coarse dead fuels is less predictable by tree species composition than litter and dead 1 hr fuels: their occurrence is more random as it depends on forest management activities such as logging and pruning or natural disturbance such as windthrow and falling branches after strong winds or heavy snowfall. Mortality can also be influenced by different soil conditions, which affect a tree's susceptibility to drought. In our case, the time lag between lidar acquisition and field measurements might have further affected the prediction, as interventions such as removal of deadwood or accumulation of branches after strong winds might not have been recorded in one of the datasets. Remote sensing can help identify major disturbance events and detect trees that may become deadwood sources after insect infestation or drought (Brodrick & Asner, 2017; Kislov et al., 2021), but accurate quantification of accumulating woody debris at the forest floor remains challenging and especially management effects will be difficult to account for as long as no direct and timely detection of deadwood is possible.

Herb and moss fuels

Understory fuel load in the herb layer was moderately well predicted using our RF models. Prediction of moss and herb fuels relied mostly on multispectral features (**Table 6.5**), as their occurrence in our study area is strongly biased towards conifer stands, which contrast strongly with broadleaved stands in the spectral domain. As expected, information on canopy characteristics was helpful in predicting herbaceous fuel loads, because canopy composition and density control the amount of light reaching the forest floor. Tree cover alone, as reflected in the lidar metrics and also estimated in the field, was not as strongly correlated with herbaceous fuel loads as the multispectral features. However, structural information from below the canopy obtained from lidar data was also useful and gained importance when herbaceous biomass was predicted independently of mosses. The variance explained with our herb load model was similar to what is reported in a study predicting herbaceous cover from airborne lidar in temperate forests (Latifi et al., 2017), but despite the high point density of our dataset, we could not reach the performance of models based on TLS-derived metrics (S. Li et al., 2021; Wallace et al., 2017). As biomass does not only depend on cover, but also on plant height and bulk density and thus on the type of understory vegetation or more specifically the species present (Bolte, 2006), these metrics need to be estimated precisely, which is unlikely to be achieved based on ALS. But even if the vegetation volume of the herb layer cannot be derived as accurately as from TLS point clouds, ALS-derived cover (and height) estimates may still allow to approximate biomass if species information is available. Such information could be derived from existing knowledge of herbaceous plant communities that develop under specific site conditions, and should take into account seasonal variations in their composition and condition (e.g., spring flowering and senescence). Our data showed that there was a slightly decreasing trend in measured herbaceous biomass over the year (Spearman's $r = -0.42$), which is important to consider for dynamic fuel estimates. Despite limitations, models based on remotely sensed structural and spectral metrics can improve the prediction of herbaceous loads compared to predictions based on forest types alone.

Shrub fuels

Shrub fuel load predictions relied almost exclusively on lidar metrics and provided reasonable accuracy for shrub woody loads, but poorer results for the more fire model-relevant fine biomass. Shrub load is species-dependent like herb load and additionally determined by wood density (Annighöfer et al., 2016), and therefore not perfectly correlated with cover and/or height extracted at plot-level. While shrub cover has been well predicted from airborne lidar point clouds (Wing et al., 2012), difficulties in estimating shrub height from lidar have been reported when different shrub species are present (Alonso-Rego et al., 2021). Having included geometric features as descriptors of point cloud shape in our study may not have been sufficient to account for the effects of different growth forms on biomass. However, these features may still offer potential for improving approaches to understory species segmentation (e.g., D. Wang, 2020) as basis for developing species-specific biomass models from point cloud data. Additionally, geometric features have been successfully applied in leaf-wood classifications of forest point clouds (Krishna Moorthy et al., 2020) and could serve to separate the fire model-relevant fine shrub load in this way. We also acknowledge that our reference shrub load data are subject to considerable uncertainty: their accuracy is limited by the availability of accurate allometric equations for calculating biomass from diameter at stem base (DAB), and by the accuracy of the biomass partitioning into different plant compartments used to estimate fine biomass in our study (see Appendix B). It is also well known that growth morphology of understory trees and shrubs, even of the same species, changes with light conditions: In our study area, despite having the same DAB, young beech trees in particular either had long stems with branches and leaves located further from the ground or remained rather small depending on light availability. This has an important impact on the biomass available near the ground that can burn in a surface fire. In addition, in a few cases there were still branches of mature trees in the surface fuel layer, but these were not included in the measurement of shrub fuels. The only way to avoid this uncertainty is to collect all the shrub material within the fire relevant layer and sort it by particle size, which is often not feasible due to time and personnel constraints. Alternatively, existing approaches to characterise shrubs from dense point clouds acquired with terrestrial laser scanning (e.g. Hudak et al., 2020; S. Li et al., 2021) could be used to calibrate better models for shrub woody and fine biomass. Overall, the inclusion of detailed structural information derived from airborne lidar was more relevant for the prediction of shrub fuel loads than for any other fuel component, and this approach should be favoured over assigning average fuel loads based on forest types. The same is true for the closely related fuelbed depth if it is not estimated from the fuel loads themselves.

6.4.2 Surface fuel maps and potential surface fire behaviour

Despite the limited performance of the remote sensing-based models, the generated fuel load maps show clear patterns that match field observations of the respective fuel components and can thus inform forest managers and firefighters about the fuel situation at a fine scale. Modelled potential fire behaviour remains unvalidated due to lack of reference data from real fires in the study area. However, our results were broadly consistent with the findings of Heisig et al. (2022), who reported similar surface fuel load ranges in a study area dominated by Scots pine, European beech and red oak in north-western Germany, and modelled fire behaviour under different environmental conditions. They used constant fuel loads depending on forest type and found the spatial patterns of fire behaviour to be close-

ly linked to those of the surface fuel models. Under the same moisture scenario and a wind speed half of ours, they simulated a mean spread rate of 2.6 m/min and flame length of 2.5 m, which is about twice as high as our values. Considering the known difficulty of predicting realistic fire behaviour based on actual fuel loads (Burgan, 1987), we conclude that the absolute values should be treated with caution. Nevertheless, we assessed how errors in fuel load estimates affect predicted fire behaviour through the mechanistic relationships in the Rothermel model and found that errors in shrub load have the strongest effect, followed by litter load. This is most likely due to the effect of the presence of shrubs on fuelbed depth, which strongly impacts bulk density of the fuelbed and thus changes the estimated rate of spread and associated fire characteristics. We also noted that the assumption of the Rothermel model that fuel particles are homogeneously distributed over the fuelbed was not fulfilled in our study: bulk density decreased from the bottom of the litter layer to the top of the fuelbed, but this was not reflected in the averaged fuelbed depth and bulk density, which probably led to underestimated fire spread rates (Cruz & Fernandes, 2008). The remarkable effect of litter load on fireline intensity and flame length is due to its influence on reaction intensity, which is a function of net fuel load (Andrews, 2018), of which litter is the largest component in this study. As the two most influential fuel components were at the same time associated with the highest prediction error in our models, we recommend that future research on surface fuels in temperate forests should focus on improving estimates of litter and shrub fuel loads, as well as fuelbed depth.

6.5 Conclusion

Statistical relationships between remotely sensed metrics describing forest composition and structure and surface fuels have some potential for estimating fuel loads in Central European forest types. Still, we confirm previous studies in other ecosystems that establishing robust relationships is challenging. Random forest regression based on multiple spectral and structural characteristics derived from airborne lidar and multispectral satellite data showed that a combination of different metric types is most useful for fuel load estimation. It also revealed that previously unexplored metrics such as geometric features calculated from lidar point clouds may be an interesting alternative to the more commonly used density-related metrics. Multispectral information is most useful for estimating canopy-related fuels such as litter and dead 1 hr fuels, but can also be linked to other relevant stand properties, such as the presence of mosses under certain tree species. Multispectral information in combination with lidar helps to estimate herb fuels, while shrub fuels can be estimated with lidar alone, and results can probably be improved by developing adequate biomass models from selected metrics. Dead woody fuels are difficult to relate to metrics aggregated at field plot level and may be better captured with object-based approaches on TLS or photogrammetric data. The data-driven regression approach and feature-selection process employed in this study are efficient; however, the application of more sophisticated (point cloud) processing methods targeting the individual fuel components and their spatial scale of variation may help to improve the estimates. For dynamic fuel load estimates, ecological processes and knowledge of management and disturbance events must also be included. Extending the method to larger areas is limited by the availability of high-resolution airborne lidar data, but spaceborne lidar data from instruments such as GEDI and spaceborne radar data could be a possible substitute that needs further research. In general, remote sensing-based fuel load predictions were more accurate than average fuel loads based

on forest type. However, the latter can be sufficient for fuel components that are relatively constant underneath a certain tree species at a certain site, e.g. litter and dead 1 hr fuels. Understory fuels and fuelbed depth, in contrast, should be estimated at finer scales, preferably using structural information derived from lidar. This is important given their strong influence on fire dynamics, which is also reflected in the high sensitivity of fire behaviour models to variations in understory, particularly shrub fuel loads.

Acknowledgements

This work was funded by the German Federal Ministry of Food and Agriculture and Federal Ministry for the Environment, Nature Conservation and Nuclear Safety as part of the project "ErWiN" (code 2219WK54A4). We would like to thank the anonymous reviewers for their valuable comments and suggestions to improve this manuscript.

7 Assessing fuel dynamics

This chapter has been submitted as:
Labenski, P., Millin-Chalabi, G., Pacheco-Pascagaza, A. M., Senn, J. A., Fassnacht, F. E., Clay G. D. (under review). An optical satellite-based analysis of phenology and post-fire vegetation recovery in UK upland moorlands.

Abstract

Vegetation fuel dynamics in upland moorlands of the United Kingdom (UK) are important in determining landscape susceptibility to wildfire. Temporal changes in fuel availability and condition occur as a result of phenology, land management activities or unplanned disturbances such as wildfires. Understanding the annual cycle of different vegetation types and their recovery after disturbance is therefore essential to assess wildfire risks and impacts. Monitoring fuel dynamics at the landscape level can be accomplished using time series of remote sensing data.

In this study, we examined the ability of optical remote sensing time series from Sentinel-2 (2017-2023) to capture phenology and vegetation recovery in four important upland land cover classes (acid grassland, heather, heather grassland, and bog). We used harmonic modelling of time series of vegetation indices (VIs) to characterise phenological changes in key fuel properties such as moisture, live and senescent biomass, and to identify periods of potentially high vegetation flammability. We also investigated the immediate and long-term effects of wildfires on remotely sensed vegetation characteristics by quantifying VI change and spectral recovery times. Therefore, we developed an efficient workflow to estimate spectral recovery in highly cloud-influenced time series and compared the remotely sensed estimates with field measurements. Finally, we assessed the influence of various environmental factors on spectral recovery times using multiple linear regression.

We found that the period of highest potential vegetation flammability spans from mid-February to early May in acid grassland, while it extends into early June in heather and heather grassland, and into late June in bog. Changes in remotely sensed fuel properties were more pronounced after summer fires compared to spring fires, with the largest spectral changes observed in moisture-related VIs. Spectral recovery of graminoid-dominated land cover was rapid, taking less than one year, and aligned well with field observations. Spectral recovery of dwarf shrub-dominated areas was slower, requiring up to three years, broadly consistent with measurements of vegetation cover on burned areas but not with height. Spectral recovery times were primarily explained by land cover class, burn severity, season, and winter snow cover (R^2=0.66). Field data confirmed the influence of pre-fire stand age on heather recovery and underscored the strong influence of grasses on the spectral signal. These results enhance our understanding of fuel dynamics in upland moorlands using satellite-based monitoring of vegetation flammability and post-fire recovery. The findings can be used to inform wildfire risk assessments and management plans.

7.1 Introduction

The UK upland moorlands are recognised as a unique landscape of significant importance, containing Sites of Special Scientific Interest (SSSI) (Galbraith & Stroud, 2022), and fulfil diverse ecosystem functions. They provide a habitat for wildlife, including rare and endangered species (Van der Wal et al., 2011), sequester significant amounts of carbon (2302 Mt) (Billett et al., 2010), and are a source of drinking water for 43.1 % of the UK population (J. Xu et al., 2018). Moreover, they provide grazing for livestock and a place for recreational activities, and thus have both cultural and economic value (Van der Wal et al., 2011). As semi-natural ecosystems, the moorlands have been maintained for centuries by grazing and burning. The most well-known land management practice is rotational burning of common heather (*Calluna* vulgaris (L.) Hull, hereafter *Calluna*) to create a mosaic of stands of varying age for red grouse (Kirkpatrick, 2013).
However, past land-use practices such as intensive agricultural drainage and peat cutting, atmospheric deposition of industrial pollutants, as well as climate change have degraded the moorlands (Shepherd et al., 2013). Wildfires also pose a significant threat, especially during periods of dry weather and high winds (Albertson et al., 2009). Severe wildfires cause damage to the ecosystem and release large amounts of carbon into the atmosphere through the combustion of aboveground biomass (Clay & Worrall, 2011), and, in particular, when burning into the peat soil (Maltby et al., 1990).
Fighting wildfires, especially in remote areas, is difficult and costly. During episodes with multiple ignitions and low fuel moisture, resource allocation becomes a major challenge for the Fire and Rescue Services (McMorrow, 2011). Additionally, the frequency of weather conditions favouring high wildfire activity are projected to double under 2 °C of global warming (M. C. Perry et al., 2022), exacerbating the risk of larger uncontrolled fires. Between 2009 and 2021, 2,495 wildfires were recorded in the English uplands, predominantly in mountainous, heath, bog and semi-natural grassland areas, burning the largest land area of all wildfires in England (43,000 ha, 54.1 %) (Forestry Commission, 2023). In addition to increasing fire danger from meteorological conditions, especially in summer (Arnell et al., 2021), future fire regime depends on ignitions and the availability of vegetation fuel. Records of wildfire incidents show that wildfires primarily occur in spring or summer, when plant material is in a flammable state due to winter desiccation or low moisture content during hot and dry summer periods (Albertson et al., 2010).

The amount of fuel available for combustion depends on the plant species and the accumulation of live and dead biomass through growth and mortality. Fuel dynamics in upland plant communities are naturally driven by the life cycle of *Calluna*, which consists of four phases: pioneer, building, mature, and degeneration (Gimingham, 1972). These growth stages are associated with changes in plant structure and vitality (Schellenberg & Bergmeier, 2022), as well as important fuel characteristics such as the relative abundance of live and dead fuels, and of fine and coarser woody fuels within the *Calluna* canopy (Davies et al., 2009; Taylor et al., 2022).
Layered onto the life cycle stage, *Calluna* also has an annual phenological cycle. It comprises spring growth, a flowering phase lasting through August and September, and leaf senescence over late summer and autumn (Mac Arthur & Malthus, 2012). The presence of other deciduous species in *Calluna*-dominated habitats, such as purple moor-grass *Molinia caerulea* (L.) Moench (hereafter *Molinia*), and fern *Pteridium aquilinum* (L.) Kuhn (hereafter bracken), contributes to a strong seasonal dynamic in fuel quantity and condition. During the grow-

ing season, green biomass is produced, which then undergoes autumnal senescence and eventually forms a pool of dead plant material (Taylor et al., 2022).
Whether plant material is in a flammable state depends primarily on its fuel moisture content (FMC). The FMC of dead plant material is strongly driven by atmospheric conditions, and very dry conditions are quickly reached through evaporation when humidity is low (<50 %), e.g. during high-pressure situations (M. C. Perry et al., 2022). Live vegetation is less responsive to weather changes, and FMC is more closely related to the plant's physiological state and soil moisture. With the seasonal transition from living to cured foliage in deciduous species, FMC can vary considerably throughout the year, from 30 % in the cured state to 250 % during green-up (Burgan, 1979). Laboratory experiments with *Molinia* have shown a high probability of ignition and almost complete consumption at less than 65 % FMC (Taylor et al., 2022). Daily measurements of live FMC in *Calluna* carried out by Davies (2005) during autumn and spring in the Scottish Highlands showed that it was comparatively low (65-100 %) and a substantial decline was observed in early spring (<45 %). The probability of ignition in *Calluna* has also been shown to depend on the amount of dead fuel in the canopy and its FMC (Santana & Marrs, 2014).

As fuel quantity and condition of the pre-fire vegetation are important drivers of fire behaviour, they directly influence the impact of the fire on the landscape. High fuel biomass in very dry condition leads to intense fires, causing severe ecosystem damage. Assessing the short-term and long-term effects of wildfires helps decide if and where costly restoration activities are needed. Also, understanding post-fire vegetation recovery is important for planning how long an area will be unavailable for livestock grazing and when management actions may be required again (Kirkpatrick, 2013).
Previous studies have shown that vegetation recovery after burning in heather moorlands depends on various factors, including fire severity (Davies, Smith, et al., 2010; Grau-Andrés et al., 2019): Low-severity fires can facilitate rapid resprouting of *Calluna* shoots from stem bases, but this ability declines as plants age. High-severity fires can damage stem bases, in which case regeneration depends on seeds (Legg et al., 1992). However, prolonged exposure of the ground to elevated temperatures destroys seed banks, resulting in slow and incomplete recovery (Maltby et al., 1990). Under such circumstances, burned areas may be particularly vulnerable to invasion by other graminoids, bryophytes and herbs (Grau-Andrés et al., 2019; Velle & Vandvik, 2014). For instance, perennial *Molinia* grass, with its large and deep root system, can withstand intense fires and produces a large amount of seeds. Growth and seed production have been shown to increase after fire, resulting in high biomass production and litter accumulation (Brys et al., 2005).

While on-the-ground assessments are indispensable to understand how wildfire alters the landscape, satellite remote sensing provides a cost- and time-effective way to obtain information on pre-fire vegetation status and post-fire development, especially in areas with limited accessibility. Time series from optical sensors, e.g., Landsat, MODIS, AVHRR and Sentinel-2, have been successfully used to observe vegetation dynamics in response to wildfires or managed burns in shrub- and grassland ecosystems (Lees et al., 2021; Potter, 2018; Sankey et al., 2013; Villarreal et al., 2016). These studies have largely focused on Normalised Difference Vegetation Index (NDVI) to track the reemergence of vegetation greenness and phenological variation. However, NDVI is sensitive to soil background in sparse vegetation and suffers from saturation problems in dense vegetation, limiting its effectiveness in monitoring vegetation status (Z. Wang et al., 2022). Accounting for the influence of soil background by using the Soil-Adjusted Vegetation Index (SAVI) has proven to be

more effective in discriminating burn areas in heathland environments (Schepers et al., 2014). However, greenness is not the only important variable in characterising vegetation, especially from a wildfire perspective, where plant senescence and moisture status are crucial factors. Limited research has been conducted on the potential of satellite data to characterise phenology and post-wildfire vegetation recovery in moorland habitats.

Al-Moustafa et al. (2012) showed that vegetation indices combining near-infrared (NIR) and shortwave infrared (SWIR) reflectance derived from airborne hyperspectral imagery strongly correlate with live FMC in *Calluna* plots at a moorland site. Similarly, Badi (2019) found a strong positive relationship between the Normalised Difference Water Index (NDWI) (B. Gao, 1996) calculated for multi-temporal Sentinel-2 and Landsat imagery and measured *Calluna* FMC. This spectral index, which is sensitive to plant water content, is also referred to as Normalised Difference Moisture Index (NDMI) (E. H. Wilson & Sader, 2002).

Senescent biomass is less frequently assessed in remote sensing studies, including those in upland moorland vegetation. However, Metzger et al. (2017) found that estimates of biomass and the green ratio in a temperate grassland fen based on NDVI were poor due to the presence of standing senescent biomass. Guerini Filho (2020) estimated senescent plant biomass in the grasslands of the Brazilian Pampa from Sentinel-2 data, using among others the Plant Senescence Reflectance Index (PSRI), with moderately accurate results. PSRI calculated from field spectroscopy has been shown to indicate phenological change in upland vegetation species and was useful for discriminating between plant functional types (Cole et al., 2014b). However, PSRI based on spectroradiometer measurements had limited correlation with leaf pigment content of *Calluna* (Nichol & Grace, 2010), leaving the applicability of the index for monitoring plant senescence across moorland land cover classes using satellite data for investigation.

Lees et al. (2021) assessed vegetation regeneration in UK moorland areas after low-severity management fires using NDVI time series, but suggested a comparison with other indices and field assessments of vegetation recovery would be beneficial. Millin-Chalabi (2016) used pre- and post-fire Synthetic Aperture Radar (SAR) signals to characterise wildfire burn scars and assess their persistence in peat moorlands. The study showed that increased SAR backscatter of burned areas can persist for more than six months post-fire and indicate incomplete vegetation recovery. However, the pre- and post-burn conditions and the effect of wildfires of varying severity on the optical remote sensing signal of different upland land cover classes have not been investigated. This is due to the challenges posed by frequent cloud cover in upland environments particularly in the UK.

Therefore, in this study, we applied a multi-index approach based on time series of Sentinel-2 data to capture key fuel characteristics of UK upland vegetation and provide a more comprehensive understanding of both phenology-driven fuel dynamics and vegetation recovery after wildfire. We utilised optical vegetation indices (VIs), which have proven useful in previous studies, to highlight specific vegetation properties. We focused on SAVI as a proxy for live/green vegetation cover, PSRI for dead/senescent vegetation cover, and NDMI as proxy for FMC. Additionally, we included the commonly used indices NDVI and Normalised Burn Ratio (NBR) in our analysis. The NBR has become a standard index to assess burn severity across different ecosystems (e.g. Boelman et al., 2011; Schepers et al., 2014). Our study aimed to evaluate the potential of optical remote sensing to characterise fuel dynamics in upland land cover classes and enhance our understanding of wildfire impacts on the landscape by addressing the following research questions:

i) What is the remotely sensed phenology of key fuel properties of UK upland land cover classes, and how is it related to records of wildfire occurrence?

ii) To what extent do remotely sensed fuel properties change, and what is the timeframe for their recovery following a wildfire?

iii) How do remote sensing observations align with field measurements of vegetation recovery?

iv) How are remotely sensed vegetation recovery times influenced by environmental factors?

7.2 Methods

This study focuses on the moorlands of the South Pennines in northern England, encompassing the Peak District National Park (PDNP) and Marsden Moor. The PDNP covers an area of 1,438 km², ranging in altitude from 12 to 636 m. While the northern part and the eastern and western margins are characterised by moorland and gritstone formations of the Dark Peak, limestone plateaus and gorges dominate the White Peak in the central and southern parts (PDNPA, 2013). The land cover classes of the Dark Peak are mainly heather moorland, bog, and acid grassland, whereas the White Peak is characterised by calcareous and improved grassland, and woodland (**Figure 7.1**). Wildfires recorded in the PDNP over the past decades have been concentrated in the Dark Peak (Moors for the Future, 2023). Therefore, acid grassland, heather, heather grassland, and bog are the focus of this study. The UK Centre for Ecology and Hydrology (UKCEH) Land Cover Map (LCM2021) (Marston et al., 2022) defines these land cover classes as follows: acid grasslands can have a variable composition of grasses, rushes, herbs, and sedges, but are often dominated by *Molinia*. Heather land cover is distinguished from heather grassland by a cover of more than 25 % *Calluna*. Bogs include areas of ericaceous, herbaceous, and moss species on deep peat soils (>0.5 m).

7.2.1 Datasets

Satellite data

We obtained time series of Sentinel-2 surface reflectance (harmonised Level-2A collection) with a spatial resolution of 10 m from Google Earth Engine (GEE). All scenes from 2017-04-01 to 2023-09-20 that covered the study area and had a maximum cloud cover of 50 % were included. Clouds were masked based on the Sentinel-2 cloud probability product using a threshold of 40 % probability for masking. Cloud shadows were removed based on NIR reflectance, while snow and ice were masked based on the scene classification band (SCL) of the Sentinel-2 product. For each of the masked scenes, we calculated the VIs listed in **Figure 7.1** using the eemont package (Montero, 2021). All processing was done via the GEE Python API in Google Colab.

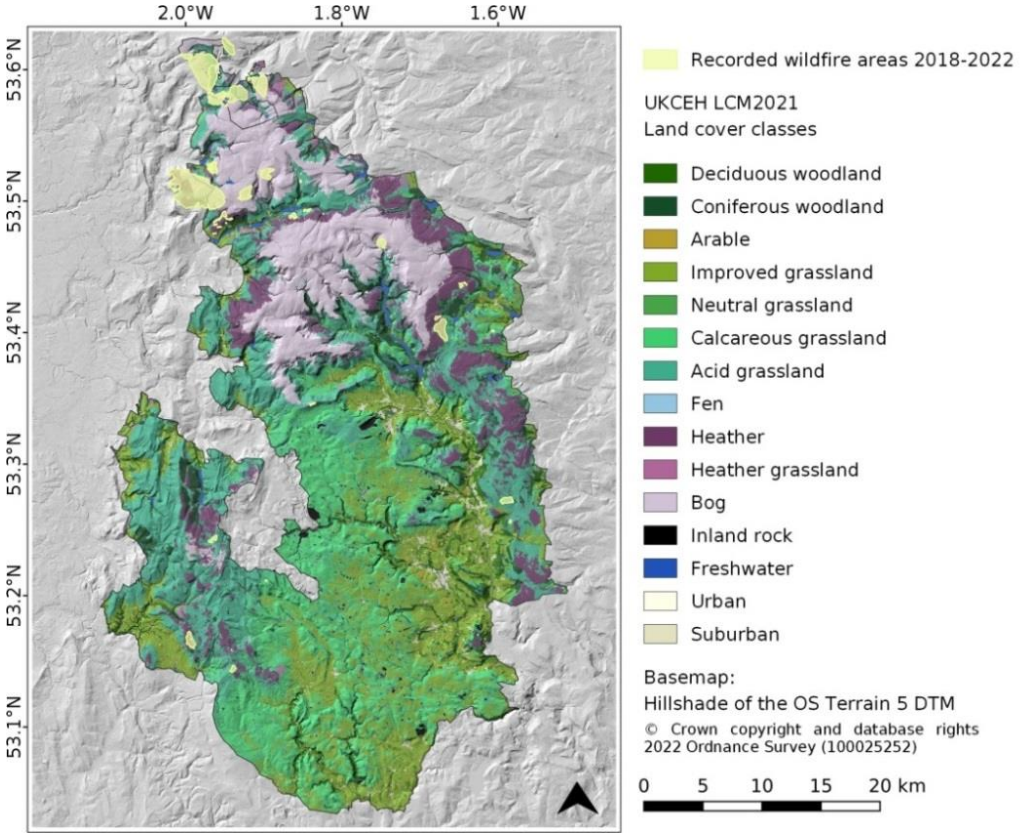

Figure 7.1: South Pennines study area showing the land cover classes and wildfire areas considered in this study.

Table 7.1: Sentinel-2 VIs used in this study. Bands were renamed as follows: B8:NIR, B9:NIR2, B11: SWIR1, B12:SWIR2, B6:RedEdge2.

index	proxy for	equation	reference
NDVI	vegetation greenness, live biomass	$\frac{NIR-Red}{NIR+Red}$	Rouse et al. (1974)
SAVI	vegetation greenness, live biomass, accounts for soil effects	$\frac{NIR-Red}{NIR+Red+L}(1+L),\ L=0.5$	Huete (1988)
NDMI	FMC	$\frac{NIR-SWIR1}{NIR+SWIR1}$	Wilson and Sader (2002)
PSRI	vegetation senescence, dead biomass	$\frac{Red-Blue}{RedEdge2}$	Merzlyak et al. (1999)
NBR	vegetation structure, intact vegetation biomass	$\frac{NIR2-SWIR2}{NIR2+SWIR2}$	Coffelt and Livingston (2002)

Wildfire data

Records of wildfire incidents in the PDNP were downloaded from the local wildfire recording system managed by the Moors for the Future Partnership (Moors for the Future, 2023). The database contains polygons that delineate wildfire perimeters based on field observations of burned areas, as well as additional information such as fire start and end dates. We cross-checked the polygons from the wildfire log with wildfires recorded in the European Forest Fire Information System (EFFIS) (San-Miguel-Ayanz et al., 2012) to ensure no large wildfires were missed. We obtained 45 wildfire polygons covering a five-year

period from 2018-01-01 to 2022-12-31. For each fire, we visually inspected the closest cloud-free pre- and post-fire RGB and NBR images from Sentinel-2. As a measure of fire severity, we calculated the differenced NBR (dNBR) for each wildfire area by subtracting post-fire from pre-fire NBR of the previously selected images. We removed wildfires with a dNBR<0.1 from the dataset, as we expected a very weak signal in the remote sensing indices from these low-severity fires. We also removed fires that were obviously management burns, as indicated by the many small burn strips in the satellite imagery. Ultimately, we obtained a dataset of 38 wildfire polygons with different severities and burned areas in the four land cover classes (**Figure 7.2**).

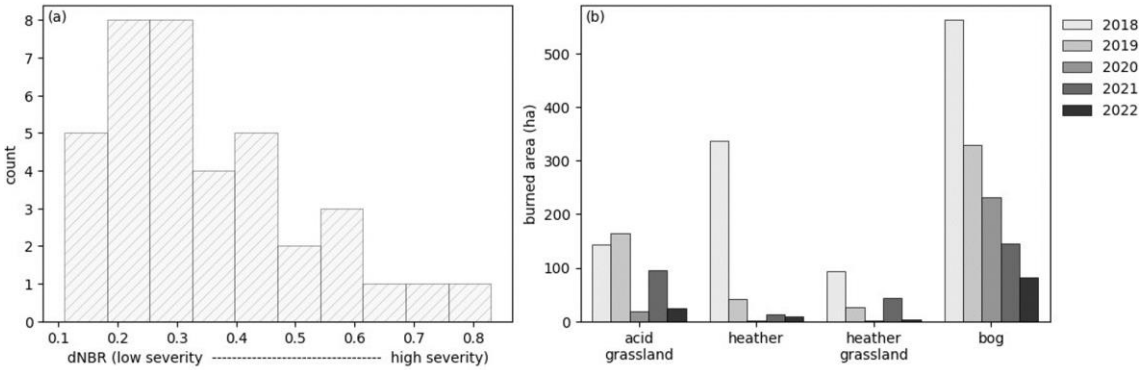

Figure 7.2: (a) Burn severity of individual wildfires and (b) burned area in different land cover classes per year.

Field data

We collected data on post-fire vegetation recovery in 14 wildfire areas in the South Pennines during a field campaign 3-14 July 2023. Long-term vegetation recovery is ideally assessed over several years, but adopting a space-for-time approach is a common strategy in ecology (e.g. Harper, 2020; Thomaz et al., 2012). We also used this approach, acknowledging that the results must be interpreted cautiously, as the burn conditions of the individual wildfires were different. We visited two to three wildfire areas from each year between 2018 and 2023 and measured vegetation cover and height in two to six plots per area, and in 15 plots in the large Tameside wildfire area (also Saddleworth Moor fire, e.g. Graham et al., 2020) (**Table C1**, Appendix C). The locations of the 10×10 m plots were selected to encompass landscape heterogeneity. We used an adapted version of the FIREMON point intercept method (Lutes et al., 2006) to sample vegetation cover, condition, and height. The sampling was conducted along three parallel 10 m transects positioned at 0, 5, and 10 m along the plot baseline. At 50 cm intervals, we documented the presence of the following plant species or functional groups: grass, rush, moss, heather, bell heather, bilberry, crowberry, bracken. We noted the condition of the plants, categorising them as live, dead/senescent or charred. Additionally, we measured vegetation height at 2 m intervals.
This data was used to calculate average cover per plant type and condition, as well as average vegetation height at different times post-fire. Due to limited resources and landscape heterogeneity, we did not establish control plots in unburnt areas. Information on post-fire vegetation condition, cover, and height on burned areas was used for comparison with remote sensing estimates of vegetation recovery. However, a direct validation of the recovery estimates per wildfire area was not possible because the field data only covered one point in time per area, and the vegetation composition of individual wildfire areas varied

considerably even within the same classified land cover.
In addition to assessing long-term vegetation recovery, we captured the immediate post-fire response at one site (Standedge) burned on 3 May 2023 by visiting the area repeatedly on 4 May, 7 June, and 3 July 2023. We collected vegetation data on three fixed plots inside the wildfire area and two plots outside the area. Measurements were carried out as described earlier, except that the sampling interval was 1 m along each transect.

7.2.2 Phenology analysis

Estimation of baseline phenology for the South Pennines

To establish a baseline phenology of vegetation fuel properties as captured by remotely sensed VIs, we randomly sampled 500 satellite image pixels per land cover class across the South Pennines. These samples were collected from every available Sentinel-2 scene, excluding known wildfire areas. Due to frequent cloud cover in the study area, the number of valid pixels per scene varied significantly. Therefore, we chose to keep only 30 pixels per land cover class and discard time steps with less than 30 valid pixels. We computed the bivariate kernel density of the 30 pixel values per time step using a Gaussian kernel density estimation following the 'npphen' approach (Chávez et al., 2023) to display the frequency distribution of the VI values along the time series. Next, we calculated the mean over the 30 pixels per time step to obtain the average time series for each VI and land cover class. We removed any remaining outliers in the time series caused by undetected clouds/haze by applying a Hampel filter (Pearson et al., 2016). Outliers at the time series ends that could not be detected using the Hampel filter were removed using fixed thresholds for each spectral index that were determined after careful investigation of the data: NDVI<0.4, SAVI<0.1, NDMI>0.5 , PSRI<-0.05, NBR>0.7. We modelled the outlier-filtered time-series of each VI using a harmonic model consisting of a series of sine and cosine terms defined in Equation 1 (cf. e.g. Z. Zhu & Woodcock, 2014):

$$y_t = \beta_0 + \beta_1 t + \beta_2 \cos(\omega t) + \beta_3 \sin(\omega t) + \beta_4 \cos(2\omega t) + \beta_5 \sin(2\omega t) + \beta_6 \cos(3\omega t) + \beta_7 \sin(3\omega t) \quad (1)$$

β_0 and β_1 are the overall mean and the inter-annual trend, respectively, β_2 to β_7 capture the intra-annual variation of the signal at different frequencies $\omega=2\pi/365.25$. The time series model was fitted using the Levenberg-Marquardt least squares optimisation implemented in the Python package 'lmfit' (Newville et al., 2014). From the modelled time series, we extracted several phenological characteristics such as mean, amplitude, maxima, minima, day of the year of minima and maxima, as well as model performance metrics.

Identification of periods of high vegetation flammability

We identified periods of high vegetation flammability from the baseline phenology of individual wildfire areas. We hypothesised that a combination of low FMC and a high proportion of dead plant material, as indicated by low NDMI and high PSRI values, would result in higher probability of successful ignition. We thus identified the overlapping periods of lowest NDMI and highest PSRI values in the annual time series by extracting the intersection points of the two VIs around their global minimum (NDMI) and maximum (PSRI). We compared the identified flammability periods with the actual wildfire occurrence dates.

7.2.3 Wildfire effects and recovery

Estimation of wildfire impact on VIs

We assessed the immediate impact of wildfires on VIs obtained from Sentinel-2 by calculating the change magnitude and change angle for key indices, namely SAVI, NDMI, and PSRI. These indices serve as primary indicators of fuel properties: green biomass, fuel moisture, and senescent biomass. Calculations were performed separately for each land cover class and for the meteorological spring (MAM) and summer (JJA) seasons. We calculated change magnitude as the Euclidean distance between the pre- and post-fire spectral data points of a land cover class and season in a 3-dimensional Cartesian space whose axes correspond to SAVI, NDMI, and PSRI. Change angle was determined from the angle between the two vectors drawn from the origin to the pre- and post-fire spectral data points according to the Spectral Angle Mapper (SAM) algorithm (Kruse et al., 1993). SAM is a common measure of the similarity between two spectral vectors, with a smaller angle indicating greater similarity. Finally, we obtained a combined estimate of the impact of wildfires on VIs by normalising both change magnitude and change angle to the range [0, 1] and then averaging the two.

Estimation of spectral recovery rates

We estimated recovery rates of the different VIs after wildfire. Therefore, we extracted the average VI time series for each land cover class within a wildfire polygon. We did not filter these time series for outliers, as potential outliers could also represent the signal from the fire. The pre-fire time series was modelled using the model from Equation (1) and then extrapolated to the post-fire period. In cases where the pre-fire period had less than two years of valid acquisitions and was difficult to model, we extracted the VI time series for the same land cover class within a 1 km buffer zone of the wildfire polygon as a substitute to obtain the model parameters. We subtracted the modelled and extrapolated time series from the actual time series of the wildfire area to obtain the residuals. To determine the time of spectral recovery, we repeatedly compared the distribution of the residuals in the post-fire period to the distribution of the pre-fire residuals. For this purpose, we used moving windows of four different sizes (n=3, 5, 10, 20), each shifted by one observation from the first post-fire satellite image to the present. We continued this process until the post-fire residuals within the window were no longer significantly different from the pre-fire residuals, as tested by Welch's test (α=0.05). If no significant difference could be found for three consecutive time steps, the area was declared as spectrally recovered. We used different window sizes to make the approach more robust to the effects of outliers, data gaps, and different recovery rates. As a visual analysis of the residuals showed that the recovery time tended to be underestimated, we obtained the final recovery time of each VI as the maximum recovery time across the four window sizes. However, for acid grassland we used a window size of five for the final recovery time, as spectral recovery was fast and overestimated with larger windows. As a single estimate of the VI-derived recovery rate per wildfire event and land cover class, we used the maximum of SAVI, NDMI and NBR recovery. We did not include PSRI in final recovery estimation because it was the index with the weakest model fit and highest scatter, which sometimes led to unrealistic recovery estimates. Instead, we used NBR, as it is sensitive to vegetation structure and therefore expected to provide a robust estimate of the long-term vegetation recovery (e.g. Pickell et al., 2016).

Analysis of drivers of spectral recovery rates

We investigated the effects of various environmental variables and wildfire-related factors (**Table 7.2**) on recovery rates using multiple linear regression models. We extracted topographic information from the OS Terrain 5 DTM product (Ordnance Survey, 2023). We obtained meteorological data from the collection of gridded and monthly aggregated land surface observations over the UK at 1 km resolution (Met Office et al., 2023) and summarised them for different pre- and post-fire periods. Since recovery rates varied across land cover classes within a wildfire area, we treated each land cover class of a burned area as an individual sample when calculating correlation coefficients and building regression models. The sample size was n=74. We used Ordinary Least Squares (OLS) and tested different combinations of the variables most strongly correlated with recovery rate. We visually inspected the model residuals for normality and homoscedasticity. The final model to explain recovery was selected based on R^2 and the Akaike's Information Criterion (AIC).

Table 7.2: Variables used to explain spectral recovery rates.

	variables	**assumed influence on**
topography	elevation	local microclimate
	slope-aspect interaction northness eastness	fire dynamics, fire severity, soil conditions
wildfire	fire severity (dNBR)	regeneration capacity
	size	distance to seed sources
	season	phenological stage, weather conditions
vegetation	land cover class	specific flammability, regeneration capacity
weather	precipitation	soil moisture, erosion
	temperature	growth activity
	wind speed	exposure, erosion, seed dispersal
	sunshine duration	seed germination, growth
	days of ground frost	soil conditions
	days of snow cover	soil conditions

7.3 Results

7.3.1 Baseline phenology for the South Pennines

The phenology analysis revealed similar patterns between the land cover classes. As expected, the remotely sensed cover of green vegetation is lowest over winter and spring (**Figure 7.3**), although NDVI and SAVI indicate a different day of year (DOY) for the location of the minimum (DOY 355-103). The lowest FMC reflected in low NDMI values is reached around the end of March/beginning of April (DOY 89-106). The latter period is also characterised by highest plant senescence (PSRI). NBR patterns closely follow NDMI as both rely on NIR and SWIR reflectance. The extracted phenological characteristics of each land cover class are listed in **Table C2** (Appendix C). While the seasonal patterns are similar, acid grassland and heather grassland exhibit larger amplitudes in the variation of green and senescent biomass ($A_{SAVI/NDVI}$=0.14, A_{PSRI}=0.08) than heather and bog ($A_{SAVI/NDVI}$=0.10, A_{PSRI}=0.06). Grass-dominated land cover classes also generally have higher

FMC (mean NDMI=0.18) than heather-dominated land cover (mean NDMI=0.12). Wildfire occurrences accumulate in spring when plant senescence is high and FMC is low in all land cover classes. This period also has the highest density of valid data points (available clear-sky observations), indicating more cloud-free days, which may be related to the dominance of high-pressure systems that can promote fuel dryness (M. C. Perry et al., 2022). Single wildfire events occurring in summer partly coincide with prolonged periods of exceptionally dry conditions, as indicated by lower-than-average NDMI observations in the summer of 2018 .

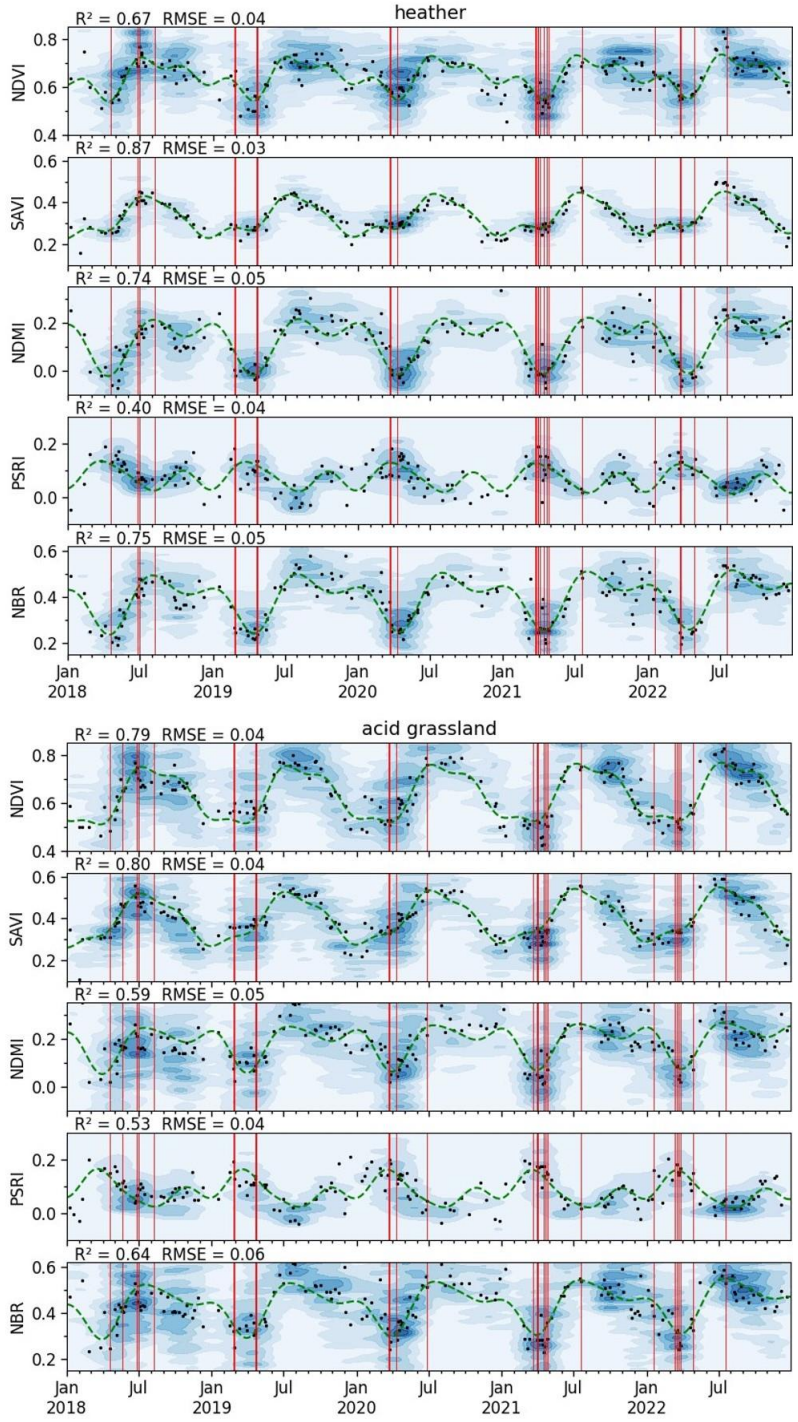

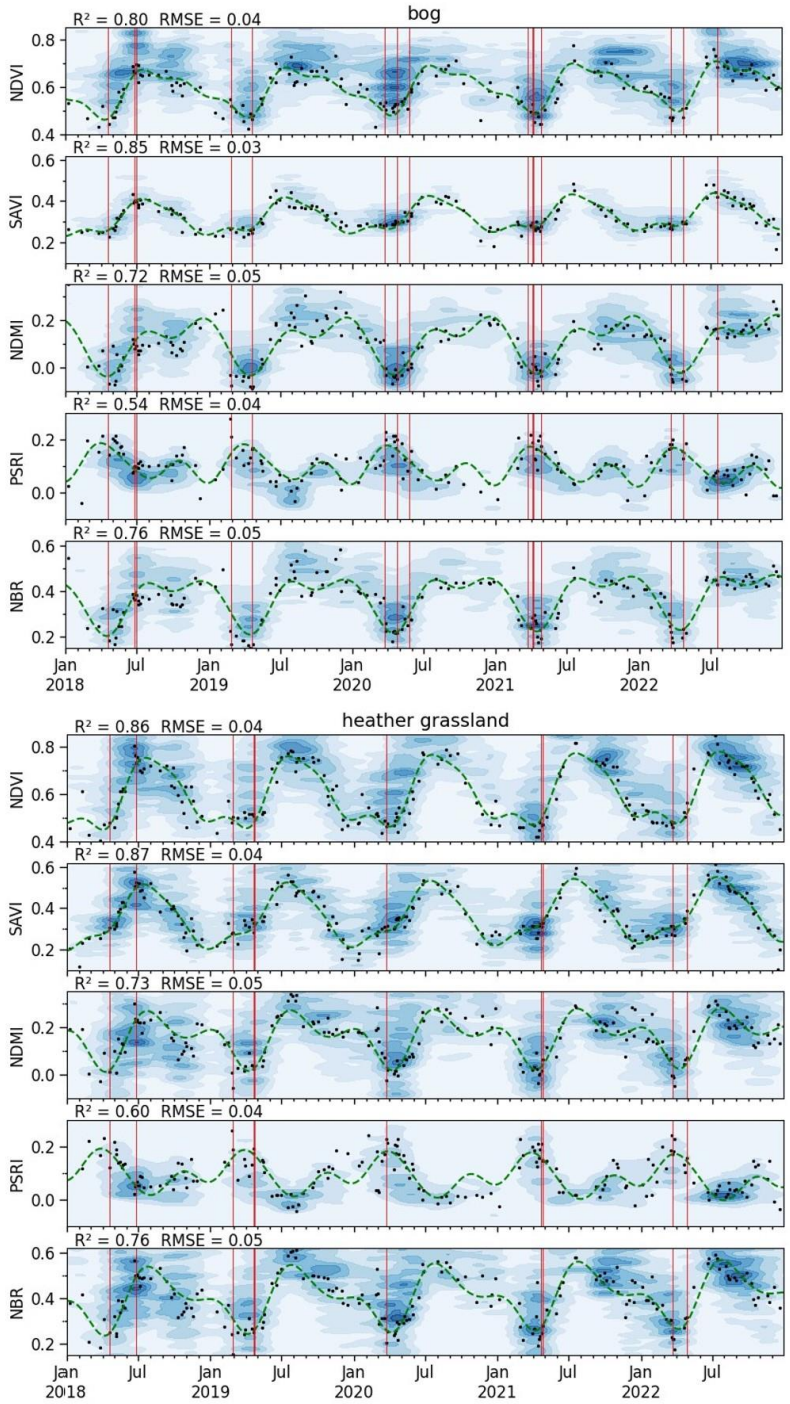

Figure 7.3: Phenological patterns of the VIs in the four land cover classes. Black dots show the mean values of the VIs in the South Pennines over the five years of observation, while the green dashed lines represent the modelled time series. Vertical red lines indicate wildfire start dates. Darker shades of blue indicate a higher bivariate density of observations (in time and across sample pixels).

7.3.2 Spring flammability window and pre-fire fuel conditions

In all land cover classes, the period of higher vegetation flammability starts in mid-February (**Figure 7.4**). It ends in early May in acid grassland, and lasts until early June in heather and heather grassland. Bog has the largest flammability window, extending into mid to late June. These periods encompass 71 % of the recorded wildfires in acid grassland, 73 % in heather, 90 % in heather grassland, and 81 % in bog. The start and end days for each land cover class are provided in **Table C3** (Appendix C).

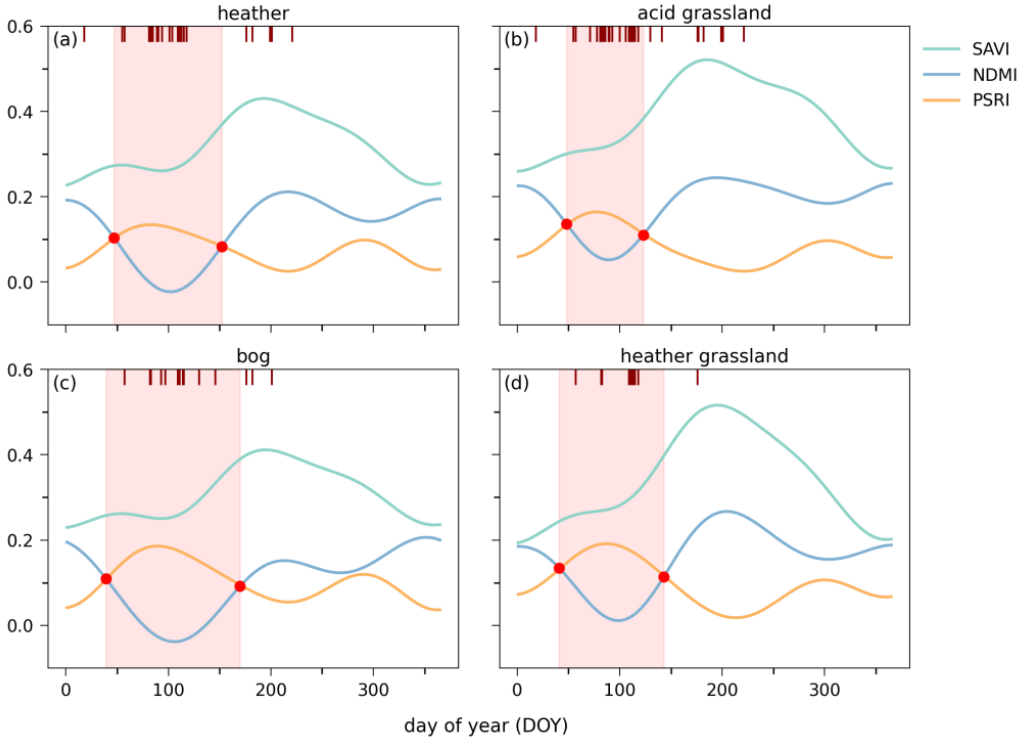

Figure 7.4: Flammability window of each land cover class. Red lines at the top of each plot indicate the occurrence of wildfires.

When comparing the remotely sensed fuel conditions in areas affected by wildfires in spring and summer to the average phenology in the South Pennines for the respective season (**Figure 7.5**), a notable finding emerges: particularly in spring, the areas impacted by wildfire showed remarkably low NDMI values compared to the average phenology. Furthermore, they had a significantly higher proportion of senescent (PSRI) relative to live vegetation cover (SAVI) just before the outbreak of the fire, especially in acid grassland and heather grassland. In summer, fuel conditions are generally less variable and characterised by less senescent cover than in spring. However, atypical conditions in wildfire-affected areas were only observed for one fire event in bog and heather (lower NDMI), which occurred in the summer of 2018 and represents the exceptionally large Tameside wildfire (circled cross in **Figure 7.5**).

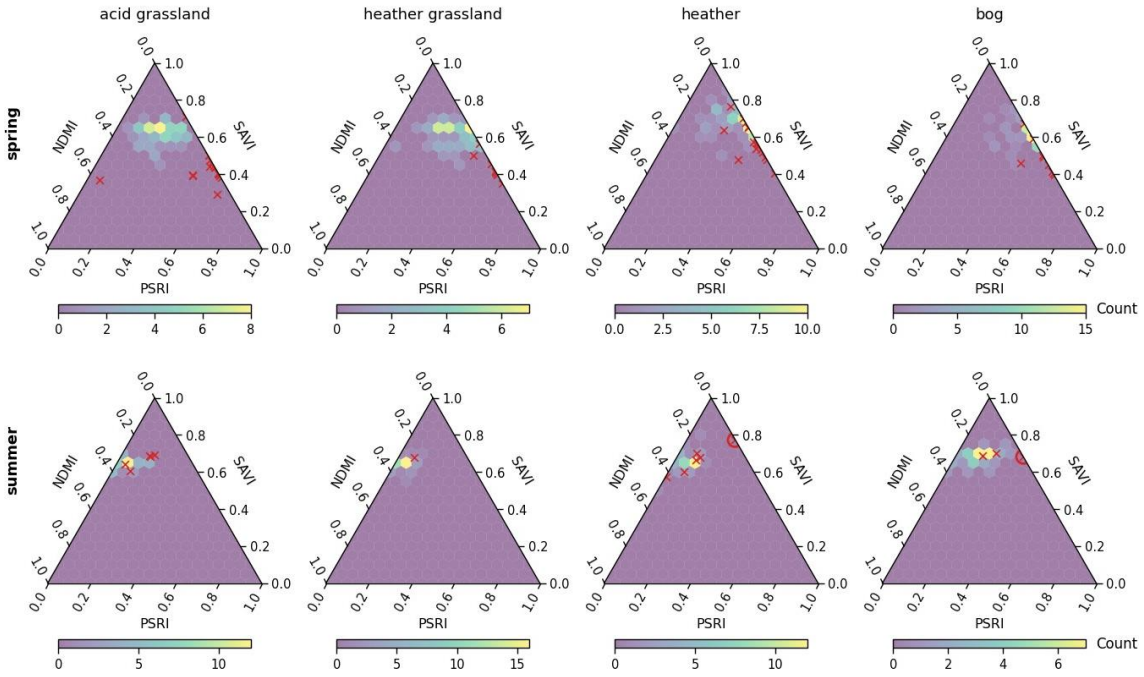

Figure 7.5: Ternary plots showing the occurrence frequency of typical proportions of SAVI, PSRI, and NDMI during spring and summer in the South Pennines' land cover classes derived from their baseline phenology (coloured filling). Red crosses show the conditions shortly before a wildfire outbreak. Note that the axes do not display the actual VI values, but their proportion (all three VIs sum to 1). Circled cross represents the Tameside wildfire in 2018.

7.3.3 Wildfire effects on VIs

The immediate impact of wildfires on fuel properties, as determined from remotely sensed VIs, was more pronounced in summer compared to spring. This is evident in the greater magnitude and angle of change observed between pre- and post-fire data of SAVI, PSRI, and NDMI across all land cover classes (**Table 7.3**, **Figure 7.6**). SAVI and NDMI showed a strong decrease after summer fires (both -0.27), indicating a substantial reduction in live green biomass, whilst there was a less pronounced decrease in spring (-0.09 and -0.13), where they had lower pre-fire levels. PSRI changed slightly, showing on average a small reduction after spring fires (-0.07) and a small increase after summer fires (+0.07). Overall, wildfire effects on VIs differed only slightly between the different land cover classes, compared to the large variability in effects between fires (**Table C4**, Appendix C).

Table 7.3: Mean change magnitude and change angle and their standard deviations. Values for heather grassland are not shown due to only one wildfire occurrence.

		magnitude	**angle**
acid grassland	spring	0.27±0.11	42.1°±22.3°
	summer	0.47±0.22	62.5°±32.8°
bog	spring	0.17±0.06	25.1°±11.9°
	summer	0.45±0.27	65.6°±32.1°
heather	spring	0.25±0.12	42.2°±21.3°
	summer	0.49±0.34	66.5°±42.6°
heather grassland	spring	0.22±0.09	32.3°±17.5°

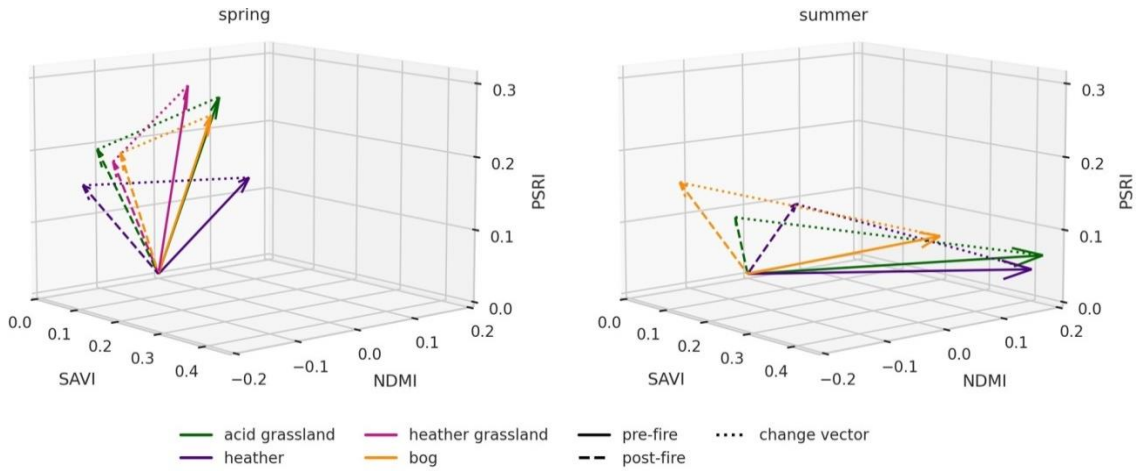

Figure 7.6: Vectors representing average pre- and post-fire VIs for each land cover class separated by season. Since there was only one fire in heather grassland in summer, the vectors are not displayed here.

7.3.4 Spectral recovery of VIs

The average spectral recovery time varied across land cover classes. Acid grassland consistently had the shortest recovery times, with mean values for the different VIs ranging from 67-131 days. Heather grassland followed with recovery times spanning 155-255 days. In bog areas, recovery estimates were more variable: PSRI recovered the fastest in approximately 203 days, while NDMI had a slower recovery time of 515 days. NDVI and SAVI also produced different results for the mean spectral recovery time in bog areas, with values of 236 and 492 days, respectively. Average heather recovery rates remained relatively consistent across all VIs, ranging from 437-527 days, except for PSRI, which showed a faster recovery time of 254 days (as shown in **Figure 7.7** and **Figure 7.8**). Notably, the variability in recovery rates was higher in heather and bog areas compared to acid grassland and heather grassland, particularly between individual wildfire events.

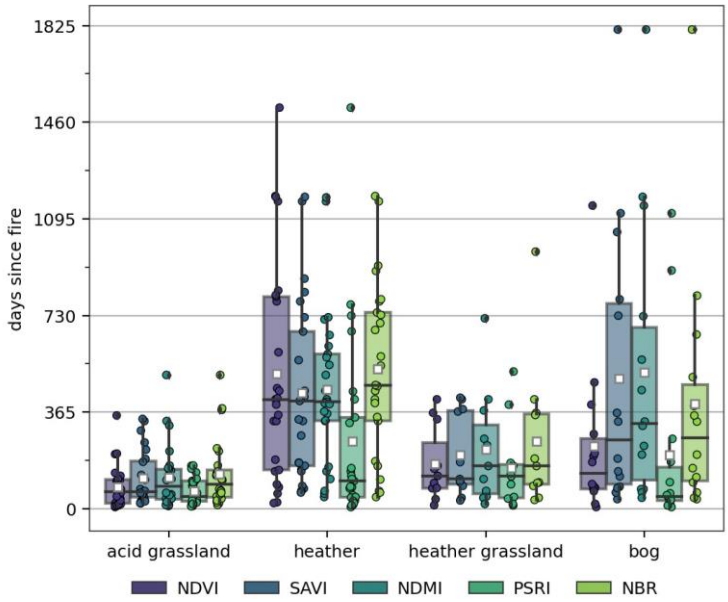

Figure 7.7: Recovery times of the VIs for different land cover classes. Mean values are shown as white squares.

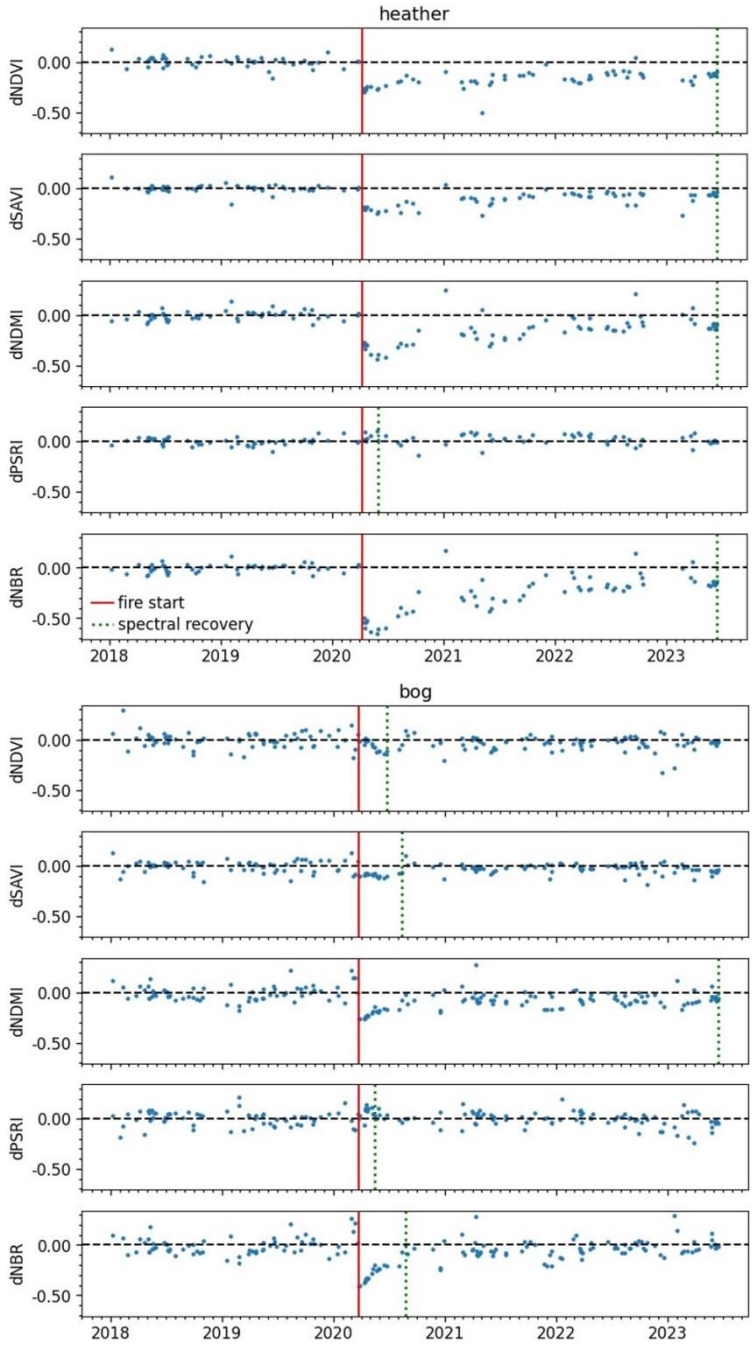

Figure 7.8: Example of the different recovery trajectories of the VIs for two wildfire events in heather (West of Didsbury intake) and bog (Kirklees) that occurred in spring 2020. Red vertical line denotes fire occurrence. Dashed green vertical line denotes point of spectral recovery.

Most wildfire areas in the South Pennines showed relatively minor changes ('low impact') in spectral VIs and tended to recover spectrally in less than two years (**Figure 7.9**, quadrant I). Large spectral changes ('high impact') and rapid recovery, often within one year, were observed particularly in acid grasslands (quadrant II). In contrast, large spectral changes coupled with slower recovery, exceeding two years, were primarily observed in heather and bog (quadrant III). Similarly, smaller spectral changes and slower recovery were prevalent in these two land cover classes (quadrant IV). A significant positive correlation between spectral change and recovery time was observed only for heather land cover (Spearman's r=0.50, p-value=0.02).

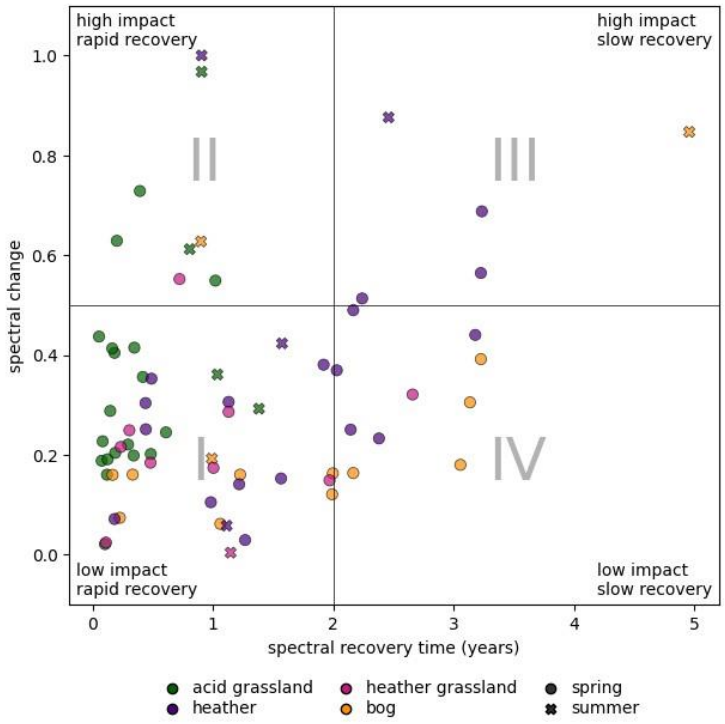

Figure 7.9: Mean recovery time of the VIs for each wildfire area versus the spectral change (combined measure of change magnitude and change angle).

7.3.5 Field-measured vegetation recovery

While we describe the field data as a true chronosequence for ease of reading, it is important to emphasise that it is a pseudo-time series created from space-for-time sampling. Vegetation cover in the sampled wildfire areas averaged approximately 69 % in the first year after the fire (**Figure 7.10 a**), with subsequent years showing further recovery. Vegetation heights also increased over time, but differed greatly between wildfire areas of the same year, i.e., different sites (**Figure 7.10 b**). We therefore differentiated our plots according to the dominance of either graminoids or dwarf shrubs.

The graminoid-dominated plots had on average 96 % vegetation cover in the first year after the fire (**Figure 7.10 c**), which aligns with the observed VI recovery times of less than one year in grassland land cover classes (**Figure 7.7**). In the first year following fire, we recorded the highest grass heights (**Figure 7.10 d**). While vegetation cover remained high in subsequent years, heights decreased to a lower level.

In the dwarf shrub-dominated land cover classes, average vegetation cover and height were initially low in the first year after the fire (48 % and 12 cm, respectively). Vegetation cover increased to about 69 % in the second year and 85 % by the third year post-fire, while vegetation heights remained low for the first three years and reached heights comparable to those in graminoid-dominated areas only in the fourth to fifth year after fire.

The development of live vegetation cover (**Figure 7.10 e**) roughly followed the pattern of total vegetation cover, but the proportion of dead vegetation was higher in graminoid-dominated plots than in dwarf shrub-dominated plots, especially from the second year post-fire (**Figure 7.10 f**).

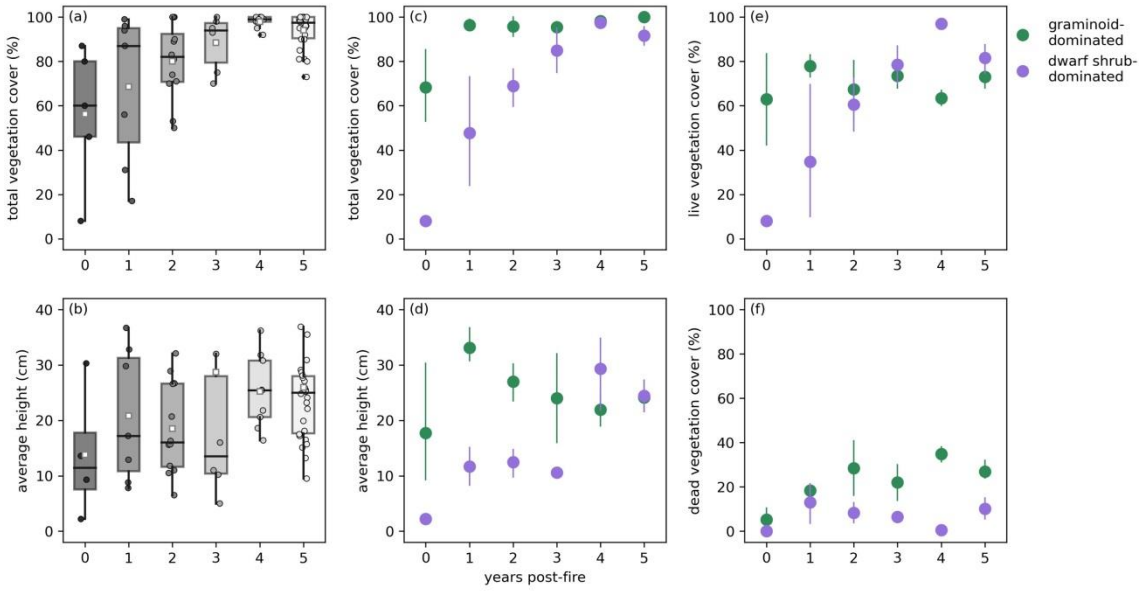

Figure 7.10: Vegetation cover fractions and heights in wildfire areas across the South Pennines in different years post-fire (0 corresponds to wildfire areas from 2023, 5 to areas from 2018). a) and b) show data from all burned areas, c) to f) show means and standard deviations of the data categorised by dominant functional group.

An assessment of vegetation recovery immediately following the Standedge wildfire shows that vegetation recovers rapidly in such grass-dominated areas (**Figure 7.11**). Within only one month post-fire, live vegetation cover in the burned area was not significantly different from the unburned area, where spring growth had just started. The (visible) cover of charred vegetation in the burned area also decreased rapidly. The cover of senescent plant material was initially high in the unburned area, but visually decreased as new grass shoots emerged. Hence, two months after the fire, burned and unburned areas had similar measured cover of dead vegetation. Vegetation height in the burned area was comparable to the unburned area two months after the fire. **Figure C1** (Appendix C) provides photographic evidence of the burned area's recovery.

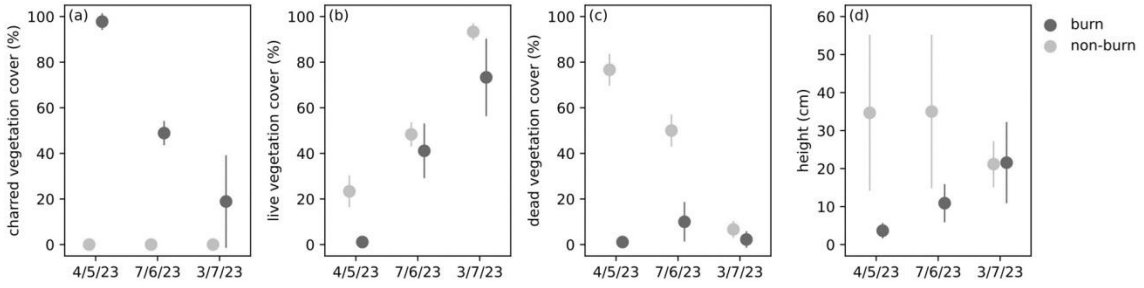

Figure 7.11: Average vegetation cover fractions (a-c) and heights (d) inside (burn) and outside (non-burn) the Standedge wildfire area (burned on 03/05/23). The last measurement of vegetation height in the non-burn plots differed from the previous ones, either because of management (e.g. grazing), different measurement teams, or the effect of precipitation causing the grass to bend. Measurements from the same date were carried out consistently. Vertical lines represent the standard deviation.

7.3.6 Drivers of spectral recovery

To explain spectral recovery times we selected a model that achieved an adjusted R^2 of 0.58 and used land cover class and season as categorical variables, along with the continuous variables burn severity and days with snow cover (**Table 7.4**). When each of the four variables was excluded from the model, we found that land cover class had the strongest influence (reduced adj. R^2=0.32), followed by burn severity (0.46), days with snow cover (0.53), and season (0.56). Recovery times increased with burn severity. In comparison to the reference category acid grassland, bog and heather were estimated to have recovery times more than one year longer, while heather grassland had recovery times less than one year longer. Summer fires recovered approximately six months faster than spring fires. Recovery times were further estimated to increase with more days of snow cover in winter. When interactions between land cover class, season, and burn severity were included in the model (**Table 7.5**), the adjusted R^2 increased to 0.66. This model revealed that burn severity in acid grassland had no significant effect on recovery times, in contrast to bog and heather. Generally, the correlations between recovery time and other environmental variables were low, with significant values (α=0.05) for elevation (Pearson's r=0.35), temperature, and sunshine duration in the year post-fire (r=-0.30 and -0.31), wind in the year post-fire (r=0.31), and days with groundfrost in winter (r=0.32). However, none of these variables were significant factors in the selected regression model.

Table 7.4: Coefficients in the selected regression model to explain spectral recovery times.

	coef	std err	P>|t|
Intercept	-292	84	0.001
Land cover – Bog	463	85	0.000
Land cover – Heather	418	72	0.000
Land cover – Heather grassland	276	94	0.005
Season – Summer	-213	101	0.038
Burn severity	1101	247	0.000
Snow cover days	11	4	0.004

Table 7.5: Coefficients in the regression model with interactions between variables.

	coef	std err	P>|t|
Intercept	17	74	0.815
Acid grassland : burn severity : spring	-169	315	0.594
Bog : burn severity : spring	1405	344	0.000
Heather : burn severity : spring	1489	266	0.000
Heather grassland : burn severity : spring	1036	412	0.015
Acid grassland : burn severity : summer	297	208	0.157
Bog : burn severity : summer	1362	248	0.000
Heather : burn severity : summer	727	209	0.001
Heather grassland : burn severity : summer	452	428	0.294
Snow cover days	12	4	0.000

7.4 Discussion

7.4.1 Baseline phenology and flammability window

Phenological patterns of key fuel characteristics are captured by remotely sensed VIs as they show expected fuel conditions (low moisture, high plant senescence) at times of increased wildfire activity. Modelling the time series effectively illustrates the typical annual progression with acceptable accuracy for most VIs (R^2=0.59-0.87) except PSRI (R^2=0.40-0.60). However, extended gaps in the time series resulting from frequent cloud cover, particularly in winter, introduce uncertainty to the modelled second peak in NDMI/NBR and the second trough in PSRI in January. Gaps in this section of the dataset are perhaps less problematic as this period tends to have lower wildfire activity, though it is an important period during which fuel can desiccate (Hancock, 2008). Spectral measurements by Cole et al. (2014b) between April and September in the PDNP also showed clear seasonal patterns in reflectance for both dwarf shrubs and graminoids, with the largest amplitudes confirmed in graminoid species. The higher stability of the SAVI time series compared to NDVI in our study suggests that SAVI is a more reliable proxy for greenness, particularly for land cover classes with bare ground exposure. The VIs also capture specific fuel properties of the land cover classes, such as the low FMC of *Calluna* and its pronounced drop in early spring (Davies, Legg, et al., 2010), consistent with previous studies that successfully related FMC in upland vegetation to spectral indices such as NDWI or Moisture Stress Index (MSI) (Al-Moustafa et al., 2012; Badi, 2019).
NDMI and PSRI further allow the identification of periods when vegetation is in a condition that is critical for burning and could be used as a complement to meteorological fire danger indicators such as the Met Office Fire Severity Index (MOFSI) (Met Office, 2005). However, it is important to note that wildfires are not limited to the period estimated by the VIs. Particularly in acid grassland, the flammability window calculated from VIs covers a short period, as the optical signal changes rapidly with the onset of spring green-up. However, the senescent biomass accumulated during winter persists as a flammable layer beneath the green grass shoots that dominate the spectral signal. This potentially contributes to the lower percentage of fires captured by the flammability window in acid grassland. These observations align with the finding of Cole et al. (2014b) that separability between graminoids and dwarf shrubs using PSRI was best in April and declined rapidly thereafter.

The longer flammability window observed for heather and heather grassland can be explained by the long winter dormancy of *Calluna*, which can last until late May or early June (Kwolek & Woolhouse, 1982). This period of dormancy is associated with low FMC and strong root resistance to water uptake (Bannister, 1964). FMC measurements in *Calluna* by Al-Moustafa et al. (2012) showed that FMC was still below 70 % in May but increased to more than 100 % in July. The longest flammability window was calculated for bog areas, despite their typically wet or waterlogged nature. However, the bogs in the South Pennines have historically experienced severe degradation, with lowered water tables transforming many sites into dry heath on peat (PDNPA, 2021). This could explain the similar phenological pattern of bog and heather, with bog sites showing even lower FMC levels in spring and summer, highlighting their vulnerability to severe wildfire events.
While spring wildfires have predominantly impacted areas with a high proportion of senescent plant material, identifying flammable conditions in summer using VIs has been more challenging. This may be due to the fact that wildfire danger in summer primarily results

from high temperatures and atmospheric drought, which leads to plant water loss but does not cause immediate mortality (Anderegg et al., 2013). Water stress can be observed to some extent in the NDMI, and other indices such as the MSI could be included, but meteorological indices may be better suited to identify critical periods over the summer.

7.4.2 Wildfire effects on VIs

Larger differences between pre- and post-fire SAVI, PSRI, and NDMI observations during the summer months indicate a higher burn severity associated with summer fires. However, these disparities could also be influenced by the higher pre-fire values of SAVI and NDMI in summer compared to spring. Removal and charring of plants generally result in a reduction of these VIs through a decrease in reflectance in the NIR range and unchanged or even increased reflectance in the SWIR range, as the absorption of the latter by leaf water is reduced (Fassnacht et al., 2021). The largest change was found in NDMI, and other studies also reported that the largest wildfire-induced decrease was in wetness indices such as NDMI and NBR (Serra-Burriel et al., 2021). Differences in PSRI, which is sensitive to the carotenoid/chlorophyll ratio (Sims & Gamon, 2002), showed subtle changes and reflected distinct behaviours between spring and summer. In spring, the abundant senescent plant material is lost from the site and partly transformed into charcoal (Clay & Worrall, 2011), leading to a reduction in carotenoid reflectance. In contrast, during summer, the carotenoid to chlorophyll ratio is typically low, and the combustion of green plants therefore affects chlorophyll pigments more than carotenoids.

7.4.3 Spectral recovery of VIs

Acid grassland

VIs demonstrated high consistency in the rapid spectral recovery of acid grasslands, often within a year or even just two or three months. The main challenge in capturing this rapid recovery with remotely sensed VIs was data gaps in the satellite time series interrupting the short-lived signal. NDVI recovery was faster than SAVI for most grassland areas (by 32 days on average), indicating a lack of sensitivity of the index to different cover conditions as previously reported (X. Gao et al., 2000). The VI-estimated recovery times align well with the field observations of vegetation recovery at the Standedge wildfire area, where live vegetation cover was restored within a few weeks post-fire. Grass shoots also rapidly reached heights comparable to the surrounding unburned area, suggesting temporarily improved nutrient availability in the burned area (San Emeterio et al., 2016). Consequently, the land may be returned to pasture fairly quickly, and improvements in forage quality have also been reported for some species (Gimingham, 1972). Since the rate of fuel load accumulation is high in grass-dominated land cover classes, fuel availability for new wildfires is only temporarily reduced, although field data indicate that the proportion of dead biomass takes longer to reach pre-fire levels (around two years post-fire). However, accurately quantifying dead biomass fraction using satellite data is challenging due to the top view of the vegetation canopy. A study in subalpine grassland, where post-fire regeneration was generally slower than in our study, predicted that the return of the litter component could take several years (Wahren et al., 2001). Acid grassland wildfires exhibited a wide range of spectral changes in the VIs, but burn severity did not significantly impact their recovery times. The data indicate that acid grasslands recover faster spectrally after spring than summer

fires, likely because areas burned in spring still have the entire growing season ahead. Following summer fires, plant growth is limited until the end of the growing season, which is why full spectral recovery can only be achieved in the following year (**Figure 7.9**).

Heather

For heather land cover, estimated spectral recovery times varied significantly among wildfire areas, ranging from less than six months to approximately three years. The NBR recovery time was generally the longest, surpassing SAVI by approximately 90 days. This suggests that SWIR-based indices may be more effective at capturing heather recovery due to their higher sensitivity to vegetation structure. Conversely, the PSRI recovery times were the shortest, indicating that the noisy signal of the index is unsuitable for capturing the (assumed long-term) return of dead material within the heather canopy.

Our model showed a significant effect of burn severity on recovery times in heather land cover, which has been reported in previous studies (Lees et al., 2021). This is typically attributed to the level of fuel consumption and ground heating affecting the regenerative capacity of *Calluna* (Gilbert, 2008; Grau-Andrés et al., 2019). Interestingly, recovery time increased more with burn severity in spring compared to summer. One possible explanation is that seed germination and plant development are delayed after severe spring fires because seeds are more likely to be exposed to drought conditions. Experiments by Birkeli et al. (2023) revealed that reduced water availability increases the time to germination and reduces the germination percentage of *Calluna* seeds, and also affects development in the seedling stage. Furthermore, post-fire development has been shown to depend on pre-fire stand age, with the ability to regenerate vegetatively strongly diminished in older stands, resulting in slower recovery (Davies, Smith, et al., 2010; Kayll & Gimingham, 1965). Since we lacked information on the age of the *Calluna* stands in our study area, we were unable to include this in the model. However, during our field campaign, we recorded the growth phase of *Calluna* on the wildfire scars and in the surrounding unburned areas, and found a similar pattern (**Figure 7.12 a**). When the unburned *Calluna* was in the mature-degenerate or degenerate phase, regeneration on the burned area primarily consisted of plants still in the pioneer phase, even on the oldest wildfire areas (from 2018). In contrast, stands burned in an earlier growth phase reached the building phase more rapidly (**Figure 7.12 b**). This aligns with the observations of Schellenberg & Bergmeier (2022), who noted that younger *Calluna* stands burned in the mature stage resprout vigorously and grow rapidly, reaching an early-mature stage after only three to four years under favourable conditions.

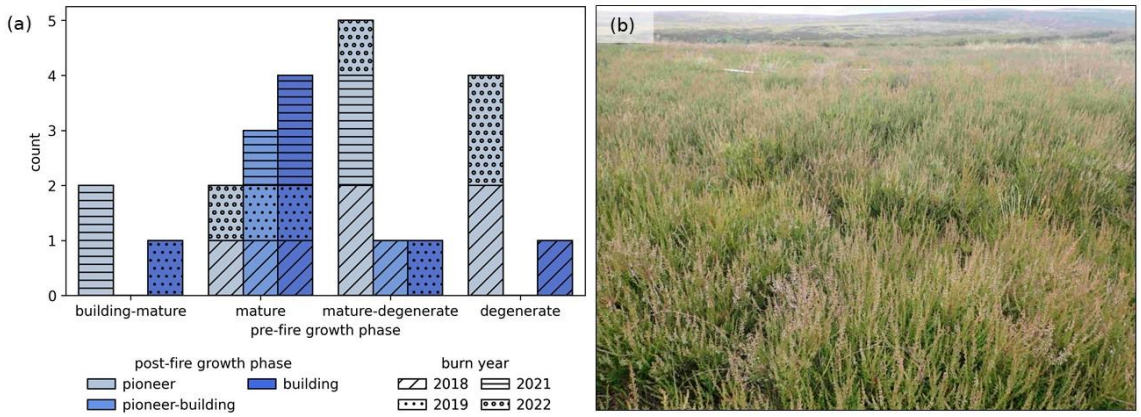

Figure 7.12: (a) *Calluna* growth phase on burned areas in relation to the pre-fire stand age. (b) Regenerated *Calluna* in the building phase in 2023 on an area burned in April 2021, pre-fire *Calluna* was in the mature phase.

Generally, the VI-estimated recovery times for heather land cover underestimate the actual recovery time. Our field data suggest that cover in dwarf shrub-dominated areas is reconstituted faster than height, the latter taking four to five years and longer. Underestimates of recovery times may be due to the limited recovery time series available for some of the more recently burned areas. Additionally, VI-estimated recovery times of less than one year for heather land cover may indicate either a misclassification in the LCM2021 or that the immediate post-fire signal is strongly dominated by other plant species, such as graminoids, herbs, and mosses. The LCM2021, as well as field observations of some rapidly recovering wildfire areas, suggest that these areas predominantly featured small *Calluna* patches before the fire, surrounded by graminoid-dominated acid grassland or bog vegetation (**Figure 7.13 a**). Where *Calluna* regeneration depends on seedling establishment, the rapid spread of pioneer species immediately after wildfire may hinder the germination of the light-sensitive *Calluna* seeds, possibly leading to a reduction in *Calluna* cover, as observed at other sites (Brys et al., 2005; Velle & Vandvik, 2014). However, if seedlings have established successfully, *Calluna* may regain dominance at a later stage of succession due to its superior competitiveness for light (Sedláková & Chytrỳ, 1999). Areas where *Calluna* is restricted to smaller patches and the potential for grass invasion from surrounding areas is high (potentially heather grasslands) could therefore be a target for post-wildfire management.

Our model also indicates that prolonged winter snow cover delays the recovery of burned areas. This could be attributed to lower seedling survival in winter when cold temperatures freeze the ground, leading to desiccation and browning of foliage (Legg et al., 1992), although a thick snow layer should prevent this. Extended periods of snow cover have also been known to be followed by plant damage caused by molds in early spring (Watson et al., 1966). They could also simply indicate sites with less favourable microclimates, such as those found at higher altitudes (**Figure 7.13 b**) or on north-facing slopes. In these areas, lower temperatures, high winds, or less sunlight limit plant growth, as suggested by this and other studies (Lees et al., 2021; Nilsen et al., 2005; Velle & Vandvik, 2014). Remaining unexplained variance in the recovery time may be attributed to differences in post-fire substrate conditions (Davies, Smith, et al., 2010).

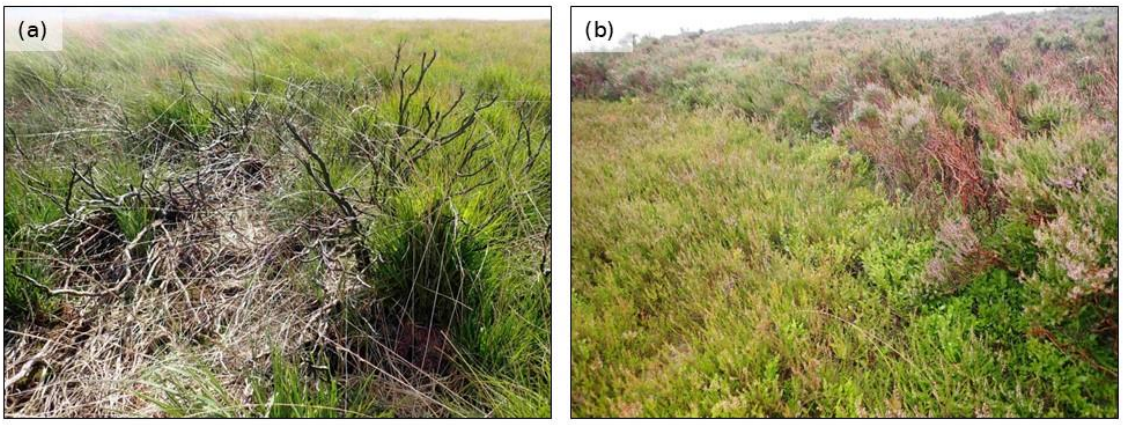

Figure 7.13: (a) Graminoid invasion of burned heather patch. (b) Slow recovery on a higher altitude site burned in 2018, showing the transition between burned (left) and unburned (right) area.

Heather grassland and bog

We do not provide a separate discussion for heather grasslands, as they can be considered to hold an intermediary status between the previously discussed land cover classes from a remote sensing perspective. We hypothesise that the strong influence of grasses on the spectral signal likely contributes to relatively short estimated recovery times.

For bog, recovery estimates were similarly variable as for heather, ranging from a few months to up to five years. Our field campaign revealed that bog areas encompassed both pure graminoid and *Calluna*-dominated habitats, as the land cover class is defined by a soil characteristic (>0.5 m peat), which explains the large variability in recovery rates. The discrepancy between NDVI and SAVI recovery suggests that soil background has a strong influence in bog areas, as darker soils in particular lead to higher NDVI values for incomplete canopies (X. Gao et al., 2000). We therefore recommend using SAVI instead. The NDMI exhibited the longest recovery time among all VIs, suggesting that wildfires can have a substantial impact on the moisture regime in moorlands. Studies have shown that pyrolysed peat soils are characterised by increased hydraulic conductivity and decreased soil moisture (Akmet'eva et al., 2014; Astiani et al., 2020), which may affect water uptake by regenerating plants.

7.4.4 Limitations and outlook

Our study focused solely on optical remote sensing data, as we aimed to investigate these data comprehensively. While they provide insight into important fuel properties, they offer limited information on the physical structure of the vegetation and therefore cannot fully capture vegetation recovery to pre-fire levels. In addition, the time series feature large gaps due to frequent cloud cover in the study area. Therefore, future studies should include complementary information from sensors that are independent of atmospheric conditions and more sensitive to vegetation structure, such as SAR. The backscatter signal from spaceborne SAR has already been successfully used to retrieve information on *Calluna* height (Schmidt et al., 2018) and to monitor post-fire vegetation recovery in Arctic tundra (Zhou et al., 2019). Previous work on using the SAR intensity and InSAR coherence signal to detect burn scars in peat moorlands in the PDNP could be developed further to under-

stand vegetation recovery in these landscapes (Millin-Chalabi et al., 2013). Canopy height and *Calluna* growth phase can also be determined from photogrammetric point clouds derived from high-resolution UAV imagery (Mead & Arthur, 2020; Neumann et al., 2020). Access to this information would facilitate more accurate assessments of when biomass (i.e., fuel load) is fully restored in burned areas. However, estimating the litter component remains difficult even with other sensors. Our study centered on the spectral recovery of remote sensing signals and the recovery of vegetation cover and height in the field, with particular emphasis on fuel availability and condition. This should not be mistaken for the ecological recovery of an area, which requires more complex criteria such as assessments of biodiversity, structural diversity, and ecosystem functionality.

7.5 Conclusion

This study demonstrated the utility of optical VIs such as SAVI, NDMI, and PSRI for characterising the phenology of important fuel properties in UK upland land cover classes and identifying periods of peak vegetation flammability. Analysis of pre- and post-fire signals allowed a better understanding of wildfire-induced changes in the VIs and their recovery patterns in different land cover classes. Bog and heather exhibited the longest spectral recovery times, heather grassland was intermediate, and acid grassland recovered most rapidly. Our results underscore the importance of distinguishing between different functional groups when estimating vegetation recovery from remote sensing data across large areas, particularly between dwarf shrubs and graminoids. In addition to land cover class, recovery times were affected by burn severity, season, and winter snow cover. The comparison with field data from wildfire areas showed that optical data tend to underestimate the time required for recovery to pre-fire conditions, especially for habitats dominated by slower-growing dwarf shrubs. Future studies could supplement the optical data with SAR imagery or point cloud data, which provide additional information on vegetation structure, to improve recovery estimates. Our results advance the knowledge of phenology-driven fuel dynamics in moorlands and help to interpret satellite-based analysis of vegetation recovery. They serve as an important foundation for the development of satellite-based monitoring of fire risk and post-fire vegetation recovery, which can ultimately inform both precautionary measures and management priorities.

Acknowledgements

PL and JAS received funding from the German Federal Ministry of Food and Agriculture as part of the project 'ErWiN' (2219WK54A4). AMPP, GM-C, and GDC were supported by funding from the Natural Environment Research Council (NE/T003553/1). We thank the following site owners and managers for permission to access the field areas: Moors for the Future Partnership, National Trust Marsden Moor, Royal Society for the Protection of Birds (RSPB) Dovestone, United Utilities, Enville and Stalybridge Estates, Staffordshire Wildlife Trust. A huge thanks goes to Martina Ettlin for her invaluable fieldwork assistance.

Part III

Synthesis

8 Synthesis

Accurately characterising and mapping surface fuels in the increasingly fire-prone, but to date insufficiently studied temperate ecosystems of Europe is a key requirement to support fire risk assessment and fire behaviour modelling as a basis for management decisions. A comprehensive assessment of new and existing approaches based on proximal and remote sensing data is needed to understand their usefulness for surface fuel characterisation in heterogeneous temperate forests and dynamic dwarf shrub heaths. The main insights of this thesis in this regard are summarised below.

8.1 Main findings

8.1.1 Proximal image data

A new deep learning-based method for identifying surface fuel types in central European forests based on proximal image data, i.e. forest photographs, was presented in this thesis (Chapter 5). The algorithm performed well in the classification task, despite the rather small dataset that had been collected for its development. The work showed that both horizontal forest stand photographs and forest floor photographs can be used to classify fuel types, and combining both leads to more stable results. While the initial results for CNN-based fuel type classification from forest photographs were promising, the accuracy of the algorithm needs to be improved before it can be used operationally. The study showed that majority voting based on multiple photographs from the same forest stand are one means to improve understory classification. Litter classification showed improvement when majority voting was applied to the predictions of multiple single-input models, which process one type of input data at a time, rather than using a multi-input model. Both classifications improved when predictions were filtered according to the class prediction probability.
Still, classification accuracies were limited particularly for litter fuel types due to the continuous transition between different litter fuelbed compositions. Also in understory classification, the presence of different fuel types in an image hampered the identification of a specific class. In such cases, however, it is also difficult for human observers to adhere to strict class boundaries. This underscores the general limitation of the classification approach and opens new lines of enquiry into whether the presence or even abundance of different fuel types can be quantified from photographs.
Overall, the work showed that proximal sensing can be a useful means to derive information on fuelbed composition in central European forests. It also proved that the approach enables discriminating a more fine-grained surface fuel classification than is possible with spaceborne or airborne remote sensing data, particularly because different understory species with their respective fuel traits can be identified. The approach effectively overcomes the canopy obstruction problem faced by many other remote sensing techniques. This opens new opportunities to extend and refine existing fuel classifications also in other ecosystems. The extent to which the surface fuel types identified in central European forests are associated with different fire behaviour still needs to be investigated using experimental approaches, but this does not affect the proposed methodology.
As shown in other deep learning applications, classification accuracies are likely to increase

as more training data become available. Expanding the dataset is therefore one of the most important ways of further improving the results. Applying the algorithm to labelled data from existing databases, such as the LUCAS photographs (see Chapter 3.2.3), would help to assess its performance on independent datasets. In the long term, the algorithm will make it possible to collect information on fuelbed composition in any region by using geo-referenced imagery that is being uploaded in increasing volumes to various online platforms. It could then serve as an alternative approach to validate fuel type maps generated based on other remote sensing datasets when geo-referenced imagery from within forest stands is available. However, as with the established method of photo series, the area represented by a photograph can be variable and also depends on the viewing direction. Therefore, precise matching of fuel type maps with geo-referenced photographs is difficult. More research is needed to determine the effect this would have on validation results.
As another use case, the algorithm could be implemented in a smartphone application for foresters and the general public that allows the collection of forest photographs and automatically relates the identified fuel type to potential fire behaviour. This could be a means of communicating knowledge about fuels and fire behaviour to the population.

8.1.2 Multispectral satellite data

Multispectral data from the Sentinel-2 satellites were employed in all three studies of this thesis, as they are easily and freely accessible for any place on Earth and have a high temporal and spatial resolution.
However, the data were of limited usefulness in the classificaton of surface fuel types in central European forests (Chapter 5). Integrating Sentinel-2 time series in the proposed deep learning approach based on forest photographs did not provide much added value for the prediction of understory and litter fuel types. When using the multispectral data as stand-alone methodology for fuel type classification, results showed that distinguishing understory fuel types was not possible based on these data. This confirms that understory characteristics are difficult to retrieve and underscores the importance of incorporating below-canopy observations (proximal data) for accurate fuelbed characterisation. However, classification of litter fuel types based on multispectral data alone was similarly accurate as predictions based on forest photographs. The higher importance of summer observations compared to winter observations for litter classification revealed that the algorithms relies more on canopy characteristics than on direct sensing of the litter layer under leaf-off conditions, showing that spaceborne multispectral data can inform indirectly about litterbed properties.
This was also observed in the quantification of surface fuels (Chapter 6), where Sentinel-2 data were used in combination with airborne laserscanning data. The results showed that multispectral satellite data were most useful for quantifying litter and fine woody fuels, which are related to canopy characteristics. The latter fuel components are more homogeneously distributed than other fuel components, and can thus be associated with forest types. Hence, multispectral satellite data can be used to make predictions on average canopy-related fine dead fuel loads depending on dominating tree species. Multispectral satellite data also helped to improve estimates of herbaceous fuel load through the link between certain tree species and the presence of mosses, and more generally between canopy density and herbaceous vegetation cover. However, multispectral satellite data provided little information about shrub fuel loads and coarse dead wood.
Time series of vegetation indices (VIs) derived from Sentinel-2 data were well suited for

monitoring seasonal changes in fuel condition in the Atlantic heathlands of western Europe (Chapter 7). As the time series were strongly disturbed by clouds, data gaps had to be bridged by harmonic modelling of the time series. This allowed for the derivation of a baseline phenology of the vegetation types present. The selected VIs effectively captured the annual dynamics of important fuel properties such as fuel greenness, senescence, and moisture. PSRI as proxy for the abundance of senescent plant material, and NDMI as proxy for fuel moisture content were well suited suited to identify periods of potentially increased vegetation flammability and thus determine the main phenological 'fire season'. In some cases, they also allowed to detect exceptional fire weather conditions (longer drought periods) during other times of the year through deviations of the NDMI observations from the baseline. While the VIs can serve to warn of periods of increased fire risk, they provide an average estimate across the fuel complex that is dominated by the canopy, and cannot resolve the condition of different fuel components needed for fine-scale fire behaviour analysis. This is also unlikely to be feasible from spaceborne measurements.
The magnitude of change in the selected VIs following wildfires was not suitable as an indicator of fire severity and post-fire recovery times, because the spectral change depended strongly on the seasonal pre-fire vegetation condition. Pre-fire vegetation status could be included in the future to normalise the estimate of change.
Similar to forest ecosystems, VIs incorporating SWIR reflectance such as NDMI and NBR were most robust in estimating vegetation recovery. However, spectral recovery times still underestimated field-assessed recovery times, particularly for life forms with low growth rates, due to the lack of remotely sensed information on structural recovery. Nevertheless, they provided insight into post-fire vegetation development in the different life forms associated with heathland environments after wildfires of varying severity.
The proposed methodological approach to monitor fuel dynamics can yet not be easily transferred to forest ecosystems. Especially the flammability of surface fuels in forest ecosystems cannot be directly sensed with spaceborne multispectral data, as the analyses in Chapter 5 and 6 have shown that information on surface fuels can only be obtained to a limited extent and only indirectly via canopy properties. It may be possible to establish such an indirect link between the condition of the overstory and surface fuel condition, but complicating effects such as competition for water resources between species and sheltering effects of the canopy on microclimatic conditions near the forest floor exist. Seasonal transfer of biomass between live and dead pools is partly directly linked to the defoliation of overstory trees, which can be detected using multispectral data. Senescence of understory vegetation is yet more difficult to capture. Monitoring surface fuel dynamics in temperate forests may thus be more challenging than in open landscapes and require greater reliance on ecological modelling approaches.

8.1.3 Airborne laserscanning data

High-density airborne laserscanning data were included in this work to estimate surface fuels loads in temperate forests (Chapter 6). In agreement with previous studies in other ecosystems, the precision of fuel component predictions decreased towards the forest floor, with best results for shrub woody fuels and weakest results for coarse woody debris. The work showed that even with high-density ALS data it is difficult to estimate ground-based fuels such as dead wood and litter, including in stands with low canopy density, emphasising the need for alternative approaches. Lidar metrics derived for the canopy were most important in estimating loads for fine dead fuels such as litter and dead 1 hr fuels,

indicating that there was little information in the direct interaction of the laser beam with the forest floor. Trade-offs between canopy closure and penetration depth, as well as the presence of understory under low-density canopies, limited direct sensing of the forest floor. Also footprint size was likely to be a limiting factor in the characterisation of fine dead fuels. Coarse woody fuel loads could not be estimated from ALS data with the approach used either, but there may be greater potential for approaches based on multispectral ALS and object-based segmentation.
Still, while airborne laserscanning data with high point densities were of limited usefulness in characterising ground-based fuels, they showed potential for understory fuel characterisation. Shrub woody fuel load was reasonably well predictable based on ALS data, however, the fine fraction of shrub fuels relevant to surface fire spread could not be quantified reliably. This had a significant impact on modelled fire behaviour in central European forests using the Rothermel surface fire spread model, indicating the urgent need to develop more accurate models for estimating shrub fine fuels. Herbaceous fuel loads were estimated with moderate accuracy from ALS by incorporating metrics based on both canopy and near-surface returns. The analyses showed that different metric types were useful for understory fuel load estimation, including density, geometric, and intensity features. In the future, these should be used in understory segmentation and leaf-wood classification of ALS point clouds before fuel loads are derived. Additionally, incorporating species-specific information was identified as likely means to improve estimates of both herbaceous and shrub fuel loads using allometric equations based on ALS-derived metrics. Species identification could be achieved using below-canopy observations to identify different understory types for example by further developing the approach presented in Chapter 5.

8.2 Summary

The aim of this work was to contribute to the advancement of remote sensing based techniques for surface fuel characterisation and to increase the knowledge of fuels in temperate ecosystems of Europe.
The proposed method of CNN-based fuel type identification using in-forest RGB imagery improves the characterisation of important surface fuelbed traits. The approach has the potential to replace the long-standing method of fuel classification based on photo series, which is highly subjective and difficult to replicate between different observers. It is therefore an important contribution to advancing fuel characterisation techniques by utilising easily accessible and low-cost images that can be acquired with simple devices such as smartphones cameras, and leveraging the visual processing capabilities of artificial intelligence (AI) methods. Furthermore, it demonstrates that deep learning approaches can be successfully applied in wildland fuel science and have potential for further development beyond fuel type classification. In particular, AI-based methods open up new ways for integrating a wide range of sensor modalities for a more precise fuel characterisation.
The study also provided a more detailed classification of surface fuel types in central European forests, which had previously been lacking. Still, the level of detail required in surface fuel type classification for practical purposes needs to be determined, e.g. through combustion experiments that enable relating the identified fuel types to observed fire behaviour.
This work further showed that accurate quantification of different surface fuel components in forests remains challenging even with detailed multispectral satellite and ALS observations, especially for ground-based fuels. The combination of spectral and structural predic-

tors generally led to improved estimates of most surface fuel components compared to using one data type alone, underlining the synergistic effect of multimodal datasets for surface fuel characterisation, which should be further explored.
The research underlined the difficulties in obtaining accurate fuel load estimates from remote sensing, also due the different spatial scales at which different fuel components vary. This demands a more flexible and scalable approach to surface fuel characterisation that incorporates different datasets, methodological approaches, and spatial scales depending on the target component and the requirements of the application, and should also translate to an adaptation of field sampling methods.
Despite the limited accuracies, this is the first time a spatially explicit representation of this key fuel property (fuel load) has been obtained in central European forests, providing a higher level of detail than conventional fuel classification maps. Fuel load maps give a better overview of the spatial distribution of surface fuels in forest stands and are thus relevant to forest managers and firefighters. In addition, they can help improve estimates of forest aboveground biomass and refine emission estimates from burning forest stands.
Furthermore, this thesis showed that dynamic changes in surface fuels due to phenology and post-fire recovery processes in open landscapes such as heathlands can be assessed to some extent using multispectral satellite time series. While changes in the potential flammability of surface fuels over the course of the year can be tracked using optical indices, long-term vegetation recovery is more difficult to assess accurately based on multispectral data alone. The most reliable results were obtained using SWIR-related indices and for areas dominated by fast-growing life forms such as grasses, whereas areas dominated by slower growing life forms such as dwarf shrubs require the integration of structural information. Analysing the potential environmental drivers of spectral recovery times contributed to a better understanding of the recovery process after wildfire, which can be incorporated in models describing fuel dynamics that can be used to update fuel maps. On the basis of the regression models presented, it is already possible to make rough predictions as to when a site can be expected to return to a similar state to before the wildfire. This will help to predict future fire risk and prepare suitable management plans. Overall, surface fuel dynamics in open landscapes can possibly be sufficiently well characterised based on multispectral and ancillary structural data, but monitoring surface fuel dynamics in forest ecosystems likely poses additional challenges.

8.3 Outlook

Overall, the approaches presented in this thesis can only capture part of the high spatial and temporal complexity of fuels, which also varies depending on the ecosystem and scale. However, timely and precise fuel information is needed particularly for the recently advanced physics-based fire behaviour models, such as FIRETEC (R. Linn et al., 2002) and WFDS (Mell et al., 2007), which rely on computational fluid dynamics (CFD) and require fine-scale, three-dimensional (3D) fuel inputs (e.g., Parsons et al., 2011). CFD models are specifically useful to understand the underlying mechanisms of fire propagation through heterogeneous fuels, however, running these models is computationally expensive. More recently, real-time simulation tools that include fire-atmosphere coupling for prescribed fire planning have been developed, which also require 3D fuel inputs (R. R. Linn et al., 2020). Still, less resource-intensive semi-empirical models such as FlamMap (Finney, 2006) may be the first choice for landscape-scale fire behaviour calculations and operational purposes.

Hence, accurate fuel representations at the landscape scale are also needed, and are further relevant for emission calculations by models such as CONSUME (Prichard et al., 2007) and FOFEM (Reinhardt, 1997).
Recently, besides emphasising the need for continuous mapping of fuel properties, fire scientists have asked for new frameworks to characterise 3D fuels for CFD models and establish linkages between different spatial scales (D. L. Peterson et al., 2022; Prichard et al., 2023). As proximal and remote sensing data from different sensors are becoming available in increasing volumes and at low cost, combining these is a promising way to achieve a more precise characterisation of surface fuels that can suit different applications and modelling scales. Multi-modal datasets have already shown promise in surface fuel characterisation, as has been demonstrated in Chapter 5 and 6. The new processing capabilities offered by AI-based methods, which require little preprocessing of data and automatically extract and select useful features, can be handy to fuse different datasets for fuel characterisation. In this Outlook, I aim to extend on previous proposals for future surface fuel characterisation by presenting my own view on what remote sensing datasets and methods could be helpful to capture surface fuel variability and impacting ecological processes at the relevant scales. **Figure 8.1** provides an overview of the proposed framework to achieve a multi-source, multi-scale, and multi-temporal characterisation of surface fuels in temperate forests and dwarf shrub heaths, and beyond.

8.3.1 Future surface fuel characterisation

At the local scale, gridded 3D information on fuels is required to run CFD models. Therefore, a voxel-based representation of fuels is needed, with each voxel being associated with information about the amount of fuel contained within the voxel (fuel load), its physico-chemical properties (fuel traits), and its condition (fuel moisture). The voxel size determines the resolution of the fuelbed. Detailed 3D point clouds of the forest understory vegetation and coarse deadwood should be collected by terrestrial laserscanning (TLS), ideally integrated with an imaging sensor that captures colour information (RGB values), or alternatively a separate external camera. While the point cloud is used to determine the presence of fuel in each voxel, e.g., by relating the return density per voxel to the occupied volume, the colour information is necessary to visually interpret the data and recognise different plant parts and their properties, such as their live/dead status. This could be realised by deep learning-based semantic segmentation of the 3D point cloud (see e.g. Zhang et al. (2023) for a recent discussion of different methods). The segmented plant parts could be associated with information on SAV, heat content, and particle density for the identified species from a trait database. Particle density and estimated volume occupied could be combined to retrieve fuel load. Moisture content of the plant parts is calculated based on weather data for dead fuels depending on their identified size, while the moisture of live fuels is determined by classification as leaf or wood and associated with respective species-specific moisture content under consideration of weather-induced drought stress.
For the litter layer and fine dead fuels, a slightly different approach might be necessary. Litter depth could be identified from a ground-penetrating radar system, which may also allow to retrieve the moisture content of the litter layer. RGB imagery could be used to identify litter types and the presence of fine woody fuels using CNNs, which could be associated with typical bulk density values of the litter layer (allowing to calculate litter fuel load) and physico-chemical properties for the species present.

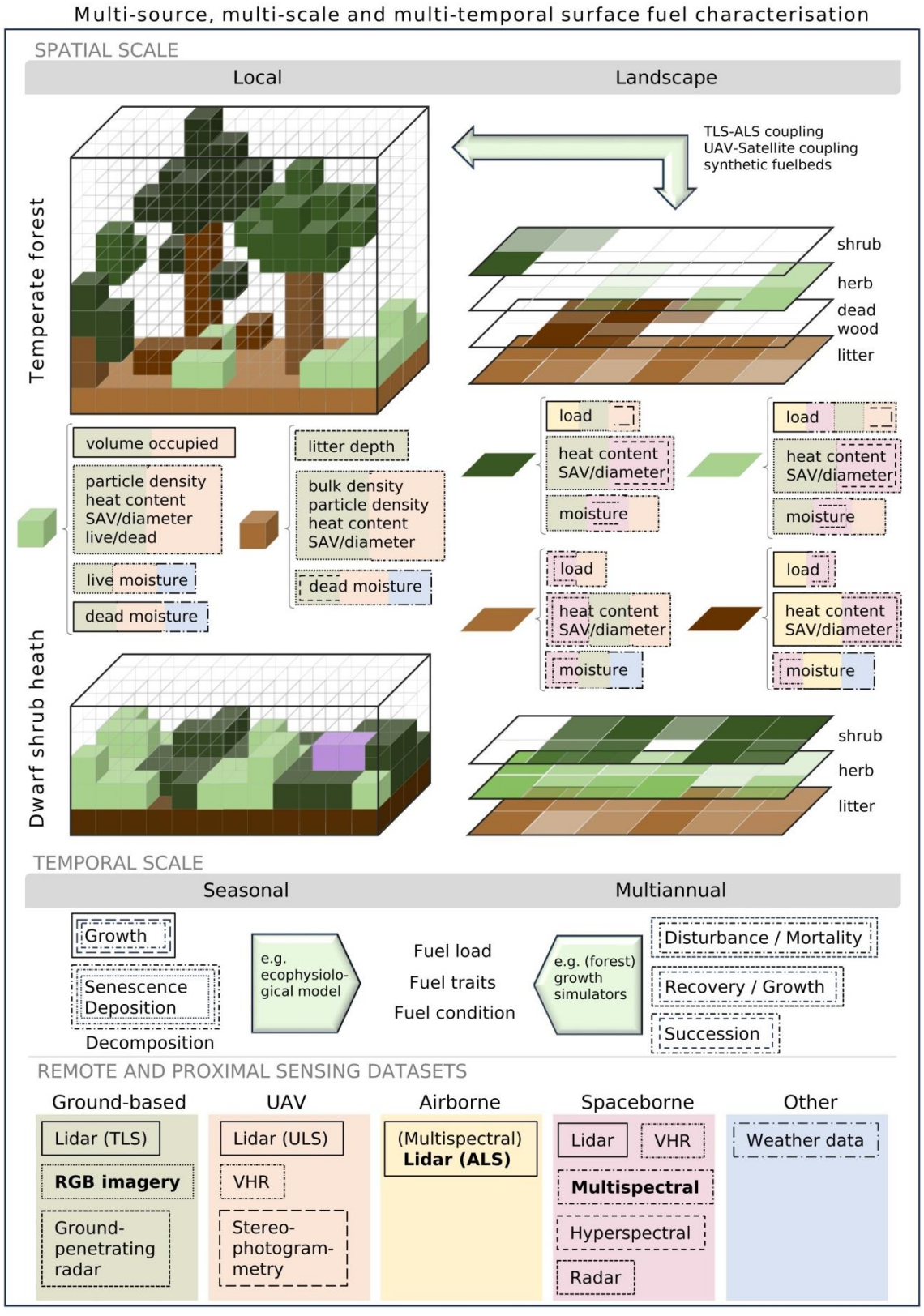

Figure 8.1: Proposed framework for surface fuel characterisation covering different spatial and temporal scales by using a variety of proximal and remote sensing datasets. Line types indicate the type of data suggested to be used to capture a surface fuel property or ecological process, while coloured fills indicate suitable platforms/locations of the respective data collecting sensor. As the ecological processes that influence temporal fuel variation also cover different spatial scales, no colours are used to indicate that different sensor platforms may be suitable. Data types printed in bold have been examined in this thesis.

In forest ecosystems, these sensors are ideally mounted on a ground vehicle that moves through the forest while collecting data. For the denser and more homogeneously vegetated dwarf shrub heaths, it might be more practical to use a UAV platform and collect the data from a top view. Difficulties in estimating the litter layer could be overcome by relating the litter production to different growth stages of the dwarf shrubs identified from the collected VHR imagery (see for example Neumann et al., 2020) or to the productivity of the graminoids under the given site conditions, while also including site-specific decomposition rates.

At the landscape scale, fuel information is provided in 2D raster layers for each fuel component, which can be combined into raster stacks, with each cell containing information on average fuel load, traits, and moisture within the grid cell. The resolution of the raster grid is coarser than that of the 3D representation and the spatial coverage is greater. The fuel information can be used to analyse fire behaviour and fire effects at the landscape scale, where topography and weather gain importance over fine-scale fuel heterogeneity. Still, a continuous representation of the fuel properties is being sought, as it has more informative value for different applications and enables better scalability between the 2D and 3D approach. High-density airborne laserscanning (ALS) data, preferably operating at different wavelengths (e.g., NIR, SWIR, green), is subject to a stepwise segmentation approach, that first separates different forest strata (e.g., Ferraz et al., 2012). Then, the intensity information of the different channels and geometric features are used to distinguish between dead and living fuels, and leaves and wood (e.g., Krishna Moorthy et al., 2020). From the segmented point cloud, the shrub total and fine biomass are estimated. Herb fuel loads are also estimated from the ALS point cloud, but multispectral satellite data is included as additional predictor capturing canopy characteristics (as has been shown to be beneficial in Chapter 6). When only low-density and/or single-channel ALS data are available, cover and height of the herbaceous and shrub layer are estimated from the point cloud, and loads are calculated by using allometric equations for the main species present, identified from point-captured below-canopy photographs using CNNs (see Chapter 5) and then extrapolated to the whole area. The species information from below-canopy observations is also needed to assign the average physico-chemical properties. Herb and shrub fuel moisture are empirically tied to the canopy multispectral or radar signal, and species-specific differences are incorporated using empirical data. Concerning the litter layer, average loads are assigned according to the dominating tree species (see Chapter 6) and site conditions. Litter traits are assigned based on canopy properties identified from multispectral satellite data and refined using forest floor photographs where available (Chapter 5). Litter moisture is determined from weather data and litter type-specific drying/wetting curves (e.g. Schunk et al., 2013). Coarse deadwood in forest ecosystems can either be identified in the multispectral ALS dataset, or a rough area-based estimate is made depending on stand age, species, and management. Inaccuracies in this fuel component are less relevant for fire behaviour estimates, but can affect fire effects models. Deadwood traits and moisture are assigned based on overstory species (multispectral data), stem size (from ALS or stand age), and weather data.

For the vertically less complex dwarf shrub heaths, it may be sufficient to create photogrammetric point clouds from UAV observations instead of acquiring more costly lidar data. The resulting canopy height model can be used together with VHR or hyperspectral imagery where the different life forms (mainly graminoids and dwarf shrubs) are segmented to calculate their respective loads based on allometric equations incorporating cover and

height. Fuel traits are assigned according to the dominating life form in the grid cell, taking into account different growth stages in the case of dwarf shrubs, which have been identified in the imagery. Moisture values are assigned as an average across the canopy based on optical or radar data, calibrated for the respective life form. Similar to the 3D approach, average litter loads are assigned based on the balance of deposition and decomposition determined empirically or through ecological modelling for the identified life forms and environmental conditions. Litter traits are also assigned based on the dominating life form, and growth stage if applicable, while litter moisture is modelled depending on weather data.

Links between small-scale 3D and larger-scale 2D representations can be established. 2D rasters of fuels may be obtained from 3D voxels by averaging/summarising the attributes of all voxels that fall within a raster grid cell and contain the fuel component of interest. Additionally, detailed TLS models of understory fuels can be coupled with ALS or even spaceborne lidar measurements. Similarly, UAV observations of fuel situations can be linked to multispectral satellite observations, thus helping to improve mapping efforts at larger scales. Synthetic TLS and ALS fuelbeds could be used to train models that can predict a plausible representation in the case that one of the two datasets is missing in an area. Furthermore, they could be used to build up a large database of possible fuelbeds, for example with the help of forest growth simulators that allow to create realistic forest stands of varying structure and composition, and also include different types of forest management (e.g., Henniger et al., 2023). Deep learning algorithms could then predict the best matching 3D fuelbed for a stand from simple forest photographs (extending the work in Chapter 5), rapidly providing the basis for fire behaviour modelling in any location.

Temporal dynamics in fuels as a result of ecological processes also need to be included in future fuel characterisation frameworks. Seasonal changes in the flammability of open landscapes such as dwarf shrub heaths can be monitored using optical satellite time series data (see Chapter 7), which allow to determine the timing of phenological events such as the onset of spring green-up or autumnal senescence. However, in forest ecosystems, below-canopy observations, e.g. from phenocams, should complement satellite-based observations, which can only inform the timing of leaf shedding from overstory trees. Still, both empirical and process-based ecological models are needed to quantify the effects of such phenological events on fuel loads, traits, and condition. In particular, processes such as decomposition and associated changes in fuel characteristics cannot be resolved with remote sensing data and require ecological modelling. Seasonal growth of fast-growing life forms can be monitored using multispectral data, but more importantly structural information from repeated lidar acquisitions or photogrammetric point clouds is needed. On time scales of multiple years, processes such as disturbance and mortality as well as subsequent recovery and succession become relevant. The occurrence of disturbance events is readily detectable with radar and multispectral satellite data acquired at high temporal resolution, and these data can also be used to monitor vegetation recovery (see Chapter 7). Detecting changes in species composition through succession, and the resulting effects on fuel loads and traits, may require higher spectral and spatial resolution, provided for example by VHR and hyperspectral imagery. However, it is inefficient to monitor such processes closely at every possible site, so generalisations based on ecological models are essential and require further research.

8.3.2 Additional research needs

The individual methods and remote sensing datasets proposed above for fuel characterisation need to be thoroughly tested and validated. Importantly, methods to combine the individual datasets and evaluation techniques within a joint framework should be explored. Future research should therefore focus primarily on methods for processing data of different structure and approaches to data fusion.
Future research will also need to address the collection of reference data, including the adaptation of field sampling protocols. 3D fuel sampling approaches have already been proposed (Hawley et al., 2018; Rowell et al., 2020) and will not be further discussed here. Extensive reference datasets are particularly urgently needed in the understudied but highly vulnerable ecosystems of central-western Europe. Standardised fuel sampling should therefore become part of national forest inventories. More data are also required to develop accurate allometric equations for a number of important species, including their partitioning of biomass into different plant compartments. Furthermore, databases of georeferenced and time-stamped forest photographs should be set up and extended with the help of citizen scientists. This would help to further improve and expand deep learning-based approaches to fuel characterisation. Lidar datasets should be made freely available within and across borders, and a library of synthetic fuelbeds should be established.
Finally, laboratory experiments at varying scales and with different species, as well as experimental burns in the field, are needed to better understand fire behaviour in central European fuelbeds. In order to be able to validate fire modelling results with data from real fires, standardised protocols for collecting data on fire behaviour characteristics during real wildfires should be established, ideally including the collection of optical and thermal data from UAV platforms.

Continuing the research on fuels and fire behaviour in temperate ecosystems is essential to respond appropriately to the increasing risk of wildfires. Better characterisation of complex fuelbeds, both at fine scales and over large areas, is a fundamental step towards a better understanding of fire dynamics and effects based on modelling approaches. Shifts in vegetation composition, productivity, arrangement, and condition associated with climate change will continue to alter fuelbed properties and need to be monitored precisely. This will provide the foundation for preparing for changes in the pattern, intensity, severity, and frequency of future wildfires in European temperate regions.

References

Abatzoglou, J. T., Williams, A. P., & Barbero, R. (2019). Global Emergence of Anthropogenic Climate Change in Fire Weather Indices. *Geophysical Research Letters*, *46*(1), 326–336. https://doi.org/10.1029/2018GL080959

Abdollahi, A., & Yebra, M. (2023). Forest fuel type classification: Review of remote sensing techniques, constraints and future trends. *Journal of Environmental Management*, *342*, 118315. https://doi.org/10.1016/j.jenvman.2023.118315

Abrams, J. F., Vashishtha, A., Wong, S. T., Nguyen, Mohamed, A., Wieser, S., Kuijper, A., Wilting, A., & Mukhopadhyay, A. (2019). Habitat-Net: Segmentation of habitat images using deep learning. *Ecological Informatics*, *51*, 121–128. https://doi.org/10.1016/j.ecoinf.2019.01.009

Adámek, M., Bobek, P., Hadincová, V., Wild, J., & Kopecký, M. (2015). Forest fires within a temperate landscape: A decadal and millennial perspective from a sandstone region in Central Europe. *Forest Ecology and Management*, *336*, 81–90. https://doi.org/10.1016/j.foreco.2014.10.014

Adámek, M., Hadincová, V., & Wild, J. (2016). Long-term effect of wildfires on temperate Pinus sylvestris forests: Vegetation dynamics and ecosystem resilience. *Forest Ecology and Management*, *380*, 285–295. https://doi.org/10.1016/j.foreco.2016.08.051

Adámek, M., Jankovská, Z., Hadincová, V., Kula, E., & Wild, J. (2018). Drivers of forest fire occurrence in the cultural landscape of Central Europe. *Landscape Ecology*, *33*(11), 2031–2045. https://doi.org/10.1007/s10980-018-0712-2

Agee, J. K., & Skinner, C. N. (2005). Basic principles of forest fuel reduction treatments. *Forest Ecology and Management*, *211*(1), 83–96. https://doi.org/10.1016/j.foreco.2005.01.034

Agee, J. K., Wright, C. S., Williamson, N., & Huff, M. H. (2002). Foliar moisture content of Pacific Northwest vegetation and its relation to wildland fire behavior. *Forest Ecology and Management*, *167*(1), 57–66. https://doi.org/10.1016/S0378-1127(01)00690-9

Agrawal, S., & Khairnar, G. B. (2019). A comparative assessment of remote sensing imaging techniques: Optical, SAR and LiDAR. *The International Archives of the Photogrammetry, Remote Sensing and Spatial Information Sciences*, *XLII-5-W3*, 1–6. https://doi.org/10.5194/isprs-archives-XLII-5-W3-1-2019

Akmet'eva, N. P., Belova, S. E., Dzhamalov, R. G., Kulichevskaya, I. S., Lapina, E. E., & Mikhailova, A. V. (2014). Natural post-fire bog recovery. *Water Resources*, *41*(4), 353–363. https://doi.org/10.1134/S0097807814040022

Albertson, K., Aylen, J., Cavan, G., & McMorrow, J. (2009). Forecasting the outbreak of moorland wildfires in the English Peak District. *Journal of Environmental Management*, *90*(8), 2642–2651. https://doi.org/10.1016/j.jenvman.2009.02.011

Albertson, K., Aylen, J., Cavan, G., & McMorrow, J. (2010). Climate change and the future occurrence of moorland wildfires in the Peak District of the UK. *Climate Research*, *45*, 105–118. https://doi.org/10.3354/cr00926

Albini, F. A. (1976). *Estimating Wildfire Behavior and Effects*. Department of Agriculture, Forest Service, Intermountain Forest and Range Experiment Station.

Albini, F. A. (1984). Wildland Fires: Predicting the behavior of wildland fires—Among nature's most potent forces—Can save lives, money, and natural resources. *American Scientist*, *72*(6), 590–597.

Alipour, M., La Puma, I., Picotte, J., Shamsaei, K., Rowell, E., Watts, A., Kosovic, B., Ebrahimian, H., & Taciroglu, E. (2023). A Multimodal Data Fusion and Deep Learning Framework for Large-Scale Wildfire Surface Fuel Mapping. *Fire*, *6*(2), 2. https://doi.org/10.3390/fire6020036

Al-Moustafa, T., Armitage, R. P., & Danson, F. M. (2012). Mapping fuel moisture content in upland vegetation using airborne hyperspectral imagery. *Remote Sensing of Environment*, *127*, 74–83. https://doi.org/10.1016/j.rse.2012.08.034

Alonso-Benito, A., Arroyo, L. A., Arbelo, M., Hernández-Leal, P., & González-Calvo, A. (2012). Pixel and object-based classification approaches for mapping forest fuel types in Tenerife Island from ASTER data. *International Journal of Wildland Fire*, *22*(3), 306–317. https://doi.org/10.1071/WF11068

Alonso-Benito, A., Arroyo, L., Arbelo, M., & Hernández-Leal, P. (2016). Fusion of WorldView-2 and LiDAR Data to Map Fuel Types in the Canary Islands. *Remote Sensing*, *8*(8), 669. https://doi.org/10.3390/rs8080669

Alonso-Rego, C., Arellano-Pérez, S., Guerra-Hernández, J., Molina-Valero, J. A., Martínez-Calvo, A., Pérez-Cruzado, C., Castedo-Dorado, F., González-Ferreiro, E., Álvarez-González, J. G., & Ruiz-González, A. D. (2021). Estimating Stand and Fire-Related Surface and Canopy Fuel Variables in Pine Stands Using Low-Density Airborne and Single-Scan Terrestrial Laser Scanning Data. *Remote Sensing*, *13*(24), 5170. https://doi.org/10.3390/rs13245170

Anderegg, L. D., Anderegg, W. R., & Berry, J. A. (2013). Not all droughts are created equal: Translating meteorological drought into woody plant mortality. *Tree Physiology*, *33*(7), 701–712. https://doi.org/10.1093/treephys/tpt044

Andersen, H.-E., McGaughey, R. J., & Reutebuch, S. E. (2005). Estimating forest canopy fuel parameters using LIDAR data. *Remote Sensing of Environment*, *94*(4), 441–449. https://doi.org/10.1016/j.rse.2004.10.013

Anderson, H. E. (1982). Aids to determining fuel models for estimating fire behavior. *U.S. Department of Agriculture, Forest Service, Intermountain Forest and Range Experiment Station*, *122*. https://doi.org/10.2737/INT-GTR-122

Andre, F., Jonard, M., & Lambot, S. (2015). Non-Invasive Forest Litter Characterization Using Full-Wave Inversion of Microwave Radar Data. *IEEE Transactions on Geoscience and Remote Sensing*, *53*(2), 828–840. https://doi.org/10.1109/TGRS.2014.2328776

Andrews, P. L. (2009). *BehavePlus fire modeling system, version 5.0: Variables* (Gen. Tech. Rep. RMRS-GTR-213WWW Revised). Department of Agriculture, Forest Service, Rocky Mountain Research Station.

Andrews, P. L. (2012). *Modeling wind adjustment factor and midflame wind speed for Rothermel's surface fire spread model* (Gen. Tech. Rep. RMRS-GTR-266). U.S. Department of Agriculture, Forest Service, Rocky Mountain Research Station.

Andrews, P. L. (2014). Current status and future needs of the BehavePlus Fire Modeling System. *International Journal of Wildland Fire*, *23*(1), 21–33. https://doi.org/10.1071/WF12167

Andrews, P. L. (2018). *The Rothermel surface fire spread model and associated developments: A comprehensive explanation* (Gen. Tech. Rep. RMRS-GTR-371). U.S. Department of Agriculture, Forest Service, Rocky Mountain Research Station.

Andrews, P. L., & Queen, Ll. P. (2001). Fire modeling and information system technology. *International Journal of Wildland Fire*, *10*(4), 343–352. https://doi.org/10.1071/WF01033

Annighöfer, P., Ameztegui, A., Ammer, C., Balandier, P., Bartsch, N., Bolte, A., Coll, L., Collet, C., Ewald, J., Frischbier, N., Gebereyesus, T., Haase, J., Hamm, T., Hirschfelder, B., Huth, F., Kändler, G., Kahl, A., Kawaletz, H., Kuehne, C., … Mund, M. (2016). Species-specific and generic biomass equations for seedlings and saplings of European tree species. *European Journal of Forest Research*, *135*(2), 313–329. https://doi.org/10.1007/s10342-016-0937-z

Apley, D. W., & Zhu, J. (2020). Visualizing the effects of predictor variables in black box supervised learning models. *Journal of the Royal Statistical Society: Series B (Statistical Methodology)*, *82*(4), 1059–1086. https://doi.org/10.1111/rssb.12377

Aragoneses, E., García, M., Salis, M., Ribeiro, L. M., & Chuvieco, E. (2023). Classification and mapping of European fuels using a hierarchical, multipurpose fuel classification system. *Earth System Science Data*, *15*(3), 1287–1315. https://doi.org/10.5194/essd-15-1287-2023

Arellano-Pérez, S., Castedo-Dorado, F., López-Sánchez, C., González-Ferreiro, E., Yang, Z., Díaz-Varela, R., Álvarez-González, J., Vega, J., & Ruiz-González, A. (2018). Potential of Sentinel-2A Data to Model Surface and Canopy Fuel Characteristics in Relation to Crown Fire Hazard. *Remote Sensing*, *10*(10), 1645. https://doi.org/10.3390/rs10101645

Argañaraz, J. P., Landi, M. A., Bravo, S. J., Gavier-Pizarro, G. I., Scavuzzo, C. M., & Bellis, L. M. (2016). Estimation of Live Fuel Moisture Content From MODIS Images for Fire Danger Assessment in Southern Gran Chaco. *IEEE Journal of Selected Topics in Applied Earth Observations and Remote Sensing*, *9*(12), 5339–5349. https://doi.org/10.1109/JSTARS.2016.2575366

Arkin, J., Coops, N. C., Daniels, L. D., & Plowright, A. (2023). Canopy and surface fuel estimations using RPAS and ground-based point clouds. *Forestry: An International Journal of Forest Research*. https://doi.org/10.1093/forestry/cpad020

Arnell, N. W., Freeman, A., & Gazzard, R. (2021). The effect of climate change on indicators of fire danger in the UK. *Environmental Research Letters*, *16*(4), 044027. https://doi.org/10.1088/1748-9326/abd9f2

Arroyo, L. A., Pascual, C., & Manzanera, J. A. (2008). Fire models and methods to map fuel types: The role of remote sensing. *Forest Ecology and Management*, *256*(6), 1239–1252. https://doi.org/10.1016/j.foreco.2008.06.048

Ascoli, D., Castagneri, D., Valsecchi, C., Conedera, M., & Bovio, G. (2013). Post-fire restoration of beech stands in the Southern Alps by natural regeneration. *Ecological Engineering*, *54*, 210–217. https://doi.org/10.1016/j.ecoleng.2013.01.032

Ascoli, D., Vacchiano, G., Motta, R., & Bovio, G. (2015). Building Rothermel fire behaviour fuel models by genetic algorithm optimisation. *International Journal of Wildland Fire*, *24*(3), 317. https://doi.org/10.1071/WF14097

Astiani, D., Widiastuti, T., Latifah, S., & Simatupang, D. (2020). Soil characteristics and CO2 emissions of ex-burnt peatland in Kubu Raya District, West Kalimantan, Indonesia. *Biodiversitas Journal of Biological Diversity*, *21*(8), 8. https://doi.org/10.13057/biodiv/d210836

Ausden, M. (2007). *Habitat Management for Conservation: A Handbook of Techniques*. Oxford University Press.

Badi, A. H. A. (2019). *Remote sensing to characterise vegetation fuel moisture content in the UK uplands* [PhD Thesis]. University of Salford (United Kingdom).

Bajocco, S., Dragoz, E., Gitas, I., Smiraglia, D., Salvati, L., & Ricotta, C. (2015). Mapping Forest Fuels through Vegetation Phenology: The Role of Coarse-Resolution Satellite Time-Series. *PLOS ONE*, *10*(3), e0119811. https://doi.org/10.1371/journal.pone.0119811

Baldridge, A. M., Hook, S. J., Grove, C. I., & Rivera, G. (2009). The ASTER spectral library version 2.0. *Remote Sensing of Environment*, *113*(4), 711–715. https://doi.org/10.1016/j.rse.2008.11.007

Bannister, P. (1964). The Water Relations of Certain Heath Plants with Reference to their Ecological Amplitude: II. Field Studies. *Journal of Ecology*, *52*(3), 481–497. https://doi.org/10.2307/2257845

Battisti, C., Poeta, G., & Fanelli, G. (2016). *An introduction to disturbance ecology: A Road Map for Wildlife Management and Conservation*. https://doi.org/10.1007/978-3-319-32476-0

Bayoudh, K., Knani, R., Hamdaoui, F., & Mtibaa, A. (2021). A survey on deep multimodal learning for computer vision: Advances, trends, applications, and datasets. *The Visual Computer*, 1–32. https://doi.org/10.1007/s00371-021-02166-7

Bayr, U., & Puschmann, O. (2019). Automatic detection of woody vegetation in repeat landscape photographs using a convolutional neural network. *Ecological Informatics*, *50*, 220–233. https://doi.org/10.1016/j.ecoinf.2019.01.012

Billett, M. F., Charman, D. J., Clark, J. M., Evans, C. D., Evans, M. G., Ostle, N. J., Worrall, F., Burden, A., Dinsmore, K. J., Jones, T., McNamara, N. P., Parry, L., Rowson, J. G., & Rose, R. (2010). Carbon balance of UK peatlands: Current state of knowledge and future research challenges. *Climate Research*, *45*, 13–29. https://doi.org/10.3354/cr00903

Birkeli, K., Gya, R., Haugum, S. V., Velle, L. G., & Vandvik, V. (2023). Germination and seedling growth of Calluna vulgaris is sensitive to regional climate, heathland succession, and drought. *Ecology and Evolution*, *13*(7), e10199. https://doi.org/10.1002/ece3.10199

Blauw, L. G., van Logtestijn, R. S. P., Broekman, R., Aerts, R., & Cornelissen, J. H. C. (2017). Tree species identity in high-latitude forests determines fire spread through fuel ladders from branches to soil and vice versa. *Forest Ecology and Management*, *400*, 475–484. https://doi.org/10.1016/j.foreco.2017.06.023

BLE. (2023). *Waldbrandstatistiken der Bundesrepublik Deutschland*. https://www.ble.de/DE/BZL/Daten-Berichte/Wald/wald.html

Bobek, P., Svobodová-Svitavská, H., Pokorný, P., Šamonil, P., Kuneš, P., Kozáková, R., Abraham, V., Klinerová, T., Švarcová, M. G., Jamrichová, E., Krauseová, E., & Wild, J. (2019). Divergent fire history trajectories in Central European temperate forests revealed a pronounced influence of broad-leaved trees on fire dynamics. *Quaternary Science Reviews*, *222*, 105865. https://doi.org/10.1016/j.quascirev.2019.105865

Boelman, N. T., Rocha, A. V., & Shaver, G. R. (2011). Understanding burn severity sensing in Arctic tundra: Exploring vegetation indices, suboptimal assessment timing and the impact of increasing pixel size. *International Journal of Remote Sensing*, *32*(22), 7033–7056. https://doi.org/10.1080/01431161.2011.611187

Boer, M. M., Nolan, R. H., Resco De Dios, V., Clarke, H., Price, O. F., & Bradstock, R. A. (2017). Changing Weather Extremes Call for Early Warning of Potential for Catastrophic Fire. *Earth's Future*, *5*(12), 1196–1202. https://doi.org/10.1002/2017EF000657

Bohlmann, J., & Keeling, C. I. (2008). Terpenoid biomaterials. *The Plant Journal*, *54*(4), 656–669. https://doi.org/10.1111/j.1365-313X.2008.03449.x

Bolte, A. (2006). Biomasse- und Elementvorräte der Bodenvegetation auf Flächen des forstlichen Umweltmonitorings in Rheinland-Pfalz. *Berichte Des Forschungszentrum Waldökosysteme, Institut Für Waldbau, Universität Göttingen*.

Bonazountas, M., Astyakopoulos, A., Martirano, G., Sebastian, A., de la fuente, D., Ribeiro, L., Viegas, D., Eftichidis, G., Gitas, I., & Toukiloglou, P. (2014). *LIFE ArcFUEL: Mediterranean fuel-type maps geodatabase for wildland & forest fire safety*. VII International Conference on Forest Fire Research. https://doi.org/10.14195/978-989-26-0884-6_189

Botequim, B., Fernandes, P. M., Borges, J. G., González-Ferreiro, E., & Guerra-Hernández, J. (2019). Improving silvicultural practices for Mediterranean forests through fire behaviour modelling using LiDAR-derived canopy fuel characteristics. *International Journal of Wildland Fire*, *28*(11), 823–839. https://doi.org/10.1071/WF19001

Brandis, K., & Jacobson, C. (2003). Estimation of vegetative fuel loads using Landsat TM imagery in New South Wales, Australia. *International Journal of Wildland Fire*, *12*(2), 185. https://doi.org/10.1071/wf03032

Breiman, L. (2001). Random Forests. *Machine Learning*, *45*(1), 5–32. https://doi.org/10.1023/A:1010933404324

Bright, B., Hudak, A., Meddens, A., Hawbaker, T., Briggs, J., & Kennedy, R. (2017). Prediction of Forest Canopy and Surface Fuels from Lidar and Satellite Time Series Data in a Bark Beetle-Affected Forest. *Forests*, *8*(9), 322. https://doi.org/10.3390/f8090322

Brodrick, P. G., & Asner, G. P. (2017). Remotely sensed predictors of conifer tree mortality during severe drought. *Environmental Research Letters*, *12*(11), 115013. https://doi.org/10.1088/1748-9326/aa8f55

Brown, J. K. (1970). Ratios of surface area to volume for common fine fuels. *Forest Science*, *16*(1), 101–105. https://doi.org/10.1093/forestscience/16.1.101

Brown, J. K. (1978). *Weight and Density of Crowns of Rocky Mountain Conifers*. Department of Agriculture, Forest Service, Intermountain Forest and Range Experiment Station.

Brown, J. K. (1981). *Downed Dead Woody Fuel and Biomass in the Northern Rocky Mountains* (INT-117). U.S. Department of Agriculture, Forest Service, Intermountain Forest and Range Experiment Station.

Brown, J. K. (1986). *Surface Fuel Loadings and Predicted Fire Behavior for Vegetation Types in the Northern Rocky Mountains* (INT-358). U.S. Department of Agriculture, Forest Service, Intermountain Research Station.

Brown, J. K., Oberheu, R. D., & Johnston, C. M. (1982). *Handbook for inventorying surface fuels and biomass in the Interior West* (INT-GTR-129). U.S. Department of Agriculture, Forest Service, Intermountain Forest and Range Experiment Station. https://doi.org/10.2737/INT-GTR-129

Brys, R., Jacquemyn, H., & De Blust, G. (2005). Fire increases aboveground biomass, seed production and recruitment success of Molinia caerulea in dry heathland. *Acta Oecologica*, *28*(3), 299–305. https://doi.org/10.1016/j.actao.2005.05.008

Burgan, R. E. (1979). *Estimating Live Fuel Moisture for the 1978 National Fire Danger Rating System*. Intermountain Forest and Range Experiment Station, Forest Service, U.S. Department of Agriculture.

Burgan, R. E. (1987). *Concepts and Interpreted Examples in Advanced Fuel Modeling* (INT-238). U.S. Department of Agriculture, Forest Service, Intermountain Research Station.

Burgan, R. E., & Rothermel, R. C. (1984). *BEHAVE: Fire Behavior Prediction and Fuel Modeling System, Fuel Subsystem* (INT-GTR-167). Intermountain Forest and Range Experiment Station, Forest Service, U.S. Department of Agriculture.

Burton, J. E., Cawson, J. G., Filkov, A. I., & Penman, T. D. (2021). Leaf traits predict global patterns in the structure and flammability of forest litter beds. *Journal of Ecology*, *109*(3), 1344–1355. https://doi.org/10.1111/1365-2745.13561

Byram, G. M. (1959). Combustion of forest fuels. *Forest Fire : Control and Use*, 61–89.

Campbell, M. J., Dennison, P. E., Hudak, A. T., Parham, L. M., & Butler, B. W. (2018). Quantifying understory vegetation density using small-footprint airborne lidar. *Remote Sensing of Environment*, *215*, 330–342. https://doi.org/10.1016/j.rse.2018.06.023

Campos-Taberner, M., García-Haro, F. J., Martínez, B., Izquierdo-Verdiguier, E., Atzberger, C., Camps-Valls, G., & Gilabert, M. A. (2020). Understanding deep learning in land use classification based on Sentinel-2 time series. *Scientific Reports*, *10*(1), 17188. https://doi.org/10.1038/s41598-020-74215-5

Cao, R., Zhu, J., Tu, W., Li, Q., Cao, J., Liu, B., Zhang, Q., & Qiu, G. (2018). Integrating Aerial and Street View Images for Urban Land Use Classification. *Remote Sensing*, *10*(10), 1553. https://doi.org/10.3390/rs10101553

Carbone, A., Spiller, D., & Laneve, G. (2023). Fuel Type Mapping Using a CNN-Based Remote Sensing Approach: A Case Study in Sardinia. *Fire*, *6*(10), 10. https://doi.org/10.3390/fire6100395

Cardíl, A., Tapia, V. M., Monedero, S., Quiñones, T., Little, K., Stoof, C. R., Ramirez, J., & de-Miguel, S. (2023). Characterizing the rate of spread of large wildfires in emerging fire environments of northwestern Europe using Visible Infrared Imaging Radiometer Suite active fire data. *Natural Hazards and Earth System Sciences*, *23*(1), 361–373. https://doi.org/10.5194/nhess-23-361-2023

Carnicer, J., Alegria, A., Giannakopoulos, C., Di Giuseppe, F., Karali, A., Koutsias, N., Lionello, P., Parrington, M., & Vitolo, C. (2022). Global warming is shifting the relationships between fire weather and realized fire-induced CO2 emissions in Europe. *Scientific Reports*, *12*(1), 1. https://doi.org/10.1038/s41598-022-14480-8

Caron, D., & Messal, L. (2020). *Jakteristics*. https://github.com/jakarto3d/jakteristics

Carrasco, L., Giam, X., Papeş, M., & Sheldon, K. (2019). Metrics of Lidar-Derived 3D Vegetation Structure Reveal Contrasting Effects of Horizontal and Vertical Forest Heterogeneity on Bird Species Richness. *Remote Sensing*, *11*(7), 743. https://doi.org/10.3390/rs11070743

Caturegli, L., Matteoli, S., Gaetani, M., Grossi, N., Magni, S., Minelli, A., Corsini, G., Remorini, D., & Volterrani, M. (2020). Effects of water stress on spectral reflectance of bermudagrass. *Scientific Reports*, *10*(1), 1. https://doi.org/10.1038/s41598-020-72006-6

Chatto, K., & Tolhurst, K. G. (1997). *Development and testing of the wiltronics TH fine fuel moisture meter* (46). Fire Management Branch, Department of Natural Resources and Environment.

Chávez, R. O., Estay, S. A., Lastra, J. A., Riquelme, C. G., Olea, M., Aguayo, J., & Decuyper, M. (2023). npphen: An R-Package for Detecting and Mapping Extreme Vegetation Anomalies Based on Remotely Sensed Phenological Variability. *Remote Sensing*, *15*(1), 1. https://doi.org/10.3390/rs15010073

Chen, L.-C., Papandreou, G., Kokkinos, I., Murphy, K., & Yuille, A. L. (2018). DeepLab: Semantic Image Segmentation with Deep Convolutional Nets, Atrous Convolution, and Fully Connected CRFs. *IEEE Transactions on Pattern Analysis and Machine Intelligence*, *40*(4), 834–848. https://doi.org/10.1109/TPAMI.2017.2699184

Chen, X., Xiang, S., Liu, C.-L., & Pan, C.-H. (2014). Vehicle Detection in Satellite Images by Hybrid Deep Convolutional Neural Networks. *IEEE Geoscience and Remote Sensing Letters*, *11*(10), 1797–1801. https://doi.org/10.1109/LGRS.2014.2309695

Chen, Y., Zhu, X., Yebra, M., Harris, S., & Tapper, N. (2017). Development of a predictive model for estimating forest surface fuel load in Australian eucalypt forests with LiDAR data. *Environmental Modelling & Software*, *97*, 61–71. https://doi.org/10.1016/j.envsoft.2017.07.007

Chetehouna, K., Courty, L., Mounaïm-Rousselle, C., Halter, F., & Garo, J.-P. (2013). Combustion Characteristics of p-Cymene Possibly Involved in Accelerating Forest Fires. *Combustion Science and Technology*, *185*(9), 1295–1305. https://doi.org/10.1080/00102202.2013.795557

Chirici, G., Scotti, R., Montaghi, A., Barbati, A., Cartisano, R., Lopez, G., Marchetti, M., McRoberts, R. E., Olsson, H., & Corona, P. (2013). Stochastic gradient boosting classification trees for forest fuel types mapping through airborne laser scanning and IRS LISS-III imagery. *International Journal of Applied Earth Observation and Geoinformation*, *25*, 87–97. https://doi.org/10.1016/j.jag.2013.04.006

Chollet, F. (2015). *Keras*. https://github.com/fchollet/keras

Christin, S., Hervet, É., & Lecomte, N. (2019). Applications for deep learning in ecology. *Methods in Ecology and Evolution*, *10*(10), 1632–1644. https://doi.org/10.1111/2041-210X.13256

Chrysafis, I., Damianidis, C., Giannakopoulos, V., Mitsopoulos, I., Dokas, I. M., & Mallinis, G. (2023). Vegetation Fuel Mapping at Regional Scale Using Sentinel-1, Sentinel-2, and DEM Derivatives—The Case of the Region of East Macedonia and Thrace, Greece. *Remote Sensing*, *15*(4), 4. https://doi.org/10.3390/rs15041015

Clark, J. S., Merkt, J., & Muller, H. (1989). Post-Glacial Fire, Vegetation, and Human History on the Northern Alpine Forelands, South-Western Germany. *Journal of Ecology*, *77*(4), 897–925. https://doi.org/10.2307/2260813

Clay, G. D., & Worrall, F. (2011). Charcoal production in a UK moorland wildfire – How important is it? *Journal of Environmental Management*, *92*(3), 676–682. https://doi.org/10.1016/j.jenvman.2010.10.006

Coffelt, J. L., & Livingston, R. K. (2002). *Second U.S. Geological Survey Wildland Fire Workshop: Los Alamos, New Mexico, October 31-November 3, 2000*. https://doi.org/10.3133/ofr0211

Cohen, J. D. (1985). *The National Fire-danger Rating System: Basic Equations* (PSW-82). U.S. Department of Agriculture, Forest Service, Pacific Southwest Forest and Range Experiment Station.

Cohen, W. B., & Spies, T. A. (1992). Estimating structural attributes of Douglas-fir/western hemlock forest stands from landsat and SPOT imagery. *Remote Sensing of Environment*, *41*(1), 1–17. https://doi.org/10.1016/0034-4257(92)90056-P

Cole, B., McMorrow, J., & Evans, M. (2014a). Empirical Modelling of Vegetation Abundance from Airborne Hyperspectral Data for Upland Peatland Restoration Monitoring. *Remote Sensing*, *6*(1), 1. https://doi.org/10.3390/rs6010716

Cole, B., McMorrow, J., & Evans, M. (2014b). Spectral monitoring of moorland plant phenology to identify a temporal window for hyperspectral remote sensing of peatland. *ISPRS Journal of Photogrammetry and Remote Sensing*, *90*, 49–58. https://doi.org/10.1016/j.isprsjprs.2014.01.010

Conedera, M., Lucini, L., Valese, E., Ascoli, D., & Pezzatti, G. B. (2010). Fire resistance and vegetative recruitment ability of different deciduous trees species after low-to moderate-intensity surface fires in southern Switzerland. *VI International Conference on Forest Fire Research*.

Conedera, M., Vassere, S., Neff, C., Meurer, M., & Krebs, P. (2007). Using toponymy to reconstruct past land use: A case study of 'brüsáda' (burn) in southern Switzerland. *Journal of Historical Geography*, *33*(4), 729–748. https://doi.org/10.1016/j.jhg.2006.11.002

Correia, D. L. P., Bouachir, W., Gervais, D., Pureswaran, D., Kneeshaw, D. D., & de Grandpre, L. (2020). Leveraging Artificial Intelligence for Large-Scale Plant Phenology Studies From Noisy Time-Lapse Images. *IEEE Access*, *8*, 13151–13160. https://doi.org/10.1109/ACCESS.2020.2965462

Costa, H., de Rigo, D., Ibertà, G., Durrant, T. H., & San-Miguel-Ayanz, J. (2020). *European wildfire danger and vulnerability under a changing climate*. Publications Office of the European Union. https://doi.org/10.2760/46951

Crespo-Peremarch, P., Tompalski, P., Coops, N. C., & Ruiz, L. Á. (2018). Characterizing understory vegetation in Mediterranean forests using full-waveform airborne laser scanning data. *Remote Sensing of Environment*, *217*, 400–413. https://doi.org/10.1016/j.rse.2018.08.033

Cruz, M. G., & Fernandes, P. M. (2008). Development of fuel models for fire behaviour prediction in maritime pine (Pinus pinaster Ait.) stands. *International Journal of Wildland Fire*, *17*(2), 194. https://doi.org/10.1071/WF07009

Darwish Ahmad, A., Abubaker, A. M., Salaimeh, A., Akafuah, N. K., Finney, M., Forthofer, J. M., & Saito, K. (2021). Ignition and burning mechanisms of live spruce needles. *Fuel*, *304*, 121371. https://doi.org/10.1016/j.fuel.2021.121371

Davies, G. M. (2005). *Fire Behaviour and Impact on Heather Moorland* [PhD Thesis]. University of Edinburgh.

Davies, G. M., Gray, A., Hamilton, A., & Legg, C. J. (2008). The future of fire management in the British uplands. *International Journal of Biodiversity Science & Management*, *4*(3), 127–147. https://doi.org/10.3843/Biodiv.4.3:1

Davies, G. M., Kettridge, N., Stoof, C. R., Gray, A., Ascoli, D., Fernandes, P. M., Marrs, R., Allen, K. A., Doerr, S. H., & Clay, G. D. (2016). The role of fire in UK peatland and moorland management: The need for informed, unbiased debate. *Philosophical Transactions of the Royal Society B: Biological Sciences*, *371*(1696), 20150342. https://doi.org/10.1098/rstb.2015.0342

Davies, G. M., & Legg, C. J. (2011). Fuel Moisture Thresholds in the Flammability of Calluna vulgaris. *Fire Technology*, *47*(2), 421–436. https://doi.org/10.1007/s10694-010-0162-0

Davies, G. M., Legg, C. J., O'hara, R., MacDonald, A. J., & Smith, A. A. (2010). Winter desiccation and rapid changes in the live fuel moisture content of Calluna vulgaris. *Plant Ecology & Diversity*, *3*(3), 289–299. https://doi.org/10.1080/17550874.2010.544335

Davies, G. M., Legg, C. J., Smith, A. A., & MacDonald, A. J. (2009). Rate of spread of fires in Calluna vulgaris-dominated moorlands. *Journal of Applied Ecology*, *46*(5), 1054–1063. https://doi.org/10.1111/j.1365-2664.2009.01681.x

Davies, G. M., Smith, A. A., MacDonald, A. J., Bakker, J. D., & Legg, C. J. (2010). Fire intensity, fire severity and ecosystem response in heathlands: Factors affecting the regeneration of Calluna vulgaris. *Journal of Applied Ecology*, *47*(2), 356–365. https://doi.org/10.1111/j.1365-2664.2010.01774.x

De Angelis, A., Bajocco, S., & Ricotta, C. (2012). Phenological variability drives the distribution of wildfires in Sardinia. *Landscape Ecology*, *27*(10), 1535–1545. https://doi.org/10.1007/s10980-012-9808-2

de Rigo, D., Libertà, G., Durrant, T. H., Vivancos, T. A., & San-Miguel-Ayanz, J. (2017). *Forest fire danger extremes in Europe under climate change: Variability and uncertainty*. Publications Office of the European Union.

DeBano, L. F., Neary, D. G., & Ffolliott, P. F. (1998). *Fire effects on ecosystems*. John Wiley & Sons.

DeCastro, A. L., Juliano, T. W., Kosović, B., Ebrahimian, H., & Balch, J. K. (2022). A Computationally Efficient Method for Updating Fuel Inputs for Wildfire Behavior Models Using Sentinel Imagery and Random Forest Classification. *Remote Sensing*, *14*(6), 6. https://doi.org/10.3390/rs14061447

Defra. (2007). *The Heather and Grass Burning Code* (Defra Publications). Department for Environment, Food and Rural Affairs.

Dell, J. E., Richards, L. A., O'Brien, J. J., Loudermilk, E. L., Hudak, A. T., Pokswinski, S. M., Bright, B. C., Hiers, J. K., Williams, B. W., & Dyer, L. A. (2017). Overstory-derived surface fuels mediate plant species diversity in frequently burned longleaf pine forests. *Ecosphere*, *8*(10), e01964. https://doi.org/10.1002/ecs2.1964

D'Este, M., Elia, M., Giannico, V., Spano, G., Lafortezza, R., & Sanesi, G. (2021). Machine Learning Techniques for Fine Dead Fuel Load Estimation Using Multi-Source Remote Sensing Data. *Remote Sensing*, *13*(9), 9. https://doi.org/10.3390/rs13091658

Dewhirst, R. A., Smirnoff, N., & Belcher, C. M. (2020). Pine Species That Support Crown Fire Regimes Have Lower Leaf-Level Terpene Contents Than Those Native to Surface Fire Regimes. *Fire*, *3*(2), 2. https://doi.org/10.3390/fire3020017

Diemont, W. H., Heijman, W. J. M., Siepel, H., & Webb, N. R. (2013). *Economy and Ecology of Heathlands: Heathland Ecology and Management*. KNNV Publishing.

Domingo, D., de La Riva, J., Lamelas, M. T., García-Martín, A., Ibarra, P., Echeverría, M., & Hoffrén, R. (2020). Fuel Type Classification Using Airborne Laser Scanning and Sentinel 2 Data in Mediterranean Forest Affected by Wildfires. *Remote Sensing*, *12*(21), 3660. https://doi.org/10.3390/rs12213660

Doran, J. D., Randall, C. K., & Long, A. J. (2004). *Fire in the wildland-urban interface: Selecting and maintaining firewise plants for landscaping.* USDA Forest Service, Southern Research Station, Southern Center for Wildland-Urban Interface Research and Information. doi.org/10.32473/edis-fr147-2023

Dormann, C. F., Bagnara, M., Boch, S., Hinderling, J., Janeiro-Otero, A., Schäfer, D., Schall, P., & Hartig, F. (2020). Plant species richness increases with light availability, but not variability, in temperate forests understorey. *BMC Ecology*, *20*(1), 43. https://doi.org/10.1186/s12898-020-00311-9

Drury, S. (2019). Fuel Continuity. In S. L. Manzello (Ed.), *Encyclopedia of Wildfires and Wildland-Urban Interface (WUI) Fires* (pp. 1–3). Springer International Publishing. https://doi.org/10.1007/978-3-319-51727-8_239-1

Duane, A., Castellnou, M., & Brotons, L. (2021). Towards a comprehensive look at global drivers of novel extreme wildfire events. *Climatic Change*, *165*(3), 43. https://doi.org/10.1007/s10584-021-03066-4

Dubayah, R., Blair, J. B., Goetz, S., Fatoyinbo, L., Hansen, M., Healey, S., Hofton, M., Hurtt, G., Kellner, J., Luthcke, S., Armston, J., Tang, H., Duncanson, L., Hancock, S., Jantz, P., Marselis, S., Patterson, P. L., Qi, W., & Silva, C. (2020). The Global Ecosystem Dynamics Investigation: High-resolution laser ranging of the Earth's forests and topography. *Science of Remote Sensing*, *1*, 100002. https://doi.org/10.1016/j.srs.2020.100002

Duff, T. J., Bell, T. L., & York, A. (2013). Predicting continuous variation in forest fuel load using biophysical models: A case study in south-eastern Australia. *International Journal of Wildland Fire*, *22*(3), 318. https://doi.org/10.1071/WF11087

Duff, T. J., Bessell, R., & Cruz, M. G. (2019). Grass Curing/Cured Fuels. In S. L. Manzello (Ed.), *Encyclopedia of Wildfires and Wildland-Urban Interface (WUI) Fires* (pp. 1–7). Springer International Publishing. https://doi.org/10.1007/978-3-319-51727-8_238-1

Duff, T. J., Keane, R. E., Penman, T. D., & Tolhurst, K. G. (2017). Revisiting Wildland Fire Fuel Quantification Methods: The Challenge of Understanding a Dynamic, Biotic Entity. *Forests*, *8*(9), 351. https://doi.org/10.3390/f8090351

Dunn, O. J. (1964). Multiple Comparisons Using Rank Sums. *Technometrics*, *6*(3), 241–252.

DWD Climate Data Center. (2023). *Historical monthly station observations (temperature, precipitation, sunshine duration, wind and cloud cover) for Germany, Version v22.3: Urn:x-wmo:md:de.dwd.cdc::obsgermany-climate-monthly-kl-historical*.

EFFIS. (2017). *European Fuel Map* (JRC Contract Number 384347; Development of a European Fuel Map). European Forest Fire Information System, European Comission.

EFFIS. (2021, October 18). *European Forest Fire Information System—Statistics Portal*. EFFIS Estimates of Burned Areas and Number of Fires. https://effis.jrc.ec.europa.eu/apps/effis.statistics/

EFFIS. (2023, January 23). *European Forest Fire Information System—Statistics Portal*. EFFIS Estimates for European Union. https://effis.jrc.ec.europa.eu/apps/effis.statistics/estimates

Elmqvist, M., Jungert, E., Lantz, F., Persson, A., & Soderman, U. (2001). Terrain modelling and analysis using laser scanner data. *International Archives of Photogrammetry Remote Sensing and Spatial Information Sciences*, *34*(3), 219–226.

Engber, E. A., & Varner, J. M. (2012). Patterns of flammability of the California oaks: The role of leaf traits. *Canadian Journal of Forest Research*, *42*(11), 1965–1975. https://doi.org/10.1139/x2012-138

Engelstad, P. S., Falkowski, M., Wolter, P., Poznanovic, A., & Johnson, P. (2019). Estimating Canopy Fuel Attributes from Low-Density LiDAR. *Fire*, *2*(3), 38. https://doi.org/10.3390/fire2030038

Ensley-Field, M., Shriver, R. K., Law, S., & Adler, P. B. (2023). Combining Field Observations and Remote Sensing to Forecast Fine Fuel Loads. *Rangeland Ecology & Management*, *90*, 245–255. https://doi.org/10.1016/j.rama.2023.04.008

Erdody, T. L., & Moskal, L. M. (2010). Fusion of LiDAR and imagery for estimating forest canopy fuels. *Remote Sensing of Environment*, *114*(4), 725–737. https://doi.org/10.1016/j.rse.2009.11.002

Eurostat. (2022). *Overview—Land cover and use—Eurostat*. https://ec.europa.eu/eurostat/web/lucas

Ewald, M., Dupke, C., Heurich, M., Müller, J., & Reineking, B. (2014). LiDAR Remote Sensing of Forest Structure and GPS Telemetry Data Provide Insights on Winter Habitat Selection of European Roe Deer. *Forests*, *5*(6), 1374–1390. https://doi.org/10.3390/f5061374

Ewald, M., Labenski, P., Westphal, E., Metzsch-Zilligen, E., Großhauser, M., & Fassnacht, F. E. (2023). Leaf litter combustion properties of Central European tree species. *Forestry: An International Journal of Forest Research*, cpad026. https://doi.org/10.1093/forestry/cpad026

Falkowski, M. J., Gessler, P. E., Morgan, P., Hudak, A. T., & Smith, A. M. S. (2005). Characterizing and mapping forest fire fuels using ASTER imagery and gradient modeling. *Forest Ecology and Management*, *217*(2–3), 129–146. https://doi.org/10.1016/j.foreco.2005.06.013

Fares, S., Bajocco, S., Salvati, L., Camarretta, N., Dupuy, J.-L., Xanthopoulos, G., Guijarro, M., Madrigal, J., Hernando, C., & Corona, P. (2017). Characterizing potential wildland fire fuel in live vegetation in the Mediterranean region. *Annals of Forest Science*, *74*(1), 1. https://doi.org/10.1007/s13595-016-0599-5

Fassnacht, F. E., Latifi, H., Stereńczak, K., Modzelewska, A., Lefsky, M., Waser, L. T., Straub, C., & Ghosh, A. (2016). Review of studies on tree species classification from remotely sensed data. *Remote Sensing of Environment*, *186*, 64–87. https://doi.org/10.1016/j.rse.2016.08.013

Fassnacht, F. E., Schmidt-Riese, E., Kattenborn, T., & Hernández, J. (2021). Explaining Sentinel 2-based dNBR and RdNBR variability with reference data from the bird's eye (UAS) perspective. *International Journal of Applied Earth Observation and Geoinformation*, *95*, 102262. https://doi.org/10.1016/j.jag.2020.102262

Fernandes, P. M., & Rego, F. C. (1998). A new method to estimate fuel surface area-to-volume ratio using water immersion. *International Journal of Wildland Fire*, *8*(3), 121–128. https://doi.org/10.1071/WF9980121

Fernandes, P. M., Vega, J. A., Jiménez, E., & Rigolot, E. (2008). Fire resistance of European pines. *Forest Ecology and Management*, *256*(3), 246–255. https://doi.org/10.1016/j.foreco.2008.04.032

Fernandez-Anez, N., Krasovskiy, A., Müller, M., Vacik, H., Baetens, J., Hukić, E., Kapovic Solomun, M., Atanassova, I., Glushkova, M., Bogunović, I., Fajković, H., Djuma, H., Boustras, G., Adámek, M., Devetter, M., Hrabalikova, M., Huska, D., Martínez Barroso, P., Vaverková, M. D., … Cerda, A. (2021). Current Wildland Fire Patterns and Challenges in Europe: A Synthesis of National Perspectives. *Air, Soil and Water Research*, *14*, 1–19. https://doi.org/10.1177/11786221211028185

Fernández-Guisuraga, J. M., Suárez-Seoane, S., & Calvo, L. (2019). Modeling Pinus pinaster forest structure after a large wildfire using remote sensing data at high spatial resolution. *Forest Ecology and Management*, *446*, 257–271. https://doi.org/10.1016/j.foreco.2019.05.028

Ferraz, A., Bretar, F., Jacquemoud, S., Gonçalves, G., Pereira, L., Tomé, M., & Soares, P. (2012). 3-D mapping of a multi-layered Mediterranean forest using ALS data. *Remote Sensing of Environment*, *121*, 210–223. https://doi.org/10.1016/j.rse.2012.01.020

Finney, M. A. (2006). An Overview of FlamMap Fire Modeling Capabilities. In P. L. Andrews & B. W. Butler (Eds.), *Fuels Management—How to Measure Success: Conference Proceedings* (Vol. 041, pp. 213–220). https://www.fs.usda.gov/treesearch/pubs/25948

Finney, M. A. (2019). Operational Wildland Fire Behavior Models and Systems. In S. L. Manzello (Ed.), *Encyclopedia of Wildfires and Wildland-Urban Interface (WUI) Fires* (pp. 1–5). Springer International Publishing. https://doi.org/10.1007/978-3-319-51727-8_246-1

Forest Europe. (2020). *State of Europe's Forests 2020*. Ministerial Conference on the Protection of Forests in Europe. https://foresteurope.org/wp-content/uploads/2016/08/SoEF_2020.pdf

Forestry Commission. (2023). *Wildfire statistics for England: Report to 2020-21*. Forestry Commission. https://assets.publishing.service.gov.uk/government/uploads/system/uploads/attachment_data/file/1136838/FC-Wildfire-statistics-for-England-Report-to-2020-21-.pdf

Forkel, M., Schmidt, L., Zotta, R.-M., Dorigo, W., & Yebra, M. (2023). Estimating leaf moisture content at global scale from passive microwave satellite observations of vegetation optical depth. *Hydrology and Earth System Sciences*, *27*(1), 39–68. https://doi.org/10.5194/hess-27-39-2023

ForstBW. (2019). *Waldentwicklungstypenkarte: Gemeinde Walzbachtal*. Landkreis Karlsruhe, Untere Forstbehörde.

ForstBW. (2023). *Geo-Daten: Waldeinteilung* (ForstBW, Ed.). https://www.forstbw.de/produkte-angebote/geo-daten/

Forzieri, G., Girardello, M., Ceccherini, G., Spinoni, J., Feyen, L., Hartmann, H., Beck, P. S. A., Camps-Valls, G., Chirici, G., Mauri, A., & Cescatti, A. (2021). Emergent vulnerability to climate-driven disturbances in European forests. *Nature Communications*, *12*(1), 1081. https://doi.org/10.1038/s41467-021-21399-7

Fosberg, M. A. (1971). *Derivation of the 1- and 10-hour Timelag Fuel Moisture Calculations for Fire-danger Rating*. Rocky Mountain Forest and Range Experiment Station, Forest Service, U.S. Department of Agriculture.

Fosberg, M. A., Lancaster, J. W., & Schroeder, M. J. (1970). Fuel Moisture Response—Drying Relationships Under Standard And Field Conditions. *Forest Science*, *16*(1), 121–128. https://doi.org/10.1093/forestscience/16.1.121

Franke, J., Barradas, A. C. S., Borges, M. A., Menezes Costa, M., Dias, P. A., Hoffmann, A. A., Orozco Filho, J. C., Melchiori, A. E., & Siegert, F. (2018). Fuel load mapping in the Brazilian Cerrado in support of integrated fire management. *Remote Sensing of Environment*, *217*, 221–232. https://doi.org/10.1016/j.rse.2018.08.018

Fréjaville, T., Curt, T., & Carcaillet, C. (2016). Tree cover and seasonal precipitation drive understorey flammability in alpine mountain forests. *Journal of Biogeography*, *43*(9), 1869–1880. https://doi.org/10.1111/jbi.12745

Furlaud, J. M., Williamson, G. J., & Bowman, D. M. J. S. (2018). Simulating the effectiveness of prescribed burning at altering wildfire behaviour in Tasmania, Australia. *International Journal of Wildland Fire*, *27*(1), 15. https://doi.org/10.1071/WF17061

Galbraith, C. A., & Stroud, D. A. (2022). *Sites of Special Scientific Interest (SSSIs) in England: Their historical development and prospects in a changing environment* (NECR414). Natural England.

Gale, M. G., Cary, G. J., van Dijk, A. I. J. M., & Yebra, M. (2021). Forest fire fuel through the lens of remote sensing: Review of approaches, challenges and future directions in the remote sensing of biotic determinants of fire behaviour. *Remote Sensing of Environment*, *255*, 112282. https://doi.org/10.1016/j.rse.2020.112282

Ganteaume, A., Camia, A., Jappiot, M., San-Miguel-Ayanz, J., Long-Fournel, M., & Lampin, C. (2013). A Review of the Main Driving Factors of Forest Fire Ignition Over Europe. *Environmental Management*, *51*(3), 651–662. https://doi.org/10.1007/s00267-012-9961-z

Gao, B. (1996). NDWI—A normalized difference water index for remote sensing of vegetation liquid water from space. *Remote Sensing of Environment*, *58*(3), 257–266. https://doi.org/10.1016/S0034-4257(96)00067-3

Gao, J., French, A. P., Pound, M. P., He, Y., Pridmore, T. P., & Pieters, J. G. (2020). Deep convolutional neural networks for image-based Convolvulus sepium detection in sugar beet fields. *Plant Methods*, *16*, 29. https://doi.org/10.1186/s13007-020-00570-z

Gao, X., Huete, A. R., Ni, W., & Miura, T. (2000). Optical–Biophysical Relationships of Vegetation Spectra without Background Contamination. *Remote Sensing of Environment*, *74*(3), 609–620. https://doi.org/10.1016/S0034-4257(00)00150-4

García, M., Popescu, S., Riaño, D., Zhao, K., Neuenschwander, A., Agca, M., & Chuvieco, E. (2012). Characterization of canopy fuels using ICESat/GLAS data. *Remote Sensing of Environment*, *123*, 81–89. https://doi.org/10.1016/j.rse.2012.03.018

García, M., Riaño, D., Chuvieco, E., Salas, J., & Danson, F. M. (2011). Multispectral and LiDAR data fusion for fuel type mapping using Support Vector Machine and decision rules. *Remote Sensing of Environment*, *115*(6), 1369–1379. https://doi.org/10.1016/j.rse.2011.01.017

García, M., Riaño, D., Yebra, M., Salas, J., Cardil, A., Monedero, S., Ramirez, J., Martín, M. P., Vilar, L., Gajardo, J., & Ustin, S. (2020). A Live Fuel Moisture Content Product from Landsat TM Satellite Time Series for Implementation in Fire Behavior Models. *Remote Sensing*, *12*(11), 11. https://doi.org/10.3390/rs12111714

Genuer, R., Poggi, J.-M., & Tuleau-Malot, C. (2015). VSURF: An R Package for Variable Selection Using Random Forests. *The R Journal*, *7*(2), 19–33.

Gilbert, J. A. (2008). *Calluna vulgaris regeneration on upland moorland post-wildfire.* [PhD Thesis]. University of Central Lancashire.

Gimingham, C. H. (1972). *Ecology of heathlands*. Chapman and Hall.

Girardin, M. P., Ali, A. A., Carcaillet, C., Blarquez, O., Hély, C., Terrier, A., Genries, A., & Bergeron, Y. (2013). Vegetation limits the impact of a warm climate on boreal wildfires. *New Phytologist*, *199*(4), 1001–1011. https://doi.org/10.1111/nph.12322

Gitas, I., Mitri, G. H., Kazakis, G., Ghosn, D., & Xanthopoulos, G. (2006). Fuel type mapping in Anopolis, Crete by employing QuickBird imagery and object-based classification. *Forest Ecology and Management*, *234*, S228. https://doi.org/10.1016/j.foreco.2006.08.255

Gitas, I., Mitri, G., Veraverbeke, S., & Polychronaki, A. (2012). Advances in remote sensing of post-fire vegetation recovery monitoring—A review. In T. Fatoyinbo (Ed.), *Remote Sensing of Biomass—Principles and Applications* (Vol. 1, p. 334). InTech.

Goëau, H., Boujemaa, N., Molino, J.-F., Duché, G., Péronnet, A., Bonnet, P., Joly, A., Bakić, V., Barbe, J., Yahiaoui, I., Selmi, S., Carré, J., & Barthélémy, D. (2013). Pl@ntNet mobile app. *Proceedings of the 21st ACM International Conference on Multimedia*. https://doi.org/10.1145/2502081.2502251

González-Ferreiro, E., Diéguez-Aranda, U., Crecente-Campo, F., Barreiro-Fernández, L., Miranda, D., & Castedo-Dorado, F. (2014). Modelling canopy fuel variables for Pinus radiata D. Don in NW Spain with low-density LiDAR data. *International Journal of Wildland Fire*, *23*(3), 350. https://doi.org/10.1071/WF13054

Grabska, E., Hostert, P., Pflugmacher, D., & Ostapowicz, K. (2019). Forest Stand Species Mapping Using the Sentinel-2 Time Series. *Remote Sensing*, *11*(10), 1197. https://doi.org/10.3390/rs11101197

Graham, A. M., Pope, R. J., Pringle, K. P., Arnold, S., Chipperfield, M. P., Conibear, L. A., Butt, E. W., Kiely, L., Knote, C., & McQuaid, J. B. (2020). Impact on air quality and health due to the Saddleworth Moor fire in northern England. *Environmental Research Letters*, *15*(7), 074018. https://doi.org/10.1088/1748-9326/ab8496

Grau-Andrés, R., Davies, G. M., Waldron, S., Scott, E. M., & Gray, A. (2019). Increased fire severity alters initial vegetation regeneration across Calluna-dominated ecosystems. *Journal of Environmental Management*, *231*, 1004–1011. https://doi.org/10.1016/j.jenvman.2018.10.113

Grootemaat, S., Wright, I. J., van Bodegom, P. M., & Cornelissen, J. H. C. (2017). Scaling up flammability from individual leaves to fuel beds. *Oikos*, *126*(10), 1428–1438. https://doi.org/10.1111/oik.03886

Guerini Filho, M., Kuplich, T. M., & Quadros, F. L. F. D. (2020). Estimating natural grassland biomass by vegetation indices using Sentinel 2 remote sensing data. *International Journal of Remote Sensing*, *41*(8), 2861–2876. https://doi.org/10.1080/01431161.2019.1697004

Guirado, E., Alcaraz-Segura, D., Cabello, J., Puertas-Ruíz, S., Herrera, F., & Tabik, S. (2020). Tree Cover Estimation in Global Drylands from Space Using Deep Learning. *Remote Sensing*, *12*(3), 343. https://doi.org/10.3390/rs12030343

Gyllin, M., & Grahn, P. (2015). Semantic assessments of experienced biodiversity from photographs and on-site observations—A comparison. *Environment and Natural Resources Research*, *5*(4), 46–62. https://doi.org/10.5539/enrr.v5n4p46

Hall, R. J., Peddle, D. R., & Klita, D. L. (2000). Mapping conifer understory within boreal mixedwoods from Landsat TM satellite imagery and forest inventory information. *The Forestry Chronicle*, *76*(6), 887–902. https://doi.org/10.5558/tfc76887-6

Hanan, E. J., Kennedy, M. C., Ren, J., Johnson, M. C., & Smith, A. M. S. (2022). Missing Climate Feedbacks in Fire Models: Limitations and Uncertainties in Fuel Loadings and the Role of Decomposition in Fine Fuel Accumulation. *Journal of Advances in Modeling Earth Systems*, *14*(3). https://doi.org/10.1029/2021MS002818

Hancock, M. H. (2008). An exceptional Calluna vulgaris winter die-back event, Abernethy Forest, Scottish Highlands. *Plant Ecology & Diversity*, *1*(1), 89–103. https://doi.org/10.1080/17550870802260772

Hänsel, S., Hoy, A., Brendel, C., & Maugeri, M. (2022). Record summers in Europe: Variations in drought and heavy precipitation during 1901–2018. *International Journal of Climatology*, *42*(12), 6235–6257. https://doi.org/10.1002/joc.7587

Hardisky, M., Klemas, V., & Smart, R. (1983). The Influence of Soil-Salinity, Growth Form, and Leaf Moisture on the Spectral Radiance of Spartina-Alterniflora Canopies. *Photogrammetric Engineering and Remote Sensing*, *49*(1), 77–83.

Harper, A. (2020). *Vegetation fires in temperate upland heaths: Environmental impacts, recovery, and management implications* [PhD Thesis]. Swansea University.

Hawley, C. M., Loudermilk, E. L., Rowell, E. M., & Pokswinski, S. (2018). A novel approach to fuel biomass sampling for 3D fuel characterization. *MethodsX*, *5*, 1597–1604. https://doi.org/10.1016/j.mex.2018.11.006

He, J., Loboda, T. V., Jenkins, L., & Chen, D. (2019). Mapping fractional cover of major fuel type components across Alaskan tundra. *Remote Sensing of Environment*, *232*, 111324. https://doi.org/10.1016/j.rse.2019.111324

Heinemeyer, A., & Ashby, M. A. (2023). Prescribed Fire in UK Heather-Dominated Blanket Bog Peatlands: A Critical Review of "Carbon Storage and Sequestration by Habitat: A Review of the Evidence (Second Edition)" by Gregg et al., 2021. *Fire*, *6*(5), 5. https://doi.org/10.3390/fire6050204

Heinsch, F. A. (2019). Fuel Model. In S. L. Manzello (Ed.), *Encyclopedia of Wildfires and Wildland-Urban Interface (WUI) Fires* (pp. 1–19). Springer International Publishing. https://doi.org/10.1007/978-3-319-51727-8_178-1

Heisig, J., Olson, E., & Pebesma, E. (2022). Predicting Wildfire Fuels and Hazard in a Central European Temperate Forest Using Active and Passive Remote Sensing. *Fire*, *5*(1), 29. https://doi.org/10.3390/fire5010029

Henniger, H., Huth, A., Frank, K., & Bohn, F. J. (2023). Creating virtual forests around the globe and analysing their state space. *Ecological Modelling*, *483*, 110404. https://doi.org/10.1016/j.ecolmodel.2023.110404

Hill, M. J. (2013). Vegetation index suites as indicators of vegetation state in grassland and savanna: An analysis with simulated SENTINEL 2 data for a North American transect. *Remote Sensing of Environment*, *137*, 94–111. https://doi.org/10.1016/j.rse.2013.06.004

Hille, M. (2006). *Fire ecology of Scots pine in Northwest Europe* [PhD Thesis]. Wageningen University.

Hille, M., Ouden, J. den, Hille*, M., & Ouden, J. den. (2005). Fuel load, humus consumption and humus moisture dynamics in Central European Scots pine stands. *International Journal of Wildland Fire*, *14*(2), 153–159. https://doi.org/10.1071/WF04026

Hislop, S., Jones, S., Soto-Berelov, M., Skidmore, A., Haywood, A., & Nguyen, T. H. (2018). Using Landsat Spectral Indices in Time-Series to Assess Wildfire Disturbance and Recovery. *Remote Sensing*, *10*(3), 460. https://doi.org/10.3390/rs10030460

Hochreiter, S., & Schmidhuber, J. (1997). Long short-term memory. *Neural Computation*, *9*(8), 1735–1780. https://doi.org/10.1162/neco.1997.9.8.1735

Hough, W. A. (1969). *Caloric Value of Some Forest Fuels of the Southern United States*. U.S. Department of Agriculture, Forest Service, Southeastern Forest Experiment Station.

Huang, S., Crabtree, R. L., Potter, C., & Gross, P. (2009). Estimating the quantity and quality of coarse woody debris in Yellowstone post-fire forest ecosystem from fusion of SAR and optical data. *Remote Sensing of Environment*, *113*(9), 1926–1938. https://doi.org/10.1016/j.rse.2009.05.001

Hudak, A. T., Dickinson, M. B., Bright, B. C., Kremens, R. L., Loudermilk, E. L., O'Brien, J. J., Hornsby, B. S., & Ottmar, R. D. (2016). Measurements relating fire radiative energy density and surface fuel con-

sumption – RxCADRE 2011 and 2012. *International Journal of Wildland Fire*, *25*(1), 25. https://doi.org/10.1071/WF14159

Hudak, A. T., Kato, A., Bright, B. C., Loudermilk, E. L., Hawley, C., Restaino, J. C., Ottmar, R. D., Prata, G. A., Cabo, C., Prichard, S. J., Rowell, E. M., & Weise, D. R. (2020). Towards Spatially Explicit Quantification of Pre- and Postfire Fuels and Fuel Consumption from Traditional and Point Cloud Measurements. *Forest Science*, *66*(4), 428–442. https://doi.org/10.1093/forsci/fxz085

Huete, A. R. (1988). A soil-adjusted vegetation index (SAVI). *Remote Sensing of Environment*, *25*(3), 295–309. https://doi.org/10.1016/0034-4257(88)90106-X

Huete, A. R. (2004). Remote Sensing for Environmental Monitoring. In J. F. Artiola, I. L. Pepper, & M. L. Brusseau (Eds.), *Environmental Monitoring and Characterization* (pp. 183–206). Academic Press. https://doi.org/10.1016/B978-012064477-3/50013-8

Immitzer, M., Vuolo, F., & Atzberger, C. (2016). First Experience with Sentinel-2 Data for Crop and Tree Species Classifications in Central Europe. *Remote Sensing*, *8*(3), 166. https://doi.org/10.3390/rs8030166

IPCC. (2019). *Climate Change and Land: An IPCC special report on climate change, desertification, land degradation, sustainable land management, food security, and greenhouse gas fluxes in terrestrial ecosystems* (P. R. Shukla, J. Skea, E. Calvo Buendia, V. Masson-Delmotte, H. O. Pörtner, D. C. Roberts, P. Zhai, R. Slade, S. Connors, R. van Diemen, M. Ferrat, E. Haughey, S. Luz, S. Neogi, M. Pathak, J. Petzold, J. Portugal Pereira, P. Vyas, E. Huntley, … J. Malley, Eds.).

IPCC. (2021). Summary for Policymakers. In V. Masson-Delmotte, P. Zhai, A. Pirani, A. L. Connors, C. Péan, S. Berger, N. Caud, Y. Chen, L. Goldfarb, M. I. Gomis, M. Huang, K. Leitzell, E. Lonnoy, J. B. R. Matthews, T. K. Maycock, T. Waterfield, O. Yelekçi, R. Yu, & B. Zhou (Eds.), *Climate Change 2021: The Physical Science Basis. Contribution of Working Group I to the Sixth Assessment Report of the Intergovernmental Panel on Climate Change*. Cambridge University Press.

Isidorov, V. A., Pirożnikow, E., Spirina, V. L., Vasyanin, A. N., Kulakova, S. A., Abdulmanova, I. F., & Zaitsev, A. A. (2022). Emission of volatile organic compounds by plants on the floor of boreal and mid-latitude forests. *Journal of Atmospheric Chemistry*, *79*(3), 153–166. https://doi.org/10.1007/s10874-022-09434-3

Jakubowksi, M. K., Guo, Q., Collins, B., Stephens, S., & Kelly, M. (2013). Predicting Surface Fuel Models and Fuel Metrics Using Lidar and CIR Imagery in a Dense, Mountainous Forest. *American Society for Photogrammetry and Remote Sensing*, *79*. https://doi.org/10.14358/PERS.79.1.37

Jarron, L. R., Coops, N. C., MacKenzie, W. H., & Dykstra, P. (2021). Detection and Quantification of Coarse Woody Debris in Natural Forest Stands Using Airborne LiDAR. *Forest Science*, *67*(5), 550–563. https://doi.org/10.1093/forsci/fxab023

Jia, G. J., Burke, I. C., Goetz, A. F. H., Kaufmann, M. R., & Kindel, B. C. (2006). Assessing spatial patterns of forest fuel using AVIRIS data. *Remote Sensing of Environment*, *102*(3–4), 318–327. https://doi.org/10.1016/j.rse.2006.02.025

Jin, S., & Chen, S.-C. (2012). Application of QuickBird imagery in fuel load estimation in the Daxinganling region, China. *International Journal of Wildland Fire*, *21*(5), 583. https://doi.org/10.1071/WF11018

Jin, S., & Sader, S. A. (2005). Comparison of time series tasseled cap wetness and the normalized difference moisture index in detecting forest disturbances. *Remote Sensing of Environment*, *94*(3), 364–372. https://doi.org/10.1016/j.rse.2004.10.012

Johnson, E. A. (1996). *Fire and Vegetation Dynamics: Studies from the North American Boreal Forest*. Cambridge University Press.

Jolly, W. M., Cochrane, M. A., Freeborn, P. H., Holden, Z. A., Brown, T. J., Williamson, G. J., & Bowman, D. M. J. S. (2015). Climate-induced variations in global wildfire danger from 1979 to 2013. *Nature Communications*, *6*, 7537. https://doi.org/10.1038/ncomms8537

Jolly, W. M., Hadlow, A. M., & Huguet, K. (2014). De-coupling seasonal changes in water content and dry matter to predict live conifer foliar moisture content. *International Journal of Wildland Fire*, *23*(4), 480–489. https://doi.org/10.1071/WF13127

Joshi, N., Mitchard, E. T. A., Brolly, M., Schumacher, J., Fernández-Landa, A., Johannsen, V. K., Marchamalo, M., & Fensholt, R. (2017). Understanding 'saturation' of radar signals over forests. *Scientific Reports*, *7*(1), 1. https://doi.org/10.1038/s41598-017-03469-3

JRC. (2011). *FUELMAP project [Final Classification and Mapping of EU Fuel Complexes] Deliverable 2/S 116-153998* (116–153998).

Jumelle, M., Kuhn-Regnier, A., & Rajaratnam, S. (2020). *ALEPython: Python Accumulated Local Effects package*. https://github.com/blent-ai/ALEPython

Kahl, S., Wood, C. M., Eibl, M., & Klinck, H. (2021). BirdNET: A deep learning solution for avian diversity monitoring. *Ecological Informatics*, *61*, 101236. https://doi.org/10.1016/j.ecoinf.2021.101236

Kälin, U., Lang, N., Hug, C., Gessler, A., & Wegner, J. D. (2019). Defoliation estimation of forest trees from ground-level images. *Remote Sensing of Environment*, *223*, 143–153. https://doi.org/10.1016/j.rse.2018.12.021

Kane, J. M., & Prat-Guitart, N. (2018). Fuel Moisture. In S. L. Manzello (Ed.), *Encyclopedia of Wildfires and Wildland-Urban Interface (WUI) Fires* (pp. 1–13). Springer International Publishing. https://doi.org/10.1007/978-3-319-51727-8_115-1

ka-news. (2022). Vier Feuer im Hardtwald Karlsruhe. *Ka-News*. https://www.ka-news.de/region/karlsruhe/erneut-feuer-im-hardtwald-karlsruhe-feuerwehr-an-zwei-brandstellen-im-einsatz-art-2831371

Kattenborn, T., Eichel, J., & Fassnacht, F. E. (2019). Convolutional Neural Networks enable efficient, accurate and fine-grained segmentation of plant species and communities from high-resolution UAV imagery. *Scientific Reports*, *9*(1), 1. https://doi.org/10.1038/s41598-019-53797-9

Kattenborn, T., Leitloff, J., Schiefer, F., & Hinz, S. (2021). Review on Convolutional Neural Networks (CNN) in vegetation remote sensing. *ISPRS Journal of Photogrammetry and Remote Sensing*, *173*, 24–49. https://doi.org/10.1016/j.isprsjprs.2020.12.010

Kauth, R. J., & Thomas, G. S. (1976). The tasselled cap – a graphic description of the spectral-temporal development of agricultural crops as seen by Landsat. *LARS Symposia*. Laboratory for Applications of Remote Sensing. http://docs.lib.purdue.edu/lars_symp/159

Kayll, A. J., & Gimingham, C. H. (1965). Vegetative regeneration of Calluna vulgaris after fire. *The Journal of Ecology*, 729–734. https://doi.org/10.2307/2257631

Keane, R. E. (2013). Describing wildland surface fuel loading for fire management: A review of approaches, methods and systems. *International Journal of Wildland Fire*, *22*(1), 51–62. https://doi.org/10.1071/WF11139

Keane, R. E. (2015). *Wildland Fuel Fundamentals and Applications*. Springer International Publishing. https://doi.org/10.1007/978-3-319-09015-3

Keane, R. E., & Dickinson, L. J. (2007). *Development and evaluation of the photoload sampling technique* (RMRS-RP-61). U.S. Department of Agriculture, Forest Service, Rocky Mountain Research Station. https://doi.org/10.2737/RMRS-RP-61

Keane, R. E., Gray, K., & Bacciu, V. (2012). *Spatial variability of wildland fuel characteristics in northern Rocky Mountain ecosystems* (RMRS-RP-98). U.S. Department of Agriculture, Forest Service, Rocky Mountain Research Station. https://doi.org/10.2737/RMRS-RP-98

Keeley, J. E., Bond, W. J., Bradstock, R. A., Pausas, J. G., & Rundel, P. W. (2011). *Fire in Mediterranean Ecosystems: Ecology, Evolution and Management*. Cambridge University Press.

Kelley, D. I., Bistinas, I., Whitley, R., Burton, C., Marthews, T. R., & Dong, N. (2019). How contemporary bioclimatic and human controls change global fire regimes. *Nature Climate Change*, *9*(9), 690–696. https://doi.org/10.1038/s41558-019-0540-7

Keramitsoglou, I., Kontoes, C., Sykioti, O., Sifakis, N., & Xofis, P. (2008). Reliable, accurate and timely forest mapping for wildfire management using ASTER and Hyperion satellite imagery. *Forest Ecology and Management*, *255*(10), 3556–3562. https://doi.org/10.1016/j.foreco.2008.01.077

Kesselmeier, J., Ciccioli, P., Kuhn, U., Stefani, P., Biesenthal, T., Rottenberger, S., Wolf, A., Vitullo, M., Valentini, R., Nobre, A., Kabat, P., & Andreae, M. O. (2002). Volatile organic compound emissions in relation to plant carbon fixation and the terrestrial carbon budget. *Global Biogeochemical Cycles*, *16*(4), 1126. https://doi.org/10.1029/2001GB001813

Keyes, C. R. (2006). Role of Foliar Moisture Content in the Silvicultural Management of Forest Fuels. *Western Journal of Applied Forestry*, *21*(4), 228–231. https://doi.org/10.1093/wjaf/21.4.228

Khabarov, N., Krasovskii, A., Obersteiner, M., Swart, R., Dosio, A., San-Miguel-Ayanz, J., Durrant, T., Camia, A., & Migliavacca, M. (2016). Forest fires and adaptation options in Europe. *Regional Environmental Change*, *16*(1), 21–30. https://doi.org/10.1007/s10113-014-0621-0

Kim, Y., Yang, Z., Cohen, W. B., Pflugmacher, D., Lauver, C. L., & Vankat, J. L. (2009). Distinguishing between live and dead standing tree biomass on the North Rim of Grand Canyon National Park, USA

using small-footprint lidar data. *Remote Sensing of Environment*, *113*(11), 2499–2510. https://doi.org/10.1016/j.rse.2009.07.010

Kirkland, M., Atkinson, P. W., Pearce-Higgins, J. W., de Jong, M. C., Dowling, T. P. F., Grummo, D., Critchley, M., & Ashton-Butt, A. (2023). Landscape fires disproportionally affect high conservation value temperate peatlands, meadows, and deciduous forests, but only under low moisture conditions. *Science of The Total Environment*, *884*, 163849. https://doi.org/10.1016/j.scitotenv.2023.163849

Kirkpatrick, H. (2013). Chapter 16: Managing moorland in the UK. In W. H. Diemont, W. J. M. Heijman, H. Siepel, & N. R. Webb (Eds.), *Economy and Ecology of Heathlands: Heathland Ecology and Management*. KNNV Publishing.

Kislov, D. E., Korznikov, K. A., Altman, J., Vozmishcheva, A. S., & Krestov, P. V. (2021). Extending deep learning approaches for forest disturbance segmentation on very high–resolution satellite images. *Remote Sensing in Ecology and Conservation*, *7*(3), 355–368. https://doi.org/10.1002/rse2.194

Knapp, E. E., & Keeley, J. E. (2006). Heterogeneity in fire severity within early season and late season prescribed burns in a mixed-conifer forest. *International Journal of Wildland Fire*, *15*(1), 37–45. https://doi.org/10.1071/WF04068

Kobayashi, H., Nagai, S., Kim, Y., Yang, W., Ikeda, K., Ikawa, H., Nagano, H., & Suzuki, R. (2018). In Situ Observations Reveal How Spectral Reflectance Responds to Growing Season Phenology of an Open Evergreen Forest in Alaska. *Remote Sensing*, *10*(7), 1071. https://doi.org/10.3390/rs10071071

Korpela, I., Ørka, H. O., Hyyppä, J., Heikkinen, V., & Tokola, T. (2010). Range and AGC normalization in airborne discrete-return LiDAR intensity data for forest canopies. *ISPRS Journal of Photogrammetry and Remote Sensing*, *65*(4), 369–379. https://doi.org/10.1016/j.isprsjprs.2010.04.003

Korpela, I., Tuomola, T., Tokola, T., & Dahlin, B. (2008). Appraisal of seedling stand vegetation with airborne imagery and discrete-return LiDAR – an exploratory analysis. *Silva Fennica*, *42*(5), 753–772. https://doi.org/10.14214/sf.466

Krawchuk, M. A., & Moritz, M. A. (2011). Constraints on global fire activity vary across a resource gradient. *Ecology*, *92*(1), 121–132. https://doi.org/10.1890/09-1843.1

Krawchuk, M. A., Moritz, M. A., Parisien, M.-A., Dorn, J. V., & Hayhoe, K. (2009). Global Pyrogeography: The Current and Future Distribution of Wildfire. *PLOS ONE*, *4*(4), e5102. https://doi.org/10.1371/journal.pone.0005102

Krisanski, S., Taskhiri, M., & Turner, P. (2020). Enhancing Methods for Under-Canopy Unmanned Aircraft System Based Photogrammetry in Complex Forests for Tree Diameter Measurement. *Remote Sensing*, *12*(10), 1652. https://doi.org/10.3390/rs12101652

Krishna, M. P., & Mohan, M. (2017). Litter decomposition in forest ecosystems: A review. *Energy, Ecology and Environment*, *2*(4), 236–249. https://doi.org/10.1007/s40974-017-0064-9

Krishna Moorthy, S. M., Calders, K., Vicari, M. B., & Verbeeck, H. (2020). Improved Supervised Learning-Based Approach for Leaf and Wood Classification From LiDAR Point Clouds of Forests. *IEEE Transactions on Geoscience and Remote Sensing*, *58*(5), 3057–3070. https://doi.org/10.1109/TGRS.2019.2947198

Krizhevsky, A., Sutskever, I., & Hinton, G. E. (2017). ImageNet classification with deep convolutional neural networks. *Communications of the ACM*, *60*(6), 84–90. https://doi.org/10.1145/3065386

Kruskal, W. H., & Wallis, W. A. (1952). Use of Ranks in One-Criterion Variance Analysis. *Journal of the American Statistical Association*, *47*(260), 583–621.

Kuželka, K., & Surový, P. (2018). Mapping Forest Structure Using UAS inside Flight Capabilities. *Sensors*, *18*(7), 2245. https://doi.org/10.3390/s18072245

Kwolek, A. V. A., & Woolhouse, H. W. (1982). Studies on the Dormancy of Calluna vulgaris (L.) Hull, during Winter: The Effect of Photoperiod and Temperature on the Induction of Dormancy and the Annual Cycle of Development. *Annals of Botany*, *49*(3), 367–376. https://doi.org/10.1093/oxfordjournals.aob.a086261

Landry, S., St-Laurent, M.-H., Pelletier, G., & Villard, M.-A. (2020). The Best of Both Worlds? Integrating Sentinel-2 Images and airborne LiDAR to Characterize Forest Regeneration. *Remote Sensing*, *12*(15), 2440. https://doi.org/10.3390/rs12152440

Langford, Z. L., Kumar, J., Hoffman, F. M., Breen, A. L., & Iversen, C. M. (2019). Arctic Vegetation Mapping Using Unsupervised Training Datasets and Convolutional Neural Networks. *Remote Sensing*, *11*(1), 69. https://doi.org/10.3390/rs11010069

Lanorte, A., & Lasaponara, R. (2008). Fuel type characterization based on coarse resolution MODIS satellite data. *IForest - Biogeosciences and Forestry*, *1*(1), 60. https://doi.org/10.3832/ifor0451-0010060

Lasaponara, R., & Lanorte, A. (2007a). On the capability of satellite VHR QuickBird data for fuel type characterization in fragmented landscape. *Ecological Modelling*, *204*(1), 79–84. https://doi.org/10.1016/j.ecolmodel.2006.12.022

Lasaponara, R., & Lanorte, A. (2007b). Remotely sensed characterization of forest fuel types by using satellite ASTER data. *International Journal of Applied Earth Observation and Geoinformation*, *9*(3), 225–234. https://doi.org/10.1016/j.jag.2006.08.001

Latifi, H., Hill, S., Schumann, B., Heurich, M., & Dech, S. (2017). Multi-model estimation of understorey shrub, herb and moss cover in temperate forest stands by laser scanner data. *Forestry*. https://doi.org/10.1093/forestry/cpw066

Lees, K. J., Buxton, J., Boulton, C. A., Abrams, J. F., & Lenton, T. M. (2021). Using satellite data to assess management frequency and rate of regeneration on heather moorlands in England as a resilience indicator. *Environmental Research Communications*, *3*(8), 085003. https://doi.org/10.1088/2515-7620/ac1a5f

Legg, C. J., Maltby, E., & Proctor, M. C. F. (1992). The ecology of severe moorland fire on the North York Moors: Seed distribution and seedling establishment of Calluna vulgaris. *Journal of Ecology*, 737–752. https://doi.org/10.2307/2260863

Leite, R. V., Silva, C. A., Broadbent, E. N., Amaral, C. H. do, Liesenberg, V., Almeida, D. R. A. de, Mohan, M., Godinho, S., Cardil, A., Hamamura, C., Faria, B. L. de, Brancalion, P. H. S., Hirsch, A., Marcatti, G. E., Dalla Corte, A. P., Zambrano, A. M. A., Costa, M. B. T. da, Matricardi, E. A. T., Silva, A. L. da, … Klauberg, C. (2022). Large scale multi-layer fuel load characterization in tropical savanna using GEDI spaceborne lidar data. *Remote Sensing of Environment*, *268*, 112764. https://doi.org/10.1016/j.rse.2021.112764

Leuschner, C., & Ellenberg, H. (2017a). *Ecology of Central European Forests: Vegetation Ecology of Central Europe, Volume I*. Springer International Publishing. https://doi.org/10.1007/978-3-319-43042-3

Leuschner, C., & Ellenberg, H. (2017b). *Ecology of Central European Non-Forest Vegetation: Coastal to Alpine, Natural to Man-Made Habitats: Vegetation Ecology of Central Europe, Volume II*. Springer International Publishing. https://doi.org/10.1007/978-3-319-43048-5

Li, S., Wang, T., Hou, Z., Gong, Y., Feng, L., & Ge, J. (2021). Harnessing terrestrial laser scanning to predict understory biomass in temperate mixed forests. *Ecological Indicators*, *121*, 107011. https://doi.org/10.1016/j.ecolind.2020.107011

Li, Y., Quan, X., Liao, Z., & He, B. (2021). Forest Fuel Loads Estimation from Landsat ETM plus and ALOS PALSAR Data. *Remote Sensing*, *13*(6), 1189. https://doi.org/10.3390/rs13061189

Lillesand, T., Kiefer, R. W., & Chipman, J. (2008). *Remote sensing and image interpretation* (6th ed.). John Wiley & Sons.

Linn, R. R., Goodrick, S. L., Brambilla, S., Brown, M. J., Middleton, R. S., O'Brien, J. J., & Hiers, J. K. (2020). QUIC-fire: A fast-running simulation tool for prescribed fire planning. *Environmental Modelling & Software*, *125*, 104616. https://doi.org/10.1016/j.envsoft.2019.104616

Linn, R., Reisner, J., Colman, J. J., & Winterkamp, J. (2002). Studying wildfire behavior using FIRETEC. *International Journal of Wildland Fire*, *11*(4), 233–246. https://doi.org/10.1071/wf02007

Liodakis, S., Bakirtzis, D., & Dimitrakopoulos, A. (2002). Ignition characteristics of forest species in relation to thermal analysis data. *Thermochimica Acta*, *390*(1), 83–91. https://doi.org/10.1016/S0040-6031(02)00077-1

Liu, H. Q., & Huete, A. (1995). A feedback based modification of the NDVI to minimize canopy background and atmospheric noise. *IEEE Transactions on Geoscience and Remote Sensing*, *33*(2), 457–465. https://doi.org/10.1109/36.377946

Liu, J., Wang, X., & Wang, T. (2019). Classification of tree species and stock volume estimation in ground forest images using Deep Learning. *Computers and Electronics in Agriculture*, *166*, 105012. https://doi.org/10.1016/j.compag.2019.105012

Long, J., Shelhamer, E., & Darrell, T. (2015). Fully convolutional networks for semantic segmentation. *Proceedings of the IEEE Conference on Computer Vision and Pattern Recognition*, 3431–3440. https://doi.org/10.1109/cvpr.2015.7298965

Lopes Queiroz, G., McDermid, G., Linke, J., Hopkinson, C., & Kariyeva, J. (2020). Estimating Coarse Woody Debris Volume Using Image Analysis and Multispectral LiDAR. *Forests*, *11*(2), 141. https://doi.org/10.3390/f11020141

Loudermilk, E. L., O'Brien, J. J., Goodrick, S. L., Linn, R. R., Skowronski, N. S., & Hiers, J. K. (2022). Vegetation's influence on fire behavior goes beyond just being fuel. *Fire Ecology*, *18*(1), 1–10. https://doi.org/10.1186/s42408-022-00132-9

Loudermilk, E. L., O'Brien, J. J., Mitchell, R. J., Cropper, W. P., Hiers, J. K., Grunwald, S., Grego, J., & Fernandez-Diaz, J. C. (2012). Linking complex forest fuel structure and fire behaviour at fine scales. *International Journal of Wildland Fire*, *21*(7), 882. https://doi.org/10.1071/WF10116

Lutes, D. C., Keane, R. E., & Caratti, J. F. (2009). A surface fuel classification for estimating fire effects. *International Journal of Wildland Fire*, *18*(7), 802. https://doi.org/10.1071/WF08062

Lutes, D. C., Keane, R. E., Caratti, J. F., Key, C. H., Benson, N. C., Sutherland, S., & Gangi, L. J. (2006). *FIREMON: Fire effects monitoring and inventory system* (RMRS-GTR-164). U.S. Department of Agriculture, Forest Service, Rocky Mountain Research Station.

Mac Arthur, A., & Malthus, T. (2012). Calluna vulgaris foliar pigments and spectral reflectance modelling. *International Journal of Remote Sensing*, *33*(16), 5214–5239. https://doi.org/10.1080/01431161.2012.659357

Maillard, A., Diquélou, S., Billard, V., Laîné, P., Garnica, M., Prudent, M., Garcia-Mina, J.-M., Yvin, J.-C., & Ourry, A. (2015). Leaf mineral nutrient remobilization during leaf senescence and modulation by nutrient deficiency. *Frontiers in Plant Science*, *6*. https://doi.org/10.3389/fpls.2015.00317

Mak, E. H. T. (1982). *The relationship between the nutrient status and flammability of forest fuels* [PhD Thesis]. The Australian National University.

Mallinis, G., Galidaki, G., & Gitas, I. (2014). A Comparative Analysis of EO-1 Hyperion, Quickbird and Landsat TM Imagery for Fuel Type Mapping of a Typical Mediterranean Landscape. *Remote Sensing*, *6*(2), 2. https://doi.org/10.3390/rs6021684

Mallinis, G., Mitsopoulos, I. D., Dimitrakopoulos, A. P., Gitas, I., & Karteris, M. (2008). Local-Scale Fuel-Type Mapping and Fire Behavior Prediction by Employing High-Resolution Satellite Imagery. *IEEE Journal of Selected Topics in Applied Earth Observations and Remote Sensing*, *1*(4), 230–239. https://doi.org/10.1109/JSTARS.2008.2011298

Maltby, E., Legg, C. J., & Proctor, M. C. F. (1990). The ecology of severe moorland fire on the North York Moors: Effects of the 1976 fires, and subsequent surface and vegetation development. *The Journal of Ecology*, 490–518. https://doi.org/10.2307/2261126

Måren, I. E., Janovský, Z., Spindelböck, J. P., Daws, M. I., Kaland, P. E., & Vandvik, V. (2010). Prescribed burning of northern heathlands: Calluna vulgaris germination cues and seed-bank dynamics. *Plant Ecology*, *207*(2), 245–256. https://doi.org/10.1007/s11258-009-9669-1

Maringer, J., Ascoli, D., Küffer, N., Schmidtlein, S., & Conedera, M. (2016). What drives European beech (Fagus sylvatica L.) mortality after forest fires of varying severity? *Forest Ecology and Management*, *368*, 81–93. https://doi.org/10.1016/j.foreco.2016.03.008

Marino, E., Ranz, P., Tomé, J. L., Noriega, M. Á., Esteban, J., & Madrigal, J. (2016). Generation of high-resolution fuel model maps from discrete airborne laser scanner and Landsat-8 OLI: A low-cost and highly updated methodology for large areas. *Remote Sensing of Environment*, *187*, 267–280. https://doi.org/10.1016/j.rse.2016.10.020

Marrs, R. H., Le Duc, M. G., Mitchell, R. J., Goddard, D., Paterson, S., & Pakeman, R. J. (2000). The Ecology of Bracken: Its Role in Succession and Implications for Control. *Annals of Botany*, *85*, 3–15. https://doi.org/10.1006/anbo.1999.1054

Marston, C., Rowland, C. S., O'Neil, A. W., & Morton, R. D. (2022). *Land Cover Map 2021 (10m classified pixels, GB)*. NERC EDS Environmental Information Data Centre. https://doi.org/10.5285/a22baa7c-5809-4a02-87e0-3cf87d4e223a

Matthews, S. (2013). Dead fuel moisture research: 1991–2012. *International Journal of Wildland Fire*, *23*(1), 78–92. https://doi.org/10.1071/WF13005

Maxwell, W. G. (1980). *Photo Series for Quantifying Natural Forest Residues in Common Vegetation Types of the Pacific Northwest*. U.S. Department of Agriculture, Forest Service, Pacific Northwest Forest and Range Experiment Station.

McAllister, S., Grenfell, I., Hadlow, A., Jolly, W. M., Finney, M., & Cohen, J. (2012). Piloted ignition of live forest fuels. *Fire Safety Journal*, *51*, 133–142. https://doi.org/10.1016/j.firesaf.2012.04.001

McGaughey, R. J. (2022). *FUSION/LDV: Software for LIDAR Data Analysis and Visualization: FUSION Version 4.40* (Pacific Northwest Research Station, Forest Service, U.S. Department of Agriculture, Ed.). http://forsys.cfr.washington.edu/software/fusion/FUSION_manual.pdf

McKenna, P., Phinn, S., & Erskine, P. D. (2018). Fire Severity and Vegetation Recovery on Mine Site Rehabilitation Using WorldView-3 Imagery. *Fire*, *1*(2), 2. https://doi.org/10.3390/fire1020022

McKenzie, D., Raymond, C. L., Kellogg, L.-K. B., Norheim, R. A., Andreu, A. G., Bayard, A. C., Kopper, K. E., & Elman, E. (2007). Mapping fuels at multiple scales: Landscape application of the Fuel Characteristic Classification SystemThis article is one of a selection of papers published in the Special Forum on the Fuel Characteristic Classification System. *Canadian Journal of Forest Research*, *37*(12), 2421–2437. https://doi.org/10.1139/X07-056

McKinney, W. (2010). Data Structures for Statistical Computing in Python. *Proceedings of the 9th Python in Science Conference*, 51–56. https://doi.org/10.25080/majora-92bf1922-00a

McMorrow, J. (2011). Wildfire in the United Kingdom: Status and key issues. *Proc. 2nd Conf. on the Human Dimensions of Wildland Fire*, *GTR-NRS-P-84*, 44–56.

Mead, L., & Arthur, M. (2020). Environmental condition in British moorlands: Quantifying the life cycle of Calluna vulgaris using UAV aerial imagery. *International Journal of Remote Sensing*, *41*(2), 573–583. https://doi.org/10.1080/2150704X.2019.1646931

Meerdink, S. K., Hook, S. J., Roberts, D. A., & Abbott, E. A. (2019). The ECOSTRESS spectral library version 1.0. *Remote Sensing of Environment*, *230*, 111196. https://doi.org/10.1016/j.rse.2019.05.015

Mell, W., Jenkins, M. A., Gould, J., & Cheney, P. (2007). A physics-based approach to modelling grassland fires. *International Journal of Wildland Fire*, *16*(1), 1–22. https://doi.org/10.1071/WF06002

Merrill, D. F., & Alexander, M. E. (1987). *Glossary of forest fire management terms* (4th ed.). Canadian Committee on Forest Fire Management, National Research Council of Canada.

Merzlyak, M. N., Gitelson, A. A., Chivkunova, O. B., & Rakitin, V. YU. (1999). Non-destructive optical detection of pigment changes during leaf senescence and fruit ripening. *Physiologia Plantarum*, *106*(1), 135–141. https://doi.org/10.1034/j.1399-3054.1999.106119.x

Met Office. (2005). *UK Fire Severity Index*. https://www.metoffice.gov.uk/public/weather/fire-severity-index/#?tab=map&fcTime=1695981600&zoom=5&lon=-4.00&lat=55.74

Met Office, Hollis, D., McCarthy, M., Kendon, M., & Legg, T. (2023). *HadUK-Grid Gridded Climate Observations on a 1km grid over the UK, v1.2.0.ceda (1836-2022)*. https://doi.org/10.5285/46f8c1377f8849eeb8570b8ac9b26d86

Metzger, C. M. H., Heinichen, J., Eickenscheidt, T., & Drösler, M. (2017). Impact of land-use intensity on the relationships between vegetation indices, photosynthesis and biomass of intensively and extensively managed grassland fens. *Grass and Forage Science*, *72*(1), 50–63. https://doi.org/10.1111/gfs.12223

Millar, C. I., & Stephenson, N. L. (2015). Temperate forest health in an era of emerging megadisturbance. *Science*, *349*(6250), 823–826. https://doi.org/10.1126/science.aaa9933

Millard, K., Darling, S., Pelletier, N., & Schultz, S. (2022). Seasonally-decomposed Sentinel-1 backscatter time-series are useful indicators of peatland wildfire vulnerability. *Remote Sensing of Environment*, *283*, 113329. https://doi.org/10.1016/j.rse.2022.113329

Miller, C., & Urban, D. L. (2000). Connectivity of forest fuels and surface fire regimes. *Landscape Ecology*, *15*(2), 145–154. https://doi.org/10.1023/A:1008181313360

Miller, G. R., & Miles, J. (1970). Regeneration of Heather (Calluna vulgaris (L.) Hull) at Different Ages and Seasons in North-East Scotland. *Journal of Applied Ecology*, *7*(1), 51–60. https://doi.org/10.2307/2401611

Millin-Chalabi, G. (2016). *Radar Multi-Temporal and Multi-Sensor Approach to Characterise Peat Moorland Burn Scars and Assess Burn Scar Persistence in the Landscape* [PhD Thesis]. The University of Manchester (United Kingdom).

Millin-Chalabi, G., McMorrow, J., & Agnew, C. (2013). Detecting a moorland wildfire scar in the Peak District, UK, using synthetic aperture radar from ERS-2 and Envisat ASAR. *International Journal of Remote Sensing*, *35*(1), 54–69. https://doi.org/10.1080/01431161.2013.860658

Mißbach, K. (1982). *Waldbrand: Verhütung und Bekämpfung* (3rd ed.). VEB Deutscher Landwirtschaftsverlag.

Mitchell, S. R., Harmon, M. E., & O'Connell, K. E. B. (2009). Forest fuel reduction alters fire severity and long-term carbon storage in three Pacific Northwest ecosystems. *Ecological Applications : A Publication of the Ecological Society of America*, *19*(3), 643–655. https://doi.org/10.1890/08-0501.1

Mitri, G. H., & Gitas, I. (2010). Mapping Postfire Vegetation Recovery Using EO-1 Hyperion Imagery. *IEEE Transactions on Geoscience and Remote Sensing*, *48*(3), 1613–1618. https://doi.org/10.1109/TGRS.2009.2031557

Modugno, S., Balzter, H., Cole, B., & Borrelli, P. (2016). Mapping regional patterns of large forest fires in Wildland–Urban Interface areas in Europe. *Journal of Environmental Management*, *172*, 112–126. https://doi.org/10.1016/j.jenvman.2016.02.013

Moghaddas, J. J., Collins, B. M., Menning, K., Moghaddas, E. E. Y., & Stephens, S. L. (2010). Fuel treatment effects on modeled landscape-level fire behavior in the northern Sierra Nevada. *Canadian Journal of Forest Research*, *40*(9), 1751–1765. https://doi.org/10.1139/X10-118

Molnar, C. (2022). *Interpretable Machine Learning: A Guide for Making Black Box Models Explainable* (2nd ed.). https://christophm.github.io/interpretable-ml-book

Moors for the Future. (2023). *Wildfire Recording System*. https://www.wildfirelog.co.uk/

Morfin-Rios, J. E., Alvarado-Celestino, E., Jardel-Pelaez, E. J., Vihnanek, R. E., Wright, D. K., Michel-Fuentes, J. M., Wright, C. S., Ottmar, R. D., Sandberg, D. V., & Najera-Diaz, A. (2008). *Photo series for quantifying forest fuels in Mexico: Montane subtropical forests of the Sierra Madre del Sur and temperate forests and montane shrubland of the northern Sierra Madre Oriental* (Special Pub. No. 1). Pacific Wildland Fire Sciences Laboratory, University of Washington, College of Forest Resources.

Moris, J. V., Reilly, M. J., Yang, Z., Cohen, W. B., Motta, R., & Ascoli, D. (2022). Using a trait-based approach to asses fire resistance in forest landscapes of the Inland Northwest, USA. *Landscape Ecology*, *37*(8), 2149–2164. https://doi.org/10.1007/s10980-022-01478-w

Moritz, M. A., Morais, M. E., Summerell, L. A., Carlson, J. M., & Doyle, J. (2005). Wildfires, complexity, and highly optimized tolerance. *Proceedings of the National Academy of Sciences*, *102*(50), 17912–17917. https://doi.org/10.1073/pnas.0508985102

Moritz, M. A., Parisien, M.-A., Batllori, E., Krawchuk, M. A., van Dorn, J., Ganz, D. J., & Hayhoe, K. (2012). Climate change and disruptions to global fire activity. *Ecosphere*, *3*(6). https://doi.org/10.1890/ES11-00345.1

Müller, M., Vilà Vilardell, L., Vacik, H., Mayer, C., Mayr, S., Carrega, P., Duche, Y., Lahaye, S., Böttcher, F., Maier, H., Schunk, C., Zimmermann, L., Ascoli, D., Cotterchio, A., Fiorucci, P., Gottero, F., Pirone, S., Rizzolo, R., Vacchiano, G., & Sautter, M. (2020). *Forest fires in the Alps—State of knowledge, future challenges and options for an integrated fire management—White Paper for policy makers*. https://doi.org/10.13140/RG.2.2.15609.42081

Murray, J., Blackburn, G. A., Whyatt, J. D., & Edwards, C. (2018). Using fractal analysis of crown images to measure the structural condition of trees. *Forestry: An International Journal of Forest Research*, *91*(4), 480–491. https://doi.org/10.1093/forestry/cpy008

Mutlu, M., Popescu, M., Stripling, C., & Spencer, T. (2008). Mapping surface fuel models using lidar and multispectral data fusion for fire behavior. *Remote Sensing of Environment*, *112*(1), 274–285. https://doi.org/10.1016/j.rse.2007.05.005

Muys, B., Angelstam, P., Bauhus, J., Bouriaud, L., Jactel, H., Kraigher, H., Müller, J., Pettorelli, N., Pötzelsberger, E., & Primmer, E. (2022). *Forest biodiversity in Europe*. European Forest Institute Joensuu, Finland. https://doi.org/10.36333/fs13

Nelson, R. M. J. (2000). Prediction of diurnal change in 10-h fuel stick moisture content. *Canadian Journal of Forest Research*, *30*(7), 1071–1087. https://doi.org/10.1139/x00-032

Neumann, C., Behling, R., Schindhelm, A., Itzerott, S., Weiss, G., Wichmann, M., & Müller, J. (2020). The colors of heath flowering – quantifying spatial patterns of phenology in Calluna life-cycle phases using high-resolution drone imagery. *Remote Sensing in Ecology and Conservation*, *6*(1), 35–51. https://doi.org/10.1002/rse2.121

Newville, M., Stensitzki, T., Allen, D. B., & Ingargiola, A. (2014). *LMFIT: Non-Linear Least-Square Minimization and Curve-Fitting for Python* (0.8.0). Zenodo. https://doi.org/10.5281/zenodo.11813

Nichol, C. J., & Grace, J. (2010). Determination of leaf pigment content in Calluna vulgaris shoots from spectral reflectance. *International Journal of Remote Sensing*, *31*(20), 5409–5422. https://doi.org/10.1080/01431160903302957

Nilsen, L. S., Johansen, L., & Velle, L. G. (2005). Early stages of Calluna vulgaris regeneration after burning of coastal heath in central Norway. *Applied Vegetation Science*, *8*(1), 57–64. https://doi.org/10.1111/j.1654-109X.2005.tb00629.x

Ordnance Survey. (2023). *OS Terrain 5*. Ordnance Survey. https://www.ordnancesurvey.co.uk/products/os-terrain-5

Ormeño, E., Céspedes, B., Sánchez, I. A., Velasco-García, A., Moreno, J. M., Fernandez, C., & Baldy, V. (2009). The relationship between terpenes and flammability of leaf litter. *Forest Ecology and Management*, *257*(2), 471–482. https://doi.org/10.1016/j.foreco.2008.09.019

Ottmar, R. D. (2014). Wildland fire emissions, carbon, and climate: Modeling fuel consumption. *Forest Ecology and Management*, *317*, 41–50. https://doi.org/10.1016/j.foreco.2013.06.010

Ottmar, R. D., Vihnanek, R. E., Miranda, H. S., Sato, M. N., & Andrade, S. M. A. (2004). Stereo photo series for quantifying biomass for the Cerrado vegetation in central Brazil. *Floresta*, *34*(2). https://doi.org/10.5380/rf.v34i2.2380

Ottosen, T.-B., Petch, G., Hanson, M., & Skjøth, C. A. (2020). Tree cover mapping based on Sentinel-2 images demonstrate high thematic accuracy in Europe. *International Journal of Applied Earth Observation and Geoinformation*, *84*, 101947. https://doi.org/10.1016/j.jag.2019.101947

Päätalo, M.-L. (1998). Factors influencing occurrence and impacts of fires in northern European forests. *Silva Fennica*, *32*, 185–202.

Page, W. G., Alexander, M. E., & Jenkins, M. J. (2013). Wildfire's resistance to control in mountain pine beetle-attacked lodgepole pine forests. *The Forestry Chronicle*, *89*(06), 783–794. https://doi.org/10.5558/tfc2013-141

Pajtík, J., Konôpka, B., & Lukac, M. (2011). Individual biomass factors for beech, oak and pine in Slovakia: A comparative study in young naturally regenerated stands. *Trees*, *25*(2), 277–288. https://doi.org/10.1007/s00468-010-0504-z

Parsons, R. A., Mell, W. E., & McCauley, P. (2011). Linking 3D spatial models of fuels and fire: Effects of spatial heterogeneity on fire behavior. *Ecological Modelling*, *222*(3), 679–691. https://doi.org/10.1016/j.ecolmodel.2010.10.023

PDNPA. (2013). *Landscape: Peak District State of the Park Report*. http://www.peakdistrict.gov.uk/microsites/sopr/landscape

PDNPA. (2021). *Climate Change Vulnerability Assessment by the Peak District National Park Authority*. https://reports.peakdistrict.gov.uk/ccva/

Pearson, R. K., Neuvo, Y., Astola, J., & Gabbouj, M. (2016). Generalized Hampel Filters. *EURASIP Journal on Advances in Signal Processing*, *2016*(1), 87. https://doi.org/10.1186/s13634-016-0383-6

Pedregosa, F., Varoquaux, G., Gramfort, A., Michel, V., Thirion, B., Grisel, O., Blondel, M., Prettenhofer, P., Weiss, R., Dubourg, V., Vanderplas, J., Passos, A., Cournapeau, D., Brucher, M., Perrot, M., & Duchesnay, E. (2011). Scikit-learn: Machine learning in Python. *Journal of Machine Learning Research*, *12*, 2825–2830.

Pérez-Cabello, F., Montorio, R., & Alves, D. B. (2021). Remote sensing techniques to assess post-fire vegetation recovery. *Current Opinion in Environmental Science & Health*, *21*, 100251. https://doi.org/10.1016/j.coesh.2021.100251

Perry, D. A., Choquette, C., & Schroeder, P. (1987). Nitrogen dynamics in conifer-dominated forests with and without hardwoods. *Canadian Journal of Forest Research*, *17*(11), 1434–1441. https://doi.org/10.1139/x87-221

Perry, M. C., Vanvyve, E., Betts, R. A., & Palin, E. J. (2022). Past and future trends in fire weather for the UK. *Natural Hazards and Earth System Sciences*, *22*(2), 559–575. https://doi.org/10.5194/nhess-22-559-2022

Persson, M., Lindberg, E., & Reese, H. (2018). Tree Species Classification with Multi-Temporal Sentinel-2 Data. *Remote Sensing*, *10*(11), 1794. https://doi.org/10.3390/rs10111794

Peterson, D. L., McCaffrey, S. M., & Patel-Weynand, T. (Eds.). (2022). *Wildland Fire Smoke in the United States: A Scientific Assessment*. Springer Nature. https://doi.org/10.1007/978-3-030-87045-4

Peterson, S. H., Franklin, J., Roberts, D. A., & van Wagtendonk, J. W. (2013). Mapping fuels in Yosemite National Park. *Canadian Journal of Forest Research*, *43*(1), 7–17. https://doi.org/10.1139/cjfr-2012-0213

Philpot, C. W. (1970). Influence of Mineral Content on the Pyrolysis of Plant Materials. *Forest Science*, *16*(4), 461–471. https://doi.org/10.1093/forestscience/16.4.461

Pickell, P. D., Chavardès, R. D., Li, S., & Daniels, L. D. (2021). FuelNet: An Artificial Neural Network for Learning and Updating Fuel Types for Fire Research. *IEEE Transactions on Geoscience and Remote Sensing*, *59*(9), 7338–7352. https://doi.org/10.1109/TGRS.2020.3037160

Pickell, P. D., Hermosilla, T., Frazier, R. J., Coops, N. C., & Wulder, M. A. (2016). Forest recovery trends derived from Landsat time series for North American boreal forests. *International Journal of Remote Sensing*, *37*(1), 138–149. https://doi.org/10.1080/2150704X.2015.1126375

Pizer, S. M., Amburn, E. P., Austin, J. D., Cromartie, R., Geselowitz, A., Greer, T., ter Haar Romeny, B., Zimmerman, J. B., & Zuiderveld, K. (1987). Adaptive histogram equalization and its variations. *Computer Vision, Graphics, and Image Processing*, *39*(3), 355–368. https://doi.org/10.1016/S0734-189X(87)80186-X

Plamondon, P. A., Black, T. A., & Goodell, B. C. (1972). The role of hydrologic properties of the forest floor in watershed hydrology. *National Symposium on Watersheds in Transition*, 341–348.

Plucinski, M. P. (2019). Fighting Flames and Forging Firelines: Wildfire Suppression Effectiveness at the Fire Edge. *Current Forestry Reports*, *5*(1), 1–19. https://doi.org/10.1007/s40725-019-00084-5

Plucinski, M. P., Gill, A. M., & Bradstock, R. A. (2009). Fuel dynamics in shrub dominated landscapes. *Proceedings of the Royal Society of Queensland*, *115*, 145–151.

Polychronaki, A., Gitas, I., & Minchella, A. (2013). Monitoring post-fire vegetation recovery in the Mediterranean using SPOT and ERS imagery. *International Journal of Wildland Fire*, *23*(5), 631–642. https://doi.org/10.1071/WF12058

Popović, Z., Bojović, S., Marković, M., & Cerdà, A. (2021). Tree species flammability based on plant traits: A synthesis. *Science of The Total Environment*, *800*, 149625. https://doi.org/10.1016/j.scitotenv.2021.149625

Potter, C. (2018). Recovery Rates of Wetland Vegetation Greenness in Severely Burned Ecosystems of Alaska Derived from Satellite Image Analysis. *Remote Sensing*, *10*(9), 9. https://doi.org/10.3390/rs10091456

Prichard, S. J., Ottmar, R. D., & Anderson, G. K. (2007). *CONSUME 3.0 User's Guide*. USDA Forest Service, Pacific Northwest Research Station, Pacific Wildland Fire Sciences Laboratory.

Prichard, S. J., Rowell, E., Keane, R. E., Hudak, A. T., Lutes, D., & Loudermilk, E. L. (2023). Wildland Fuel Characterization Across Space and Time. In *Landscape Fire, Smoke, and Health* (pp. 53–68). American Geophysical Union (AGU). https://doi.org/10.1002/9781119757030.ch4

Prichard, S. J., Rowell, E. M., Hudak, A. T., Keane, R. E., Loudermilk, E. L., Lutes, D. C., Ottmar, R. D., Chappell, L. M., Hall, J. A., & Hornsby, B. S. (2022). Fuels and Consumption. In D. L. Peterson, S. M. McCaffrey, & T. Patel-Weynand (Eds.), *Wildland Fire Smoke in the United States: A Scientific Assessment* (pp. 11–49). Springer International Publishing. https://doi.org/10.1007/978-3-030-87045-4_2

Puhe, J., & Ulrich, B. (2001). Human Impacts on Central European Forests: Summary and Conclusions. In J. Puhe & B. Ulrich (Eds.), *Global Climate Change and Human Impacts on Forest Ecosystems: Postglacial Development, Present Situation, and Future Trends in Central Europe* (pp. 463–476). Springer. https://doi.org/10.1007/978-3-642-59531-8_9

Pyne, S. J. (1984). *Introduction to wildland fire. Fire management in the United States.* John Wiley & Sons.

Qi, Y., Dennison, P. E., Jolly, W. M., Kropp, R. C., & Brewer, S. C. (2014). Spectroscopic analysis of seasonal changes in live fuel moisture content and leaf dry mass. *Remote Sensing of Environment*, *150*, 198–206. https://doi.org/10.1016/j.rse.2014.05.004

R Core Team. (2022). *R: A language and environment for statistical computing*. R Foundation for Statistical Computing. https://www.R-project.org/

Rao, K., Williams, A. P., Flefil, J. F., & Konings, A. G. (2020). SAR-enhanced mapping of live fuel moisture content. *Remote Sensing of Environment*, *245*, 111797. https://doi.org/10.1016/j.rse.2020.111797

Reeves, M. C., Kost, J. R., & Ryan, K. C. (2006). Fuels products of the LANDFIRE project. In P. L. Andrews & B. W. Butler (Eds.), *Fuels Management-How to Measure Success: Conference Proceedings: Vol. RMRS-P-41* (pp. 239–252). US Department of Agriculture, Forest Service, Rocky Mountain Research Station.

Reich, R. M., Lundquist, J. E., & Bravo, V. A. (2004). Spatial models for estimating fuel loads in the Black Hills, South Dakota, USA. *International Journal of Wildland Fire*, *13*(1), 119. https://doi.org/10.1071/WF02049

Rein, G., Cleaver, N., Ashton, C., Pironi, P., & Torero, J. L. (2008). The severity of smouldering peat fires and damage to the forest soil. *CATENA*, *74*(3), 304–309. https://doi.org/10.1016/j.catena.2008.05.008

Reinhardt, E. D. (1997). *First Order Fire Effects Model: FOFEM 4.0, User's Guide*. U.S. Department of Agriculture, Forest Service, Intermountain Forest and Range Experiment Station.

Resco De Dios, V. (2020). *Plant-Fire Interactions: Applying Ecophysiology to Wildfire Management* (Vol. 36). Springer International Publishing. https://doi.org/10.1007/978-3-030-41192-3

Restaino, J. (2019). Fuel Loading. In S. L. Manzello (Ed.), *Encyclopedia of Wildfires and Wildland-Urban Interface (WUI) Fires* (pp. 1–4). Springer International Publishing. https://doi.org/10.1007/978-3-319-51727-8_228-1

Riaño, D. (2003). Modeling airborne laser scanning data for the spatial generation of critical forest parameters in fire behavior modeling. *Remote Sensing of Environment*, *86*(2), 177–186. https://doi.org/10.1016/S0034-4257(03)00098-1

Riaño, D., Chuvieco, E., Salas, J., Palacios-Orueta, A., & Bastarrika, A. (2002). Generation of fuel type maps from Landsat TM images and ancillary data in Mediterranean ecosystems. *Canadian Journal of Forest Research*, *32*(8), 1301–1315. https://doi.org/10.1139/x02-052

Ringland, J., Bohm, M., & Baek, S.-R. (2019). Characterization of food cultivation along roadside transects with Google Street View imagery and deep learning. *Computers and Electronics in Agriculture*, *158*, 36–50. https://doi.org/10.1016/j.compag.2019.01.014

Rivera, J. de D., Davies, G. M., & Jahn, W. (2012). Flammability and the Heat of Combustion of Natural Fuels: A Review. *Combustion Science and Technology*, *184*(2), 224–242. https://doi.org/10.1080/00102202.2011.630332

Romeiro, J. M. N., Eid, T., Antón-Fernández, C., Kangas, A., & Trømborg, E. (2022). Natural disturbances risks in European Boreal and Temperate forests and their links to climate change – A review of modelling approaches. *Forest Ecology and Management*, *509*, 120071. https://doi.org/10.1016/j.foreco.2022.120071

Rothermel, R. C. (1972). *A Mathematical Model for Predicting Fire Spread in Wildland Fuels*. U.S. Department of Agriculture, Forest Service, Intermountain Forest and Range Experiment Station.

Rouse, J. W., Haas, R. H., Schell, J. A., & Deering, D. W. (1974). Monitoring vegetation systems in the Great Plains with ERTS. *NASA. Goddard Space Flight Center 3d ERTS-1 Symp.*

Rowell, E., Loudermilk, E. L., Hawley, C., Pokswinski, S., Seielstad, C., Queen, Ll., O'Brien, J. J., Hudak, A. T., Goodrick, S., & Hiers, J. K. (2020). Coupling terrestrial laser scanning with 3D fuel biomass sampling for advancing wildland fuels characterization. *Forest Ecology and Management*, *462*, 117945. https://doi.org/10.1016/j.foreco.2020.117945

Ryan, K. C., & Reinhardt, E. D. (1988). Predicting postfire mortality of seven western conifers. *Canadian Journal of Forest Research*, *18*(10), 1291–1297. https://doi.org/10.1139/x88-199

Saatchi, S., Halligan, K., Despain, D. G., & Crabtree, R. L. (2007). Estimation of forest fuel load from radar remote sensing. *IEEE Transactions on Geoscience and Remote Sensing*, *45*(6), 1726–1740. https://doi.org/10.1109/TGRS.2006.887002

San Emeterio, L., Múgica, L., Ugarte, M. D., Goicoa, T., & Canals, R. M. (2016). Sustainability of traditional pastoral fires in highlands under global change: Effects on soil function and nutrient cycling. *Agriculture, Ecosystems & Environment*, *235*, 155–163. https://doi.org/10.1016/j.agee.2016.10.009

Sandberg, D. V., Ottmar, R. D., & Cushon, G. H. (2001). Characterizing fuels in the 21st Century. *International Journal of Wildland Fire*, *10*(4), 381–387. https://doi.org/10.1071/WF01036

Sandberg, D. V., Riccardi, C. L., & Schaaf, M. D. (2007). Reformulation of Rothermel's wildland fire behaviour model for heterogeneous fuelbeds. *Canadian Journal of Forest Research*, *37*(12), 2438–2455. https://doi.org/10.1139/X07-094

Sankey, J. B., Wallace, C. S. A., & Ravi, S. (2013). Phenology-based, remote sensing of post-burn disturbance windows in rangelands. *Ecological Indicators*, *30*, 35–44. https://doi.org/10.1016/j.ecolind.2013.02.004

San-Miguel-Ayanz, J., Durrant, T., Boca, R., Liberta', G., Branco, A., De, R. D., Ferrari, D., Maianti, P., Artes, V. T., Pfeiffer, H., Loffler, P., Nuijten, D., Leray, T., & Jacome, F. O. D. (2019). *Forest Fires in Europe, Middle East and North Africa 2018*. JRC Publications Repository. https://doi.org/10.2760/1128

San-Miguel-Ayanz, J., Durrant, T., Boca, R., Maianti, P., Liberta', G., Artes, V. T., Jacome, F. O. D., Branco, A., De, R. D., Ferrari, D., Pfeiffer, H., Grecchi, R., Onida, M., & Loffler, P. (2022). *Forest Fires in Europe, Middle East and North Africa 2021*. JRC Publications Repository. https://doi.org/10.2760/34094

San-Miguel-Ayanz, J., Durrant, T., Boca, R., Maianti, P., Libertá, G., Artés-Vivancos, T., Oom, D., Branco, A., de Rigo, D., Ferrari, D., Pfeiffer, H., Grecchi, R., Nuijten, D., Onida, M., & Löffler, P. (2021). *Forest Fires in Europe, Middle East and North Africa 2020* (JRC1267665). JRC Publications Repository. https://doi.org/10.2760/216466

San-Miguel-Ayanz, J., Schulte, E., Schmuck, G., Camia, A., Strobl, P., Libertà, G., Giovando, C., Boca, R., Sedano, F., Kempeneers, P., McInerney, D., Withmore, C., Oliveira, S., Rodrigues, M., Durrant, T., Corti, P., Oehler, F., Vilar, L., & Amatulli, G. (2012). Comprehensive Monitoring of Wildfires in Europe: The European Forest Fire Information System (EFFIS). In *Approaches to Managing Disaster—Assessing Hazards, Emergencies and Disaster Impacts*. https://doi.org/10.5772/28441

Santana, V. M., & Marrs, R. H. (2014). Flammability properties of British heathland and moorland vegetation: Models for predicting fire ignition. *Journal of Environmental Management*, *139*, 88–96. https://doi.org/10.1016/j.jenvman.2014.02.027

Savitzky, Abraham., & Golay, M. J. E. (1964). Smoothing and Differentiation of Data by Simplified Least Squares Procedures. *Analytical Chemistry*, *36*(8), 1627–1639. https://doi.org/10.1021/ac60214a047

Schellenberg, J., & Bergmeier, E. (2022). The Calluna life cycle concept revisited: Implications for heathland management. *Biodiversity and Conservation*, *31*, 119–141. https://doi.org/10.1007/s10531-021-02325-1

Schepers, L., Haest, B., Veraverbeke, S., Spanhove, T., Vanden Borre, J., & Goossens, R. (2014). Burned Area Detection and Burn Severity Assessment of a Heathland Fire in Belgium Using Airborne Imaging Spectroscopy (APEX). *Remote Sensing*, *6*(3), 3. https://doi.org/10.3390/rs6031803

Schiefer, F., Kattenborn, T., Frick, A., Frey, J., Schall, P., Koch, B., & Schmidtlein, S. (2020). Mapping forest tree species in high resolution UAV-based RGB-imagery by means of convolutional neural networks. *ISPRS Journal of Photogrammetry and Remote Sensing*, *170*, 205–215. https://doi.org/10.1016/j.isprsjprs.2020.10.015

Schiller, C., Schmidtlein, S., Boonman, C., Moreno-Martínez, A., & Kattenborn, T. (2021). Deep learning and citizen science enable automated plant trait predictions from photographs. *Scientific Reports*, *11*(1), 16395. https://doi.org/10.1038/s41598-021-95616-0

Schimmel, J., & Granström, A. (1997). Fuel succession and fire behavior in the Swedish boreal forest. *Canadian Journal of Forest Research*, *27*(8), 1207–1216. https://doi.org/10.1139/x97-072

Schmidt, J., Fassnacht, F. E., Förster, M., & Schmidtlein, S. (2018). Synergetic use of Sentinel-1 and Sentinel-2 for assessments of heathland conservation status. *Remote Sensing in Ecology and Conservation*, *4*(3), 225–239. https://doi.org/10.1002/rse2.68

Schroeder, T. A., Wulder, M. A., Healey, S. P., & Moisen, G. G. (2011). Mapping wildfire and clearcut harvest disturbances in boreal forests with Landsat time series data. *Remote Sensing of Environment*, *115*(6), 1421–1433. https://doi.org/10.1016/j.rse.2011.01.022

Schunk, C., Leutner, C., Leuchner, M., Wastl, C., Menzel, A., Schunk, C., Leutner, C., Leuchner, M., Wastl, C., & Menzel, A. (2013). Equilibrium moisture content of dead fine fuels of selected central European tree species. *International Journal of Wildland Fire*, *22*(6), 797–809. https://doi.org/10.1071/WF12105

Schuster, M., & Paliwal, K. K. (1997). Bidirectional recurrent neural networks. *IEEE Transactions on Signal Processing*, *45*(11), 2673–2681. https://doi.org/10.1109/78.650093

Schwilk, D. W., & Caprio, A. C. (2011). Scaling from leaf traits to fire behaviour: Community composition predicts fire severity in a temperate forest. *Journal of Ecology*, *99*(4), 970–980. https://doi.org/10.1111/j.1365-2745.2011.01828.x

Scott, J. H., & Burgan, R. E. (2005). *Standard Fire Behavior Fuel Models: A Comprehensive Set for Use with Rothermel's Surface Fire Spread Model*. U.S. Department of Agriculture, Forest Service, Rocky Mountain Research Station.

Scott, N. A., & Binkley, D. (1997). Foliage litter quality and annual net N mineralization: Comparison across North American forest sites. *Oecologia*, *111*(2), 151–159. https://doi.org/10.1007/s004420050219

Sedláková, I., & Chytrỳ, M. (1999). Regeneration patterns in a Central European dry heathland: Effects of burning, sod-cutting and cutting. *Plant Ecology*, *143*, 77–87. https://doi.org/10.1023/A:1009807411654

Seidl, R., Schelhaas, M.-J., Rammer, W., & Verkerk, P. J. (2014). Increasing forest disturbances in Europe and their impact on carbon storage. *Nature Climate Change*, *4*(9), 806–810. https://doi.org/10.1038/nclimate2318

Seielstad, C. A., & Queen, L. P. (2003). Using airborne laser altimetry to determine fuel models for estimating fire behavior. *Journal of Forestry*, *101*(4), 10–15. https://doi.org/10.1093/jof/101.4.10

Selvaraju, R. R., Cogswell, M., Das, A., Vedantam, R., Parikh, D., & Batra, D. (2017). Grad-CAM: Visual Explanations from Deep Networks via Gradient-Based Localization. *Proceedings of the IEEE International Conference on Computer Vision*, 618–626. https://doi.org/10.1109/iccv.2017.74

Serra-Burriel, F., Delicado, P., Prata, A. T., & Cucchietti, F. M. (2021). Estimating heterogeneous wildfire effects using synthetic controls and satellite remote sensing. *Remote Sensing of Environment*, *265*, 112649. https://doi.org/10.1016/j.rse.2021.112649

Sesnie, S. E., Eagleston, H., Johnson, L., & Yurcich, E. (2018). In-Situ and Remote Sensing Platforms for Mapping Fine-Fuels and Fuel-Types in Sonoran Semi-Desert Grasslands. *Remote Sensing*, *10*(9), 9. https://doi.org/10.3390/rs10091358

Shaik, R. U., Laneve, G., & Fusilli, L. (2022). An Automatic Procedure for Forest Fire Fuel Mapping Using Hyperspectral (PRISMA) Imagery: A Semi-Supervised Classification Approach. *Remote Sensing*, *14*(5), 5. https://doi.org/10.3390/rs14051264

Shepherd, M. J., Labadz, J., Caporn, S. J., Crowle, A., Goodison, R., Rebane, M., & Waters, R. (2013). *Natural England review of upland evidence—Restoration of Degraded Blanket Bog* (NEER003; Natural England Evidence Review). Natural England.

Sikkink, P. G., & Keane, R. E. (2008). A comparison of five sampling techniques to estimate surface fuel loading in montane forests. *International Journal of Wildland Fire*, *17*(3), 363–379. https://doi.org/10.1071/WF07003

Silván-Cárdenas, J., Corona, N., Galeana-Pizaña, J., Núñez, J. M., & Madrigal, J. (2015). Geospatial Technologies to Support Coniferous Forests Research and Conservation efforts in Mexico. In R. P. Weber (Ed.), *Old-Growth Forests and Coniferous Forests: Ecology, Habitat and Conservation* (pp. 67–123). Nova Science Publishers.

Simonyan, K., & Zisserman, A. (2015). Very Deep Convolutional Networks for Large-Scale Image Recognition. *Conference Track Proceedings of the 3rd International Conference on Learning Representations*. https://doi.org/10.48550/arXiv.1409.1556

Sims, D. A., & Gamon, J. A. (2002). Relationships between leaf pigment content and spectral reflectance across a wide range of species, leaf structures and developmental stages. *Remote Sensing of Environment*, *81*(2), 337–354. https://doi.org/10.1016/S0034-4257(02)00010-X

Singh, K. K., & Gray, J. (2020). Mapping Understory Invasive Plants in Urban Forests with Spectral and Temporal Unmixing of Landsat Imagery. *Photogrammetric Engineering & Remote Sensing*, *86*(8), 509–518. https://doi.org/10.14358/PERS.86.8.509

Skowronski, N. S., Clark, K., Nelson, R., Hom, J., & Patterson, M. (2007). Remotely sensed measurements of forest structure and fuel loads in the Pinelands of New Jersey. *Remote Sensing of Environment*, *108*(2), 123–129. https://doi.org/10.1016/j.rse.2006.09.032

Skowronski, N. S., & Gallagher, M. R. (2018). Fuels Characterization Techniques. In S. L. Manzello (Ed.), *Encyclopedia of Wildfires and Wildland-Urban Interface (WUI) Fires* (pp. 1–10). Springer International Publishing. https://doi.org/10.1007/978-3-319-51727-8_84-1

Sladojevic, S., Arsenovic, M., Anderla, A., Culibrk, D., & Stefanovic, D. (2016). Deep Neural Networks Based Recognition of Plant Diseases by Leaf Image Classification. *Computational Intelligence and Neuroscience*, *2016*, 3289801. https://doi.org/10.1155/2016/3289801

Smith, C. W., Panda, S. K., Bhatt, U. S., & Meyer, F. J. (2021). Improved Boreal Forest Wildfire Fuel Type Mapping in Interior Alaska Using AVIRIS-NG Hyperspectral Data. *Remote Sensing*, *13*(5), 5. https://doi.org/10.3390/rs13050897

Smith, W. G. (1902). The origin and development of heather Moorland. *Scottish Geographical Magazine*, *18*(11), 587–597. https://doi.org/10.1080/00369220208733402

Solans Vila, J. P., & Barbosa, P. (2010). Post-fire vegetation regrowth detection in the Deiva Marina region (Liguria-Italy) using Landsat TM and ETM+ data. *Ecological Modelling*, *221*(1), 75–84. https://doi.org/10.1016/j.ecolmodel.2009.03.011

Spalt, K. W., & Reifsnyder, Wi. E. (1962). *Bark characteristics and fire resistance: A literature survey*. U.S. Department of Agriculture, Forest Service, Southern Forest Experiment Station.

Spinoni, J., Vogt, J. V., Naumann, G., Barbosa, P., & Dosio, A. (2018). Will drought events become more frequent and severe in Europe? *International Journal of Climatology*, *38*(4), 1718–1736. https://doi.org/10.1002/joc.5291

Spits, C., Wallace, L., & Reinke, K. (2017). Investigating Surface and Near-Surface Bushfire Fuel Attributes: A Comparison between Visual Assessments and Image-Based Point Clouds. *Sensors*, *17*(4), 4. https://doi.org/10.3390/s17040910

Stefanidou, A., Dragozi, E., Stavrakoudis, D., & Gitas, I. (2018). Fuel type mapping using object-based image analysis of DMC and Landsat-8 OLI imagery. *Geocarto International*, *33*(10), 1064–1083. https://doi.org/10.1080/10106049.2017.1333532

Stefanidou, A., Gitas, I., & Katagis, T. (2022). A national fuel type mapping method improvement using sentinel-2 satellite data. *Geocarto International*, *37*(4), 1022–1042. https://doi.org/10.1080/10106049.2020.1756460

Stefanidou, A., Gitas, I., Korhonen, L., Georgopoulos, N., & Stavrakoudis, D. (2020). Multispectral LiDAR-Based Estimation of Surface Fuel Load in a Dense Coniferous Forest. *Remote Sensing*, *12*(20), 3333. https://doi.org/10.3390/rs12203333

Strobl, C., Malley, J., & Tutz, G. (2009). An introduction to recursive partitioning: Rationale, application, and characteristics of classification and regression trees, bagging, and random forests. *Psychological Methods*, *14*(4), 323–348. https://doi.org/10.1037/a0016973

Szpakowski, D. M., & Jensen, J. L. R. (2019). A Review of the Applications of Remote Sensing in Fire Ecology. *Remote Sensing*, *11*(22), 22. https://doi.org/10.3390/rs11222638

Talhelm, A. F., & Smith, A. M. S. (2018). Litter moisture adsorption is tied to tissue structure, chemistry, and energy concentration. *Ecosphere*, *9*(4), e02198. https://doi.org/10.1002/ecs2.2198

Tanskanen, H., Granström, A., Venäläinen, A., & Puttonen, P. (2006). Moisture dynamics of moss-dominated surface fuel in relation to the structure of Picea abies and Pinus sylvestris stands. *Forest Ecology and Management*, *226*(1), 189–198. https://doi.org/10.1016/j.foreco.2006.01.048

Taylor, A., Bruce, M., Britton, A., Owen, J., Gagkas, Z., Pohle, I., Fielding, D., & Hadden, R. (2022). *Fire Danger Rating System (FDRS) Report* [Technical Report]. James Hutton Institute.

Terrier, A., Girardin, M. P., Périé, C., Legendre, P., & Bergeron, Y. (2013). Potential changes in forest composition could reduce impacts of climate change on boreal wildfires. *Ecological Applications*, *23*(1), 21–35. https://doi.org/10.1890/12-0425.1

Thomaz, S. M., Agostinho, A. A., Gomes, L. C., Silveira, M. J., Rejmánek, M., Aslan, C. E., & Chow, E. (2012). Using space-for-time substitution and time sequence approaches in invasion ecology. *Freshwater Biology*, *57*(11), 2401–2410. https://doi.org/10.1111/fwb.12005

Tiiva, P., Tang, J., Michelsen, A., & Rinnan, R. (2017). Monoterpene emissions in response to long-term night-time warming, elevated CO2 and extended summer drought in a temperate heath ecosystem. *Science of The Total Environment*, *580*, 1056–1067. https://doi.org/10.1016/j.scitotenv.2016.12.060

Tinner, W., Colombaroli, D., Heiri, O., Henne, P. D., Steinacher, M., Untenecker, J., Vescovi, E., Allen, J. R. M., Carraro, G., Conedera, M., Joos, F., Lotter, A. F., Luterbacher, J., Samartin, S., & Valsecchi, V. (2013). The past ecology of *Abies alba* provides new perspectives on future responses of silver fir forests to global warming. *Ecological Monographs*, *83*(4), 419–439. https://doi.org/10.1890/12-2231.1

Tinner, W., Conedera, M., Ammann, B., & Lotter, A. F. (2005). Fire ecology north and south of the Alps since the last ice age. *The Holocene*, *15*(8), 1214–1226. https://doi.org/10.1191/0959683605hl892rp

Tinner, W., Conedera, M., Gobet, E., Hubschmid, P., Wehrli, M., & Ammann, B. (2000). A palaeoecological attempt to classify fire sensitivity of trees in the southern Alps. *The Holocene*, *10*(5), 565–574. https://doi.org/10.1191/095968300674242447

Tompoulidou, M., Stefanidou, A., Grigoriadis, D., Dragozi, E., Stavrakoudis, D., & Gitas, I. (2016). National fuel type mapping methodology using geographic object based image analysis and Landsat 8 OLI imagery. *Proceedings*. GEOBIA 2016: Solutions and Synergies, University of Twente Faculty of Geo-Information and Earth Observation (ITC).

Tompson, J., Goroshin, R., Jain, A., LeCun, Y., & Bregler, C. (2015). Efficient Object Localization Using Convolutional Networks. In *Proceedings of the IEEE conference on computer vision and pattern recognition* (pp. 648–656). http://arxiv.org/pdf/1411.4280v3

Torres, M., & Qiu, G. (2016). Habitat image annotation with low-level features, medium-level knowledge and location information. *Multimedia Systems*, *22*(6), 767–782. https://doi.org/10.1007/s00530-014-0445-2

Toukiloglou, P., Eftychidis, G., Gitas, I., & Tompoulidou, M. (2013). ArcFuel methodology for mapping forest fuels in Europe. *First International Conference on Remote Sensing and Geoinformation of the Environment (RSCy2013)*, *8795*, 482–500. https://doi.org/10.1117/12.2028213

Trouet, V., Babst, F., & Meko, M. (2018). Recent enhanced high-summer North Atlantic Jet variability emerges from three-century context. *Nature Communications*, *9*(1), 180. https://doi.org/10.1038/s41467-017-02699-3

Tucker, C. J. (1979). Red and photographic infrared linear combinations for monitoring vegetation. *Remote Sensing of Environment*, *8*(2), 127–150. https://doi.org/10.1016/0034-4257(79)90013-0

Tymstra, C., Bryce, R. W., Wotton, B. M., Taylor, S. W., & Armitage, O. B. (2010). *Development and structure of Prometheus: The Canadian wildland fire growth simulation model* (NOR-X-417; Information Report NOR-X-417). Natural Resources Canada, Canadian Forest Service, Northern Forestry Centre.

UNEP. (2022). *Spreading like Wildfire – The Rising Threat of Extraordinary Landscape Fires: A UNEP Rapid Response Assessment*. United Nations Environment Programme.

U.S. Geological Survey. (2023). *EarthExplorer*. https://earthexplorer.usgs.gov/

Van der Wal, R., Bonn, A., Monteith, D., Reed, M., Blackstock, K., Hanley, N., Thompson, D., Evans, M., & Alonso, Isabel. (2011). Chapter 5: Mountains, Moorlands and Heaths. In *The UK National Ecosystem Assessment Technical Report*. (pp. 105–160). UK National Ecosystem Assessment, UNEP-WCMC.

van Rossum, G., & Drake, F. L. (2009). *Python 3 Reference Manual*. CreateSpace.

Van Wagtendonk, J. W., & Root, R. R. (2003). The use of multi-temporal Landsat Normalized Difference Vegetation Index (NDVI) data for mapping fuel models in Yosemite National Park, USA. *International Journal of Remote Sensing*, *24*(8), 1639–1651. https://doi.org/10.1080/01431160210144679

Varner, J. M., Kane, J. M., Kreye, J. K., & Engber, E. (2015). The Flammability of Forest and Woodland Litter: A Synthesis. *Current Forestry Reports*, *1*(2), 91–99. https://doi.org/10.1007/s40725-015-0012-x

Veira, A., Lasslop, G., & Kloster, S. (2016). Wildfires in a warmer climate: Emission fluxes, emission heights, and black carbon concentrations in 2090-2099. *Journal of Geophysical Research: Atmospheres*, *121*(7), 3195–3223. https://doi.org/10.1002/2015JD024142

Velle, L. G., & Vandvik, V. (2014). Succession after prescribed burning in coastal C alluna heathlands along a 340-km latitudinal gradient. *Journal of Vegetation Science*, *25*(2), 546–558. https://doi.org/10.1111/jvs.12100

Venäläinen, A., Korhonen, N., Hyvärinen, O., Koutsias, N., Xystrakis, F., Urbieta, I. R., & Moreno, J. M. (2014). Temporal variations and change in forest fire danger in Europe for 1960–2012. *Natural Hazards and Earth System Sciences*, *14*(6), 1477–1490. https://doi.org/10.5194/nhess-14-1477-2014

Veraverbeke, S., Somers, B., Gitas, I., Katagis, T., Polychronaki, A., & Goossens, R. (2012). Spectral mixture analysis to assess post-fire vegetation regeneration using Landsat Thematic Mapper imagery: Accounting for soil brightness variation. *International Journal of Applied Earth Observation and Geoinformation*, *14*(1), 1–11. https://doi.org/10.1016/j.jag.2011.08.004

Verrelst, J., Halabuk, A., Atzberger, C., Hank, T., Steinhauser, S., & Berger, K. (2023). A comprehensive survey on quantifying non-photosynthetic vegetation cover and biomass from imaging spectroscopy. *Ecological Indicators*, *155*, 110911. https://doi.org/10.1016/j.ecolind.2023.110911

Vihnanek, R. E., Balog, C. S., Wright, C. S., Ottmar, R. D., & Kelly, J. W. (2009). *Stereo photo series for quantifying natural fuels. Volume XII: Post-hurricane fuels in forests of the Southeast United States.* (PNW-GTR-803). U.S. Department of Agriculture, Forest Service, Pacific Northwest Research Station. https://doi.org/10.2737/PNW-GTR-803

Villarreal, M. L., Norman, L. M., Buckley, S., Wallace, C. S. A., & Coe, M. A. (2016). Multi-index time series monitoring of drought and fire effects on desert grasslands. *Remote Sensing of Environment*, *183*, 186–197. https://doi.org/10.1016/j.rse.2016.05.026

Wahren, C.-H., Papst, W. A., & Williams, R. J. (2001). Early post-fire regeneration in subalpine heathland and grassland in the Victorian Alpine National Park, south-eastern Australia. *Austral Ecology*, *26*(6), 670–679. https://doi.org/10.1046/j.1442-9993.2001.01151.x

Wäldchen, J., & Mäder, P. (2018). Machine learning for image based species identification. *Methods in Ecology and Evolution*, *9*(11), 2216–2225. https://doi.org/10.1111/2041-210X.13075

Waldhauser, C., Hochreiter, R., Otepka, J., Pfeifer, N., Ghuffar, S., Korzeniowska, K., & Wagner, G. (2014). Automated Classification of Airborne Laser Scanning Point Clouds. In *Solving Computationally Expensive Engineering Problems* (pp. 269–292). Springer, Cham. https://doi.org/10.1007/978-3-319-08985-0_12

Wallace, L., Hillman, S., Reinke, K., & Hally, B. (2017). Non–destructive estimation of above–ground surface and near–surface biomass using 3D terrestrial remote sensing techniques. *Methods in Ecology and Evolution*, *8*(11), 1607–1616. https://doi.org/10.1111/2041-210X.12759

Wang, D. (2020). Unsupervised semantic and instance segmentation of forest point clouds. *ISPRS Journal of Photogrammetry and Remote Sensing*, *165*, 86–97. https://doi.org/10.1016/j.isprsjprs.2020.04.020

Wang, L., Quan, X., He, B., Yebra, M., Xing, M., & Liu, X. (2019). Assessment of the Dual Polarimetric Sentinel-1A Data for Forest Fuel Moisture Content Estimation. *Remote Sensing*, *11*(13), 1568. https://doi.org/10.3390/rs11131568

Wang, S., Di Tommaso, S., Faulkner, J., Friedel, T., Kennepohl, A., Strey, R., & Lobell, D. B. (2020). Mapping Crop Types in Southeast India with Smartphone Crowdsourcing and Deep Learning. *Remote Sensing*, *12*(18), 2957. https://doi.org/10.3390/rs12182957

Wang, Z., Ma, Y., Zhang, Y., & Shang, J. (2022). Review of Remote Sensing Applications in Grassland Monitoring. *Remote Sensing*, *14*(12), 12. https://doi.org/10.3390/rs14122903

Watson, A., Miller, G., & Green, F. H. W. (1966). Winter browning of Heather (Calluna vulgaris) and other moorland plants. *Transactions of the Botanical Society of Edinburgh*, *40*, 195–203. https://doi.org/10.1080/03746606608685143

Weikert, R. M., Wedler, M., Lippert, M., Schramel, P., & Lange, O. L. (1989). Photosynthetic performance, chloroplast pigments, and mineral content of various needle age classes of spruce (Picea abies) with and without the new flush: An experimental approach for analysing forest decline phenomena. *Trees*, *3*(3), 161–172. https://doi.org/10.1007/BF00226652

Weinacker, H., Koch, B., & Weinacker, R. (2004). TREESVIS: A software system for simultaneous ED-real-time visualisation of DTM, DSM, laser raw data, multispectral data, simple tree and building models. *International Archives of Photogrammetry, Remote Sensing and Spatial Information Sciences*, *36*, 90–95.

Weinmann, M., Jutzi, B., Hinz, S., & Mallet, C. (2015). Semantic point cloud interpretation based on optimal neighborhoods, relevant features and efficient classifiers. *ISPRS Journal of Photogrammetry and Remote Sensing*, *105*, 286–304. https://doi.org/10.1016/j.isprsjprs.2015.01.016

Weir, J. R., & Scasta, J. D. (2022). *Global Application of Prescribed Fire*. Csiro Publishing.

Weise, D. R., & Wright, C. S. (2014). Wildland fire emissions, carbon and climate: Characterizing wildland fuels. *Forest Ecology and Management*, *317*, 26–40. https://doi.org/10.1016/j.foreco.2013.02.037

Weiss, M., & Baret, F. (2016). *S2ToolBox Level 2 products: LAI, FAPAR, FCOVER* (ESA, Ed.). http://step.esa.int/docs/extra/atbd_s2toolbox_l2b_v1.1.pdf

Wells, A. G., Munson, S. M., Sesnie, S. E., & Villarreal, M. L. (2021). Remotely Sensed Fine-Fuel Changes from Wildfire and Prescribed Fire in a Semi-Arid Grassland. *Fire*, *4*(4), 84. https://doi.org/10.3390/fire4040084

White, J. C., Wulder, M. A., Vastaranta, M., Coops, N. C., Pitt, D., & Woods, M. (2013). The Utility of Image-Based Point Clouds for Forest Inventory: A Comparison with Airborne Laser Scanning. *Forests*, *4*(3), 3. https://doi.org/10.3390/f4030518

White, J., Wulder, M., Hermosilla, T., Coops, N., & Hobart, G. (2017). A nationwide annual characterization of 25 years of forest disturbance and recovery for Canada using Landsat time series. *Remote Sensing of Environment*, *194*, 303–321. https://doi.org/10.1016/j.rse.2017.03.035

White, R. H., & Zipperer, W. C. (2010). Testing and classification of individual plants for fire behaviour: Plant selection for the wildland–urban interface. *International Journal of Wildland Fire*, *19*(2), 213–227. https://doi.org/10.1071/WF07128

Wilson, B. A., Ow, C. F. Y., Heathcott, M., Milne, D., McCaffrey, T. M., Ghitter, G., & Franklin, S. E. (1994). Landsat MSS Classification of Fire Fuel Types in Wood Buffalo National Park, Northern Canada. *Global Ecology and Biogeography Letters*, *4*(2), 33–39. https://doi.org/10.2307/2997751

Wilson, E. H., & Sader, S. A. (2002). Detection of forest harvest type using multiple dates of Landsat TM imagery. *Remote Sensing of Environment*, *80*(3), 385–396. https://doi.org/10.1016/S0034-4257(01)00318-2

Wing, B. M., Ritchie, M. W., Boston, K., Cohen, W. B., Gitelman, A., & Olsen, M. J. (2012). Prediction of understory vegetation cover with airborne lidar in an interior ponderosa pine forest. *Remote Sensing of Environment*, *124*, 730–741. https://doi.org/10.1016/j.rse.2012.06.024

Woodall, C. W., & Monleon, V. J. (2008). *Sampling protocol, estimation, and analysis procedures for the down woody materials indicator of the FIA program*. U.S. Department of Agriculture, Forest Service, Northern Research Station. https://doi.org/10.2737/NRS-GTR-22

Wotton, B. M., Alexander, M. E., & Taylor, S. W. (2009). *Updates and revisions to the 1992 Canadian forest fire behavior prediction system* (GLC-X-10). Natural Resources Canada, Canadian Forest Service, Great Lakes Forestry Centre.

Wright, C. S., Eagle, P. C., & Olson, D. L. (2010). A high-quality fuels database of photos and information. *Fire Management Today. Forest Service of the U.S. Department of Agriculture, Washington, DC*, *70*(3), 27–31.

Xi, Y., Ren, C., Tian, Q., Ren, Y., Dong, X., & Zhang, Z. (2021). Exploitation of Time Series Sentinel-2 Data and Different Machine Learning Algorithms for Detailed Tree Species Classification. *IEEE Journal of Selected Topics in Applied Earth Observations and Remote Sensing*, *14*, 7589–7603. https://doi.org/10.1109/JSTARS.2021.3098817

Xu, G., Zhu, X., Fu, D., Dong, J., & Xiao, X. (2017). Automatic land cover classification of geo-tagged field photos by deep learning. *Environmental Modelling & Software*, *91*, 127–134. https://doi.org/10.1016/j.envsoft.2017.02.004

Xu, J., Morris, P. J., Liu, J., & Holden, J. (2018). Hotspots of peatland-derived potable water use identified by global analysis. *Nature Sustainability*, *1*(5), 5. https://doi.org/10.1038/s41893-018-0064-6

Yan, Y., & Ryu, Y. (2021). Exploring Google Street View with deep learning for crop type mapping. *ISPRS Journal of Photogrammetry and Remote Sensing*, *171*, 278–296. https://doi.org/10.1016/j.isprsjprs.2020.11.022

Yebra, M., Quan, X., Riaño, D., Rozas Larraondo, P., van Dijk, A. I. J. M., & Cary, G. J. (2018). A fuel moisture content and flammability monitoring methodology for continental Australia based on optical remote sensing. *Remote Sensing of Environment*, *212*, 260–272. https://doi.org/10.1016/j.rse.2018.04.053

You, H., Wang, T., Skidmore, A., & Xing, Y. (2017). Quantifying the Effects of Normalisation of Airborne LiDAR Intensity on Coniferous Forest Leaf Area Index Estimations. *Remote Sensing*, *9*(2), 163. https://doi.org/10.3390/rs9020163

Zackrisson, O. (1977). Influence of Forest Fires on the North Swedish Boreal Forest. *Oikos*, *29*(1), 22–32. https://doi.org/10.2307/3543289

Zeilhofer, P., Sanches, L., Vourlitis, G. L., & de Andrade, N. L. R. (2012). Seasonal variations in litter production and its relation with MODIS vegetation indices in a semi-deciduous forest of Mato Grosso. *Remote Sensing Letters*, *3*(1), 1–9. https://doi.org/10.1080/01431161.2010.523025

Zeng, P., Zhang, W., Li, Y., Shi, J., & Wang, Z. (2022). Forest Total and Component Above-Ground Biomass (AGB) Estimation through C- and L-band Polarimetric SAR Data. *Forests*, *13*(3), 442. https://doi.org/10.3390/f13030442

Zhang, R., Wu, Y., Jin, W., & Meng, X. (2023). Deep-Learning-Based Point Cloud Semantic Segmentation: A Survey. *Electronics*, *12*(17), 17. https://doi.org/10.3390/electronics12173642

Zhong, L., Hu, L., & Zhou, H. (2019). Deep learning based multi-temporal crop classification. *Remote Sensing of Environment*, *221*, 430–443. https://doi.org/10.1016/j.rse.2018.11.032

Zhou, Z., Liu, L., Jiang, L., Feng, W., & Samsonov, S. V. (2019). Using long-term SAR backscatter data to monitor post-fire vegetation recovery in tundra environment. *Remote Sensing*, *11*(19), 2230. https://doi.org/10.3390/rs11192230

Zhu, L., Webb, G. I., Yebra, M., Scortechini, G., Miller, L., & Petitjean, F. (2021). Live fuel moisture content estimation from MODIS: A deep learning approach. *ISPRS Journal of Photogrammetry and Remote Sensing*, *179*, 81–91. https://doi.org/10.1016/j.isprsjprs.2021.07.010

Zhu, X. X., Tuia, D., Mou, L., Xia, G.-S., Zhang, L., Xu, F., & Fraundorfer, F. (2017). Deep Learning in Remote Sensing: A Comprehensive Review and List of Resources. *IEEE Geoscience and Remote Sensing Magazine*, *5*(4), 8–36. https://doi.org/10.1109/MGRS.2017.2762307

Zhu, Z., & Woodcock, C. E. (2014). Continuous change detection and classification of land cover using all available Landsat data. *Remote Sensing of Environment*, *144*, 152–171. https://doi.org/10.1016/j.rse.2014.01.011

Ziegler, J. P., Hoffman, C. M., & Mell, W. (2019). FirebehavioR: An R Package for Fire Behavior and Danger Analysis. *Fire*, *2*(3), 41. https://doi.org/10.3390/fire2030041

Appendices

A – Appendix of Chapter 5

Description of fuel sampling and field data preparation:

We sampled all surface fuel components in 179 circular plots with a radius of 7.5 m (176.6 m^2): We recorded all understory trees and shrubs with DBH <7 cm by counting the number of individuals per species in classes of different root collar diameter (RCD). We recorded cover and average height of each herbaceous species and moss type with cover >1 %. Dead woody fuels were tallied in four different size classes related to their rate of drying (1 hr, 10 hr, 100 hr and 1000 hr fuels) along three 7.5 m transects in azimuths of 30°, 150° and 270° from the plot center following the sampling protocol of the Forest Inventory and Analysis (FIA) program of the USDA Forest Service (Woodall & Monleon, 2008). Litter samples were collected at the end of each transect from 0.18 m × 0.18 m microplots. We visually estimated cover and measured the average height (depth) of the shrub, herb and litter layers. The species, their diameter at breast height (DBH) and canopy cover of overstory trees were also recorded.

Understory shrub and tree counts were used in species-specific allometric equations based on RCD to compute biomass (Annighöfer et al., 2016). If equations were not available for a species, we estimated biomass based on equations for species with similar wood density and preferably similar growth form. We estimated herb and moss biomass from growth form-specific equations incorporating height and cover (PhytoCalc model, Bolte, 2006). Biomass of dead woody fuels was estimated from field counts using species-specific density values for coarse (1000 hr) fuels and an average bulk density value for smaller fuel particles. Correction factors for decayed material and sloped terrain were included (Woodall & Monleon, 2008). Litter samples were dried for 72 hours at 60 °C and then weighted to obtain dry matter biomass. All biomass values were related to the respective sampling area to obtain the loading, i.e. biomass per unit area, for each fuel component.

Table A1: Averaged class-wise precision, recall and f1-scores for all models after cross-validation, as well as occurrences per class (support). Maximum scores across models are highlighted in bold.

	precision					**recall**					**f1-score**					**support**
	floor	horizontal	horizontal +floor	horizontal +floor +sentinel	sentinel	floor	horizontal	horizontal +floor	horizontal +floor +sentinel	sentinel	floor	horizontal	horizontal +floor	horizontal +floor +sentinel	sentinel	
bl	0.75	0.74	0.72	0.73	**0.84**	0.71	0.65	0.72	0.69	**0.81**	0.72	0.68	0.71	0.69	**0.82**	88
bl-ln	**0.55**	0.39	0.44	0.49	0.41	0.44	**0.47**	0.42	0.46	**0.47**	**0.47**	0.42	0.41	0.46	0.43	54
bl-sn	0.30	0.34	0.37	0.32	**0.45**	0.35	0.29	0.35	0.34	**0.43**	0.32	0.30	0.34	0.32	**0.41**	44
ln	0.69	0.73	0.66	0.71	**0.76**	**0.74**	0.73	0.73	0.72	0.68	0.69	**0.71**	0.68	0.69	0.68	53
sn	0.71	0.71	**0.73**	0.72	0.55	0.64	**0.70**	0.62	0.60	0.43	0.66	**0.69**	0.65	0.64	0.46	73
sn-fwd	0.45	**0.53**	0.38	0.45	0.24	0.60	0.55	0.47	**0.62**	0.34	0.45	**0.52**	0.41	0.46	0.27	22
mean	**0.57**	0.57	0.55	0.57	0.54	**0.58**	0.56	0.55	0.57	0.53	**0.55**	**0.55**	0.53	0.54	0.51	
bl	0.71	**0.77**	0.73	0.72	0.74	0.74	0.66	0.77	0.80	**0.86**	0.72	0.70	0.74	0.75	**0.80**	88
ln	0.74	0.73	**0.75**	0.69	0.69	0.68	0.71	**0.76**	0.73	0.65	0.69	0.72	**0.74**	0.70	0.65	73
mixed	0.55	0.49	0.57	**0.58**	0.54	0.52	0.54	**0.55**	0.49	0.46	0.53	0.50	**0.56**	0.52	0.48	98
sn	0.77	0.79	**0.82**	0.80	0.75	0.77	0.76	0.74	**0.78**	0.75	0.76	0.77	0.76	**0.78**	0.74	95
mean	0.69	0.69	**0.72**	0.70	0.68	0.68	0.67	**0.71**	0.70	0.68	0.67	0.67	**0.70**	0.69	0.67	
dwarf-shrub	**0.93**	0.78	**0.93**	0.91	0.50	0.92	0.73	**0.95**	0.92	0.68	0.90	0.74	**0.93**	0.90	0.53	23
grass	**0.78**	0.58	0.70	0.75	0.33	0.70	0.61	**0.75**	**0.75**	0.21	0.70	0.58	0.71	**0.73**	0.25	39
herb	0.72	0.67	0.75	**0.76**	0.35	**0.79**	0.60	0.77	0.75	0.50	0.74	0.63	0.74	**0.75**	0.40	41
litter	0.82	0.80	**0.87**	0.85	0.70	0.77	0.77	**0.83**	0.77	0.34	0.79	0.78	**0.84**	0.81	0.44	112
moss	0.67	**0.71**	0.70	0.68	0.41	0.67	**0.71**	0.64	0.67	0.43	0.66	0.66	0.64	**0.67**	0.36	34
shrub-broadleaf	0.76	0.64	**0.84**	0.73	0.34	0.77	0.73	0.79	**0.80**	0.62	0.76	0.68	**0.81**	0.76	0.44	47
shrub-needle	0.58	0.59	**0.63**	0.62	0.33	0.56	0.59	**0.64**	0.63	0.27	0.55	0.57	**0.61**	**0.61**	0.27	40
mean	0.75	0.68	**0.78**	0.76	0.42	0.74	0.68	**0.77**	0.76	0.44	0.73	0.66	**0.76**	0.75	0.38	

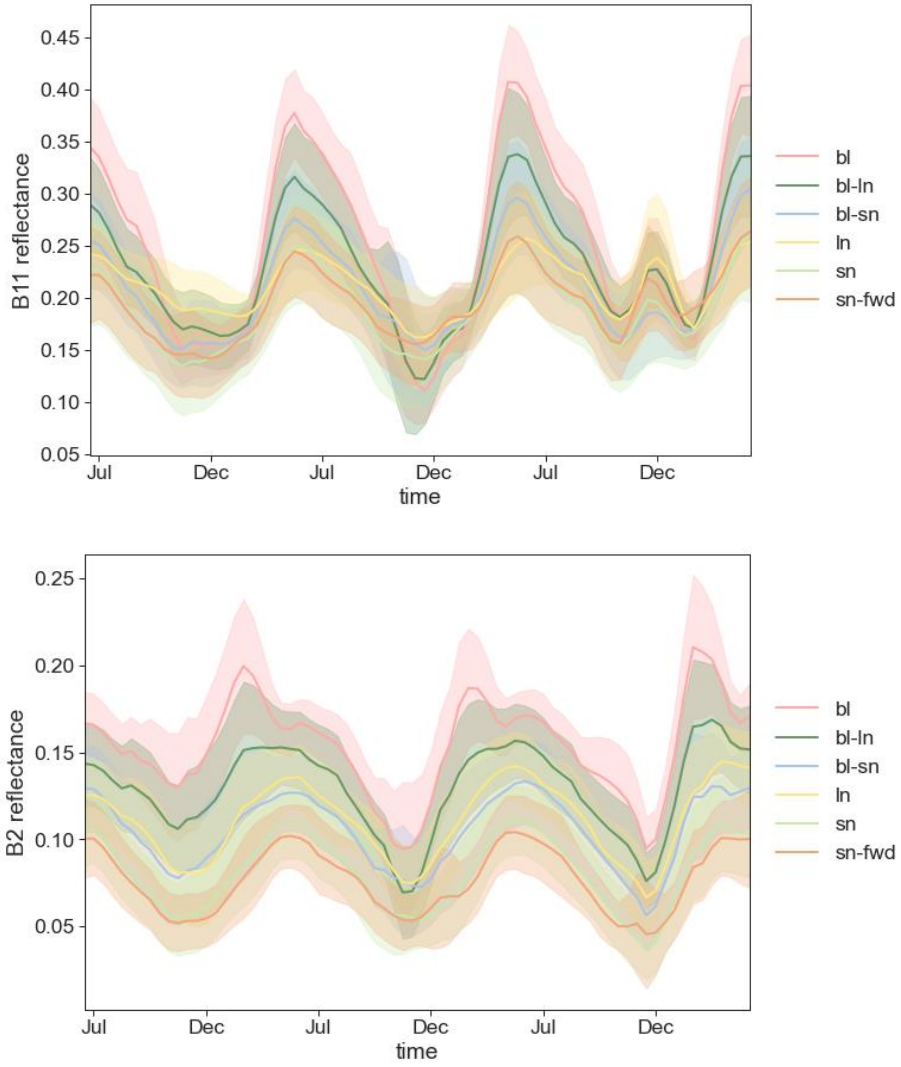

Figure A1: Averaged time series of Sentinel-2 bands 11 (SWIR, upper panel) and 2 (blue, lower panel) by litter fuel type. Shaded areas show standard deviations.

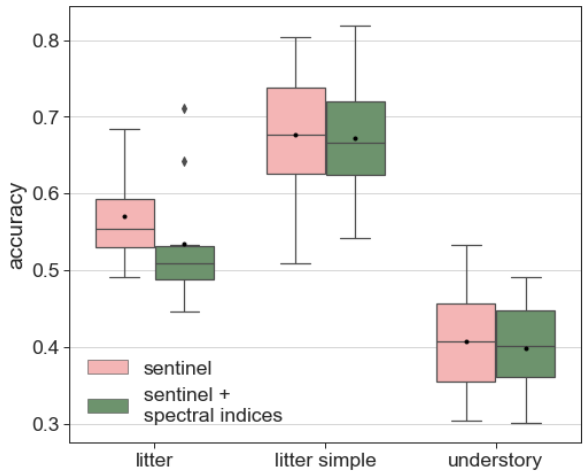

Figure A2: Test accuracy of Sentinel-only classification after 10-fold cross-validation for the original Sentinel-2 dataset (10 spectral bands + NDVI) and the original dataset plus three additional spectral indices (tasselled cap wetness, tasselled cap greenness and NDMI).

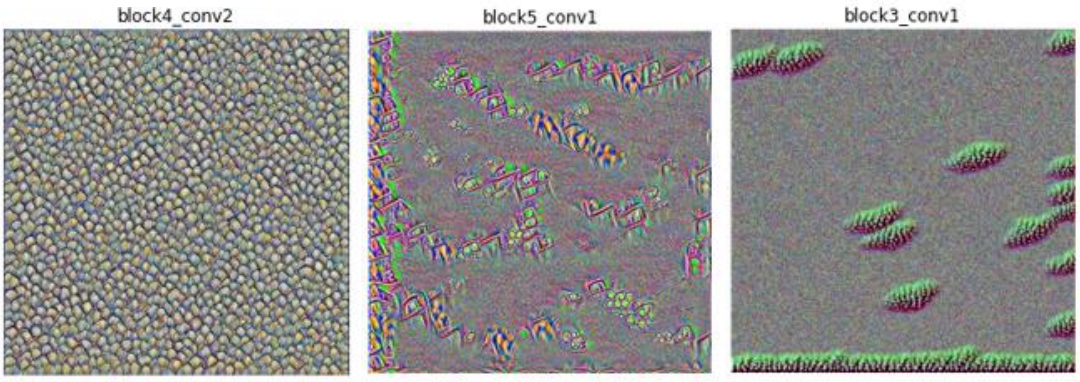

Figure A3: Examples of synthetic images that maximize activations of frequently activated filters in litter classification.

B – Appendix of Chapter 6

Description of field measurements and data preparation

Surface fuel components (dead woody fuels, litter, live herbaceous and shrub fuels) were sampled in 119 circular field plots with a radius of 7.5 m (176.6 m^2). Dead woody fuels were recorded along three transects of 7.5 m length starting at the plot center and laid out in azimuths of 30°, 150° and 270°. All woody fuels that intersected the transect were tallied following Woodall & Monleon (2008). Counts were recorded separately for each of four diameter classes, as the size of the fuel particle determines how quickly they dry out (1 hr, 10 hr, 100 hr and 1000 hr fuels). At the end of each transect, a small frame of 0.18 m x 0.18 m was placed and all litter particles within the frame were collected to the top of the duff layer. All herbaceous species and mosses with cover >1 % were recorded with their relative cover on the plot area and their average height. For the shrub fuels, all understory trees and shrubs with DBH <7 cm were counted in classes of different stem diameter at base (DAB), and the species was recorded. Finally, the cover of the tree, shrub, herb and litter layer was estimated visually and the average height/depth of shrub, herb and litter layer was measured. Tree species in each plot were recorded and the diameter at breast height (DBH) of each individual measured.

The fuel load of the dead woody fuel particles was estimated from the tallies, using species-specific wood density values for the coarsest particle size class and an average bulk density value for smaller fuel particles. We accounted for different stages of decay in the 1000 hr fuels and tallies along sloped terrain by applying correction factors (Woodall & Monleon, 2008). Litter loads were obtained after drying the samples for 72 hours at 60 °C, measuring dry weight and averaging the three samples per plot. Herbaceous fuel load was estimated from height and cover measurements by using growth form-specific equations (PhytoCalc model, Bolte, 2006). Shrub woody fuel load was calculated from species-specific allometric equations based on DAB for each of the recorded species (Annighöfer et al., 2016). For species where own allometric equations were lacking, the equation of a species with similar wood density and a similar growth form was used. The fine shrub load (plant parts with diameter <6 mm) within 2 m of the ground was estimated based on shrub woody biomass by using the relative contribution of different plant compartments to total biomass in different species as a function of diameter at base (DAB) following Pajtík et al. (2011). For young broadleaved trees with DAB >5 cm, we set the fine biomass to zero, as we observed that in most cases none of the fine plant parts fell below the 2 m limit, while for DAB between 3 and 5 cm we assumed that half of the fine biomass was still within the 2 m limit. In the coniferous species, we reduced the fine biomass to half only when DAB exceeded 5 cm.

Table B1: Equations for the geometric features calculated from the lidar point cloud in this study.

$$\text{Anisotropy} = \frac{\lambda1 - \lambda3}{\lambda1} \qquad \text{Planarity} = \frac{\lambda2 - \lambda3}{\lambda1}$$

$$\text{Eigenentropy} = -\sum_{i=1}^{3} \lambda i \cdot \ln(\lambda i) \qquad \text{Sphericity} = \frac{\lambda3}{\lambda1}$$

$$\text{Omnivariance} = (\lambda1 \cdot \lambda2 \cdot \lambda3)^{1/3} \qquad \text{Verticality} = 1 - \frac{\lambda3}{\lambda1 + \lambda2 + \lambda3}$$

$$\text{Sum} = \lambda1 + \lambda2 + \lambda3 \qquad \text{Surface Variation} = \frac{\lambda3}{\lambda1 + \lambda2 + \lambda3}$$

$$\text{Linearity} = \frac{\lambda1 - \lambda2}{\lambda1}$$

with eigenvalues λ1, λ2 and λ3 derived from the covariance matrix of all points within a certain neighbourhood area (of radius r) centered around a point. Calculated for each point inside a vertical stratum and aggregated on plot-level by calculating the mean over the vertical stratum.

Table B2: Physical fuel properties and environmental parameters used in the Rothermel model for surface fire behaviour modelling in the study area.

parameter	**fuel component**	**value**	**unit**	**source**
surface area to volume (SAV) ratio	litter	6000	m^2/m^3	within the range reported by Ascoli et al. (2015) and Cruz & Fernandes (2008)
	1hr	1600	m^2/m^3	Scott & Burgan (2005)
	10hr	358	m^2/m^3	Scott & Burgan (2005)
	100hr	98	m^2/m^3	Scott & Burgan (2005)
	live herb	11500	m^2/m^3	Schimmel & Granström (1997)
	live fine shrubs	5000	m^2/m^3	within the range reported by Ascoli et al. (2015) and Cruz & Fernandes (2008)
fuel moisture	litter	3	%	Scott & Burgan (2005)
	1hr	3	%	Scott & Burgan (2005)
	10hr	4	%	Scott & Burgan (2005)
	100hr	5	%	Scott & Burgan (2005)
	live herb	30	%	Scott & Burgan (2005)
	live fine shrubs	60	%	Scott & Burgan (2005)
extinction moisture	all	30	%	Scott & Burgan (2005)
heat content	all	18622	J/g	Andrews (2009)
terrain slope	-	0	%	set to zero to isolate effect of surface fuel loads
open wind speed	-	15	km/h	DWD Climate Data Center, July maximum
wind adjustment factor	-	0.2	-	Andrews (2012) for sheltered fuel

Table B3: Pre-selected variables for each surface fuel component sorted by variable type and forest stratum.

		litter load	**litter depth**	**fuelbed depth**	**dead 1hr**
geometry	herb	linearity 0.1-0.5 m, r = 0.5 m	eigenentropy 0.1-0.5 m, r = 0.5 m	eigenvalue sum 0.5-1 m, r = 1 m	verticality 0.25-0.5 m, r = 0.5 m
		omnivariance 0.1-0.5 m, r = 0.5 m	planarity 0.5-1 m, r = 0.5 m	verticality 0.1-0.5 m, r = 1 m	sphericity 0.5-1 m, r = 1 m
	shrub	surface variation 0.5-2 m, r = 0.5 m	surface variation 0.5-2 m, r = 0.5 m	omnivariance 0.5-5 m, r = 1 m	planarity 4-5 m, r = 1 m
		planarity 0.5-5 m, r = 1 m	planarity 0.5-2 m, r = 0.5 m	linearity 0.5-2 m, r = 1 m	linearity 4-5 m, r = 0.5 m
	canopy	anisotropy 10-15 m, r = 0.5 m	omnivariance max-5 m - max, r = 0.5 m	surface variation 5-10 m, r = 0.5 m	verticality max-1 m - max, r = 1 m
		surface variation 5-10 m, r = 0.5 m	verticality 5-10 m, r = 1 m	eigenvalue sum 15-20 m, r = 1 m	planarity 10-15 m, r = 0.5 m
density	herb	returns 0.1-0.5 m / all returns	returns 0.25-0.5 m / all returns	returns 0.5-1 m / returns below 1 m	returns 0.1-0.5 m / returns below 0.5 m
		returns 0.25-0.5 m / returns below 0.5 m	returns 0.25-0.5 m / returns below 0.5 m	returns 0.25-0.5 m / returns below 0.5 m	returns 0.25-0.5 m / returns below 0.5 m
	shrub	returns 0.5-2 m / all returns	returns 0.5-2 m / all returns	returns 0.5-2 m / returns below 2 m	returns 4-5 m / returns below 5 m
		returns 3-4 m / returns below 4 m	returns 3-4 m / returns below 4 m	returns 2-3 m / returns below 3 m	returns 1-2 m / returns below 2 m
	canopy	returns 25-30 m / all returns	returns max-5 m - max / all returns	returns 10-15 m / returns below 15 m	returns max-1 m - max / all returns
		returns 30 m - max / all returns	returns 15-20 m / returns below 20 m	returns 15-20 m / returns below 20 m	returns max-5 m - max / all returns
intensity	herb	intensity skew herb layer	intensity skew herb layer	mean intensity herb layer	intensity skew herb layer
		intensity variance herb layer	intensity variance herb layer	intensity variance herb layer	coef. of var. of intensity herb layer
	shrub	intensity variance 0.5-2 m	intensity variance 0.5-2 m	intensity skew 0.5-5 m	coef. of var. of intensity 0.5-2 m
		intensity skew 0.5-5 m	intensity skew 0.5-2 m	coef. of var. of intensity 0.5-5 m	intensity variance 0.5-5 m
	canopy	intensity skew max-5 m - max	intensity skew max-5 m - max	mean intensity max-5 m - max	intensity variance max-5 m - max
		intensity skew max-2 m - max	intensity variance max-5 m - max	intensity variance max-2 m - max	intensity skew max-5 m - max
voxel	herb	non-empty voxels 0-0.5 m	non-empty voxels 0-0.5 m	non-empty voxels 0.5-1 m	coef. of var. of pts. per voxel 0-0.5 m
		std. dev. of leaf area density 0-0.5 m	non-empty voxels 0.5-1 m	std. dev. of pts. per voxel 0.5-1 m	mean nb. of pts. per voxel 0.5-1 m
	shrub	std. dev. of leaf area density 3-4 m	std. dev. of leaf area density 3-4 m	non-empty voxels 1-2 m	std. dev. of pts. per voxel 2-3 m
		std. dev. of leaf area density 1-2 m	std. dev. of leaf area density 1-2 m	non-empty voxels 3-4 m	std. dev. of pts. per voxel 4-5 m
	canopy	std. dev. of leaf area density 10-15 m	std. dev. of pts. per voxel 5-10 m	non-empty voxels 15-20 m	std. dev. of leaf area density 20-25 m
		coef. of var. of pts. per voxel 20-25 m	coef. of var. of pts. per voxel 30 m - max	non-empty voxels 10-15 m	std. dev. of pts. per voxel 10-15 m
height	height	10th percentile	10th percentile	variance of heights 0.1-0.5 m	maximum height
		mean height	coef. of var. of heights	coef. of var. of heights	variance of heights max-1 m - max
spectral	all layers	red reflectance 2020-04-04	red reflectance 2020-04-04	NIR (740 nm) reflectance 2020-09-21	green reflectance 2020-04-04
		blue reflectance 2020-07-23	red edge reflectance 2020-09-21	blue reflectance 2020-09-21	SWIR (2190 nm) reflectance 2020-09-21
indices	all layers	NDVI 2020-07-23	NDVI 2020-04-04	tasseled cap wetness 2020-05-19	NDMI 2020-04-04
		FCOVER 2020-04-04	FAPAR 2020-09-21	EVI 2020-09-21	LAI 2020-11-30

		herb+moss load	herb load	shrub woody load	shrub fine load
geometry	herb	linearity 0.25-0.5 m, r = 0.5 m	eigenentropy 0.1-0.5 m, r = 0.5 m	verticality 0.25-0.5 m, r = 1 m	verticality 0.1-0.5 m, r = 1 m
		omnivariance 0.1-0.5 m, r = 0.5 m	planarity 0.5-1 m, r = 0.5 m	eigenvalue sum 0.5-1 m, r = 1 m	omnivariance 0.5-1 m, r = 1 m
	shrub	linearity 0.5-2 m, r = 0.5 m	linearity 0.5-2 m, r = 0.5 m	anisotropy 0.5-5 m, r = 1 m	eigenentropy 1-2 m, r = 1 m
		planarity 0.5-5 m, r = 1 m	planarity 0.5-5 m, r = 1 m	linearity 4-5 m, r = 1 m	linearity 3-4 m, r = 1 m
	canopy	eigenentropy max-5 m - max, r = 0.5 m	eigenentropy max-5 m - max, r = 0.5 m	omnivariance 5-10 m, r = 0.5 m	eigenentropy 5-10 m, r = 0.5 m
		verticality 5-10 m, r = 1 m	anisotropy 15-20 m, r = 1 m	linearity 10-15 m, r = 0.5 m	surface variation 5-10 m, r = 1 m
density	herb	returns 0.1-0.5 m / all returns	returns 0.25-0.5 m / all returns	returns 0.5-1 m / returns below 1 m	returns 0.5-1 m / returns below 1 m
		returns 0.25-0.5 m / returns below 0.5 m	returns 0.25-0.5 m / returns below 0.5 m	returns 0.1-0.5 m / returns below 0.5 m	returns 0.25-0.5 m / all returns
	shrub	returns 0.5-2 m / all returns	returns 0.5-2 m / all returns	returns 0.5-5 m / returns below 5 m	returns 1-2 m / returns below 2 m
		returns 3-4 m / returns below 4 m	returns 3-4 m / returns below 4 m	returns 0.5-2 m / all returns	returns 3-4 m / all returns
	canopy	returns max-5 m - max / all returns	returns 5-10 m / returns below 10 m	returns 15-20 m / returns below 20 m	returns 15-20 m / returns below 20 m
		returns 5-10 m / returns below 10 m	returns max-5 m - max / all returns	returns 20-25 m / returns below 25 m	returns 20-25 m / returns below 25 m
intensity	herb	intensity skew herb layer	intensity skew herb layer	coef. of var. of intensity herb layer	intensity variance herb layer
		intensity variance herb layer	intensity variance herb layer	mean intensity herb layer	mean intensity herb layer
	shrub	mean intensity 0.5-2 m	mean intensity 0.5-2 m	intensity skew 0.5-5 m	intensity skew 0.5-5 m
		intensity skew 0.5-5 m	intensity skew 0.5-5 m	coef. of var. of intensity 0.5-5 m	coef. of var. of intensity 0.5-5 m
	canopy	coef. of var. of intensity max-1 m - max	coef. of var. of intensity max-1 m - max	mean intensity max-2 m - max	mean intensity max-2 m - max
		mean intensity max-2 m - max	mean intensity max-2 m - max	mean intensity max-5 m - max	intensity variance max-2 m - max
voxel	herb	non-empty voxels 0-0.5 m	non-empty voxels 0.5-1 m	non-empty voxels 0.5-1 m	non-empty voxels 0.5-1 m
		non-empty voxels 0.5-1 m	non-empty voxels 0-0.5 m	std. dev. of pts. per voxel 0.5-1 m	std. dev. of pts. per voxel 0.5-1 m
	shrub	coef. of var. of pts. per voxel 3-4 m	coef. of var. of pts. per voxel 3-4 m	non-empty voxels 2-3 m	non-empty voxels 1-2 m
		coef. of var. of leaf area density 1-2 m	non-empty voxels 3-4 m	std. dev. of pts. per voxel 1-2 m	non-empty voxels 3-4 m
	canopy	coef. of var. of pts. per voxel 30 m - max	coef. of var. of pts. per voxel 5-10 m	mean nb. of pts. per voxel 5-10 m	non-empty voxels 15-20 m
		coef. of var. of pts. per voxel 5-10 m	coef. of var. of pts. per voxel 30 m - max	non-empty voxels 20-25 m	mean nb. of pts. per voxel 10-15 m
height	height	10th percentile	10th percentile	skewness of heights	skewness of heights
		coef. of var. of heights	coef. of var. of heights	variance of heights 0.25-0.5 m	variance of heights 0.1-0.5 m
spectral	all layers	NIR (842 nm) reflectance 2020-09-21	NIR (842 nm) reflectance 2020-09-21	SWIR (2190 nm) reflectance 2020-11-30	NIR (783 nm) reflectance 2020-11-30
		SWIR (1610 nm) reflectance 2020-11-30	red edge reflectance 2020-09-21	SWIR (2190 nm) reflectance 2020-05-19	SWIR (2190 nm) reflectance 2020-09-21
indices	all layers	EVI 2020-09-21	EVI 2020-09-21	NDMI_2 2020-11-30	tasseled cap wetness 2020-07-23
		NDVI 2020-04-04	NDVI 2020-04-04	tasseled cap wetness 2020-09-21	NDMI_2 2020-11-30

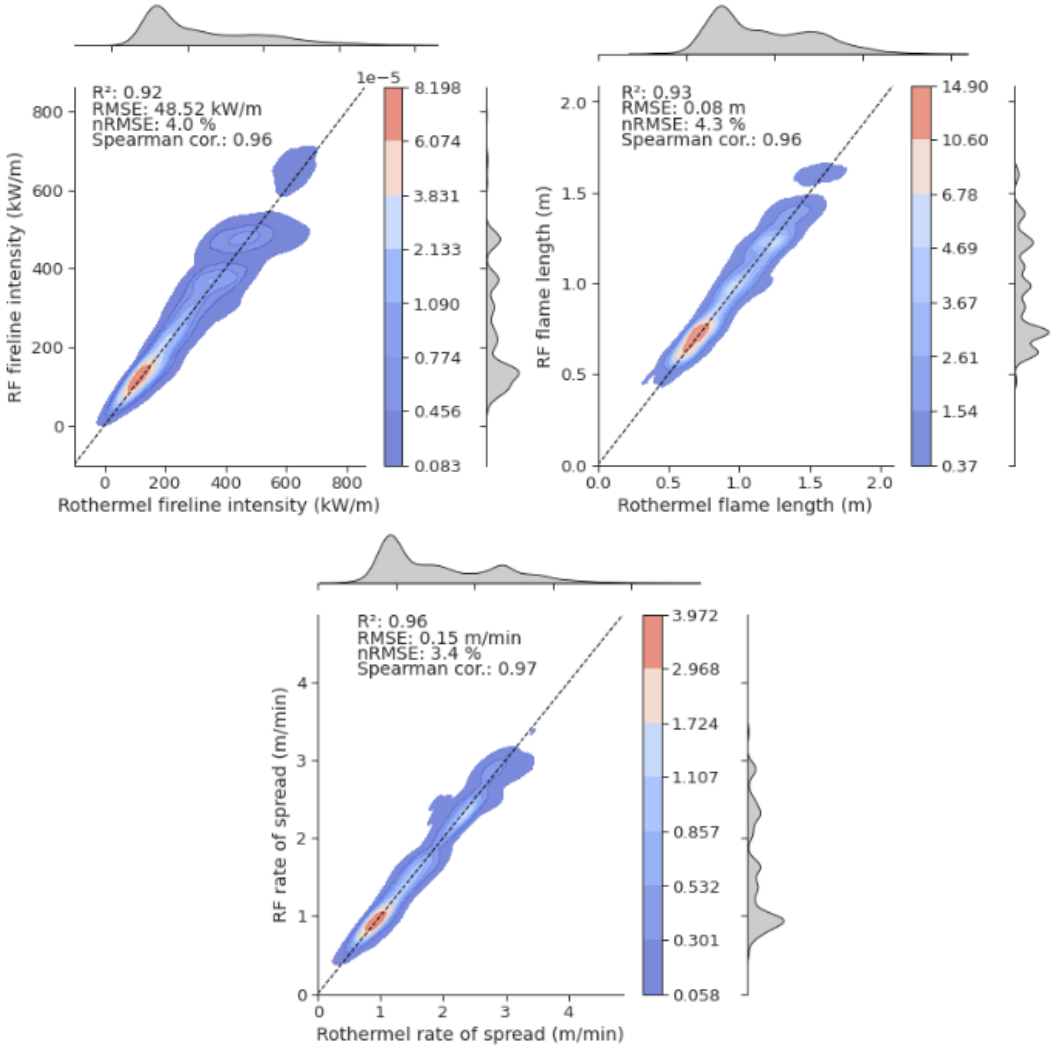

Figure B1: Fire behaviour characteristics modelled using random forest regression on fuel loads (y-axis) vs. reference fire behaviour characteristics calculated using the Rothermel surface fire spread model (x-axis).

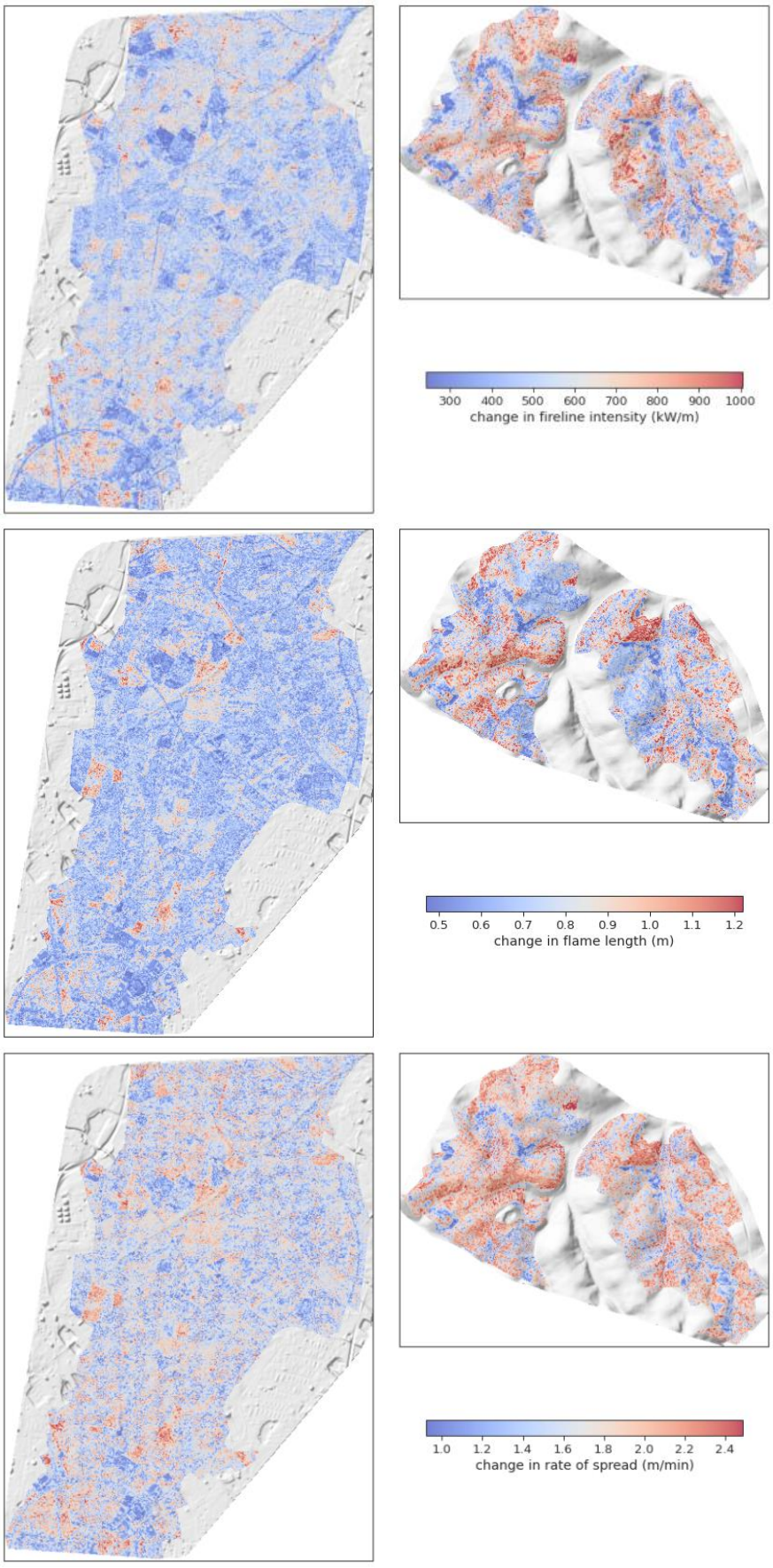

Figure B2: Absolut change in the three fire behaviour characteristics after adding the RMSE of litter and shrub load predictions to every pixel in the study area (extreme scenario).

C – Appendix of Chapter 7

Table C1: Overview of wildfire areas visited during the field campaign. Centroid coordinates of the wildfire areas are projected to the British National Grid (EPSG:27700).

wildfire area	burn year	land cover type	size (ha)	number of sampling plots	centroid coordinates (m)
Dovestone	2018	acid grassland, bog	42	5	402435, 403195
Tameside	2018	heather grassland, heather, bog	1010	15	400970, 401261
Roaches	2018	heather	64	6	400492, 363202
Saddleworth North	2019	bog, acid grassland	441	5	401468, 411702
High Peak	2019	heather	23	4	403164, 399110
Kirklees	2020	bog	158	3	406449, 410225
West of Didsbury intake	2020	heather	1	3	403518, 398539
South of Mount Road	2021	acid grassland, bog	283	6	403811, 409322
Tintwistle Low Moor	2021	heather	2	3	402922, 398194
Middle of Tintwistle Low Moor	2021	heather	2	3	402617, 398402
Slathwaite Moor	2022	bog	83	3	403717, 413471
North of Didsbury intake	2022	heather	6	4	403811, 398869
Standedge	2023	bog	116	3 (+2 outside)	401668, 410461
Harrow Hill	2023	acid grassland, bog	24	2	406001, 410259

Table C2: Phenological characteristics of each VI in each land cover type derived from modelling VI time series with a harmonic modell. Model performance metrics are also shown.

	index	mean	maximum	DOY of max.	minimum	DOY of min.	amplitude	R^2	RMSE
heather	NDVI	0.65	0.73	186	0.55	103	0.09	0.67	0.04
	SAVI	0.33	0.44	193	0.24	355	0.10	0.87	0.03
	NDMI	0.13	0.22	217	-0.02	102	0.12	0.74	0.05
	PSRI	0.07	0.13	82	0.02	217	0.05	0.40	0.04
	NBR	0.40	0.50	213	0.25	105	0.13	0.75	0.05
acid grassland	NDVI	0.63	0.76	189	0.52	84	0.12	0.79	0.04
	SAVI	0.40	0.54	185	0.28	364	0.13	0.80	0.04
	NDMI	0.19	0.26	195	0.06	89	0.10	0.59	0.05
	PSRI	0.08	0.16	78	0.02	221	0.07	0.53	0.04
	NBR	0.44	0.54	197	0.30	88	0.12	0.64	0.06
bog	NDVI	0.60	0.69	197	0.48	100	0.11	0.80	0.04
	SAVI	0.32	0.43	195	0.25	359	0.09	0.85	0.03
	NDMI	0.11	0.21	351	-0.03	106	0.12	0.72	0.05
	PSRI	0.09	0.18	89	0.03	362	0.07	0.54	0.04
	NBR	0.37	0.46	346	0.22	105	0.12	0.76	0.05
heather grassland	NDVI	0.60	0.77	200	0.46	92	0.15	0.86	0.04
	SAVI	0.36	0.53	195	0.22	360	0.16	0.87	0.04
	NDMI	0.16	0.27	204	0.02	98	0.13	0.73	0.05
	PSRI	0.09	0.18	87	0.01	213	0.09	0.60	0.04
	NBR	0.41	0.55	206	0.25	96	0.15	0.76	0.05

Table C3: Day of year (DOY) of the beginning and end of the spring flammability window in different land cover classes and proportion of actual fires that fell within the calculated period.

	DOY start	DOY end	length (days)	% fires within	N fires total
acid grassland	48	123	75	71	24
heather	47	152	105	73	25
heather grassland	41	148	107	90	11
bog	39	170	131	81	14

Table C4: Mean pre-fire VIs and mean differences between pre- and post-fire VIs, plus standard deviations. Values for heather grassland are not shown due to only one wildfire occurrence.

		pre SAVI	pre NDMI	pre PSRI	dSAVI	dNDMI	dPSRI
acid grassland	spring	0.20±0.05	-0.04±0.09	0.28±0.10	-0.07±0.08	-0.15±0.16	-0.06±0.12
	summer	0.46±0.09	0.17±0.10	0.07±0.02	-0.28±0.12	-0.31±0.20	0.06±0.05
bog	spring	0.22±0.07	-0.07±0.06	0.26±0.08	-0.07±0.07	-0.10±0.08	-0.05±0.07
	summer	0.38±0.08	0.05±0.08	0.10±0.02	-0.25±0.22	-0.25±0.29	0.07±0.21
heather	spring	0.26±0.04	-0.03±0.11	0.17±0.07	-0.12±0.06	-0.19±0.14	0.00±0.06
	summer	0.47±0.14	0.14±0.10	0.06±0.03	-0.29±0.19	-0.26±0.33	0.08±0.13
heather grassland	spring	0.20±0.04	-0.09±0.06	0.30±0.06	-0.09±0.05	-0.06±0.16	-0.11±0.09

Figure C1: Standedge wildfire area burned on 03/05/2023. Photos were taken on 04/05/06 (upper left), 07/06/2023 (upper right), and 03/07/2023 (lower left).